OPTIMAL DESIGN OF ELECTRICALLY-SMALL LOOP ANTENNA INCLUDING SURROUNDING MEDIUM EFFECTS

A Thesis
Presented to
The Academic Faculty

by

Timothy Bolton

In Partial Fulfillment
of the Requirements for the Degree
Master of Science in the
School of Electrical and Computer Engineering

Georgia Institute of Technology
May 2016

OPTIMAL DESIGN OF ELECTRICALLY-SMALL LOOP ANTENNA INCLUDING SURROUNDING MEDIUM EFFECTS

Approved by:

Dr. Morris Cohen, Advisor
School of Electrical and Computer Engineering
Georgia Institute of Technology

Dr. Andrew Peterson
School of Electrical and Computer Engineering
Georgia Institute of Technology

Dr. Glenn Smith
School of Electrical and Computer Engineering
Georgia Institute of Technology

Date Approved: April 25, 2016

ACKNOWLEDGEMENTS

I wish to thank everyone who assisted me through this effort and over the years. This includes my thesis advisor and committee; the Georgia Institute of Technology administration, faculty, and Low Frequency Lab; colleagues at the Naval Undersea Warfare Center (NUWC) Division Newport; and family and friends. A special thanks goes to Jess and Lily.

This thesis was made possible through support I received from the NUWC Fellowship Program. I wish to thank the NUWC Fellowship Committee, NUWC Training Department, and mentor Dr. John P. Casey for their support and honoring me with this opportunity.

TABLE OF CONTENTS

LIST OF TABLES

LIST OF FIGURES

LIST OF SYMBOLS

"	Unit of length (inches)
//	Parallel to or relative to
$\emptyset$	Diameter
α	Attenuation constant (nepers per meter)
β	Phase constant (radians per meter)
β_0	Phase constant of free-space (radians per meter)
β_{med}	Phase constant in medium (radians per meter)
γ	Propagation constant (nepers per meter)
Δf	Bandwidth (hertz)
δ	Skin depth (meters)
δ_{cond}	Skin depth in conductor (meters)
δ_{med}	Skin depth in medium (meters)
ε	Absolute permittivity (farads per meter)
ε_r	Relative permittivity
$\varepsilon_0 = 8.85419 \ldots \times 10^{-12}$	Absolute permittivity of free-space (farads per meter)
η	Characteristic impedance (ohms)
η_0	Characteristic impedance of free-space (ohms)
η_{med}	Characteristic impedance of surrounding medium (ohms)
θ_i	Incident angle from vertical (radians)
λ	Electromagnetic wavelength (meters)
μ	Absolute permeability (henries per meter)
μ_r	Relative permeability
$\mu_0 = 4\pi \times 10^{-7}$	Absolute permeability of free-space (henries per meter)
$\mu_a, \mu_{ext}, \mu_{int}$	Relative apparent/external/internal permeability (real)
$\mu_{vol,ext}, \mu_{vol,int}$	Volumetric-averaged relative internal/external permeability
μ_i	Relative initial (nominal, intrinsic, toroidal) permeability of magnetic material (real)
$\pi = 3.14159 \ldots$	Mathematical circle constant
ρ	Electrical resistivity (ohms per meter)
σ	Electrical conductivity (siemens per meter)
φ	Azimuth angle (radians)
χ_e, χ_m	Electrical/magnetic susceptibility
ψ	Coil pitch angle (radians)
Ω	Unit of electrical resistance (ohms)

ω	Angular frequency (radians)
^{o}	Unit of angular measure (degrees)
^{o}C	Unit of temperature (degrees Celsius)
B	Magnetic flux
$Ber(), Ber'(), Bei(), Bei'()$	Kelvin Bessel functions and their derivatives
C	Capacitance (farads)
C_{leads}	Wire leads' external capacitance (farads)
C_{self}	Coil (distributed, parallel, stray) self-capacitance (farads per meter)
D, D_0	Antenna directivity
D_{ant}	Largest antenna dimension (meters)
d_{coil}	Coil diameter (average) (meters)
d_{cond}	Wire conductor diameter (bare) (meters)
d_{core}	Magnetic core outer diameter (meters)
d_{hollow}	Magnetic core inner diameter (meters)
$d_{ins,loop}$	Loop radome insulation outer diameter (meters)
d_{sep}	Separation distance (meters)
d_{strand}	Litz strand diameter (bare) (meters)
d_{wire}	Wire outer diameter including insulation (meters)
E	Electric field (volts per meter)
E_{med}	Incident electric field in surrounding medium (volts per meter)
$E_{ei2}()$	Elliptic integral of the 2nd kind
$e = 2.71828 \ldots$	Natural logarithm constant
F_{gap}	Air gap permeability factor
$F_{L,prox}, F_{L,skin}$	Conductor inductance proximity/skin factor
$F_{R,prox}, F_{R,skin}$	Conductor resistance proximity/skin factor
f	Frequency (hertz)
G_{abs}	Absolute gain (decibels, isotropic)
H	Magnetic field (amperes per meter)
H_{med}	Incident magnetic field in surrounding medium (amperes per meter)
h_e	Effective height (meters)
$J_n(x),\ J_n'(x)$	Bessel function of the 1st kind (order n) and its derivative
j	Imaginary unit
$K_{ei1}()$	Elliptic integral of the 1st kind
k_λ	Wave number (radians per meter)
$k_B = 1.38065 \ldots \times 10^{-23}$	Boltzmann constant (joules per kelvin)

k_{fm}	Fluxmetric-magnetometric correction factor
k_L	Lorenz's (or Nagaoka's) fringing flux correction factor
k_m	Rosa's mutual-inductance correction factor
k_{rad}	Radiation efficiency
k_s	Rosa's self-inductance correction coefficient
L	Inductance (henries)
L_{coil}	Coil external inductance, net including mutual (henries)
L_{leads}	Wire leads' external inductance (henries)
L_{leak}	Leakage inductance (henries)
L_{mut}	Mutual inductance (henries)
L_{self}	Coil external inductance, alone (henries)
l_{coil}	Coil length, measured between the starting and ending wire centers (meters)
l_{core}	Magnetic core length (meters)
l_{gap}	Total length of air gaps (meters)
l_{wire}	Wire length (meters)
l/d_{core}	Length/diameter ratio of magnetic core
$\ln()$	Natural logarithm
$\log_{10}()$	Base-10 logarithm
M	Magnetization field (amperes per meter)
m_{mag}	Magnetic moment (ampere – square meter)
N	Demagnetization factor
N_{axial}	Demagnetization factor along axis of symmetry
N_{ell}	Ellipsoidal demagnetization factor
N_f	Fluxmetric (ballistic, central, short-coil) demagnetization factor
$N_{local,toroidal}$	Local toroidal demagnetization factor
N_m	Magnetometric (long-coil) demagnetization factor
N_{radial}	Demagnetization factor normal to axis of symmetry
N_x, N_y, N_z	Demagnetization factor in x-/y-/z-direction
n_l	Number of coil layers
$n_{t/l}$	Number of coil turns per layer
$P_v^\mu(), Q_v^\mu()$	Associated Legendre functions (order μ, degree v)
$P_v'(), Q_v'()$	Assoc. Legendre function derivatives (order zero, degree v)
p	Winding pitch length (meters)
R	Electrical resistance (ohms)
R_{ant}	Antenna series resistance (ohms)

R_{ac}	Alternating-current resistance (ohms)
R_{core}	Magnetic core resistance (ohms)
R_{dc}	Direct-current resistance (ohms)
R_{med}	Resistance due to surrounding medium (ohms)
R_{rad}	Radiation resistance (ohms)
r_{coil}	Radius of coil (average) (meters)
r_{cond}	Radius of wire conductor (bare) (meters)
r_{wire}	Wire outer radius including insulation (meters)
S_{min}	Magnetic sensitivity (volts-second-meter per ampere)
T	Temperature (degrees Celsius or Kelvin)
t	Time (seconds)
t_{coil}	Thickness of coil (meters)
t_{ins}	Insulation thickness (meters)
$v_0 = 2.99792 \ldots \times 10^8$	Speed of light in free-space (meters per second)
V	Volume (cubic meters)
V_{ant}	Voltage on antenna (volts)
V_n	Noise voltage (volts)
V_{oc}	Open-circuit voltage (volts)
X	Electrical reactance (ohms)
X_{med}	Reactance due to surrounding medium (ohms)
Z	Electrical impedance (ohms)
Z_{ant}	Antenna impedance (ohms)
Z_{in}	Input impedance (ohms)

LIST OF ABBREVIATIONS

μH	Micro-henry (10^{-6} henries)
A	Unit of current (amperes)
AC	Alternating current
CCW	Counter-counter-wound (series-aiding)
CS	Current sheet
CW	Counter-wound (series-opposing)
DC	Direct current
dB	Logarithmic (base-10) ratio unit (decibels)
dBi	Logarithmic (base-10) isotropic radiation (decibels isotropic)
E-field	Electric field
ESL	Electrically-small loop
F	Unit of electrical capacitance (farads)
H	Unit of electrical inductance (henries)
H-field	Magnetic field
ID	Inner diameter
in	Unit of length (inches)
kHz	Kilohertz (10^{3} hertz)
m	Unit of length (meters)
m^2	Unit of area (square meters)
mH	Milli-henry (10^{-3} henries)
MHz	Megahertz (10^{6} hertz)
MN60	Ceramics Magnetics, Inc. manganese zinc ferrite material
MnZn	Manganese zinc ferrite
MPL	Mean magnetic path length (meters)
NAA	Very low frequency transmitter station (Cutler, Maine)
NiZn	Nickel zinc ferrite
Np	Logarithmic (natural) ratio unit (nepers)
OC	Open-circuit
OD	Outer diameter
pF	Pico-farad (10^{-12} farads)
rad	Unit of angular measure (radians)
S	Unit of electrical conductance (siemens)
s	Unit of time (seconds)
SC	Short-circuit

SRF	Self-resonant frequency
T	Unit of magnetic flux/strength (tesla)
TEM	Transverse Electromagnetic
ul	Unit-less
V	Unit of electrical potential (volts)

SUMMARY

Electrically-small loop antennas are a complex topic, with many design concepts to consider. These concepts include: effective magnetic core permeability and demagnetization, solid and Litz wire impedance including eddy current effects, coil inductance and self-capacitance, antenna radiation, effects due to a surrounding medium, and optimization approaches. There is a plethora of literature available covering these disparate subjects but many conflict, compete, or may be overall lacking. We address these concerns by introducing relevant concepts, discussing and analyzing analytical theory and empirical results from an extensive list of literature, and validating with measurements where possible. As a proof of concept, an optimization example is given along with results.

CHAPTER 1

INTRODUCTION

The subject of loop antennas encompasses a wide variety of antennas utilizing magnetic fields from near-field communications to wireless power transfer to geophysics to far-field communications. We will present the design of far-field receiving, electrically-small loop (ESL) antennas including considerations for when insulated & immersed in an electrically-large, dissipative (conducting) medium; many concepts also apply to near-field applications. Most of this thesis is not new in principle, but to wit, the broad collation is new—bringing together literature from the fields of antennas & electromagnetics, inductors & transformers, and magnetometers—as well as attempting to use consistent symbols. Part of the difficulty of collating into one tome is the expanse of loop antenna material spreading over nearly one and a half centuries, but the effort is worthwhile in order to design an optimal antenna. Furthermore, data from a variety of performed measurements are given and analyzed, a noticeable contrast to the plethora of literature lacking empirical data.

It has been attempted to use clear and concise terminology when possible, but it is still easy to be confounded. For example: the terms coil, helix, inductor, loop, solenoid, and winding can conjure different pictures in one's mind but can be synonymous in most aspects under electrically-small assumptions (presented later). Another example is sensor classification: some technical fields divide magnetic field sensors depending on the measured magnetic field strength—magnetometers (<1 mT) and gaussmeters (>1 mT) [Macintyre 1999]. Electromagnetics and radio frequency communications typically use the general term antenna (or aerial), as any antenna radiates (and receives) both electric- and magnetic-fields, though one may be dominant in certain circumstances.

It is assumed that the reader has at least a basic understanding of antennas and electromagnetics—such as that loops are sensitive to magnetic fields, plane transverse electromagnetic (TEM) waves; etc. However, it is not assumed that the reader is familiar with everything under the sun related to loop antennas and electromagnetics. The reader should be aware that there are a variety of magnetic material classifications (ferrimagnetic, ferromagnetic, etc.) and any are usable, but the specific type commonly used in with antennas are soft ferrite (ferrimagnetic) and magnetic foils/tapes/thin-films/alloys because of their relative advantages. It is beyond the scope to delve deeply into the complexities of magnetic materials, but a general introduction is given to cover the salient features of common materials.

While many applications can assume free-space conditions, there are many that must incorporate effects due to surrounding media that are electrically near the antenna—where "near" can be hard to quantify. Three major applications immediately come to mind: seawater communications, ground sensing/communications, and human body sensing/communications. In any of these cases, the surrounding medium(s) can not only affect electromagnetic propagation but also the impedance of the antenna, which is important for antenna matching. Therefore, an antenna designer must be cognizant of the application environment. We will present a brief introduction into general effects of surrounding media, but the subject matter is complicated and difficult to simplify; the reader is recommended to further pursue the literature including references given herein.

Electrically-small magnetic dipoles—which an ESL is—can have significant application advantages over electrically-small electric dipoles. One example is that magnetic dipoles can be easier to impedance match to 50 Ω than electric dipoles [Best 2007, pg. 6-23]. Another example is dipoles immersed in a conductive/dielectric medium where it can be shown that a magnetic dipole is superior to the electric dipole because of less losses but otherwise comparable radiation properties [Moore 1967; Wait 1957;

Galejs 1963; Manteghi and Ibraheem 2014]. Magnetic dipoles have less losses in the presence of a conductive/dielectric medium because their electric near-field is smaller than an electric dipole's [Galejs 1963]; this means the opposite is true for a surrounding medium that is magnetic, which is rare. This is true for both near- and far-field, with the difference in dipole losses becoming more pronounced as electrical size decreases [Manteghi and Ibraheem 2014].

However, this doesn't imply that an ESL is the best antenna in most applications but rather that it can be more efficient for a given volume than an electric dipole, especially since a loop can have multiple turns. For example, it can be shown that a long, trailing wire antenna (floating, insulated conductor) can be preferable to a submerged dipole (of either type) in overall far-field performance in the presence of a conductive medium [Moore 1967].

The following sub-sections round out the introduction by presenting common loop antenna variants, circuit models, the assumptions herein, and describing measurement methods. Following chapters describe and discuss materials and media; radiation; effective permeability; wire impedance; coil inductance and capacitance; optimization approaches and a design example; measured and calculated data; and a conclusion. Useful tables are given in the Appendices, which are referenced by the following chapters where appropriate. Finally, a list of references used herein is given.

Common Loop Antenna Variants

In order to foment understanding of the types of loop antennas and antennas that don't exactly qualify as loop antennas, this section will describe common antenna types involving coils. Some photographs are also included to aid in understanding. Finally, an overview of some classifications of magnetic sensors and antennas is given.

The primary loop antenna variants include the following: air-core loop, crossed loops, loop array, ferrite-core loop, and toroidal antenna. These antennas are listed in Table 1.1 along with common aliases, as the literature is rife with synonyms and variants. Photos of some ESLs are presented in Figure 1.1. Crossed loops and loop arrays are combinations of other loop antenna types, but include considerations of their own. Symbol notation also varies across the literature, so it has been herein attempted to always use descriptive notation, using the common notation when possible.

Table 1.1 – List of Common Types of Loop Antennas

Name Herein	Lit. Aliases/Variants	Typical Electrical Size
Air-core loop	• Circular/square/polygonal loop • Box antenna • Coil antenna • Cylindrical antenna • Frame antenna • Helical antenna • Helicoidal antenna • Inductor antenna • Magnetic dipole (horizontal/vertical) • Multi-turn loop • Solenoid antenna • Induction coil/magnetometer • Search coil	Small – Large
Crossed loop(s)	• Orthogonal coils • Two-/three-axial coil	Small
Loop array		Large
Ferrite- / magnetic-core loop	• Ferrite (-loaded) loop • (Ferrite) rod antenna • Loopstick • Magnetic-core loop	Small
Toroidal loop	Toroidal loop	Small

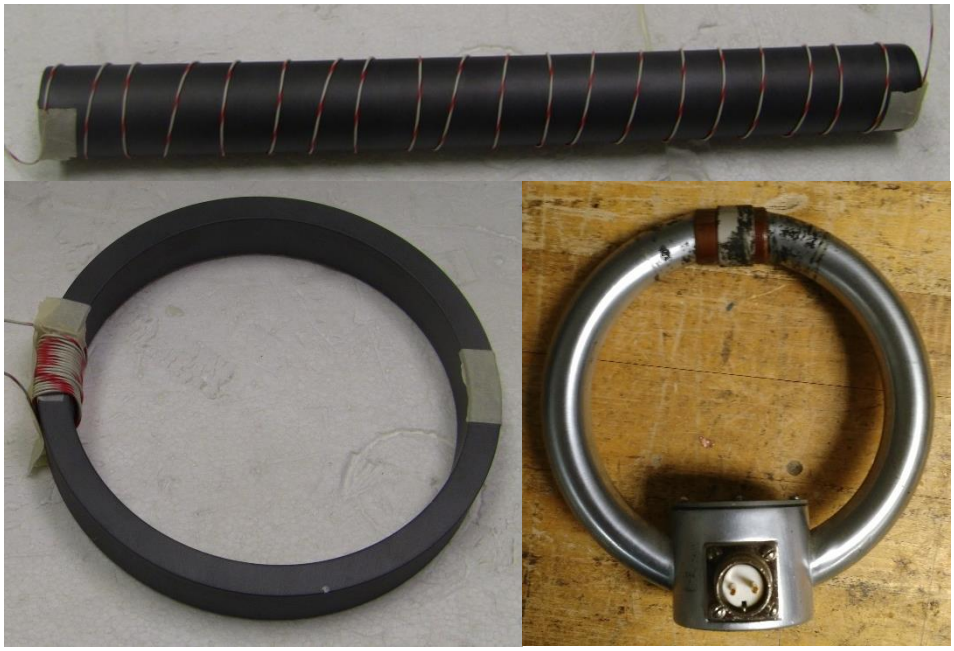

Figure 1.1 – Photos of Some Electrically-Small Loop Antennas
Ferrite-Core Loop (*top*), Ferrite-Core Toroidal Loop (*left*), Shielded Air-Core (*right*)

It is worthwhile introducing helical antennas which do not operate the same as the loop antenna presented herein. Rather, they are their own type of antennas, which can certainly foment confusion as the terms helical and helix are geometrically synonymous with solenoid; see Table 1.2 for a list of common variants. They have physical similarities to loop antennas but the coil may be open-circuited such as for normal- (broadside, electrically-small) and axial-mode (end-fire, electrically-large) helical/helix antenna or a toroidal helix antenna which consists of a coil revolved around an axis. Helical coils, which support traveling waves, have been analyzed extensively in literature for different variations. An electrically-small helix antenna's symmetry axis is effectively an electric dipole [Corum and Corum 1987; Wait 1995].

Table 1.2 – List of Common Non-Loop Helical/Helix Antennas

Lit. Aliases/Variants	Typical Electrical Size
Broadside or normal-mode helical/helix	Small
Axial-mode, end-fire, or quadrifilar (quad) helical/helix	Large
Contra-wound or single-wound toroidal helix antenna	Small-Large

Other common types of magnetic sensors are shown in Figure 1.2 and some notable characteristics in Table 1.3; note that the reference uses the term "induction coil" and "search coil" for ESL. Superconducting quantum interference devices (SQUID) magnetometers are the most sensitive but the limitations can be significant (especially the cooling equipment) in constrained applications such as submerged communications (e.g. [Dinger and Davis 1976; Davis et al. 1977]). It can be seen that an ESL has the largest possible range both in resolution (or sensitivity) but that air- and magnetic-core ESLs (along with fluxgates) can have sensitivities approximately three orders worse than SQUIDs, which is still very good [Tumanski 2011, Table 4.1]. For more details on non-ESL magnetic field sensors/antennas, see the literature (e.g. [Macintyre 1999; Musmann and Afanassiev; Tumanski 2011]).

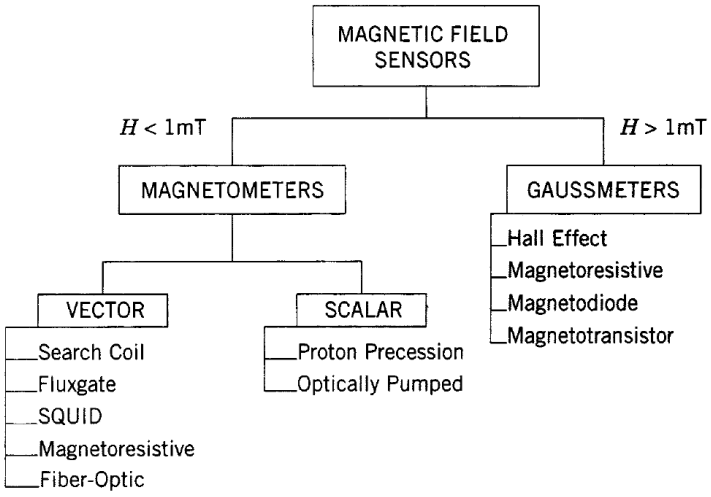

Figure 1.2 – Common Types of Magnetic Field Sensors [Macintyre 1999, Fig. 48.1]

Table 1.3 – Characteristics of Common Magnetic Field Sensors
[Macintyre 1999, Table 48.1]

Instrument	Range (mT)	Resolution (nT)	Bandwidth (Hz)	Comment
Induction coil	10^{-10} to 10^{6}	Variable	10^{-1} to 10^{6}	Cannot measure static fields
Fluxgate	10^{-4} to 0.5	0.1	dc to 2×10^{3}	General-purpose vector magnetometer
SQUID	10^{-9} to 0.1	10^{-4}	dc to 5	Highest sensitivity magnetometer
Hall effect	0.1 to 3×10^{4}	100	dc to 10^{8}	Best for fields above 1T
Magnetoresistance	10^{-3} to 5	10	dc to 10^{7}	Good for mid-range applications
Proton precession	0.02 to 0.1	0.05	dc to 2	General-purpose scalar magnetometer
Optically pumped	0.01 to 0.1	0.005	dc to 5	Highest resolution scalar magnetometer

From all of this, it can be seen that the terminology for antennas and coils is vast. Part of that comes from the many uses and applications of antennas and sensors made from a coil.

Loop Antenna Circuit Models

The classic, lumped-element, low-frequency circuit model for an inductor (which an ESL is) is that of a resistor and inductor in series with a parallel capacitor, illustrated below in Figure 1.3. This model is accurate following certain assumptions, but breaks down as the inductor approaches resonance. In order to extend this classic model but keep it lumped-element, [Rhea 2000] and [Green 2001] proposed cumbersome modifications. However, it may be better to consider a coil as a helical transmission line and the classic, lumped-element, low-frequency coil model as a special case [Corum et al. 2006; Knight 2013a]; helical transmission line models include the (Ollendorf) sheath-helix and the tape-helix. If the assumptions herein (presented in the next sub-section) are maintained, then the classic, lumped-element, low-frequency model is appropriate for an ESL.

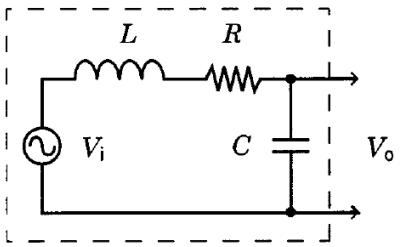

Figure 1.3 – Low-Frequency, Lumped-Element Model of an Inductor [Macintyre 1999, Fig. 48.5]

The generated voltage in a receiving loop is typically measured into an open-circuit and is therefore commonly symbolized as V_{oc} (shown in the preceding figure as V_i). The equivalent series resistance (R in the preceding figure) is commonly abbreviated "ESR" and is typically dominated by internal wire resistance and magnetic core losses (if any). The equivalent series inductance (L in the preceding figure) is typically dominated by the external coil inductance, and is sometimes symbolized as L_0. The parallel capacitance (C in the preceding figure) goes by many names (see Chapter 6); sometimes an external capacitor is added in parallel (wherein capacitances add together) to resonate at a particular frequency. Constituent properties to consider and the symbols used herein are listed in Table 1.4, which are presented and discussed in later chapters. Note that lead wires are technically a cascaded circuit that is identical to Figure 1.3 but may not be ignorable (discussed later, though [Simpson 2007] states they typically can). Our measurements, presented in Chapter 8, show that the lead wires' impedance internal wire resistance and inductance as well as external inductance can be simply added in series to the antenna resistance and inductance with good results.

Table 1.4 – Lumped-Element Model Constituent Impedances

Lumped Element	Constituents
$R = R_{ant}$	External radiation resistance R_{rad}
	Internal wire resistance R_{cond}
	Diss. medium resistance R_{med}
	Magnetic core loss resistance R_{core}
$L = L_{ant}$	External coil inductance L_{coil}
	Mutual coil inductance L_{mut}
	Internal wire inductance L_{cond}
	Diss. medium inductance L_{med}
$C = C_{ant}$	Self-capacitance C_{self}
	External parallel capacitor (if any) C_{ext}

Assumptions Herein

In order to simplify the math and theory considerably from the general equations—which can be open-form (that is, no closed solution but can be numerically analyzed)—there are certain assumptions made by various authors in analyzing loop antennas. Listed in Table 1.5 is the collection of assumptions herein and the benefits thereby attained for analyzing an electrically-small loop antenna; formulas presented later will list the exact assumption(s) used when possible.

Table 1.5 – ESL Assumptions

Theoretical	Practical	Simplifications Allowed
$D_{ant} \ll \lambda_{med}$ [Wait 1957]	$D_{ant} \leq 0.1\lambda_{med}$	Quasi-static analysis
$l_{core} \ll \lambda_{core}$	$l_{core} < 0.5\lambda_{core}$ [DeVore and Bohley 1977, eq. (12)]	Quasi-static analysis
$r_{cond} \ll r_{coil}$ [Smith 2007]	$r_{cond} \leq 0.1r_{coil}$	Simplified current distribution
$l_{wire} \ll \lambda_0$ [Smith 2007]	$l_{wire} \leq 0.1\lambda_0$ [Smith 2007]	Uniform longitudinal current
$l_{coil} \ll \lambda_{core}$ [Knight 2016; Smith 2007]	$l_{coil} \leq 0.1\lambda_{core}$	Lumped-element model
$f \ll f_{res}$ [Kazimierczuk 2014]	$f \leq 0.25f_{res}$ [Smith 2007, ref. 2]	Lumped-element model and uniform current
$n\beta_{med}r_{coil} \ll 1$ [Smith 2007, ref. 2] or $(n)r_{coil} \ll \lambda_{med}$ [Nikolova 2014, pg. 2]	$n\beta_{med}r_{coil} \leq 0.1$ [Smith 2007, ref. 2] or $(n)\beta_{med}r_{coil} < 0.1$ [Galejs 1965, pg. 229] or $(n)r_{coil} < 0.2\lambda_{med}$ [Nikolova 2014, pg. 9]	Uniform current
$\mu_{med} \approx 1$		Various
Materials/mediums linear, homogenous, and isotropic		$\sigma, \varepsilon, \& \mu$ not spatially dependent
$\mu_0\mu_{ext}H_{med} \ll B_{sat}$	$\mu_0\mu_{ext}H_{med} \leq 0.5B_{sat}$	Negligible core saturation
$\delta_{core} \gg (r_{core} - r_{hollow})$ [Kazimierczuk 2014]	$\delta_{core} > (d_{core} - d_{hollow})$ [Kazimierczuk 2014]	Uniform flux in magnetic core
Coil centered on axial core		Simplified analysis
Coil evenly-spaced		Simplified analysis
Far-field TEM [Bansal 1999] or surface wave [King 1986]	See [Bansal 1999] or [King 1986]	Uniform field; $\lvert E_{med}\rvert = \lvert\eta_{med}\rvert\lvert H_{med}\rvert$

Where D_{ant} is the antenna's largest dimension, including insulation (which may include other layers not strictly attributed to the antenna); λ_{med} is the wavelength in the surrounding medium; l_{core} is the core length; λ_{core} is the wavelength in the core; r_{cond} is the bare conductor radius; r_{coil} is the mean coil radius; l_{wire} is the wire length; λ_0 is the wavelength of free-space; l_{coil} is the coil length; f is the operating frequency; f_{res} is the resonant frequency; n is the number of coil turns; β_{med} is the phase constant of the medium; μ_{med} is the relative permeability of the surrounding medium; μ_0 is the

permeability of free-space; μ_{ext} is the relative effective external permeability; H_{med} is the incident external magnetic field in the surrounding medium; B_{sat} is the saturation flux density of the core; δ_{core} is the skin depth of the core; r_{core} is the outer radius of the core; r_{hollow} is the inner, hollow radius of the core; d_{core} is the outer diameter of the core; d_{hollow} is the inner, hollow diameter of the core; E_{med} is the incident electric field in the surrounding medium; and η_{med} is the intrinsic impedance of the surrounding medium.

Note that [Smith 2007] states that a multi-turn solenoid must have a length-to-diameter ratio of at least 3, as well as other electrically-short assumptions, in order for the assumption of uniform current to be valid. Smith references the work of [Medhurst 1947b, pg. 86] where Medhurst's measurements (Fig. 10) show that self-resonant frequency is directly related to an air-core coil's length/diameter ratio and length of wire used. The measurements fit the presented analytical expressions very well and reasonably asymptote to resonance at $l_{wire} = 0.5\lambda_0$. A more generalized constraint is $f \leq 0.25 f_{res}$ where Smith notes that it is reasonable to assume uniform current [Smith 2007, ref. 2].

The assumption of uniform current is very important for simplifying analysis of impedance and radiation, and allows the lumped-element model to be used. For an ESL in a lossless dielectric medium, this assumption is valid for $n\beta_{med} r_{coil} < 0.1$. For a conductive (lossy) dielectric medium, the assumption is valid when $(n)\beta_{med} r_{coil} < 0.3$ for susceptance but $(n)\beta_{med} r_{coil} < 0.05$ for conductance [Galejs 1965, pg. 229; n has been added]. Therefore, a practical limit of $n\beta_{med} r_{coil} < 0.1$ seems plausible but $n\beta_{med} r_{coil} < 0.05$ is conservative. The latter matches Nikolova's claimed $(n) r_{coil} < 0.2\lambda_{med}$ which can be re-arranged as $n\beta_{med} r_{coil} < 1/\pi \approx 0.03$, assuming $\beta_{med} \gg \alpha_{med}$, where α_{med} is the attenuation constant of the surrounding medium.

The current distribution is also a function of the loop's insulation properties and thickness [Galejs 1965; King and Smith 1981, §10.3] and submerged depth. Although only evaluated for a bare, horizontal loop, Row estimates that the submerged depth should be greater than the coil radius for steady-state conditions [Row 1969, pg. 565] which is also coincidentally approximately $0.1\delta_{med}$ [Row 1969, Fig. 1 – note that δ_{med} is actually 2.51m]. The reader is recommended to investigate literature if considering an application near a planar interface as well as attenuation and propagation effects in a conducting medium (e.g. [Balanis 2012; King et al. 1992; Kraichman 1970]. These assumptions due to a conducting medium are presented in Table 1.6, which also includes that the surrounding medium be considered semi-infinite for steady-state conditions (so there are no further reflections to consider).

Table 1.6 – Additional Assumptions for a Surrounding Conducting Medium

Theoretical	Practical	Simplifications Allowed
$D_{med} \to \infty$ (semi-infinite medium)	$D_{med} \geq 10\lambda_{med}$	Steady-state conditions
$z_{depth} \to \infty$		Impedance effects not a function of depth
$t_{ins,antenna} > 0$ [Galejs 1965; King and Smith 1981, pg. 599]	$t_{ins,antenna} > t_{coil} \times \begin{cases} 2 & \tan(\delta_{e,med}) \to 0 \\ 0.2 & \tan(\delta_{e,med}) \to \infty \end{cases}$ [Galejs 1965, Fig. 5]	Uniform current

Where D_{med} is the dimensions of the surrounding medium; z_{depth} is the depth of the antenna in the medium from a planar interface; $t_{ins,antenna}$ is the insulation thickness on the overall antenna; t_{coil} is the coil thickness; and $\delta_{e,med}$ is the loss tangent of the surrounding medium.

Some further, general assumptions are listed in Table 1.7.

Table 1.7 – General Assumptions

Theoretical	Practical	Simplifications Allowed
Suppressed time-dependence	$e^{j\omega t} \rightarrow 1$	Simplified notation
Room Temperature	$T \approx 20\ ^{o}C$	Simplified analysis

Where e is the natural exponential function; j is the imaginary unit; ω is the angular frequency; t is time; and T is temperature.

The geometry of solenoidal coil over a core is presented in Figure 1.4. In very old literature, the coil length is "mean over-all length including the insulation on the first and last wires" [Rosa 1906]; this is discussed further in [Knight 2016]. However, modern literature typically has the coil length measured from the middle of the first turn to the middle of the last turn. The difference is likely inconsequential for most applications, but it seems odd to also include the insulation on the first and last wires.

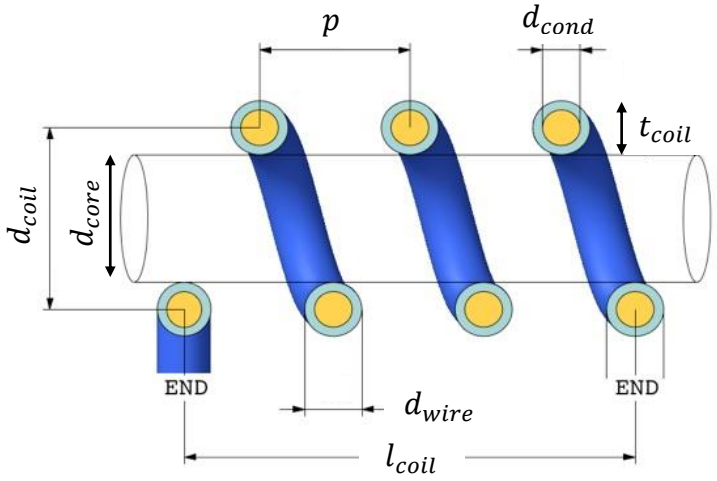

Figure 1.4 – Coil, Core, and Wire Geometry
(Adapted from [http://electronbunker.ca/eb/InductanceCalc_files/HelixSectiononly.jpg])

Note that pitch p can have two different derivations, depending on if the coil is helical (as in the previous picture) or if the coil turns are represented as parallel rings. The latter is possible, but isn't common. The key is to pay attention to the start and end of complete turns. Wire pitch is calculated as:

$$p = \begin{cases} l_{coil}/n & Helical\ coil \\ l_{coil}/(n-1) & Non-helical \end{cases} \quad m$$

Having knowledge of the assumptions and geometry enables accurate calculations. Indeed, there are many articles and texts that forego stating assumptions (or are not clear), which is discouraging.

Measurement Approaches

In general, ESL measurements are easy to make with a balanced impedance analyzer or network analyzer. However, care must be taken in some circumstances. One example is the wire leads, which should be relatively short compared to the total wire used in the coil as well as physically not being separated by more than the coil length [Simpson 1999, pg. 511]; ideally the leads' resistance and inductance have a negligible impact, but this isn't always true in practice.

In literature, it is pointed out that the series-measured resistance R_{meas} and inductance L_{meas} can be converted to the equivalent series resistance R_{series} and L_{series} if enough of the variables are known [Kazimierczuk 2014, pg. 521-3]. The following three equations, taken from [Kazimierczuk 2014, eq. (9.3), (9.4), & (9.17)], are all that are known including total parallel capacitance C and self-capacitance C_{self}, assuming the circuit as described previously in Figure 1.3 (neglecting wire leads) measured by an impedance meter in series-circuit mode:

$$R_{meas} = \frac{R_{series}}{(1-\omega^2 L_{series} C)^2 + (\omega C R_{series})^2} \quad \Omega$$

$$L_{meas} = L_{series} \frac{1 - \omega^2 L_{series} C - C R_{series}^2 / L_{series}}{(1-\omega^2 L_{series} C)^2 + (\omega C R_{series})^2} \quad \text{H}$$

$$f_{res} = \frac{1}{2\pi} \sqrt{\frac{L_{series} - R_{series}^2 C}{L_{series}^2 C}} \approx \frac{1}{2\pi\sqrt{L_{series} C_{self}}} \quad [\![C \approx C_{self}, L_{series} \gg R_{series}^2 C_{self}]\!] \ Hz$$

Note that f_{res} is the self-resonant frequency (SRF) when $C = C_{self}$, i.e. no other capacitances are considered.

While these equations can be arranged and potentially numerically evaluated, it is not trivial. Indeed, while there are three unknown variables, there are only two broadband equations as $X_{meas} = \omega L_{meas} = 0$ at SRF, so either L_{series} must be assumed/calculated at resonance or the inductor must be resonated at a frequency significantly less than SRF with an external capacitor in parallel (and then its impedance measured sans external capacitor). Instead, an assumption can be applied to simplify these equations: at frequencies significantly lower than SRF, C_{self} can be neglected resulting in $R_{series} \approx R_{meas}$ and $L_{series} \approx L_{meas}$ after applying these assumptions to the preceding equations [Kazimierczuk 2014, pg. 523]. Indeed, this seems to be the conventional wisdom.

However, as the frequency approaches resonance, such simplifications are no longer valid since $R_{series}, L_{series}, \& C_{self}$ are functions of frequency. R_{series} typically increases with frequency due to wire eddy currents and magnetic core losses; L_{series} typically decreases due to wire eddy currents and decreasing core permeability; and C_{self} is typically assumed constant for typical material permittivities (up to approximately 30 Megahertz (MHz)) [Kazimierczuk 2014, pg. 523]. Therefore, the simplest method to measure C_{self} is by way of self-resonant frequency, where the phase equals zero (Method I in [Kazimierczuk 2014, pg. 559]). However, this can be a poor choice for coils with magnetic cores as L_{series} $(f = SRF)$ is not easy to measure, so it must be calculated and may not be accurate unless the material permeability is accurately known at SRF.

If the previous is a problem, a better method is to have the ESL resonated at two different frequencies f_{r1} & f_{r2} using external capacitors C_1 & C_2 in parallel with the ESL respectively (Method III in [Kazimierczuk 2014, pg. 560]), ideally resonated at a

frequency significantly less than SRF and measuring the inductances L_1 & L_2 at the resonant frequencies. The capacitance C_{self} is then calculated as:

$$C_{self} = \frac{C_2 L_2 f_{r2}^2 - C_1 L_1 f_{r1}^2}{L_1 f_{r1}^2 - L_2 f_{r2}^2} \quad [\![L_{series} \gg R_{series}^2 C_{1,2}]\!] \quad F$$

When measuring the physical dimensions of a coil, it quickly becomes apparent that measuring the cross-sectional dimensions of a helical coil is not always easy, unless the coil is very tight and consistent. Another approach is to measure the coil length and the length of conductor in order to calculate the effective diameter; in many cases, this approach will be more accurate [Knight 2016b, pg. 22]. As many of the coils built herein were not rigorously constructed with tight tolerances upon the core, including the wire being too stiff to not tightly bend around the square cores, this can be a more accurate approach. By re-arrangement per [Knight 2016b, eq. (5.8)], coil diameter is:

$$d_{coil} = \frac{\sqrt{l_{wire\ (no\ leads)}^2 - l_{coil}^2}}{\pi n} \quad m$$

where d_{coil} is the mean coil diameter and π is the mathematical constant.

It isn't exactly clear what effective diameter to use for multi-layer coils, but the mean coil diameter is used herein (as the coil was still relatively thin). Although many equations exist specifically for multi-layer coils, there are still times when an overall effective diameter is useful—averaging the volumetric permeability being one example. The only equation found in literature is the following equation of [Tumanski 2011, eq. (4.18)], solved for coil area:

$$A_{coil} = \frac{\pi\left(d_{coil,outer}^3 - d_{coil,inner}^3\right)}{12\left(d_{coil,outer} - d_{coil,inner}\right)} \quad m^2$$

where A_{coil} is the coil area and $d_{coil,inner}$ & $d_{coil,outer}$ are the inner and outer diameters of the coil, respectively. However, it comes with the caveat that it is "of limited accuracy ... it is better to determine the resultant area of the coil experimentally by means of

calibration in a known field" and instead recommends using the mean/average coil diameter [Tumanski 2011, pg. 165].

Accurately measuring loop antenna parameters is paramount to accurate analysis and comparison to predictions. However, as shown here, there are some complexities that complicate measurement and analysis. These difficulties can be overcome by judicious assumptions and appropriate techniques.

CHAPTER 2

MATERIALS AND MEDIA

This chapter presents the properties and effects of various materials and media related to loop antennas. The first section introduces general electromagnetic principles, including various variables used throughout. The following sections describe magnetic materials' permeability, permittivity, and conductivity; magnetic materials' resistive losses; and the effects of surrounding media upon antenna impedance.

Electromagnetic Properties

In this section, the electromagnetic properties of general media will be presented and discussed. This includes common materials in order to give a general background of their properties, which helps to simplify which material to choose when. It

General electromagnetic wave properties can be described using the following variables given in Table 2.1, some of which assume a TEM wave.

Table 2.1 – General Electromagnetic Variables (TEM)

	Exact	Good Dielectric ($\sigma \ll \omega\varepsilon$, $\mu'' \approx 0$)	Good Conductor ($\sigma \gg \omega\varepsilon$, $\mu'' \approx 0$)
Complex Wave Number $\sqrt{j}k_{wave}$ (Np/m)	$= \beta - j\alpha$ $= \omega\sqrt{\dot{\varepsilon}\dot{\mu}}$	$\simeq \beta$ $\simeq \omega\sqrt{\mu\varepsilon}$	$\simeq -j\alpha$ $\simeq -j\sqrt{\frac{\omega\mu\sigma}{2}}$
Complex Propagation Constant γ (Np/m)	$= \alpha + j\beta$ $= \omega\sqrt{j\dot{\mu}\dot{\varepsilon}}$	$\simeq j\beta$ $\simeq j\omega\sqrt{\mu\varepsilon}$	$\simeq \alpha \simeq \sqrt{\frac{\omega\mu\sigma}{2}}$
Attenuation Constant α (Np/m)	$= imag(k_{wave})$ $= real(\gamma)$	$\simeq \frac{\sigma}{2}\sqrt{\frac{\mu}{\varepsilon}}$	$\simeq \sqrt{\frac{\omega\mu\sigma}{2}}$
Phase Constant β (rad/m)	$= real(k_{wave})$ $= imag(\gamma) = k_\lambda$	$\simeq \omega\sqrt{\mu\varepsilon}$	$\simeq \sqrt{\frac{\omega\mu\sigma}{2}}$
Complex Intrinsic Impedance η (Ω)	$= \sqrt{\frac{j\omega\dot{\mu}}{\sigma + j\omega\varepsilon}}$	$\simeq \sqrt{\frac{\mu}{\varepsilon}}$	$\simeq (1+j)\sqrt{\frac{\omega\mu}{2\sigma}}$
Wavelength λ (m)	$= \frac{2\pi}{\beta}$	$\simeq \frac{2\pi}{\omega\sqrt{\mu\varepsilon}}$	$\simeq 2\pi\sqrt{\frac{2}{\omega\mu\sigma}}$
Velocity v (m/s)	$= \frac{\omega}{\beta}$	$\simeq \frac{1}{\sqrt{\mu\varepsilon}}$	$\simeq \sqrt{\frac{2\omega}{\mu\sigma}}$
Skin Depth δ (m)	$= \frac{1}{\alpha}$	$\simeq \frac{2}{\sigma}\sqrt{\frac{\varepsilon}{\mu}}$	$\simeq \sqrt{\frac{2}{\omega\mu\sigma}} = \frac{1}{\sqrt{\pi f\mu\sigma}}$
Conductivity σ (S/m)	$= \sigma_{DC} + \sigma_{AC} = \omega\varepsilon_0\varepsilon_r''$		
Resistivity ρ (Ω-m)	$= 1/\sigma$		
***Complex Permittivity $\dot{\varepsilon}$ (F/m)**	$= \varepsilon' - j\varepsilon'' = \varepsilon_0(\varepsilon_r - j\varepsilon_r'') = \varepsilon_0\varepsilon_r - j\frac{\sigma}{\omega} = \varepsilon_0(1 + \dot{\chi}_e)$		
***Complex Permeability $\dot{\mu}$ (H/m)**	$= \mu' - j\mu'' = \mu_0(\mu_r - j\mu_r'') = \mu_0(1 + \dot{\chi}_m)$		
***Complex Electric Susceptibility $\dot{\chi}_e$**	$= (\varepsilon_r - 1) - j\varepsilon_r'' = (\varepsilon_r - 1) - j\frac{\sigma}{\omega}$		
***Complex Magnetic Susceptibility $\dot{\chi}_m$**	$= (\mu_r - 1) - j\mu''$		
***Electric Loss Tangent $\tan\delta_e$**	$= \varepsilon''/\varepsilon' = \sigma/\omega\varepsilon_0\varepsilon_r$		
***Magnetic Loss Tangent $\tan\delta_m$**	$= \mu''/\mu'$		
* Literature (and herein) typically assume that $\varepsilon/\mu/\chi$ sans accents (e.g. μ', $\dot{\chi}$) are *real*			
Note: Permeabilities and permittivities herein with a subscript (e.g. μ_{ext}) are relative, except μ_0, ε_0			

Where ε' & ε'' are the absolute real and imaginary permittivities, respectively; ε_0 is the absolute permittivity of free-space; ε_r & ε_r'' are the relative real and imaginary permittivities, respectively; μ' & μ'' are the absolute real and imaginary permeabilities, respectively; and μ_r & μ_r'' are the relative real and imaginary permeabilities, respectively.

Permeability and permittivity can be complex, and can be fully described as a function of frequency with dispersion equations. The permeability dispersion equation, taken from [Tsutaoka 2003, eq. (1)], is:

$$\dot{\mu} = 1 + \frac{\omega_d^2 \chi_{d0}}{\omega_d^2 + \omega + j\omega\beta_d} + \frac{(\omega_s + j\omega\alpha_s)\omega_s\chi_{s0}}{(\omega_s + j\omega\alpha_s)^2 - \omega^2} \quad H/m$$

where definition of $\omega_d, \chi_{d0}, \beta_d, \omega_s, \alpha_s, \& \chi_{s0}$ can be found in the reference.

At low frequencies, most materials have static electromagnetic properties independent of frequency and can be assumed to be linear, homogenous, and isotropic; see Table 2.2 for a list of common materials' properties. However, large bodies of media (e.g. soil, water) may rather be composed of stratified layers and can vary globally—for a global conductivity reference, consider International Telecommunications Union report ITU-R P.832. Also, materials' properties can be a function of temperature and pressure as well as alloy composition, external fields, etc. Note that "low frequencies" will vary by material.

Table 2.2 – Common Materials' Low-Frequency Electromagnetic Properties

	Material	μ_r	ε_r	σ (S/m) at 20 ºC
Large Media	Air	1.000 000 37 [a]	1.000 59 (0 ºC, 1 bar) [b]	3×10^{-15} to 8×10^{-15} [c]
	Fresh Water	0.999 992 [a]	80 [d]	3×10^{-3} [d]
	Ice (Fresh Water)	1	3 – 27 (-10/-1 ºC) [d]	10^{-5} - 10^{-4} (-10/-1 ºC) [d]
	Medium-Dry Ground	1	15 [d]	10^{-3} [d]
	Sea Water	0.999 992 [a]	70 - 81 [various]	3 - 5 [various]
	Very Dry Ground	1	3 [d]	10^{-4} [d]
	Wet Ground	1	30 [d]	10^{-2} [d]
Insulators	Acrylic (Plexiglas)	1	2.7 – 4.5 [e]	0
	Concrete (no rebar)	1 [a]	4.5 [b]	0
	Epoxy Resin (Cast)	1	3.6 [e]	0
	FR-4	1	4.3 – 5.0 [e]	0
	Neoprene	1	6.7 [b]	0
	Nylon	1	4.0 – 5.0 [e]	0
	Polyethylene (XLPE)	1	2.25 [b]	0
	Polypropylene	1	2.2 – 2.36 [b]	0
	Polystyrene	1	2.4 – 2.7 [b]	0
	Polyvinyl Chloride (PVC)	1	2.8 – 3.4 [e]	0
	PTFE (Teflon)	1.0000 [a]	2.1 [b]	10^{-25} to 10^{-23} [c]
	Pyrex Glass	1	4.7 [e]	10^{-15} to 10^{-11} [c]
	Silicone Rubber	1	3.2 – 9.8 [e]	10^{-14} [c]
	Wood (Dry)	1	2 – 6 [e]	10^{-16} to 10^{-14} [c]
	Wood (Wet)	1	10 – 30 [e]	10^{-4} – 10^{-3} [c]
Conductors	Aluminum	1.000 022 [a]	1	3.50×10^{7} [c]
	Carbon Steel (1010)	~100 [a]	1	6.99×10^{6} [c]
	Copper (Annealed)	0.999 994 [a]	1	5.80×10^{7} [c]
	Gold	0.999 96 [k]	1	4.10×10^{7} [c]
	Iron (99.8 – 99.96%)	5,000 – 2.8×10^{5} [k]	1	1.00×10^{7} [c]
	Silver	0.999 98 [11]	1	6.30×10^{7} [c]
	Stainless Steel	1 – 1,800 [a]	1	1.45×10^{6} [c]
Magnetic	Fair-Rite 75	5,000 [f]	~ 10^{5} [j]	0.3 [f]
	HyMu 80	5×10^{4} – 2×10^{5} [g]	1	1.72×10^{6} [g]
	Metglas 2714A	7.04×10^{5} [h]	1	7.04×10^{6} [h]
	MN60 (10 kHz, 22 ºC)	6,500 – 8,500 [i]	~ 10^{5} [j]	0.2 [i]
	MuMETAL	5×10^{4} – 3.5×10^{5} [j]	1	1.7×10^{6} [j]

[a] https://en.wikipedia.org/wiki/Permeability_(electromagnetism)
[b] https://en.wikipedia.org/wiki/Relative_permittivity
[c] https://en.wikipedia.org/wiki/Electrical_resistivity_and_conductivity
[d] International Telecommunications Union report ITU-R P.527-3
[e] http://www.thelen.us/1dielectric.php
[f] http://fair-rite.com/newfair/materials75.htm
[g] http://www.hightempmetals.com/techdata/hitempHymu80data.php
[h] http://www.metglas.com/products/magnetic_materials/2714A.asp
[i] http://www.cmi-ferrite.com/Materials/Datasheets/MnZn/MN60.pdf
[j] http://www.mu-metal.com/technical-data.html
[k] [Kazimierczuk 2014, Table 2.3; pg. 96]
[j] [Van Uitert 1956, Fig. 3 & Table I; Stadler et al. 2010; Huang et al. 2008c]

[a-j] accessed Sept. 14, 2015

Magnetic Material Permeability, Permittivity, and Conductivity

As mentioned in Chapter 1, there are various types of magnetic materials that are usable in an ESL. The desired core material for ESLs is an ideal "soft" magnetic material, which has a narrow "B-H" curve (see literature, e.g. [Kazimierczuk 2014]) such that the permeability is independent of frequency and magnetic field strength, and there is very little remanence. The permeability, permittivity, and conductivity will be expanded upon here as well as the consideration for lamination. Data and analysis will be given for Ceramic Magnetics, Inc. MN60 ferrite as it is used for measurements reported later. Note that the most common ferrites are ferrite (Fe_2O_3 iron oxide) compounds including manganese and zinc (MnZn) or nickel and zinc (NiZn); MN60 is a MnZn ferrite.

Permeability is generally presented as relative permeability, with both real $\mu_r' = \mu_i = \mu_{tor}$ and imaginary μ_r'', where μ_i is "initial" permeability and μ_{tor} is "toroid" permeability. It is important to note that these are a function of frequency and temperature. The imaginary permeability reflects magnetic losses (not electric, which also exist but are typically not given in data sheets). As an example, MN60's permeability vs. frequency is shown in Figure 2.1 showing specified ("spec") manufacturer data (after curve fitting) and nonlinear least mean square fit per analytical dispersion equation (presented previously). The MN60 ferrite samples were not measured before-hand for conformity to specification, but it should be noted that the relative permeability tolerance is approximately ± 25% which is generally true for all ferrites [NMG MN60; Kazimierczuk 2014]. Note that the effective permeabilities observed—resembled by μ_{ext} & μ_{int} herein for the relative, real, effective external and internal permeabilities, respectively—are discussed in a later chapter.

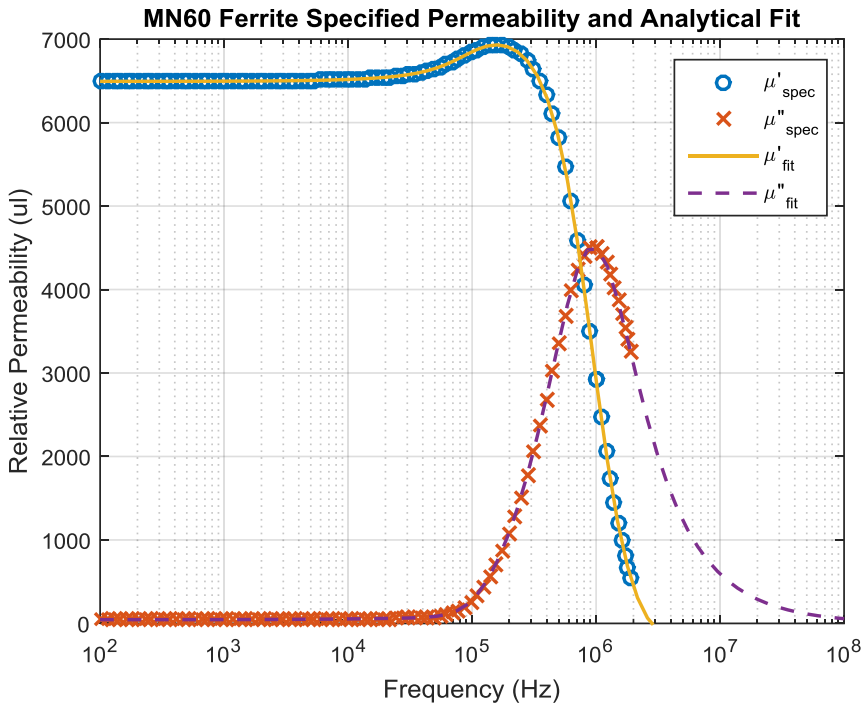

Figure 2.1 – MN60 Ferrite's Permeability (Real and Imaginary) vs. Frequency (Specified data from [http://www.cmi-ferrite.com/Materials/Datasheets/MnZn/MN60.pdf])

It is quickly noticed that manufacturer material data sheets for magnetic materials rarely include relative permittivity. Focusing specifically on ferrite, there are some available literature (see [Ferroxcube, pg. 13; Kazimierczuk 2014; Stadler et al. 2010; Van Uitert 1956; Abdeen 1999; Fiorillo et al. 2014; Pozar 2011, Appendix H; Kazimierczuk 2014; Balanis 2012]). Unfortunately, the given permittivity value can range significantly in literature. This is highlighted in empirical testing where Sullivan's results match the expected permittivity ($\approx 8.5 \cdot 10^4$ at 1.5 MHz) yet Ng used a static permittivity value of 10 vs. frequency, both using MN60 ferrite [Sullivan and Harris 2011, pg. 14; Ng 2004]. However, while Sullivan's measurement was simple and recommends further testing to validate, Ng's measurements poorly match his predictions (see [Ng 2004, Fig. 4]).

The confusion can be dispelled by approximating the ferrite as a leaky capacitor [Ferroxcube, pg. 13; Van Uitert 1956]. Such a model involves a resistor in parallel with a capacitor such that at low frequencies, the resistor has significantly less impedance and

will allow a relatively large current—therefore high permittivity—while at high frequencies the capacitor has less impedance than the resistor, approaching the "basic" permittivity [Cohen 2016]. Indeed, this phenomena is best seen in Figure 2.2 and Figure 2.3, clearly showing that general ferrites do asymptote to a relative permittivity of approximately 10. The DC resistivities listed in Figure 2.2 (ρ in right table) also generally uphold the leaky capacitor model, wherein higher resistivity (lower conductivity) implies the parallel resistor having an increased resistance, increasing the low-frequency permittivity and lowering the turnover frequency for which the capacitor dominates (that is, approaching a relative permittivity of ~10 sooner).

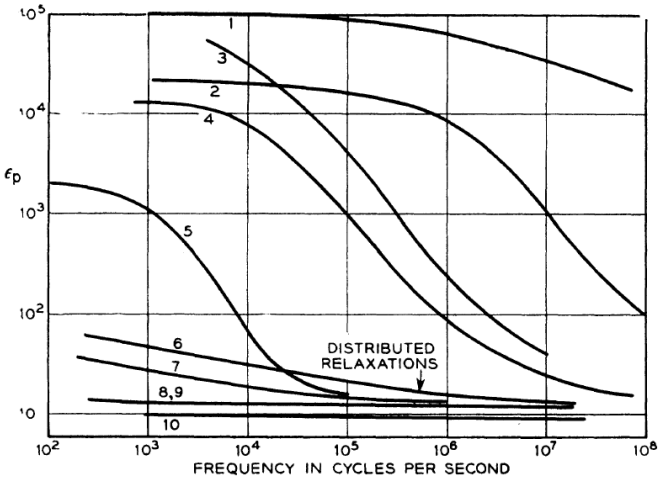

Fig. 3—Parallel dielectric constants as a function of frequency for ferrites listed in Table 1.

TABLE I

Fig. 3 No.	Ferrite	Ref.	$\rho 10^3$ Ω cm	$\rho(x)$ Ω cm	(x)
1	Mn-Zn	2	130	10	10^8
2	Ferramic B	13	2×10^6	80	10^8
3	Cu-Zn	8	1×10^8	400	10^7
4	Ferramic I	13	5×10^6	3×10^8	10^7
5	Ni-Zn	7	2×10^6	$5\times10^{6*}$	10^6
6	NM1350	14	8×10^5	1×10^5	10^7
7	N1250	14	6×10^6	4×10^5	10^7
8	NM1250	14	2×10^9	1×10^7	10^7
9	Crowloy BX113	13	6×10^8	3×10^6	10^7
10	Ferramic A	13	2×10^9	1×10^7	10^7

* Would be $\sim5\times10^4$ at 10^7 cps.

Figure 2.2 – Various Ferrites' Relative Permittivity vs. Frequency [Van Uitert 1956]

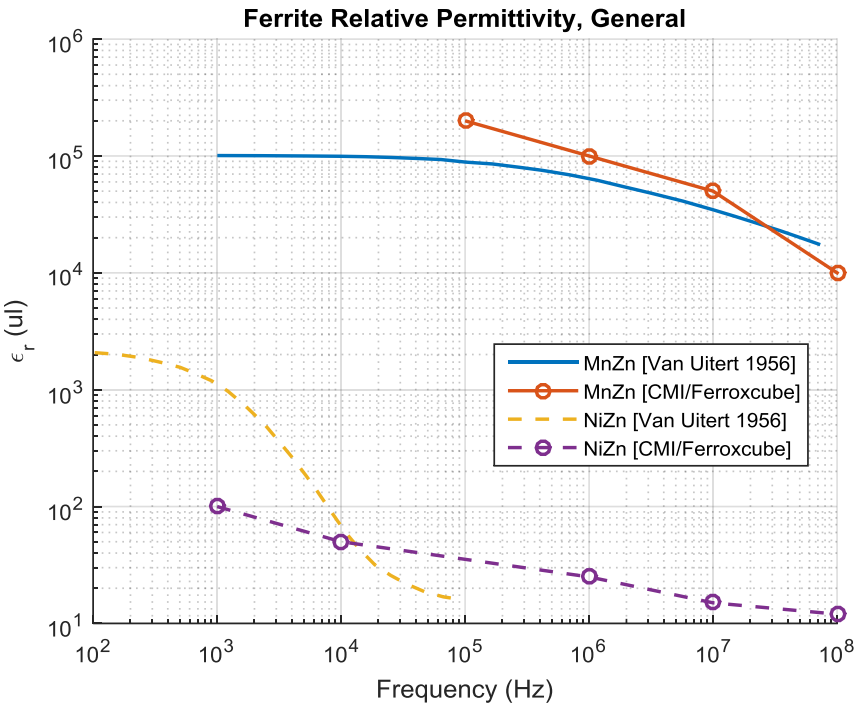

Figure 2.3 – MnZn and NiZn Ferrite Permittivity Values from Literature

Unfortunately, most literature focuses on lower frequencies, so it isn't clear exactly when MnZn and NiZn ferrites approach their high frequency upper permittivity limit of ~10. Continuing with the leaky capacitor model and noting that the resistivity of MnZn is 5 magnitude orders greater than for NiZn—even as a function of frequency—it can be assumed that the MnZn's turnover frequency is 5 magnitude orders above NiZn's [Ferroxcube, pg. 13; Van Uitert 1956, Fig. 3 & Table I; Cohen 2016]. Crudely extrapolating relative permittivities in Figure 2.3, it appears that NiZn approaches 10 around 1 GHz and MnZn (using the previous analysis) may approach 10 around 1 THz (10^{12} Hz). Analytical fitting using the leaky capacitor model and more data from literature could be attempted, but is unnecessary herein. Therefore, stating a static value for permittivity can be misleading.

Some comparisons of general magnetic materials' properties are presented in Figure 2.4 and Figure 2.5 (note low resolution as per sources). It can be seen that in

general, ferrites have low saturating magnetic flux densities and medium permeabilities as compared to other common types of materials, but can work at frequencies higher than 100 kilohertz (kHz)—especially nickel ferrites.

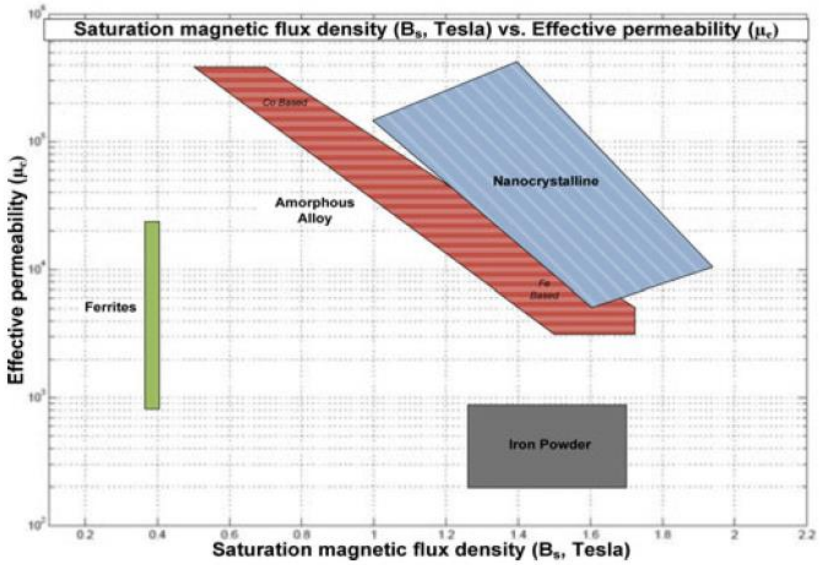

Figure 2.4 – Magnetic Materials' Initial Permeability vs. Saturation Flux Density [Roc'h and Leferink 2012, Fig. 3]

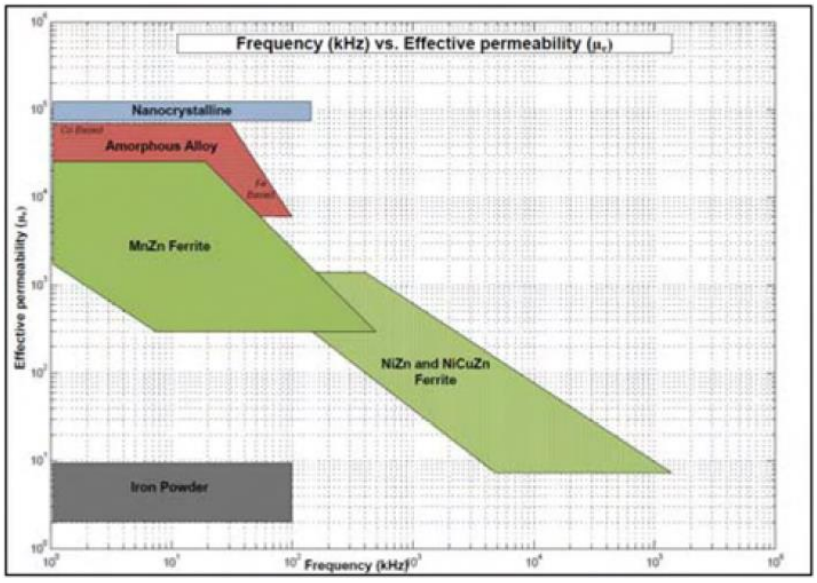

Figure 2.5 – Magnetic Materials' Initial Permeability vs. Frequency [Roc'h et al. 2009, Fig. 2]

It is worth considering core conductivity, which is typically measured at DC but can vary significantly vs. frequency [Fiorillo et al. 2014; Ferroxcube]. For ferrites, a particularly good (yet simple) model is to consider a core made up of grains separated by boundary layers as a grain resistance in series with a parallel resistor and capacitor representing the boundary layers, which matches empirical data "satisfactorily" (see Figure 2.6, dashed vs. solid lines) [Fiorillo et al. 2014; Fiorillo and Beatrice 2015]. Although not given directly, the resulting conductivity (or its reciprocal, resistivity) vs. frequency is found using the following equations in [Fiorillo and Beatrice 2015, eq. (1)]:

$$\frac{1}{\sigma} = \rho = s \times real\left(R_g + \frac{R_b - j\omega R_b^2 C_b}{1 + (\omega R_b C_b)^2}\right) \quad \Omega$$

where $R_g = \frac{\rho_g}{s}$ Ω; $R_b = \frac{\rho_b t_b}{s^2}$ Ω; $C_b = \frac{\varepsilon_0 \varepsilon_b s^2}{t_b}$ F; $s, t_b, \rho_g, \rho_b, \varepsilon_b$ – see reference.

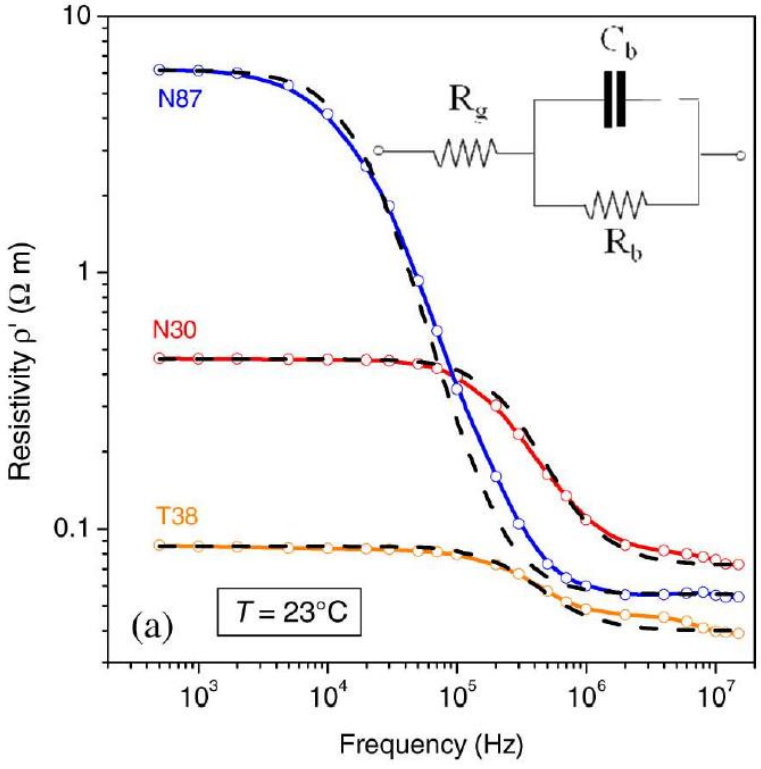

Figure 2.6 – Theoretical and Measured Ferrite Resistivity vs. Frequency [Fiorillo et al. 2014, Fig. 5a]

Noting the similarity in the parameters of MN60 ferrite with that of N87 ferrite used in literature, values were chosen to fit MN60 to a similar curve that has the appropriate low-frequency resistivity specification of 5 Ω-m [Fiorillo et al. 2014; Fiorillo and Beatrice 2015]. The resulting parameters are listed in Table 2.3 and the conductivity vs. frequency plotted in Figure 2.7, demonstrating a significant increase in conductivity between 10 kHz and 1 MHz. An increase in conductivity results in an increase of electric eddy current losses.

Table 2.3 – MN60 Ferrite Resistivity Fitted Parameters (Estimate, Room Temp.)

$s\ (\mu m)$	$t_b\ (nm)$	$\rho_g\ (\Omega m)$	$\rho_b\ (\Omega m)$	$\varepsilon_b\ (ul)$
15	0.6	$5 \cdot 10^{-2}$	$1.25 \cdot 10^{5}$	10

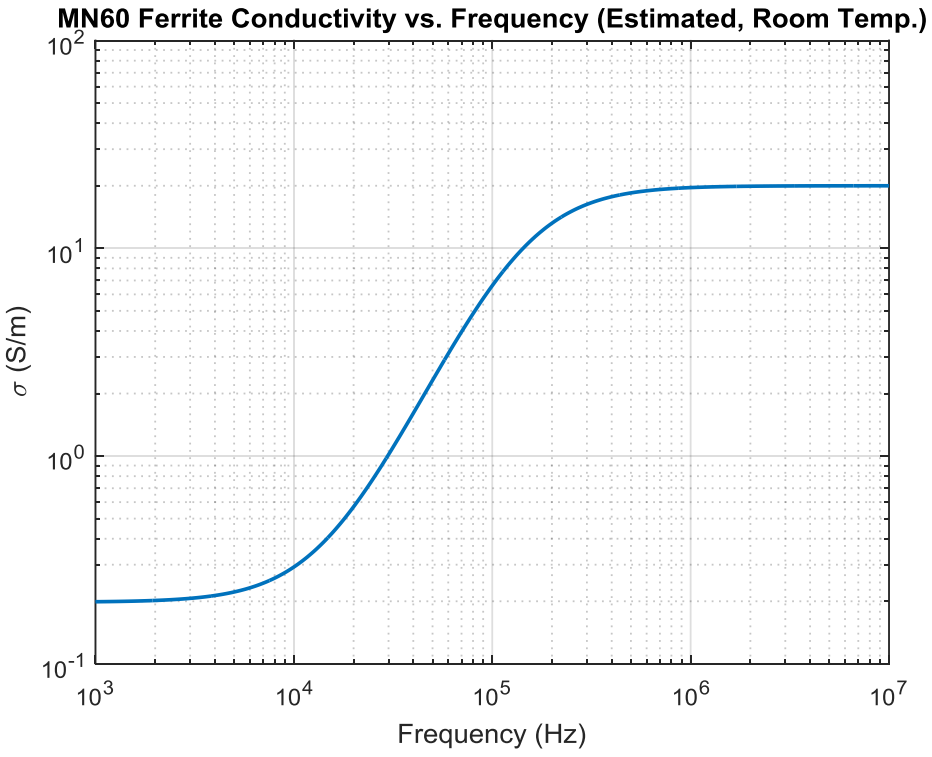

Figure 2.7 – MN60 Ferrite Conductivity vs. Frequency (Estimate, Room Temp.)

While room temperature is generally assumed, temperature effects should be considered for ferrite materials (and is typically included in material specifications) as it can significantly affect permeability, permittivity, and losses. This means that reception strength is a function of temperature, which can be less than ideal for measurements unless paired with proper temperature measurements and compensation in signal processing; it also means adjusting the temperature can be of significant advantage. Generally, as temperature increases: permeability increases (primarily at low frequencies), magnetic losses decrease at low frequencies but slightly increase at high frequencies, permittivity increases, and electric losses (conductivity) increase [Fiorillo et al. 2009; Abdeen 1999; Hamilton 2015; Stadler et al. 2010]. Note that permeability drops to zero around the Curie temperature. An example plot of ferrite permeability vs. frequency and temperature is shown in Figure 2.8.

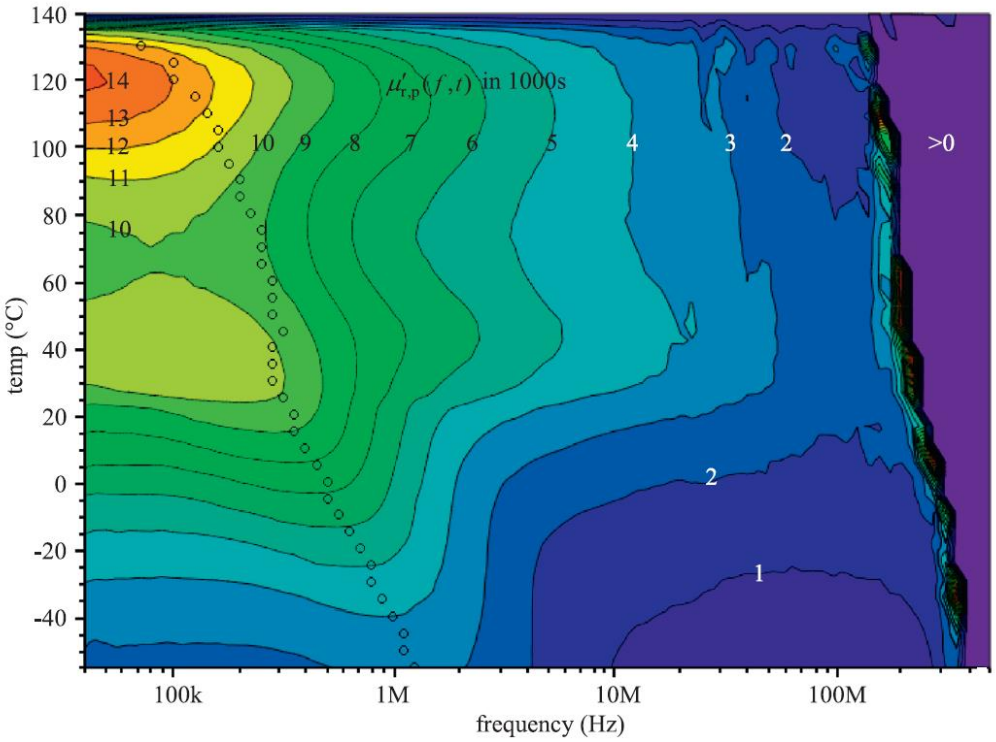

Figure 2.8 – T38 MnZn Ferrite Permeability vs. Frequency and Temperature [Hamilton 2015, Fig. 6]

Although ferrites are very commonly used, they are not the only viable material, with metallic thin-films (amorphous ribbons) being a relevant competitor, especially as research and literature increases on them [Fiorillo et al. 2010]. While metallic thin-films can have higher losses than ferrites, they can also have higher permeabilities—with proper laminations, they still can maintain higher permeability and actually have less losses than solid ferrite (whose eddy current losses, if significant, could also be decreased by lamination) at all frequencies [Fiorillo et al. 2010; Magni et al. 2012]. Although material and lamination costs may surpass that of ferrite for a typical application, metallic thin-films come with the advantages of higher heat dissipation and flexibility (and relatively insensitive to stresses) [Fiorillo et al. 2010; Fiorillo and Beatrice 2011]. The latter advantage can be huge, as ferrite antennas are heavy yet brittle, requiring extra weight for shock absorption and general robustness. Typical lamination insulation thickness is 0.015 mm [Kazimierczuk 2014, pg. 383].

Lamination of ferrites deserves some additional comments: while it can decrease eddy currents, it also affects permeability beyond that expected due to less permeability per volume (typically negligible). The effect upon permeability is two-fold and can be significant as found by one set of measurements: at low frequencies (e.g. kHz) the permeability is decreased due to lamination, but at high frequencies (e.g. MHz) the permeability can be increased [Zhu et al. 2000]. Later analysis revealed that displacement currents due to high apparent permittivity ($\varepsilon_r \approx 10^5$, e.g. MnZn ferrites) creates a magnetic field which is in-phase with the incident field at low frequencies, increasing the net magnetic field; core losses at high frequencies make the displacement current out-of-phase which decreases the net magnetic field [Zhang 2007]. This implies that permeability can be theoretically enhanced by inducing displacement current at frequencies of low loss [Zhang 2007]. Note also that if the core is thicker than its skin depth, laminations are advised—otherwise the supported magnetic fields are using less

than the whole core, decreasing the effective permeability [Kazimierczuk 2014]. One-dimensional analysis of field distribution in a core is worked out in [Kazimierczuk 2014, pg. 393-4].

As described in this section, the various properties of a magnetic materials can be significantly dependent on frequency, temperature, and external magnetic flux. This adds difficulty in evaluating them for broadband uses, and may require lamination to overcome eddy current losses. Further, there are a wide variety of materials with various properties, which makes it attractive to stick with the materials commonly used in similar applications. However, the proper choice of a material can be worth it to maximize performance.

Magnetic Material Resistive Losses

No realizable material is without loss, and that includes magnetic materials. In this section, the loss mechanisms in magnetic cores will be presented as well as analytical treatment as a series loss resistance. Some formulas will be given that are explicitly for magnetic-core rod ESLs, with validating measurements.

There are two primary loss mechanisms: hysteresis (internal resistance to magnetic re-alignment) and eddy currents (induced magnetic field that opposes the external field); a third loss mechanism is the Barkhausen effect (or flicker noise, excess noise) [Kazimierczuk 2014; Musmann and Afanassiev 2010]. One typical way to characterize material magnetic loss is to capture it as imaginary permeability as a function of frequency, which can also be presented as the magnetic loss tangent $\tan(\delta_m)$. Other methods include the Steinmetz equation (and corresponding coefficients) or first-order approximations [Kazimierczuk 2014].

For a magnetic-core loop, this intrinsic material loss can be used to calculate an effective series core loss resistance R_{core} as in the following formula. Perhaps counter-

intuitively, these losses are relative to the internal-field permeability, not external-field permeability [Smith 2007; Kazimierczuk 2014]. The inductance to use in the following equation is likely the coil external inductance and not the internal wire inductance, but the latter is typically negligible so it is a moot consideration. In general, our measurements validated the following formula [Kazimierczuk 2014, eq. (2.254)-(2.255)]:

$$R_{core} = R_{core,hys} + R_{core,eddy} + R_{core,Barkhausen} = \frac{\omega \mu'' L}{\mu'} = \omega L \tan(\delta_m) \quad \Omega$$

where $R_{core,hys}, R_{core,eddy}, \& R_{core,Barkhausen}$ are the core loss resistances due to hysteresis, eddy currents, and Barkhausen effects, respectively.

Note that some literature by Ted Simpson agrees, and some disagrees, with the above. In [Simpson and Zhu 2007; Simpson and Cahill 2007], they square a term within their equivalent μ_{int}, but their reasoning seems odd—they claim this correction is necessary because not all of the flux flows through the magnetic core, but this fact is already factored into inductance *L* (including their derivation). Simpson's preceding literature has it correct in [Simpson and Zhu 2006] and returns back to the correct formula in [Simpson 2008].

Antenna textbooks such as [Hansen and Collin 2011, eq. (3.53); Smith 2007, eq. (5-18)] present additional modifiers, seen after simplifying as:

$$R_{core} = \begin{cases} \dfrac{120\pi^2 k_{\lambda(?)} \mu_{int} \tan(\delta_m)\, n^2 r_{coil}^2}{l_{coil}} \approx \omega L \tan(\delta_m) \sqrt{\mu_{r(?)} \varepsilon_{r(?)}} \;\; [\![(?)\; Good\; dielectric]\!] \\ \dfrac{\omega \mu_0 \mu_r'' F_R n^2 A_{coil}}{l_{coil}} \left(\dfrac{\mu_{a,f}}{\mu_r'}\right)^2 \approx \omega L \tan(\delta_m) \left(\dfrac{\mu_{a,f}}{\mu_i}\right) \;\; [\![\mu_{int} \approx \mu_{a,f} F_R]\!] \end{cases} \quad \Omega$$

where the relative apparent fluxmetric permeability $\mu_{a,f}$ is presented in the following chapter and F_R can be found in [Smith 2007, Fig. 5-9].

Unfortunately, neither reference presents their derivation. Worse, the first reference (Hansen and Collin) does not clarify for which material the wave constant k_λ pertains to, but it seems unrealistic to be the magnetic core—for example, for MN60 ferrite $k_{\lambda,core} = \sqrt{\mu\varepsilon} \approx 2.5 \times 10^4$. It is intriguing that the second reference (Smith) has

the extra term $\mu_{a,f}$ (independent of a corresponding factor F_R) which represents the flux averaged at the center of the core regardless of the coil geometry (presented in the following chapter). Also, it can be confusing to see four different μ subscripts in one equation! However, empirical results herein validate the second by Smith, which proved to be more accurate than the general $\omega L \tan(\delta_m)$ for the case of ferrite rods.

For validation of the previous, see Figure 2.9 as an example for measurements on a ferrite prism versus theoretical. Various analytical approaches are given: Kazimierczuk's ($\omega L \tan \delta_m$), Smith's using the external permeability of the rod using solid-core axial demagnetization, a combination of Kazimierczuk's and Smith's, and Smith's using hollow-core axial demagnetization (the ferrite prism is 1x1" outside dimensions with 0.25x0.25" inside hollow dimensions). Measurements include the measured difference between two similar coils—one with MN60 for the core and one with wood (effectively air), wherein the difference should primarily be the core resistance (neglecting core effects upon wire impedance like proximity effect)—as well as net measured resistance (including wire). The theoretical compare decently to measured versus air-core, with Kazimierczuk's typically significantly over-estimating the core resistance. The comparison depends on the measured case—in a different ferrite core geometry (6"-long prism, same cross-section as above), Smith's approach matched very well, but another case (1"-diameter, 12"-long MN60 cylinder) is similar to that shown below. It should be reminded that a lot of assumptions go into analytical prediction (e.g. material general magnetic core loss, which was not measured as described previously). Also, error bounds were not put on "Meas. // Air-Core" but error would likely increase significantly as measured resistance approaches zero—subtraction of two small numbers, each with their own non-trivial error bounds.

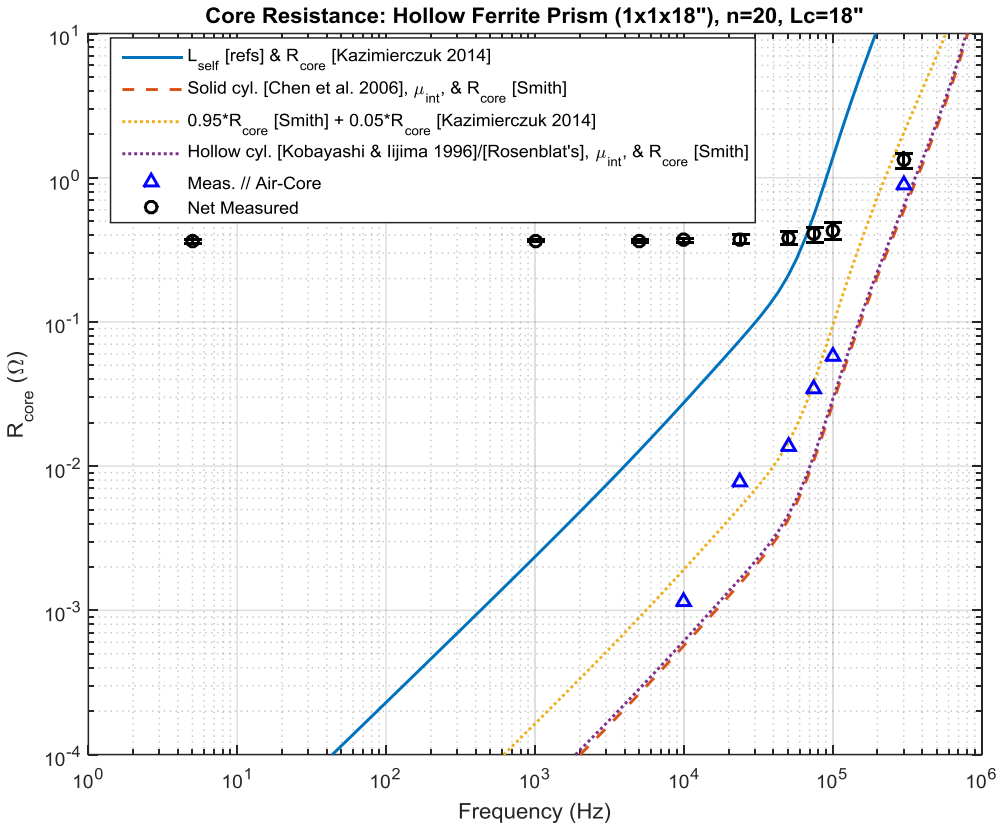

Figure 2.9 – Measured and Theoretical Magnetic Core Resistance vs. Frequency

As mentioned previously, the imaginary permeability contains several loss mechanisms. Hysteresis and eddy losses are relatively straight-forward to calculate, while the Barkhausen effect is due to micro-scale defects' magnetic domain hysteresis [Musmann and Afanassiev 2010]. Intuitively, Barkhausen noise is proportional to H_c and magnetostriction, and inversely proportional to μ_i and temperature [Musmann and Afanassiev 2010, 3.4 – 3.6]. Eddy loss can be reduced by dividing a core into laminations that are parallel to the flux direction and insulated from each other; this reduces the eddy current loss by the number of laminations, squared (assuming approximately equal permeable volume) [Kazimierczuk 2014, eq. (6.25)]. It should be noted that eddy currents can indeed be significant for ferrite cores with cross-section relatively electrically-large (as is likely the case for an antenna application) despite their

relatively-low conductivity [Fiorillo et al. 2014]. If not using measured imaginary permeability, the following equations from [Kazimierczuk 2014, eq. (2.77)-(2.78), (2.86), & (2.114)] can be used to estimate the core hysteresis and eddy losses:

$$R_{core,hys} \approx \frac{8\mu_0\mu_{int}fn^2A_{core}\sin(angle\ of\ B-H\ loop)}{MPL} \approx \frac{8\mu_0\mu_{int}fn^2A_{core}}{MPL}\ \ \Omega$$

$$R_{core,eddy} = \frac{\pi\sigma_{core}(\mu_0\mu_{int}nA_{core}f)^2}{2MPL}\ \ [\![\delta_{core} \gg r_{core}]\!]\ \Omega$$

where MPL is the magnetic path length of the circuit; σ_{core} is the conductivity of the core; and A_{core} is the area of the core. The Barkhausen noise is estimated as in [Musmann and Afanassiev 2010, 3.4 – 3.7]:

$$R_{core,Barkhausen} = \frac{\left(\omega n\mu_{int}A_{coil}B_{n,Barkhausen}\right)^2}{4k_BT\Delta f}\ \ \Omega$$

$$B_{n,Barkhausen} \approx \begin{cases} 7\times10^{-12} - 2\times10^{-9} & f < 1\ Hz \\ 3\times10^{-12} - 2\times10^{-9} & f \geq 1\ Hz \end{cases}\ T$$

where k_B is Boltzmann's constant; T is the temperature (in Kelvin); and Δf is the frequency bandwidth.

More rigorous measurement and analysis of losses can be performed, and exist in literature, which also include electric losses (e.g. [Sullivan 2013; Fiorillo et al. 2014; Huang and Zhang 2008; Brockman et al. 1950; Albach et al. 2007; Zaman et al. 1989]). It is clear from the literature that ferrite losses are complex and require careful measurements (and corrections) to extensively characterize ferrite losses.

Impedance Effects due to Surrounding Medium

When submersed in a medium other than free-space, the antenna's impedance will be affected—sometimes significantly so. When near a planar interface, the effect becomes a function of distance, but it will be assumed to be immersed in a semi-infinite medium here. The analytical treatment of impedance effects will be described here as

well as the use of various types of insulation in order to minimize these effects. The case of when loaded with a magnetic core is analyzed as is some controversy regarding radiation resistance in a medium.

Medium dissipation is modeled as a resistance loss due to conduction and displacement currents [Moore 1963]. In a good-conducting medium like seawater (at practical frequencies), displacement currents are negligible and can be ignored [Moore 1963]. These losses are typically modeled as an incremental change in impedance $\Delta Z = \Delta R + j\Delta X$ in addition (or in some literature, multiplied) to the antenna's free-space impedance Z_0; here, the added incremental resistance and reactance will be denoted R_{med} and X_{med}. In order to minimize this incremental change in impedance, which is desired, the loop should be thickly insulated—the greater the separation from the conducting medium, the less the effect upon impedance.

The four common insulation cases considered in literature are (in order of efficacy): thinly-insulated, thickly-insulated (e.g. toroidal), wedge insulation, and spherical insulating cavity [King and Smith 1981]. Wedge insulation has been explored experimentally, but not theoretically. For equations for bare, thinly- and thickly-insulated (toroidal), and spherical insulating cavity, see Table 2.4. Three of these insulations are visualized in Figure 2.10. A bare, un-insulated ESL immersed in a conducting medium differs significantly from the classic ESL and therefore is not worth pursuing here, but it will be referenced here for posterity. Interestingly, a simple method to estimate the impedance of a bare antenna in air to in a conducting medium is possible, using the ratio of medium properties [Deschamps 1962; Ancona 1978; Liao et al. 2012].

Table 2.4 – Equations for ESL's Resistance Due to Dissipative Medium

Description	Z_{med} ⟦ESL⟧ (Ω)	Reference
Bare	$= (1/Y)(\mu_{ext}n)^2 - R_{rad} - j\omega L_{self}$ Y, see reference R_{rad} − radiation resistance L_{self} − coil inductance	[Chen and King 1963, eq. (11)-(17); King et al. 1964; Smith 1976; King and Smith 1981]
Thinly-insulated, in a good conductor, low-accuracy	$= R_{med} + jX_{med}$ $R_{med} = \omega\mu_0 r_{coil}(\mu_{ext}n)^2\left[\frac{4}{3}(\beta_{med}r_{coil})^2 - \frac{\pi}{3}(\beta_{med}r_{coil})^3 + \frac{2\pi}{15}(\beta_{med}r_{coil})^5 - \cdots\right] - R_{rad}$ $X_{med} = \omega\mu_0 r_{coil}(\mu_{ext}n)^2\left[-\frac{\pi}{3}(\beta_{med}r_{coil})^3 + \frac{4}{15}(\beta_{med}r_{coil})^4 - \cdots\right]$ $\llbracket \sigma_{med} \gg \omega\varepsilon_0\varepsilon_{med}, d_{coil} \gg d_{wire}, F_{R,prox} \approx 0 \rrbracket$	[Kraichman 1962, eq. (7) & (15)]
Thinly-insulated, high-accuracy	$= (1/Y)(\mu_{ext}n)^2 - R_{rad} - j\omega L_{self}$ Y, see reference	[King and Smith 1981, eq. (5.10) on pg. 562]
Thickly-insulated, low-accuracy	$= Z(\mu_{ext}n)^2 - R_{rad} - j\omega L_{self}$ Z, see reference	[Galejs 1965, eq. (30)]
Spherical insulating cavity, low-accuracy	$= \frac{(\sigma_{med}+j\varepsilon_0\varepsilon_{med}\omega)}{6\pi r_{ins}}(\omega\mu_0\mu_{med}\mu_{ext}nA_{coil})^2\left[1 + \frac{9}{280}\left(\frac{r_{coil}}{r_{sphere}}\right)^4\right]$ $\llbracket \mu_{med} = \mu_{sphere}, \varepsilon_{sphere} = 1, d_{sphere} \ll \lambda_0, \lvert\gamma_{med}\rvert \gg \gamma_{sphere} \rrbracket$ $(r, d, \mu, \varepsilon, \gamma)_{sphere}$ − radius, diameter, relative permittivity, relative permeability, and propagation constant of the insulating sphere, respectively	[Wait and Spies 1964, eq. (10)]
Spherical insulating cavity, medium-accuracy	See reference $\llbracket \mu_{med} = \mu_{sphere}, \varepsilon_{sphere} = 1, d_{sphere} \ll \lambda_{sphere}, \lvert\gamma_{med}\rvert \gg \gamma_{sphere} \rrbracket$	[Wait and Spies 1964, eq. (9)]
Spherical insulating cavity, open-form	See references $\llbracket r_{sphere} \ll \lambda_{sphere} \rrbracket$	[King and Smith 1981, eq. (5.7) on pg. 598; Pavlov 1963; Wait 1957 and Wait and Spies 1964; Cruzan 1959; Row 1965]
Spherical insulating cavity, eccentrically-located in sphere	See reference	[An and Smith 1980]

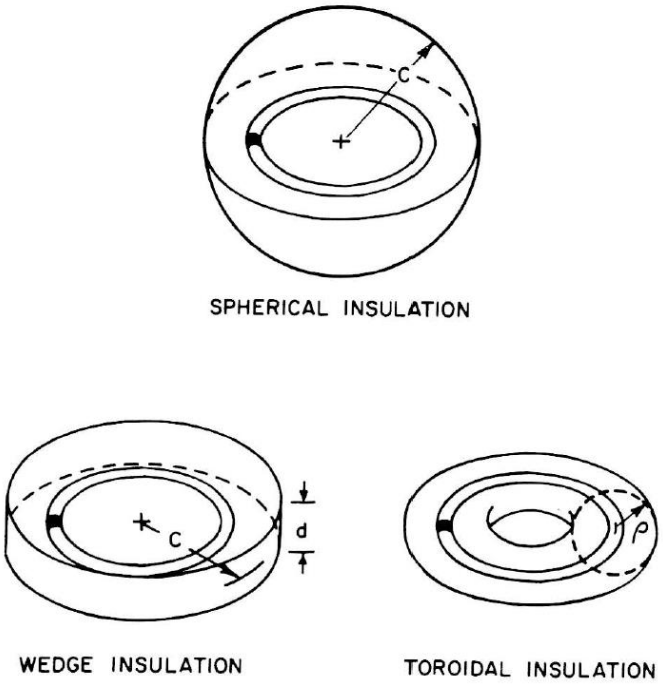

Figure 2.10 – Illustration of Various ESL Insulations
[King and Smith 1981, Fig. 10.1.1]

Thickly-insulated (toroidal), wedge, and spherical insulated cavity are compared graphically in Figure 2.11 with empirical data for all three (of equivalent minimum insulation thickness) in a simulated seawater medium and theoretical for the spherical cavity. Focusing on the electrically-small ("$k_1 b$" $\ll 1$) sub-plots, it can be seen that the insulation shape matters, noting that the reference only equalized the minimum insulation thickness ($d_{sphere} - d_{coil} = t_{wedge}/2 = d_{toroidal}$ where t_{wedge} is the wedge insulation thickness and $d_{toroidal}$ is the diameter of the toroidal insulation) and used the same coil [King and Smith 1981, pg. 602]. Examining the insulation by volume (with the additional knowledge that $r_{coil} = 0.9\, r_{sphere}$ and neglecting the coil wire volume), it is seen that the impedance effect is not linearly proportional to the volume of insulating material: the sphere is approximately 5.7 and the wedge 1.7 times more by insulation volume than the toroidal, but the relative differences in incremental resistance is approximately 1.7 and 1.3 times less, respectively. This shows that the toroidal

insulation is the most efficient by volume, which is intuitive as the fields radiate from the coil wire.

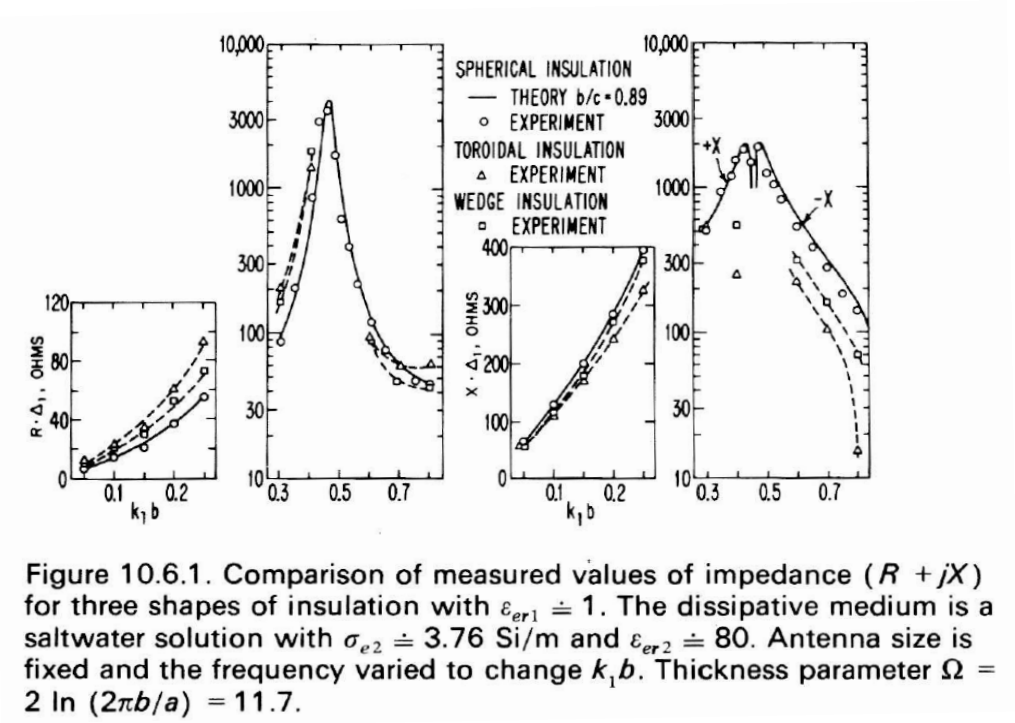

Figure 10.6.1. Comparison of measured values of impedance ($R + jX$) for three shapes of insulation with $\varepsilon_{er1} \doteq 1$. The dissipative medium is a saltwater solution with $\sigma_{e2} \doteq 3.76$ Si/m and $\varepsilon_{er2} \doteq 80$. Antenna size is fixed and the frequency varied to change $k_1 b$. Thickness parameter $\Omega = 2 \ln (2\pi b/a) = 11.7$.

Figure 2.11 – Impedance of an ESL Immersed in Seawater for Various Insulations [King and Smith 1981]

Less resistance is generally desirable, so increasing the insulation in general increases the mean distance to the lossy medium, decreasing loss. The reader is referred to [King and Smith 1981] for further analytical treatment of general antennas (including the ESL) immersed in matter, which includes rigorous analytical theory and comparing theory to measurements—the latter usually with good agreement, as is stated repeatedly for their ESL equations.

Many of the above references are explicitly for an ESL without a permeable core, and therefore do not include a μ_{ext}^2 term (they may also not include a n^2 term but readily mention how to include it). However, the presence of a spherical, permeable core inside

a loop within a spherical insulating cavity has been explored by various authors, notably [Cruzan 1959], [Pavlov 1963], [Williams 1965], and [King and Smith 1981]. From these, it becomes apparent that multiplication factors for the permeable core are approximately equal to that expected by the apparent permeability formula for a sphere (which is somewhat explored in [Pavlov 1963])—and since they assume a single, centered coil, the effective external permeability is equivalent—therefore the equations in Table 2.4 have been appropriately adjusted. In other words, these authors proved the effect of demagnetization from a different approach, for the specific case of a sphere.

In order to prove the apparent equivalency, consider the primary permeable-core factor $(1 + K_1)$ in the references (e.g. [King and Smith 1981, eq. (5.14) on pg. 601])—note that the other terms are negligible, as noted by the reference authors—which appears as a linear factor for magnetic dipole moment (and therefore effective height). This factor is squared for incremental impedance just as is μ_{ext}. The proof is:

$$(1 + K_1) = 1 + 2\frac{(\mu_i - 1)}{(\mu_i + 2)}\left(\frac{r_{core}}{r_{coil}}\right)^3 \quad [\![sphere, n = 1]\!]$$

$$\mu_i \gg 2 \;\&\; r_{core} \approx r_{coil} \rightarrow (1 + K_1) \approx 3$$

$$\mu_{ext\,\{sphere\}} \approx \mu_a = \frac{\mu_i}{1 + N(\mu_i - 1)}$$

$$\mu_i \gg 3 \;\&\; N_{\{sphere\}} = \frac{1}{3} \rightarrow \mu_{ext} \approx \mu_a \approx 3$$

$$\therefore (1 + K_1) \cong \mu_{ext}$$

where μ_a (relative apparent permeability) and N (demagnetization factor) are described in Chapter 4.

External resistance is comprised of radiation resistance (presented later) and dissipative resistance due to surrounding medium, though no literature to wit words it thusly nor distinctly separates the two, instead presenting $R_0 + \Delta R$ where $R_0 = R_{rad,air}$ since there are no dissipative losses in free-space. Separating the two is important for

analysis of transmitting or antenna gain as an increase in radiation resistance compared to other resistances means an increase in efficiency and antenna gain, but is purely academic otherwise. Since radiation resistance is not a function of the surrounding conducting medium if the antenna is insulated (see following chapter), any change in the external resistance would be dissipative loss. There are, however, some literature that claim the opposite (e.g. [Moore 1967, eq. (20); Hansen 1963, Table I; Jenkins et al. 2014, eq. (2)]) which might lead one to decrease insulation in an effort to increase the radiation resistance, all else being equal.

Further analysis into these statements shows them to be misleading. The statements by Moore and Jenkins et al. is likely due to their citing of [Kraichman 1962], wherein Kraichman derives the loop's external resistance (ignoring internal wire resistance), but he does not claim this to be the radiation resistance. Indeed, Kraichman then proceeds to give the "radiation resistance" for a loop in air and at the end of the paper, contrasts his incremental insulation resistance for a thinly-insulated ring $\Delta R_{med,ins(thin)}$ with Wait's for an insulated sphere $\Delta R_{med,ins(spher.)}$ concluding that thick spherical insulation compared to thinly-insulated "clearly shows the effectiveness of the spherical insulating cavity in reducing losses" (emphasis added) [Kraichman 1962, pg. 503]. Hansen's equation is a direct derivation from that of $\Delta R_{med,ins(spher.)}$ (with appropriate assumptions) in [Wait 1952; Wait 1957; Wait and Spies 1964], merely performing algebraic manipulation (e.g. $\eta_0/6\pi \approx 20$, where η_0 is the intrinsic impedance of free-space)—which is odd as Wait never describes $\Delta R_{med,ins(spher.)}$ as radiation resistance. Furthermore, Wait shows that an electrically-small insulating spherical cavity practically does not affect the far-field radiated field, but does significantly affect the power dissipated into the surrounding medium for a given current [Wait 1957, pg. 134-6]. It should also be obvious from the effective height equation (presented later) being independent of insulation.

The confusion over radiation resistance might be approached another way. The external resistance does directly relate to the power "supplied to the surrounding medium" which does count as "radiated"—although most of this energy dissipates in the near-field [Wait and Spies 1964, pg. 1250]. From a near-field perspective, this radiated power may be desirable. However, from a far-field perspective, the power dissipated into the near-field in the surrounding medium is a loss as it never reaches the far-field—thus decreasing the efficiency of the antenna. Therefore, the meaning of "radiation resistance" is not as clear-cut for non-free-space applications and depends on the application. For good analysis on the fields in- and out-side a spherical cavity, see [Wait 1952; Cruzan 1959; Pavlov 1963; Butler and Van Bladel 1964; Row 1965].

As has been shown, the impedance effects of a lossy surrounding medium can be mitigated with insulation. If the surrounding medium isn't very lossy, the change in impedance may be ignorable. We have also shown that the special case for a loop with a spherical magnetic core isn't actually special and can be generalized for any magnetic core. Finally, the controversy over what counts as radiation resistance in a medium has been discussed with the conclusion that the definition is a function of the application. The difficulty in analytically calculating the radiation resistance in a medium is discussed in the following chapter, as well as other radiation considerations.

CHAPTER 3

RADIATION CONSIDERATIONS

This chapter presents considerations for radiation such as radiation pattern, electromagnetic fields and currents, effective height and antenna gain, and shielding. Radiation pattern will be limited to the far-field.

Far-Field Radiation Pattern

Knowledge of the radiation pattern of an ESL is important for determining if it is an appropriate antenna for a given application as well as maximizing its alignment. In this section, the far-field pattern will be presented. In addition, the concept of null depth is introduced and considerations for radiation pattern in a lossy medium are included.

The ESL in free-space (vacuum) has the classic cosine, figure-eight far-field radiation pattern as illustrated in Figure 3.1. This radiation pattern is the corollary to an electrically-small (Hertzian) electric dipole, as the ESL is a magnetic dipole. An electrically-large loop antenna's far-field radiation pattern scallops similarly as its electric dipole cousin's, which is obviously undesirable for omni-directional antennas. If far-field criteria are not met, such as in near-field communications, a single-turn loop antenna is still well understood; multi-turn and/or ferrite-core loop antennas, however, are probably best analyzed by modeling software in the near-field.

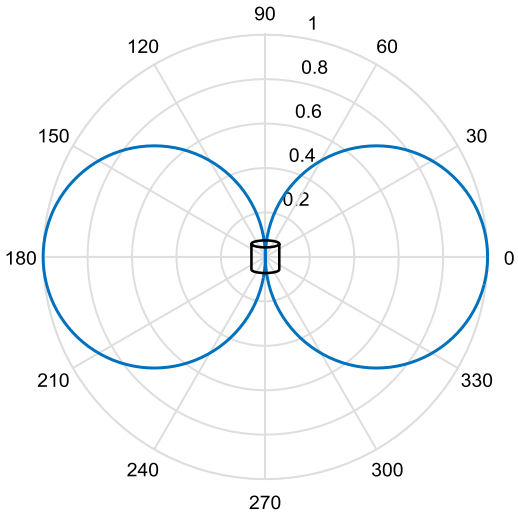

Figure 3.1 – ESL Far-Field Radiation Pattern vs. Incident Angle (Parallel H-Field)

Although not common, a coil can be wrapped such that each coil turn has no length parallel to the coil axis—making the coil non-helical—and each coil turn is connected by a straight run of wire parallel to the coil axis. This has the desired effect of maximizing a pure figure-eight pattern by minimizing the coil cross-sectional area not parallel to the coil axis, but at a cost of longer wire length (and therefore higher wire resistance) and increased construction complexity (probably not feasible to machine-wind). Such a coil can likely still be approximated by solenoidal equations, especially if using an equation that does not compensate for helicity. Since there is no pure figure-eight pattern in the real world, an ESL's null-depth may be quantified as the minimum signal received relative to the maximum versus aspect angle (i.e. azimuth for a horizontal rod). A "good" null depth is 30-40 dB (30 dB is "very common") while 60 dB is top-notch [Carr and Hippisley 2011, pg. 343].

An ESL in/near dissipative media may have a significantly different radiation pattern than in free-space unless both insulated and significantly immersed. The latter are assumed, as the bare ESL isn't typically desirable due to its significantly higher losses and change in radiation pattern, and operating close to an interface between media

significantly complicates the analysis. With the assumptions herein, a submerged ESL does have a far-field radiation pattern equivalent to that in free-space due to the uniform current distribution [King and Smith 1981, pg. 567 and Figure 9.5.5]. King and Smith point out that such is "valid for any electrically small structure that can be accurately represented by an elementary magnetic dipole in the dissipative medium ... [e.g.] a multi-turn loop, ferrite-loaded loop, or insulated loop ..." [King and Smith 1981, pg. 567].

Equations for electric and magnetic fields (near and far) as well as voltages and currents are readily available in the literature for ESLs in free-space or immersed in a medium (e.g. [Werner 1996 and correction; King and Smith 1981]). It should be noted that fields and currents are inter-related. Fields and currents are more difficult to derive for solenoidal coils, but these also exist in literature (e.g. [Conway 2001; Conway 2006]). An ESL's far-field is the same regardless of geometry, as long as ESL assumptions are met.

Effective Height, Antenna Gain, and Radiation Resistance

Low-frequency antennas are commonly characterized by effective (electrical) height h_e and high-frequency antennas by absolute antenna gain G_{abs}. Another property commonly described is radiation resistance R_{rad}. These definitions are defined and discussed here.

One reason effective height is useful is because a voltage generated by an incident vertical electric field (or horizontal magnetic field) is easy to measure. However, it is important to measure effective height into a high impedance (typically one mega-ohm) that approaches an open-circuit, as this is the very definition. The open-circuit voltage is defined as given by [Smith 2007, eq. (5-12), (5-16), & (5-23)]:

$$V_{oc} = j\omega\mu_{ext} n A_{coil} B_{med} \cos(\psi_i) \left[\sin(\theta_i) - j2\beta r_{coil} \cos(\phi_L)\right] \; V$$

where $\psi_i, \theta_i, \& \phi_L$ are defined in the reference. The effective height is then defined as [Smith 2007, eq. (5-13)]:

$$h_e \equiv \frac{V_{oc}}{E_{med}} \ \ m$$

Typically, an antenna's effective height focuses on the antenna's maximum performance and not the particulars of the incident angle and polarization of the magnetic field, therefore the sine and first cosine terms can be dropped. The last cosine term can be dropped for an ESL. Furthermore, although effective height is technically a function of the medium properties it is immersed in, it is typically calculated in air:

$$\left[air \rightarrow \omega B_{med} = \omega\left(\frac{\mu_0 E_{med}}{\eta_0}\right) = \beta_0 E_i\right] \rightarrow h_e = j\beta_0 \mu_{ext} n A_{coil} \cos(\psi_i) \sin(\theta_i) \ \ [\![ESL\ in\ air]\!] \ \ m$$

where β_0 is the phase constant of free-space. The maximum effective height is thusly:

$$\max(|h_e|) = \beta_0 \mu_{ext} n A_{coil} \ \ [\![ESL\ in\ air]\!] \ \ m$$

For a toroidal loop, the effective height needs to account for the orientation of the loop coil relative to the perpendicular magnetic field. If the coil turns are not coaxial (besides being offset laterally), then the radiation pattern is not a figure-eight and the distribution of the coil turns must be considered. Assuming a magnetic field incident on the center of a toroidal coil and a coil equally-spread out with normal vectors tangent to the toroid, the effective height should be multiplied by the following factor:

$$\int \overrightarrow{coil} \circ \vec{H}_{med} = \frac{1}{n}\sum_1^n \cos(\theta_n) = \frac{2}{n}\sum_1^{n/2} \cos(\theta_n) \approx \cos\left(\frac{\theta_{coil}}{\pi}\right)$$

$$[\![\theta_{coil} \leq \pi, turns\ not\ coaxial, coil\ evenly\ spread, centered\ vector\ \vec{H}_{med}]\!]$$

where $\theta_{coil} = \frac{2l_{coil}}{d_{core}}$ is the angular extent of the coil on the toroid (in radians). Note that the cosine summation can be replaced with an exact trigonometric identity. Therefore, a non-coaxial toroidal loop's maximum effective height is:

$$\max(|h_e|) \approx \beta_0 \mu_{ext} n A_{coil} \cos\left(\frac{\theta_{coil}}{\pi}\right) \ \ m$$

$$[\![toroidal\ ESL\ in\ air, \theta_{coil} \leq \pi, turns\ not\ coaxial, coil\ evenly\ spread]\!]$$

Effective height is also intuitive because vertical electric fields are typically the priority in far-field, low-frequency communications as the horizontal electrical field surface wave attenuates significantly faster. Since far-field electric and (corresponding perpendicular) magnetic fields are inter-related by the medium's intrinsic impedance η_{med}, it simplifies comparison to keep everything relative to the electric field; at first, this can seem like a confusing extra step for loop antenna calculations. Note that the term effective (electrical) length can be synonymous with effective height in literature or may refer to voltage generated by an incident horizontal electric field (or vertical magnetic field), so the reader must be diligent in confirming the context.

Radiation resistance R_{rad} is a fictitious, equivalent series resistance that models the electrical power transmitted or received by the antenna, and uses the electrical properties of its surrounding insulation [King and Smith 1981, pg. 598]. Typically, the surrounding electrical properties are assumed similar to free-space. For an ESL, it will almost always be negligible relative to other resistances, hence why it is difficult to directly measure. Note that some references (e.g. [Hansen and Collin 2011, eq. (3.52)]) simplify $\eta_0/6\pi = 19.9862 \approx 20$. Additionally, some literature will present radiation resistance for a single-turn, air-core ESL, but the factor $(\mu_{ext}n)^2$ scales for permeable core and/or multiple turns. The radiation resistance, as in [Kraichman 1962, eq. (8)], is:

$$R_{rad} = \frac{\eta_{ins}}{6\pi}\beta_{ins}^4(\mu_{ext}nA_{coil})^2 = \frac{\pi}{6v_{ins}^3}\omega^4\mu_0\mu_{ins}r_{coil}^4(\mu_{ext}n)^2 \quad [\![ESL, \sigma_{ins} \approx 0]\!] \quad \Omega$$

where $\eta_{ins}, \beta_{ins}, v_{ins}, \& \sigma_{ins}$ are the characteristic impedance, phase constant, velocity, and conductivity, respectively, of the insulation.

With all of the resistances known, the absolute gain of an antenna can be calculated. The antenna gain is classically defined as:

$$G_{abs} = 10\log_{10}(k_{rad}D) \quad dBi$$

where D is the antenna directivity and the radiation efficiency k_{rad} is defined as:

$$k_{rad} = \frac{R_{rad}}{R_{ant}} = \frac{R_{rad}}{R_{rad} + R_{cond} + R_{core} + R_{med}}$$

Note that the maximum directivity is 1.5 for an ESL.

Care must also be taken when attempting calculations that rely on assumptions only present in free-space conditions. For example, the traditional approach to deriving antenna radiation resistance is by "computation of the average flow of power through a sphere surrounding the antenna ... which works well in air for all sorts of antennas including short dipoles, [but] fails in a conducting medium because of dissipation in the 'induction field' and 'static field'" [Moore 1963]. Therefore, the resistance in a conducting medium will include resistance terms not seen in free-space, but the radiation resistance is the same as in air for an ESL assuming a non-magnetic medium.

As pointed out in [Hansen and Collin 2011], at low frequencies a magnetic antenna (e.g. loop) is sometimes considered to receive less external noise than an electrical antenna; this is because external electric fields generated in the neighboring near-/mid-field have not fully developed a complementing magnetic field. This is also true because low frequency external noise is typically from lightning and electrical storms. This is a disadvantage, obviously, if desiring to measure lightning activity with an ESL, though any complementing magnetic field generated will still likely be very strong due to minimal propagation loss and lightning E-field intensity.

Shielding

Shielding an ESL helps to maintain the ideal figure eight radiation pattern, which can be distorted by the ESL's non-negligible reception of the E-field and/or currents in the electromagnetic vicinity. There is a plethora of good literature on design and effects of shields. A concise introduction and application examples are given in [Smith 2007, §5.4] and more exposition (and examples) in [Lindsay and Münter 1983; Padhi 1965;

Carobbi et al. 2000; Libby 1946]. Commonly a shield will be a tube enclosing a coil, but shielded wire can be used for the coil (even multi-turn). Because the shield's purpose is to reduce E-field pick-up, it is commonly called electrostatic shielding.

Effective electrostatic shield design requires a conducting shield that is: electrically thick ($\gg \delta$) so the external fields only directly interact with the external shield; shield circumference electrically-short (overall shield diameter $d_{shield} \leq \frac{\pi\lambda_{med}}{2}$) to prevent shield current reversing phase [Libby 1946, pg. 642]; physical shield size D_{shield} electrically-small relative to the wavelength in the surrounding medium ($D_{shield} \ll \lambda_{med}$) [Padhi 1965, pg. 1000] likely so as to not cause a significant wave reflection; and has at least one slit (air gap) along the axis of magnetic flux [Padhi 1965; Carobbi and Bonci 2014; Smith 2007]. The inner shield and the loop/coil within form a non-radiating transmission line [Padhi 1965]. [Carobbi and Bonci 2014] point out that a shield "actively takes part to radiation" (whether transmitting or receiving) due to current induced on the inner shield surface; the current has a net magnitude of zero. In a receiving case, the current creates a magnetic field opposing the external field inside of the shield—which the loop is sensitive to. In other words, the inner shield is mutually coupled to the enclosed loop, engendering mutual coupling equations. This mutual coupling impacts a coil's impedance (both inductance and capacitance) because of mutual inductance and eddy-current effects [Massarini et al. 1996; Simpson 1999]; these effects are explored in a later chapter.

CHAPTER 4

EFFECTIVE PERMEABILITY

Magnetic core permeability realized in an application can vary distinctly from the given material properties. In this chapter, the concept of effective permeability is introduced. This is followed by a discussion of demagnetization, followed by discussion on flux distribution in a cylinder.

Introduction to Effective Permeability

Magnetic materials' stated permeability is typically confined to its real relative permeability ($\mu_r' = \mu_i = \mu_{tor}$) and imaginary relative permeability (μ_r''). However, more relative permeability terms abound in literature: apparent (μ_a), coil ($\mu_{coil} = \mu_{int}$), effective (μ_e, μ_{eff}), rod ($\mu_{rod} = \mu_{a,f\,\{rod\}}$), etc. It is not always apparent which is correct to use and when, or if it is accurately calculated. This section will introduce the concepts which will be further expanded upon in the following sections.

To better understand how a magnetic core affects magnetic fields and therefore the permeability exhibited in the application, first consider how a magnetic field may be generated. Generated magnetic fields (or flux, which is directly related) can be separated into two types: internal and external. Internal magnetic fields are practically generated at or inside a magnetic core, such as by a coil wrapped around the core. External magnetic fields are generated by external sources such as from a transmitting antenna. To be consistent with this approach and because disparate terms abound in literature, the effective internal and effective permeabilities realized will use μ_{int} and μ_{ext} respectively.

In a closed-path core such as a toroid, the internal fields from a coil tightly-wound on the core will create a complete circuit through the core and through the surrounding

air. The higher the core permeability, the more the fields stay internal to the core and do not "leak" out of the core through the surrounding air. Because closed-path (i.e. toroid) magnetic cores are easy to measure, have low leakage flux, and are commonly utilized in industry (e.g. transformers, inductors), material permeability is often measured with a toroid (hence why μ_{tor} is seen in some literature instead of the more common μ_r' & μ_i). In contrast, an open-path core (e.g. rod) made of the same material will not have the same field concentration due to higher leakage and will therefore have a realized permeability different than specified for the material. A non-permeable core ($\mu = \mu_0$) is obviously un-affected by geometry and application.

A different phenomena is of interest for external fields. In magnetic materials, internal magnetic dipole moments can oppose applied fields; this is known as magnetization M. This is why a material with very low initial permeability can have an effective permeability less than that of free-space. The net magnetic field H_{core} inside the magnetic core relative to the external field in the surrounding medium H_{med} is characterized by the demagnetization factor N and magnetization M [Chen et al. 1991]:

$$H_{core} = H_{med} - NM \;\; A/m$$

Therefore, the measured flux in the core B_{core} can be related to the external field by the effective external permeability [Chen et al. 1991]:

$$B_{core} = \mu_0\mu_i(H_{med} + M) = \mu_0\mu_{ext}H_{med} \;\; T$$

Commonly, the relative apparent permeability μ_a is seen in literature and used for both internal and external permeabilities; it will also be used herein. The effective internal and external permeabilities μ_{int}, μ_{ext} can be related to μ_a and depends on the specific derivation of μ_a as clarified in the following section. The apparent permeability is related to the demagnetization factor as in [Chen et al. 1991]:

$$\mu_a = \frac{\mu_i}{1 + N(\mu_i - 1)}$$

Parallel magnetic cores can negatively affect the flux in each other [Mel'nikov and Mel'nikova 1974]. This means that two identical magnetic-core ESL's in parallel will have a combined effective height between 1-2 times that of one alone. The cited authors' suggest the following approximation for two parallel rods:

$$\mu_{a,f\,\{1\}} = \mu_{a,f\,\{1\ alone\}}\left[1 - 0.5e^{(-5.6d/l_{core})}\right] \ [\![2\ identical\ rods]\!]$$

where $\mu_{a,f}$ is the relative apparent, fluxmetric permeability of the core (presented in next section) and d is the separation distance.

The effective permeability is also a function of incorporated air gaps. As stated in [Kazimierczuk 2014, pg. 52], material permeability has a typical tolerance of ±25% so high-accuracy magnetic devices will purposefully introduce air-gaps into a closed-path core to result in a more repeatable effective permeability. This is important to consider for some open-path cores as well, because larger or complex cores may be glued together. There is no high-permeability glue/adhesive [DeBonte and Butherus 1977], so glue gaps are effectively air gaps and should be minimized. If a core has a thin glue line, any deleterious effects can likely be assumed negligible. For a closed-path core, the air gap's effect on internal permeability can be modeled as suggested in [Kazimierczuk 2014, eq. (1.355)-(1.365) & (1.357)]:

$$\mu_{core} = \frac{\mu_i}{F_{gap}}$$

where $F_{gap} = 1 + \frac{\mu_i \Sigma(l_{gap})}{MPL}$. The magnetic path length MPL is discussed in [Clarke 2014] where it is shown for a toroid to be:

$$MPL \cong \frac{2\pi \ln(r_{core}/r_{hollow})}{1/r_{hollow} - 1/r_{core}} \ [\![toroid]\!]\ m$$

The following sections clarify how to calculate the demagnetization factor to attain the apparent permeability. From the apparent permeability, the effective permeabilities can be calculated.

Demagnetization Factor

The demagnetization factor N relates magnetic core geometry with the material's initial permeability as presented in the previous section. Demagnetization is commonly presented in one of three types: N_f is fluxmetric/ballistic/central, N_m is magnetometric, and N_{local} is local. Ellipsoids are a special case but their demagnetization factor N_{ell} is also commonly seen. This section will present and analyze demagnetization factors for some cases.

The demagnetization factors and applicable geometries are illustrated in Figure 4.1. N_f expresses the relative permeability at the middle of the core, while N_m is averaged across the whole core volume; in other words, N_f applies to coils centered on the magnetic core and N_m to coils encompassing the whole core length. N_{local} is that encompassing the local volume/area of interest, commonly seen for ring cores wound toroidally. For a coil that does not explicitly meet these cases, corrections and/or assumptions must be made or the coil should be modeled in software.

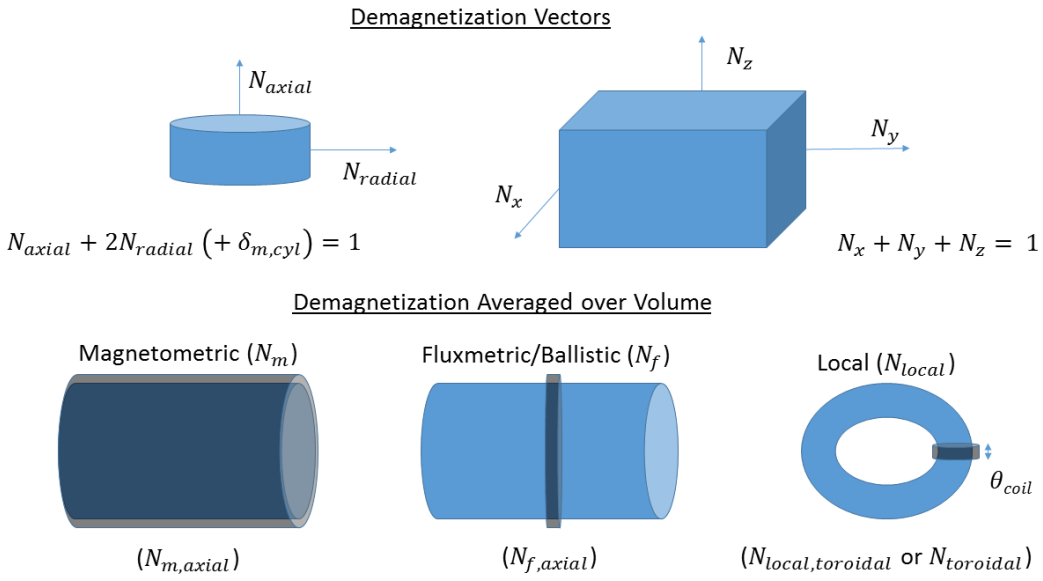

Figure 4.1 – Demagnetization Factors and Geometry

An excellent introduction into the science and history of demagnetization is available in [Chen et al. 1991]. It will also be noticed that literature by Chen have improved in accuracy such that some literature supersedes prior works (and noted so by Chen et al.)—a result of both computational capability and demagnetization theory having improved even in the last several decades. In Eastern European literature, the empirical work by Rosenblat (note that various English variants exist) from 1954 continues to be cited and modified, and whose general formula's "reliability has been proven in practice" [Matyuk and Osipov 2000].

The following equations express the demagnetization factors algebraically. Technically, the demagnetization will also be a function of the uniformity of the permeability of the material, but this can be generally assumed to be uniformly distributed. Interestingly, a magnetic core's perceived Curie temperature is a function of its demagnetization factor [Zverev et al. 2011]. The fluxmetric, magnetometric, and local demagnetization factors are defined such as in [Chen et al. 2006]:

$$N_f = \frac{H_{med}}{M\{core, middle\}} - \frac{1}{\mu_i - 1}$$

$$N_m = \frac{H_{med}}{M\{core, volume\}} - \frac{1}{\mu_i - 1}$$

$$N_{local} = \frac{H_{med}}{M\{core, local\ cross\ section\}} - \frac{1}{\mu_i - 1}$$

Calculating the realized effective external permeability depends on the coil distribution. Because these demagnetization factors are geometry-dependent and tedious to analyze, there usually isn't a simple, accurate formula to translate between fluxmetric and magnetometric in case a coil does not meet either criteria. There do exist some equations for rods and long prolate ellipsoids in the axial direction (presented in the following section), but are typically expressed starting from fluxmetric ($\mu_{a,f}$). However,

if the external flux distribution can be characterized by some factor F_{ext}, either $\mu_{a,f}$ or $\mu_{a,m}$ (magnetometric apparent permeability) can be used:

$$\mu_{ext} = \mu_{a,f} F_{ext,f} = \mu_{a,m} F_{ext,m} = \mu_{a,m} \frac{F_{ext,f}}{F_{ext,f}\{l_{coil} \to l_{core}\}}$$

For local toroid flux, the flux is assumed as the $\cos(\theta)$ model (see e.g. [De Graef and Beleggia 2006, eq. (1)]).

It is important to note that demagnetization N is commonly expressed as a scalar, but it is technically a tensor ($\widetilde{N}$) equal to one—note that some literature (e.g. [Bozorth and Chapin 1942; Osborn 1945]) set it equal to 4π, but it can be factored out. The reader must pay attention to the respective direction of demagnetization if N is given as a scalar as well as whether it is referring to fluxmetric/ballistic, magnetometric, or local. The demagnetization tensor is:

$$\widetilde{N} = N_x + N_y + N_z = N_{axial} + 2N_{radial} + \delta_{m,cyl} = 1$$

where $\delta_{m,cyl}$ is a correction factor for cylinders' N_m [Chen et al. 2001].

The above relationship shows that for objects with axial symmetry (e.g. cylinders, spheroids), it is easy to convert between N_{axial} and N_{radial} for N_f but an additional correction factor is necessary for N_m. This discrepancy is due to the influence of the surface upon volumetric demagnetization and is a function of length/diameter ratio [Chen et al. 2001]. For $N_{f,radial}$ there is, however, some discrepancy in the literature when comparing [Kobayashi et al. 1996] ($N_{radial} \to N_{axial}$) and [Chen et al. 2006] but the latter is likely more trustworthy due to higher accuracy—indeed, the latter includes extensive accuracy analysis while the former has little (and less precision).

Demagnetization has been explored empirically, analytically, and/or numerically for the following geometries: cube, sphere, ellipsoid, spheroid, cylinder (solid and hollow/ring), torus, oval ring (hollow rectangular prism), rectangular and equilateral triangular prism, and dumbbell; see Appendix A for equations and references for

ellipsoidal, fluxmetric, magnetometric, and local toroidal demagnetization factors. Note that [Chen et al. 2002] show that there is small difference ($\leq 3.5\%$) between N_f & N_m for a cylinder or square bar of equivalent cross-sectional area, so cylinders and square bars are practically equivalent. Chen et al.'s demagnetization factors for solid cylinders and prisms are recommended and well matched measurements (see Chapter 8).

The most common core shape for an ESL is a cylindrical rod, therefore it has been studied extensively. For a cylindrical rod, the apparent fluxmetric permeability has been graphically displayed for many decades based on [Bozorth and Chapin 1942] (and references within); see Figure 4.2. As can be seen, the apparent permeability can be significantly less than the material's initial permeability, and is a function of the rod's length and diameter. This implies that a material with moderate permeability properties can be practically equivalent to a material with very high permeability, depending on the core length/diameter ratio. Note that $\mu_{rod} = \mu_{a,f}$. Further, this means that even with a large material tolerance for permeability (e.g. ±25%), a rod's apparent permeability can effectively have a tight tolerance.

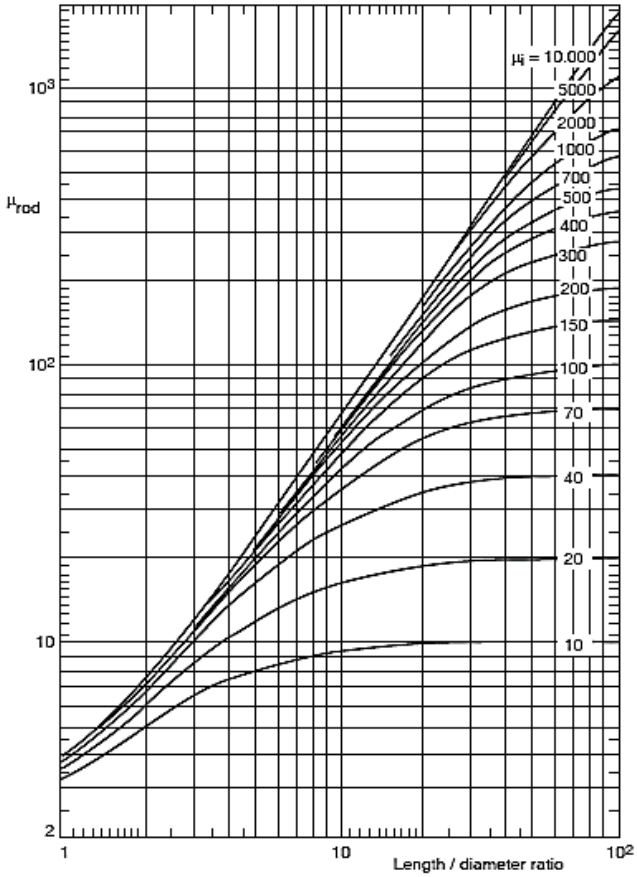

Rod permeability (μ_{rod}) as a function of length to diameter ratio with material permeability as a parameter

Figure 4.2 – Cylindrical Rod Apparent Fluxmetric Permeability [http://www.vkham.com/Info/ferro/mu-rod-1.png]

Unfortunately, the curves of Figure 4.2 are derived from data across various literature (primarily German) which are not tabulated in a single place but are reproduced in various literature, nor were any approximating formulas given in the early literature. Three later literature references present a useful formula to approximate the curves with varying accuracy and are reproduced in Table 4.1; there are additional formulations for extreme permeabilities listed in Appendix A. Note that of the first two (Poole and Pettengill et al.) the first is more accurate at low length/diameter ratios (<< 10), both are reasonably accurate at large length/diameter ratios (>> 10), but the first under-estimates while the second over-estimates at moderate ratios (~10)—so an averaging of the two

may be recommended for moderate ratios. Cross's is the most accurate without any limits to wit.

Table 4.1 – Cylindrical Rod Flux. Apparent Permeability Approximate Formulas

$\mu_{a,f}$ or N_f	Reference
$\mu_{a,f} \approx \frac{\mu_i\left[\left(l/d_{core}\right)^{5/3}+2.5\right]}{\mu_i+\left[\left(l/d_{core}\right)^{5/3}+2.5\right]}$	[Poole 2004, pg. 7]
$N_f \approx 0.37\left(l/d_{core}\right)^{-1.44} \quad [\![2 \le l/d_{core} < 20]\!]$	[Pettengill et al. 1977, eq. (11)]
$\mu_{a,f} \approx \frac{\mu_i}{1+N_{corr}k_{corr}(\mu_i-1)}$ $N_{corr} = \frac{N_{ell}}{1.2+\frac{0.05}{0.3+[\log_{10}(m)-0.7]^2}}$ $k_{corr} = \left(1+\left[\frac{m}{1.178769\,\mu_i^{5/7}}\right]^{4/3}\right)^{-1/2}$	[Cross 2007, spreadsheet]

Where l/d_{core} is the length/diameter ratio of the core and is symbolized variously in literature (e.g. m, λ).

Ellipsoidal magnetic cores have the unique property that the demagnetization factor does not depend on the choice of averaging—that is, $N_{f,ell} = N_{m,ell} = N_{ell}$—nor core permeability, assuming homogenous core material and uniform applied field [Chen et al. 1991]. This is because the "uniform applied field produces a magnetization and a demagnetizing field that are both uniform" [Chen et al. 1991, pg. 3610]. Comparing spheroids (symmetrical ellipsoids) to circular rod cores for very high initial permeabilities, the following is observed (see also Figure 4.3):

$$\begin{cases} N_{ell} > N_{m\,\{rod\}} > N_{f\,\{rod\}} & (l/d)_{core} < 10 \\ N_{m\,\{rod\}} \ge N_{ell} > N_{f\,\{rod\}} & 10 \le (l/d)_{core} \le 10^3 \\ N_{ell} \to N_{f\,\{rod\}} & (l/d)_{core} > 10^3 \end{cases}$$

$$[\![spheroidal\ ellipsoid, circ./square\ rod, \mu_i \to \infty]\!]$$

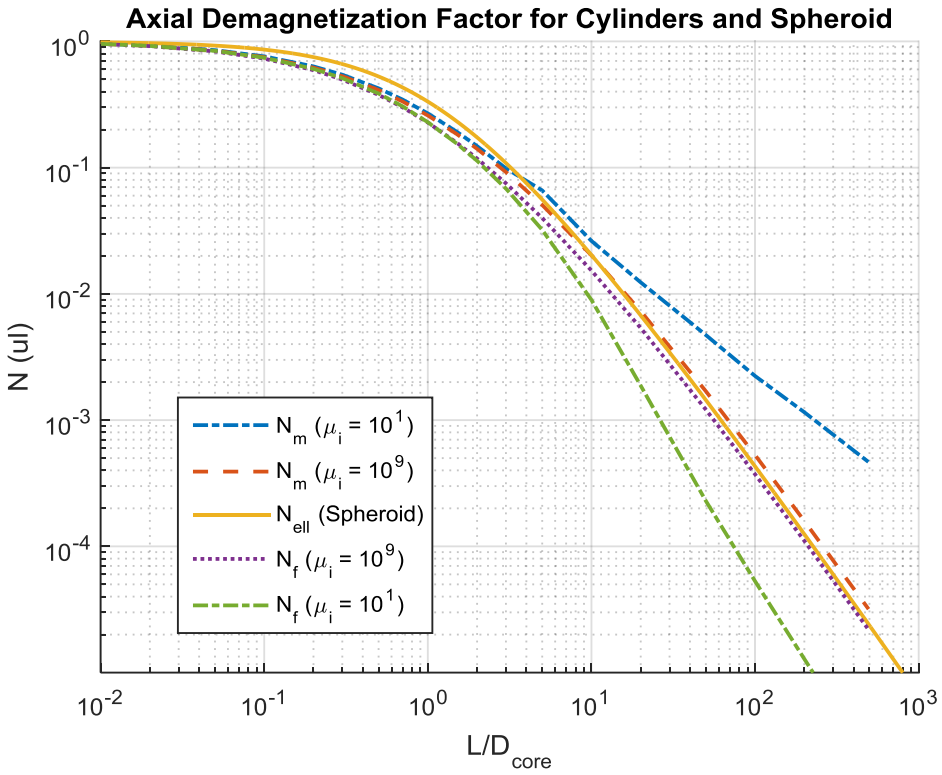

Figure 4.3 – Axial Demagnetization Factors for Cylinders and Spheroids

The above is important because closed-form analytical equations exist for spheroids, which can be conveniently used to reasonably estimate a rod (cylindrical or square) for very high permeabilities without resorting to a table or numerical computations. However, since excellent tables do exist by Chen et al. for cylindrical and rectangular rods as a function of shape and susceptibility, they should be utilized for more accuracy.

As if not complicated enough, non-ellipsoidal (i.e. prisms and cylinders) geometries' N can also be a function of the material's μ_i, which is has been explored in [Bozorth and Chapin 1942], [Chen et al. 2002], and [Chen et al. 2006]. Closed-form "exact" equations in literature for non-ellipsoidal geometries are typically either for $\mu_i \to 1$ $(\chi \to 0)$ or for $\mu_i/\chi \to \infty$; this is explored graphically in [Chen et al. 2002, figure 6]. Unless clearly stated, the reader can usually assume the demagnetization factor was

derived for $\mu_i \to 1$ ($\chi \to 0$) under "uniform magnetization" [Chen et al. 2001]. The case of $\mu_i \to 1$ ($\chi \to 0$) may appear nonsensical, but as mentioned previously, μ_a may not approach 1 as $\mu_i \to 1$. Materials with $\mu_i \to 1$ are: diamagnets, paramagnets, and saturated ferromagnets (whose permeability is then a "differential" permeability) [Prat-Camps et al. 2012].

In general, the dependence on μ_i cannot be considered a second-order concern unless $\mu_i \to 1 \; or \; \infty$ (and the appropriate equation/approximation for the demagnetization factor is used). For high-accuracy, the reader should consult the tabulated tables in the respective table in [Chen et. al 2001/2005/2006] or use approximate interpolation equations for a high length/area ratio in the direction of N [Chen et al. 2002].

The literature for hollow cores is lacking, but some exists for fluxmetric and local toroidal demagnetization of hollow cylinders. As summarized in [Matyuk et al. 2007] and [Sandomirskii 2008], various approaches have been proposed including estimating the hollow cylinder's demagnetization as the difference between that of two solid cylinders, of outer and inner radius respectively; some empirical validation is given in both (though Sandomirskii notes the inaccuracy of cited data). Many of the referenced literature are not readily available nor likely in English, and so have not been explored further here. Unfortunately, all of the hollow core analysis assumes $\mu_i \to \infty$ ("$\mu_i \gg 1$") with the exception of [Kobayashi and Iijima 1996]. The complicated integral formula given in [Matyuk et al. 2007] was not replicated here, but Rosenblat's formula is—which is analyzed by the former to be appropriate for $(l/d)_{core} \geq 7$. Note that [Sandomirskii 2008] may appear to be for fluxmetric demagnetization (using the term "central" which appears in Eastern European literature) but further scrutiny of the paper as well as comparing results reveals it to be for local toroidal demagnetization.

The results of some hollow cylinder approaches for axial, fluxmetric demagnetization are given in Figure 4.4 for three inner/outer core diameter ratios

(0.2/0.5/0.8, per [Kobayashi and Iijima 1996]) for infinite core permeability; solid core interpolations are included for comparison. Several conclusions can be drawn: thick cores ($ID/OD \leq 0.2$) are essentially the same as solid; demagnetization factor decreases noticeably as the core becomes thinner; and Rosenblat's formula appears reasonable for $(l/d)_{core} \geq 7$ and can be used to extend [Kobayashi and Iijima 1996] which ends at $(l/d)_{core} = 8$. Comparing the tables of [Kobayashi and Iijima 1996], it is noticed that there is little dependence on permeability for $\mu_i \gg 10$. For higher accuracy and applicability at high permeabilities, [Matyuk et al. 2007, eq. (19)] should be examined.

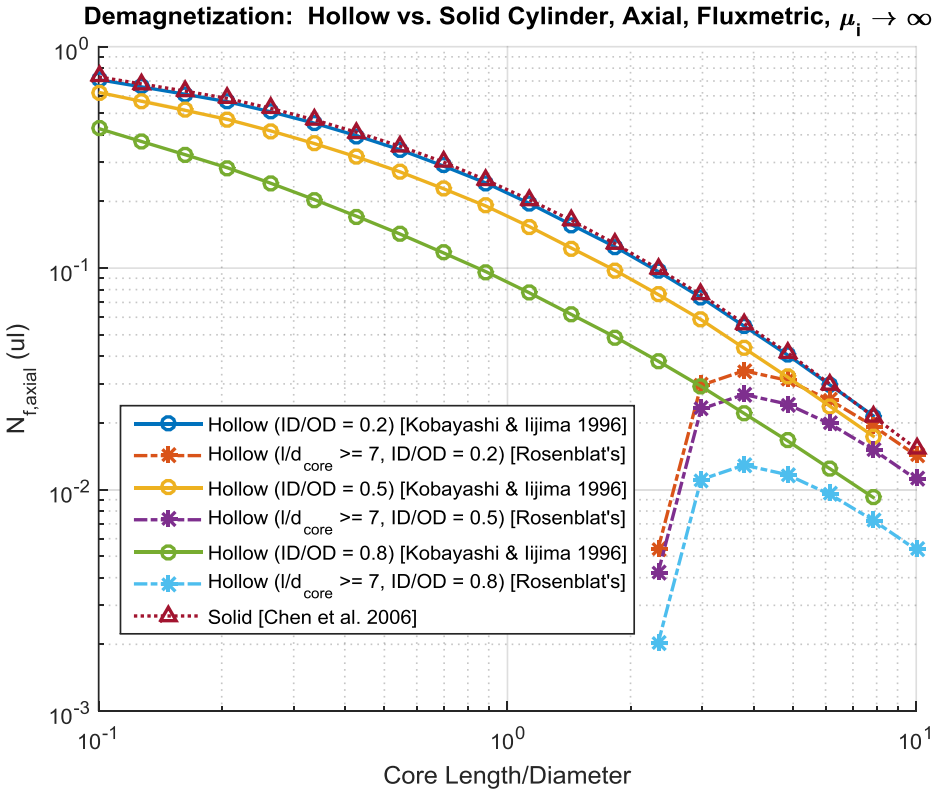

Figure 4.4 – Demagnetization Factor of Hollow Cylinders vs. Geometry

A geometry could be a larger hollow geometry with smaller magnetic cores distributed throughout. The demagnetization factor would then be that of the larger geometry multiplied by the aligned magnetic cores' surface area [Coillot et al. 2014, eq.

(11)]. For example, rods could form the edges of a cube as in Figure 4.5; in that case, the demagnetization factor would be as given by [Coillot et al. 2014, eq. (11)]:

$$N_{x,y,z} = \left(\frac{1}{3}\right)\frac{4A_{coil}}{l_{core}^2} \quad [\![orth.\ hollow\ cubic]\!]$$

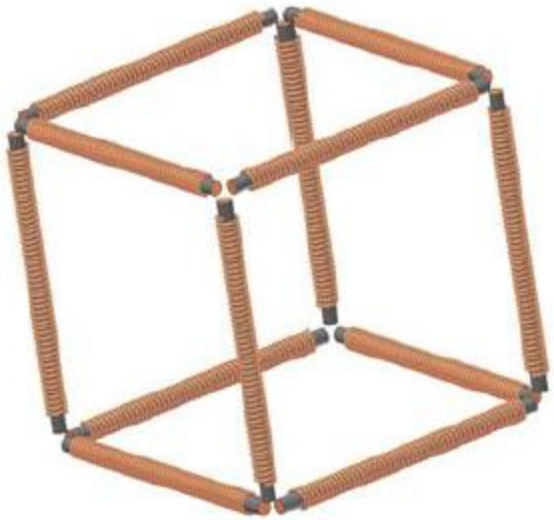

Figure 4.5 – Orthogonal Hollow Cubic ESL
[Coillot et al. 2014]

There has been considerable recent work into calculating the demagnetization factor with geometries at the scale of magnetic (nano-) particles. For example, randomly packed spherical particles [Bjork and Bahl 2013], assembly of identical particles [Martinez-Huerta et al. 2013], or chains of identical particles [Phatak et al. 2011]. They are all viable even at macro-scale, but [Phatak et al. 2011] is probably the most interesting: it derives the demagnetization factor for straight or curved chains of identical geometries (e.g. cube, sphere, cylinder) including separation gap. All of these articles are likely derived for uniform magnetization ($\mu_i \to 1$).

The vast amount of literature behind demagnetization belies the difficulty and importance in calculating it. However, once the demagnetization factor is known—or

reasonably estimated—the apparent permeability can be calculated. The following section focuses on cylinders to calculate effective permeability from apparent.

Flux Distribution in Cylinders

Continuing with the example of the rod, it is important to consider the non-uniform flux distribution across the length of the rod, hence effective permeabilities different than apparent (or "true" as in [Bozorth and Chapin 1942]). Therefore, in order to more accurately calculate the effective permeabilities that will be realized, more analysis is necessary. This section presents this analysis for cylinders for effective external permeability μ_{ext} (used for calculating effective height) and μ_{int} (for inductance and core loss). Different approaches found in literature are presented, discussed, and compared to our measurements.

Bozorth and Chapin show (referencing calculations and measurements by Würschmidt) that external flux distribution in a rod is "nearly parabolic" as $\mu_i \to \infty$, hence why first-order coil/core length ratio factors are quadratic. Indeed, the peak of the external flux is at the center of the core and decays parabolically such that the flux approaches zero just past the end of the core (therefore, a coil spanning the whole rod core will have a factor less than 1).

The approximate distribution of external flux density B_{ext} in a rod core fits the following form of [Bozorth and Chapin 1942, Fig. 3] for very high permeabilities:

$$\frac{B_{ext}}{B_{ext(max)}} \approx 1 - 0.85\left(\frac{2x}{l_{core}}\right)^2 \quad \left[\!\left[-\frac{l_{core}}{2} \le x \le \frac{l_{core}}{2}, cyl.rod, \mu_{a,f} \to \infty\right]\!\right]$$

Note that similar is found in other references: [Miron 2006, eq. (8.4)] has 0.9 instead of 0.85; [Mel'nikov and Mel'nikova 1974, eq. (4)] is similar; and [Macintyre 1999] gives constants bounded between 0.74 – 0.96 instead of 0.85.

In order to extend the external flux distribution to effective external permeability, the flux has to be integrated over the length of the coil. The following math integrates the above parabolic fit for a centered coil or a general case:

$$F_{ext,f} = \frac{1}{l_{coil}} \int_{x_{start}}^{x_{end}} \frac{B_{ext}}{B_{ext(max)}} dx$$

$$\approx \begin{cases} 1 - 0.28\left(\frac{l_{coil}}{l_{core}}\right)^2 & [\![centered\ coil]\!] \\ \frac{1}{l_{coil}}\left[\frac{1.13}{l_{core}^2}(x_{start}^3 - x_{end}^3) + x_{end} - x_{start}\right] & [\![general]\!] \end{cases}$$

$$\left[\!\left[-\frac{l_{core}}{2} \le x \le \frac{l_{core}}{2}, cyl.rod, \mu_{a,f} \to \infty\right]\!\right]$$

where x is the position along the core; x_{start} & x_{end} are the coil starting and ending positions along the core, respectively.

The flux distribution is no longer well-approximated by a simple parabolic fit as permeability decreases, such that a parabolic inflection point occurs closer to the end as $\mu_{a,f} \to 1$ [Bozorth and Chapin 1942]. Bozorth and Chapin suggest Stäblein and Schlechtweg's 1935 paper (see [Bozorth and Chapin 1942]) for a laborious approach to cylinder external flux distribution including as a function of permeability. Data from [Bozorth and Chapin 1942, Fig. 3-4] are plotted in Figure 4.6 including a referenced analytical fit by Würschmidt and parabolic fit by the authors (but the equation was not given) as well as the approximate parabolic fit $1 - 0.85(2x/l_{core})^2$. The authors used two rods of different initial permeabilities and a varying applied magnetic field to achieve varying apparent permeabilities, including saturating magnitudes; only data believed to be below saturation was included here as saturation can cause flux distribution phenomena of its own. While the simple parabolic fit does indeed do well for high apparent permeabilities, practical core geometries can have apparent permeabilities of several hundred or less, so the parabolic fit may not be as appropriate. As most coils are

close to fluxmetric or magnetometric, a more accurate flux distribution approximation including dependence on $\mu_{a,f}$ will not be attempted here.

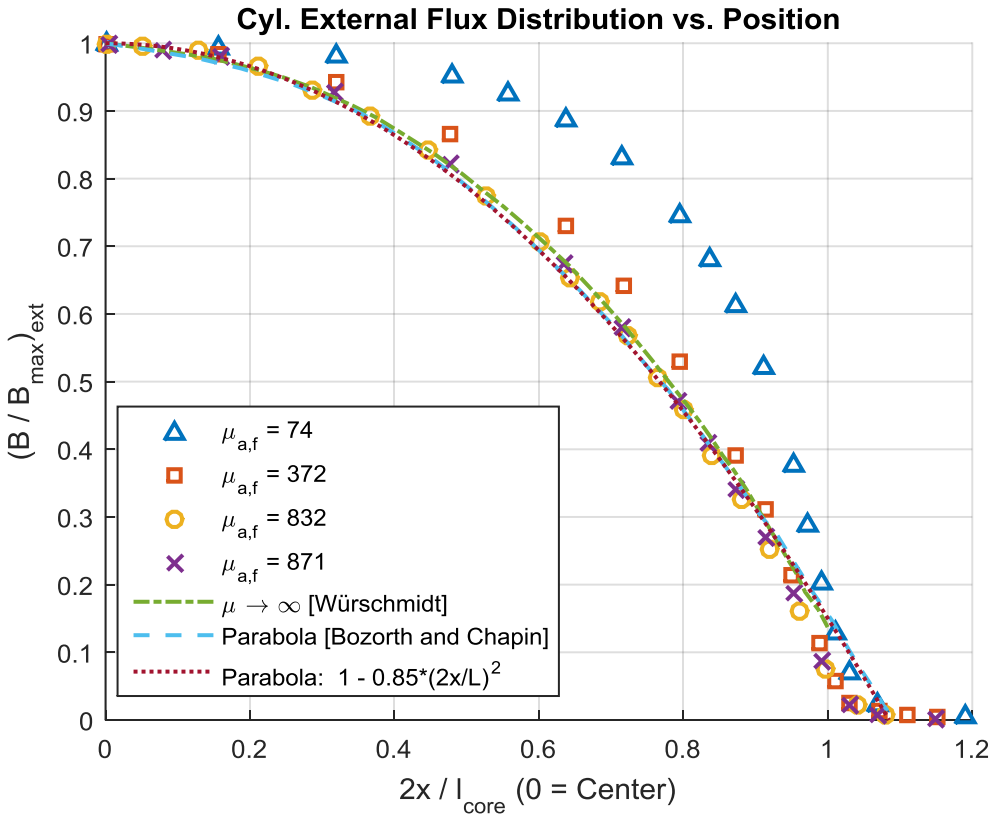

Figure 4.6 – Cylinder External Flux Distribution vs. Coil Position (Measured Data from [Bozorth and Chapin 1942])

The previous analytical approach for infinite initial permeability compares well to effective external permeability factors found in literature—listed in Table 4.2, which includes both internal and external flux factors. Note that a coil centered and evenly spaced on a magnetic core is assumed in literature—which is optimal for almost all applications—but [Maksimenko 1991] includes a factor for handling off-center coils. Further note that these approaches are all considered fluxmetric, and have to be manipulated before being applied to magnetometric computations. Note that [Hansen

and Collin 2011, pg. 108] mistakenly claims that the coil length has no significant ("critical") effect upon effective permeability—it most certainly can.

It is assumed that the coil is centered because this maximizes the flux (both internal and external) and greatly simplifies the analysis. Empirical data on varying the coil center can be found in [Stuart 1966, Fig. 5; Belrose 1955, Fig. 6]. With the goal of maximizing antenna sensitivity, Belrose concluded from measurements that centering the coil is still preferred [Belrose 1955, pg. 45].

There do exist direct formulas for $\mu_{ext/int}$ of prolate (both solid and hollow) and solid oblate spheroids, which can also be used to approximate a rod especially as $l_{core} \gg d_{core}$. Equations for spheroids' μ_{int} are listed in Table 4.3; spheroids' $\mu_{ext} = \mu_a$ (see previous section) use the equations listed in Table A.1. Note that Simpson et al. assume quasi-static conditions and a spheroid covered end-to-end by foil turns, thereby stating a limitation of $n > 7$ & $l_{coil} \rightarrow l_{core}$ but these limitations only apply to μ_{int}, not μ_{ext}. Indeed, calculations show that Wait's and Simpson and Zhu's μ_{ext} for a solid prolate spheroidal are equivalent, even though Wait assumes a short, centered coil while Simpson and Zhu assume a full-length coil. Oblate spheroidal equations were not reproduced or investigated herein, but are included for reference.

Table 4.2 – Cylindrical Rod Effective Permeability (Centered Coil, Axial)

μ_{int} (ul)	μ_{ext} (ul)	Reference
	$= \mu_{a,f} F$ $F = 1 - 0.28\left(\frac{l_{coil}}{l_{core}}\right)^2$ $[\![\mu_i \to \infty]\!]$	Integration of [Bozorth and Chapin 1942]
$= \mu_{a,f} F$ $F = \begin{cases} F_L & For\ L_{self} \\ F_R & For\ R_{core} \end{cases}$ $F_L = -0.79\left(\frac{l_{coil}}{l_{core}}\right)^2 + 1.40\left(\frac{l_{coil}}{l_{core}}\right) + 0.09$ $F_R = -0.54\left(\frac{l_{coil}}{l_{core}}\right)^2 + 1.09\left(\frac{l_{coil}}{l_{core}}\right) + 0.01$ (fit to curves)	$= \mu_{a,f} F_V$ $F_V = 1 - 0.21\left(\frac{l_{coil}}{l_{core}}\right)^2$ (fit to curve)	[Smith 2007, eq. (5-16)-(5-19) and Figure 5-9]
$= \left[1 + \left(\frac{d_{core}}{d_{coil}}\right)^2 (\mu_{a,f} F - 1)\right] \frac{l_{coil}}{l_{core}}$ $F = 1.9088 - 0.8672\left(\frac{l_{coil}}{l_{core}}\right) - 1.1217\left(\frac{l_{coil}}{l_{core}}\right)^2 + 0.8263\left(\frac{l_{coil}}{l_{core}}\right)^3$	$= 1 + \left(\frac{d_{core}}{d_{coil}}\right)^2 (F - 1)$ $F = \mu_{a,f}\left[1 - \frac{k}{3}\left(\frac{l_{coil}}{l_{core}}\right)^2\right]$ $0.74 \le k \le 0.96$	[Macintyre 1999, eq. (48.19), & (48.23)-(48.27)] Note: highlighted are our corrections to reference
$= \mu_{a,f} F$ $F = \left(\frac{l_{coil}}{l_{core}}\right)^{0.4}$		[Coillot et al. 2015, eq. (18)]
$= \mu_{a,f} F$ $F = \left(\frac{l_{coil}}{l_{core}}\right)^{0.6}$		[Yan et al. 2013, eq. (8)-(9), '-' typo]
	$= \mu_{a,f} F$ $F = 1 - 0.765\left(\frac{2\Delta x}{l_{coil}}\right)^2 - 0.255\left(\frac{l_{coil}}{l_{core}}\right)^2$ Δx is the displacement of the coil from center	[Maksimenko 1991, eq. (1)]
$= \left\{\left(2 + \frac{l_{core}}{d_{core}}\right)\left[1 - \frac{\left(1+\frac{150}{\mu_i}\right)\left(2+\frac{l_{core}}{d_{core}}\right)}{145}\right]^2\right\}\left\{1 + \left(\frac{l_{coil}}{l_{core}}\right)\left(\frac{l_{core}}{d_{core}}\right)^{3/4}\right\}$ $\left[\!\left[\frac{l_{core}}{d_{core}} \le 40, \frac{l_{coil}}{l_{core}} < 0.25\right]\!\right]$		[Poole 2004, pg. 22-23, with typos fixed according to accompanying spreadsheet]

Table 4.3 – Effective Internal Permeability Equations for Spheroids

Core Geometry	μ_{int} (ul)
Prolate spheroid, solid	$= \mu_i F \;\; [\![n > 7, l_{coil} \to l_{core}]\!]$ $F = \frac{aQ_1'(a)}{aQ_1'(a) - \mu_{int_i} Q_1(a)}$ $a = \frac{l_{core}}{\sqrt{l_{core}^2 - d_{core}^2}}$ [Simpson and Zhu 2006, eq. (12) & (23)] and [Wait 1953b, eq. (3)]
Prolate spheroid, hollow	$= FQ_1'(a) \;\; [\![n > 7, l_{coil} \to l_{core}]\!]$ $F = \frac{\mu_i[1 + GQ_1'(a)]}{\mu_i Q_1(a) + GQ_1'(a)Q_1(a)[\mu_i - 1] - aQ_1'(a)}$ $G = \frac{b[(\mu_i/\mu_{r\{hollow\}}) - 1]}{Q_1(b) - (\mu_i/\mu_{r\{hollow\}})bQ_1'(b)}$ $a = \frac{l_{core}}{\sqrt{l_{core}^2 - d_{core}^2}}$ $b = \sqrt{1 + \frac{d_{hollow}^2(a^2-1)}{d_{core}^2}}$ [Simpson 2008, eq. (2) & (13)] and [Wait 1953b, eq. (3)-(4)]
Oblate spheroid, solid	See [Simpson and Cahill 2007]

Where Q_v' is the derivative of the associated Legendre function Q_v (order zero, degree v).

To wit, there is only one magnetometric-based formula for effective permeability (seen in manufacturer literature) but the accuracy of which is dubious; also, it isn't clear if it is for μ_{int} or μ_{ext} and it blows up as $l_{coil} \to 0$ [Poole 2004, pg. 8]:

$$\mu_{int}, \mu_{ext} \approx \mu_a\{N_m\} \sqrt[3]{l_{core}/l_{coil}} \;\; [\![cyl.rod, not\ recommended]\!]$$

In the previous table, [Macintyre 1999] includes a volumetric factor for the size of the coil relative to the core: the effective permeability decreases as the coil gets larger than the rod, which is intuitive as the volume's permeability is now a ratio of magnetic core and air. However, this doesn't lower the net effective height, because the coil area is now larger. Normally, the coil is situated tightly on a solid core with a very high effective permeability—correction factors aren't necessary for that case as the core's diameter can be used as the effective coil diameter—but to be rigorous, an averaged volumetric permeability factor should be included (and that in [Macintyre 1999] ignored).

It should be noted for hollow cores that unless a volumetric factor is applied, the demagnetization factor is for the core alone (a fact overlooked in most references except [Prat-Camps et al. 2016]) except for the hollow spheroid apparent permeability by Wait and Simpson.

To a first order, averaging permeability over volume, ignoring geometry effects on field/flux distribution, and maintaining the list of assumptions (especially $\delta_{core} > (d_{core} - d_{hollow})$), the volumetric-averaged relative permeability μ_{vol} would be:

$$\mu_{vol} \approx \frac{1}{V}\sum\left(V_j \mu_j\right) \quad [\![V = volume]\!]$$

As the typical geometry is likely a hollow or solid rod (extruded in one dimension) or wound toroidally, this can be simplified as:

$$\mu_{vol} \approx \begin{cases} \frac{1}{r_{coil}^2}\left[(\mu r^2)_{hollow} + \mu_{int/ext}(r_{core}^2 - r_{hollow}^2) + \mu_{outer}(r_{coil}^2 - r_{core}^2)\right] & [\![rod]\!] \\ \frac{1}{\pi r_{coil}^2}\left[\mu_{int/ext} l_{core}(r_{core} - r_{hollow}) + \mu_{outer}\left(\pi r_{coil}^2 - l_{core}(r_{core} - r_{hollow})\right)\right] & [\![toroidal]\!] \end{cases}$$

Calculated permeabilities have been herein corrected thusly with μ_{hollow} & $\mu_{outer} = 1$. Volumetric averages should be performed for both external and internal permeability ($\mu_{vol,ext}, \mu_{vol,int}$) though measured data (see Chapter 8) suggests that while this is a decent approach for external, it is not for internal. The volumetric average can be significantly less than nominal, so it is important to consider it.

Some limiting cases of field/flux distribution can be considered, assuming the non-core materials' permeabilities to be that of free-space. In an infinitely-long core of infinite permeability and a coil wound tightly on the core, all of the magnetic flux is contained in the core (and parallel to the external field) and none in the inner hollow area nor outside the core (outer direction), resulting in the apparent permeability being that of the magnetic core's [Prat-Camps et al. 2012, pg. 3; Paul 2011, pg. 134]. That case is valid for both internal and external fields in the radial or axial direction. Another limiting case is for an infinitely-long core with zero permeability (perfect diamagnetic or ideal

superconductor) with an external field in the radial direction, in which the fields inside the hollow are likewise zero but the fields outside the core (outer direction) are nonzero and are proportional to $(R/r_{core})^2$ [Prat-Camps et al. 2012]. A third limiting case is toroidal loops (or transformers) tightly wound on a core of infinite permeability, whereupon the internal fields are wholly in the core and none outside (either direction). Otherwise, some fields (both internal and external) do exist outside the core (both inner and outer directions).

It is interesting to compare the rod effective internal permeability predictions in literature (Table 4.2) graphically; see Figure 4.7 below. As illustrated, the internal flux is approximately zero for very short coils (relative to the core length) due to the open-flux path, and approaches a value of 55-100% the apparent flux for a full-length coil. It is worth mentioning that [Smith 2007] appears to be the most vigorous relative to referencing measured data and isn't as overly-simplified as [Coillot et al. 2015; Yan et al. 2013] while [Macintyre 1999] gives the most complicated equation (without reference to its derivation). Measurements reported by [Stuart 1966], [Belrose 1955], and our measured data (see Chapter 8) have been added. The first two are calculated using the reported inductance values and using $\mu_{a,f}$ as interpolated from [Chen et al. 2006].

Our measured data is presented three times to implicate the difficulty in calculating relative to an equivalent air-core vice directly measuring against an equivalent air-core; all three used the measured apparent permeability which closely matched predicted according to [Chen et al. 2006]. The first (blue circles) divides the measured inductance by that predicted for an equivalent air-core using [Snow/Weaver] plus conductor inductance and estimated external inductance due to the wire leads. The second (orange square) and third (yellow triangle) neglect internal conductor and external leads' inductance, with the second ("L // Corr. Sol") still using [Snow/Weaver] and the third ("L // CS") instead using a current-sheet solenoid un-corrected for round-wire. The

latter is that indirectly recommended by [Smith 2007]. As can be seen, the measured data (ours and in literature) as well as literature predictions vary significantly and depend on the analytical derivation. According to our results discussed in Chapter 8, "Meas./Calc. L" (blue circles) is the most accurate.

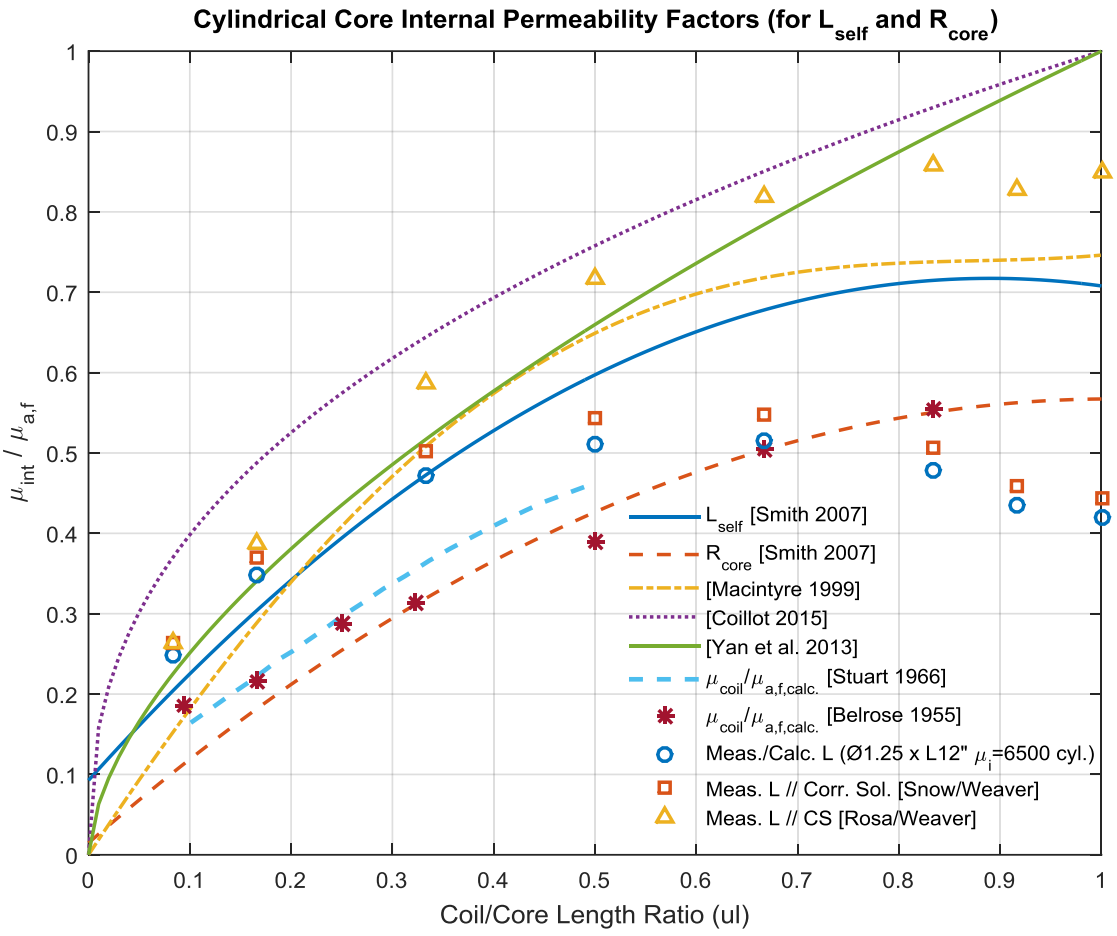

Figure 4.7 – Effective Internal Permeability vs. Coil Length (Cyl. Rod, Axial, Flux.)

Further analysis of the preceding measured vs. predicted is warranted. Smith's curve (for inductance) is based on an average of measured data, citing Snelling [Smith 2007, ref. 11]. Snelling reports (indirectly) that the factor $\mu_{int}/\mu_{a,f}$ is, as expected, a function of permeability and coil/core geometry [Snelling 1969, pg. 189]. However, he

does state that it is "very nearly independent" of $\mu_{a,f}$, "depends almost solely" on coil/core length ratio, and "within reason ... [does] not depend on the radial thickness of the winding." Yet he also recommends using the mean of his measured data vs. coil/core length ratio, which results in an "error ... less than about 12%" which is quite dramatic. This begs the question (which Snelling doesn't answer): where is the significant variance coming from? In an earlier section, Snelling does give curves for specific core geometries and permeabilities, but only gives a shaded band for the inductance factor. Therefore, this factor requires further research before accurate predictions can be made.

The external flux factor, seen in Figure 4.8, is the opposite: it starts as 100% the apparent flux for a very short coil—which it should, since that was how $\mu_{a,f}$ was calculated—and then approaches a value of 68-79% the apparent flux for a full-length coil. It is encouraging that the literature references are very similar, although only [Smith 2007] directly cites references with empirical results. At first, [Macintyre 1999] deviates significantly from the other formulas for both internal and external effective permeability; upon further review, the author made an integration mistake and the fix has been applied herein. Unfortunately, quality empirical data was scant in the literature for external permeability factor—for example, data may only foment 1st-order comparison (e.g. [Belrose 1955]) and/or under-reporting necessary parameters; data presented in [Bozorth and Chapin 1942] could be integrated to present an empirical factor for finite μ_i. Measured data (see Chapter 8) have been added and well match theoretical.

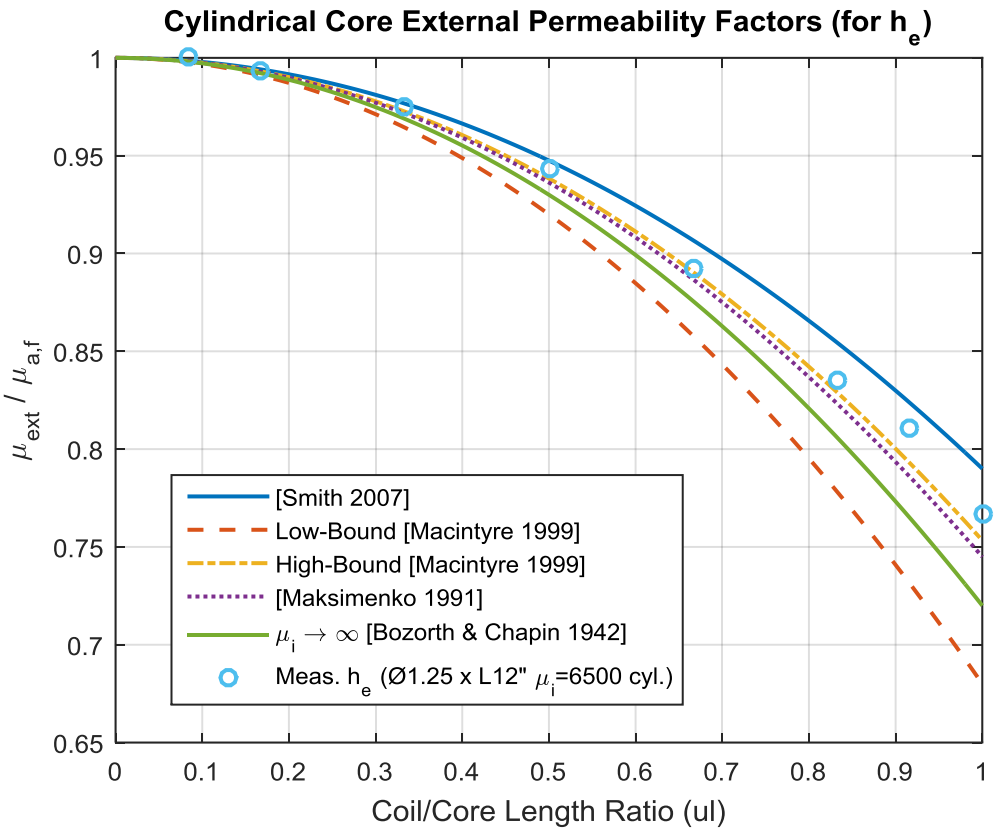

Figure 4.8 – Effective External Permeability vs. Coil Length (Cyl. Rod, Axial, Flux.)

Despite the lack of literature on flux distribution as a function of coil length, core geometry, and permeability, further analysis can be performed for the external permeability of rods. This is possible due to the extensive tables by Chen et al. for fluxmetric ($l_{coil}/l_{core} \to 0$) and magnetometric ($l_{coil}/l_{core} \to 1$) demagnetization for both cylindrical and rectangular rods. At the least, this allows the analysis of the external permeability factor as $\mu_{a,f} \leq \mu_{ext} \leq \mu_{a,m}$ as a function of coil/core length. Logarithmically interpolating numerical demagnetization factors from Chen et al. for cylindrical rods, the ratio $1 - \mu_{a,m}/\mu_{a,f}$ is plotted in Figure 4.9 (note: some manual smoothing added) for various initial permeabilities and length/diameter ratios.

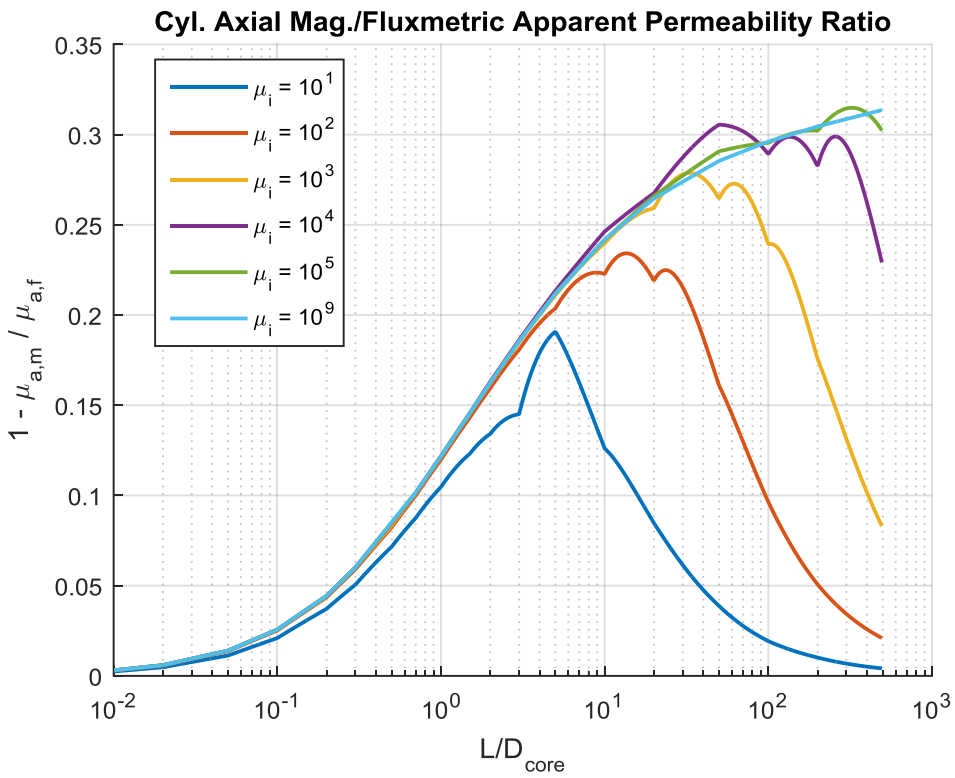

Figure 4.9 – Magneto-/Flux-metric Ratio vs. Core Geometry (Cyl. Rod, Axial) (Interpolated from [Chen et al. 2006])

Since the external permeability factors in literature correct for coil/core length ratio by utilizing a simple parabolic relationship of $1 - Constant(l_{coil}/l_{core})^2$ such that the constant is equal to approximately 0.2 – 0.3, it will be noticed that this constant is equal to $1 - \mu_{a,m}/\mu_{a,f} = k_{fm}$. These constants of 0.2 – 0.3 are reasonable for practical cores ($l/d_{core} \gg 1, \mu_i \gg 10$). The suggested external flux correction factor is the following, with no assumption on core geometry or permeability except a solid cylinder:

$$\mu_{ext} = \mu_{a,f} F_V \approx \mu_{a,f}\left[1 - \left(1 - \mu_{a,m}/\mu_{a,f}\right)\left(\frac{l_{coil}}{l_{core}}\right)^2\right] \quad [\![solid\ cyl., centered\ coil]\!]$$

A similar analysis cannot be extended to internal permeability, as demagnetization factor is calculated for applied uniform, external fields. There is still some relationship to demagnetization, and literature typically uses $\mu_{a,f}$—which is

directly derived from N_f—as a starting point for μ_{int}. Upon further thought, it would seem that a current-sheet correction (Lorenz/Nagaoka's correction factor k_L) using l_{core} in lieu of d_{coil} could be an intuitive first-order approach to handle coil length as a function of core length, as they both share the goal of characterizing the flux linkage of a solenoid. As can be seen in Figure 4.10, Smith's internal flux correction factors bound k_L, validating this as a reasonable first-order approach—but as discussed above, there is more work necessary to accurately predict this factor.

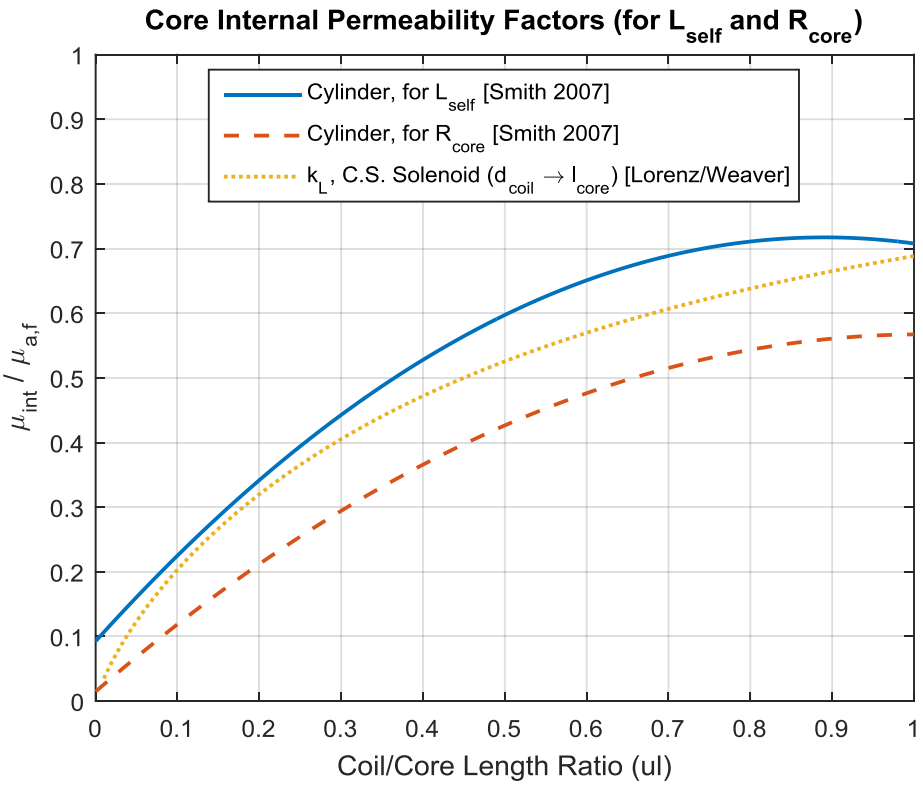

Figure 4.10 – Effective Internal Permeability and Mod. Current-Sheet Factor

There are other analytical and numerical approaches in literature, not to mention commercial computer modeling software. A reasonable analytical approach can be taken by treating a core as a spheroidal ellipsoid and evaluating the magnetic vector potential (see [Wait 1966; Islam 1963]). This approach has been also been used to evaluate a

hollow rod as a transmitter [Jordan et al. 2009]; their external flux results likely translate well to internal inductive flux. Yet another approach is by method of moments, such as a "qualitatively useful" spreadsheet program for ferrite cylinders' flux distribution (and other useful calculations and documentation) [Cross 2007]. There are also examples of numerical approaches that evaluate the magnetic vector potential of ferrite rods (e.g. [Giri and King 1978; Albach et al. 2007; Stadler 2011]). Stadler's "semi-numerical" calculations (and some validating measurements) for a ferrite rod's internal flux distribution are given in [Stadler 2011, Fig. 8 & 11]; they compare their numerical model to Finite Element Method (FEM) modeling, concluding excellent accuracy.

Due to the prevalence of cylindrical cores to ESLs, effective permeability analysis is well understood for cylinders with the caveat that some of the literature is overly-simplified (and has some errors). However, the internal effective permeability still requires further investigation to attain accurate, dependable predictions. External effective permeability predictions, though, can be accurate and dependable.

CHAPTER 5

SOLID AND LITZ WIRE IMPEDANCE

Three are four primary types of wire used: solid round, stranded round, foil, and Litz round. Square wires also exist, but aren't typically used due to relative cons such as cost. This chapter introduces the concepts of wire impedance and then presents sections for resistance and inductance. A section on lead wires is also given.

Wire Impedance Introduction

Wire conductor impedance is a function of the conductor's conductivity, the wire geometry (cross-section and nearby wire segments), and the operating frequency which causes skin and proximity eddy current effects. This section will introduce these effects, discuss common wire types, and give formulas for general use. Specific equations for wire resistance and inductance for differing geometries and applications will be given in the sub-sections with some measured data as validation.

Annealed copper is the typical conductor material utilized, but aluminum also has merits (discussed later). Note that conductivity is also a function of temperature, which is usually assumed to be approximately room temperature (20 ºC, 68 ºF); copper's dependence on temperature T (in degrees Celsius) is [Kazimierczuk 2014, eq. (3.5)]:

$$\sigma_{\{copper\}} = \frac{5.80 \times 10^7}{1 + 0.00393(T_{\circ C} - 20)} \ \ S/m$$

Electrical current with no alternating frequency—known as direct current (DC)—utilizes the whole cross-section of a wire. As the current alternates with some frequency, the current begins to favor the conductor surface due to the skin effect. The other alternating-current effect is called proximity effect, whereby adjacent current-carrying

conductors' fields interact with each other. See Figure 5.1 for an illustration of the skin and proximity effects upon the current distribution within a round conductor. Both of these factors are referred to as eddy current effects. They are shown to be orthogonal effects in [Kazimierczuk 2014] but this seems a simplification and are not considered orthogonal in other literature [Knight 2016a; Fraga et al. 1998].

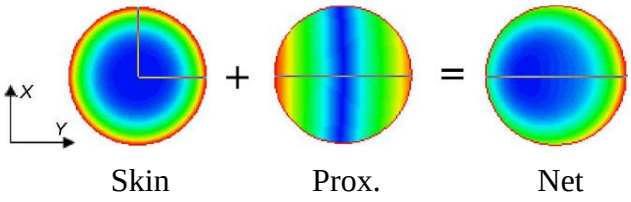

Figure 5.1 – Eddy Current Effects on Round Conductor (Adapted from [Zhang et al. 2011])

It should be noted that wire proximity effects are not uniform throughout a coil, with the ends turns being the lowest in an air-core [Knight 2016a]. Some proximity effect equations presented later have little (no) dependence on turn numbers, hence a factor k_{end} (added later where appropriate) can be utilized. This factor is a first-order approximation of the lesser proximity effects at the ends (specifically, the two ends receive half the effect when using a non-permeable core) [Knight 2016a; Medhurst 1947a]. This factor approaches unity quickly for turns $n \gg 1$.

Magnetic cores change the proximity effects due to the flux lines being drawn more through the magnetic core. For an illustration of this effect, see Figure 5.2. Turns nearest an air-gap of a magnetic core (e.g. ends of a ferrite rod) have the highest proximity effect as the magnetic field reaches its highest values there [Spang and Albach 2008; Sullivan and Zhang 2014]. In cases of many coil turns (e.g. inductor), this effect can be minimized by keeping the windings as far from the ends as possible such as by a trapezoidal geometry [Spang and Albach 2008]. These edge effects are further explored in [Dimitrakakis and Tatakis 2009].

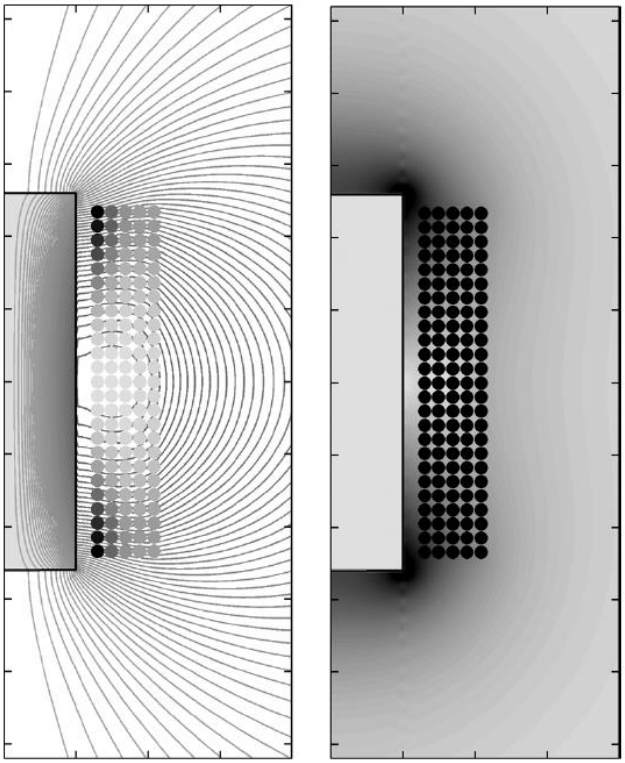

Fig. 2. (a) Magnetic flux lines of a coil with a rod core. The turns with higher proximity losses are drawn darker. (b) Absolute value of the magnetic field strength outside the core.

Figure 5.2 – Magnetic Flux and Proximity Loss Distribution of a Coil (Ferrite-Core) [Spang and Albach 2008]

The total impedance requires knowing the total wire length. Wire length can either be measured or calculated. The following formulas, taken from [Knight 2013a, eq. (5.1)-(5.2)], tended to accurately estimate the wire length:

$$l_{coil} = np \;\; m$$

$$l_{wire} = \sqrt{(n\pi d_{coil})^2 + l_{coil}^2} = n\pi d_{coil}/\cos(\psi) \;\; m$$

$$\psi = \tan^{-1}\left(\frac{l_{coil}}{n\pi d_{coil}}\right) = \tan^{-1}\left(\frac{p}{2\pi r_{coil}}\right) \;\; rad$$

For a tight coil, this simplifies to:

$$l_{wire} = n\pi d_{coil} \;\; [\![\psi \to 0 \; (tight \; coil)]\!] \;\; m$$

Solid round wire is relatively easy to analyze and has been exhaustively analyzed in literature. Stranded wire—that is, a cable of individual strands which are not insulated—is more difficult to analyze and is not treated much in literature. Because of the gaps between strands, stranded wire will have a resistance somewhere between solid and Litz due to partial eddy current suppression [Xu Tang and Sullivan 2003, pg. 289]. However, for small wires it should suffice to transform the stranded conductor into a round conductor of equivalent conductive area using the specified DC resistance to account for additional length due to twisting; this assumption was validated by our empirical measurements (see Chapter 8). Otherwise, rigorous analysis of stranded conductors in literature mostly pertains to helically-wound cabling used by the mains power industry (typically aluminum strands surrounding steel strands) [Morgan 2013].

Litz wire is commonly used to reduce alternating current (AC) resistance at low frequencies as compared to a solid, round wire of the same overall diameter. The cons are increased cost and soldering complexity as well as decreased window utilization (decreased conductor-to-insulator ratio). It reduces AC resistance by two physical effects: splitting the conductor into multiple, individually-insulated strands (which reduces the skin effect by increasing surface area) and twisting the strands (reducing the proximity effect)—both are necessary to suppress eddy currents, thus distinguishing Litz from simple stranded wire. There is a plethora of literature on analysis techniques and optimization approaches with compromises between complexity and accuracy, backed by empirical measurements; good summaries are found in [Barrios et al. 2015; Sullivan and Zhang 2014; Väisänen et al. 2013; Wojda and Kazimierczuk 2012].

Conductor Internal Resistance Equations

Solid wire of any geometry is typically described as a DC resistance R_{dc} modified by skin and proximity factors to attain the AC resistance R_{ac}:

$$R_{dc} = \frac{l_{wire}}{\sigma_{cond} A_{cond}} \quad [\![f \to 0]\!] \quad \Omega$$

$$R_{ac} = R_{dc} F_R = R_{dc}\left(F_{R,skin} + F_{R,prox}\right) \quad \Omega$$

where σ_{cond} is the conductivity of the conductor; A_{cond} is the cross-sectional area of the conductor (bare); F_R is an AC resistance factor; and $F_{R,skin}$ & $F_{R,prox}$ are skin and proximity factors, respectively.

The following sub-sections present equations for solid round and Litz wire. Foil analysis is not included here but exists in literature (e.g. [Kazimierczuk 2014]).

Solid Round Wire

Skin factors for round wire conductors are presented in Table B.1 and proximity factors in Table B.2. It is this author's recommendation for round wire skin factor to use Knight's "TEDML" analytical approach or use the exact equation (but check to ensure round-off error does not occur). For proximity factor, use Knight's modification of Medhurst's for air-core; for ferrite-core, Dowell's approach is tentatively recommended.

Proximity factor is more difficult to analyze due to it being a function of geometry. Dowell's method is referenced extensively, but its accuracy (and other classic equations') has been explored in [Dimitrakakis and Tatakis 2009] and in other works, with the conclusion that it is more accurate than Butterworth's and Ferreira's; [Xi Nan and Sullivan 2003] note that Dowell's can have errors upwards of 60%, and [Kazimierczuk 2014] notes that the accuracy is proportional to the number of layers n_l. [Shinagawa et al. 2009] show that magneto-plated wire can substantially reduce the proximity effect. Note that Dowell's method and its empirical derivatives require a high-permeability magnetic core with $\mu_{int} \to \infty$, which is approximately satisfied for $\mu_{int} \geq$

150 [Dimitrakakis and Tatakis 2009]. Further note that Butterworth's work is discussed in numerous works, but Medhurst concludes that Butterworth's proximity factor accuracy (and validity) can vary significantly [Medhurst 1947a]. Also note that [Kazimierczuk 2014] states multiple times that proximity factor can be neglected for single-layer coils—this may be approximately true for magnetic cores with permeability $\mu_{int} \to \infty$ (not simply μ_i) which is typically true for transformer geometries; it also assumes a tight coil.

As mentioned above, the factor k_{end} is recommended for air-cores (and is added to Table B.2 appropriately). Another recommended factor is for handling frequency dependency: Medhurst analyzed Butterworth's correction factor for frequency effects—estimating an accuracy of ± 2%—but noted that Butterworth's values were suspect so that data shouldn't be used [Medhurst 1947b]. Medhurst (and Butterworth's high-frequency values) assume a wire significantly thicker than skin depth [Medhurst 1947b]. Knight suggests his own correction factor for frequency and states that another person has validated it by experiment [Knight 2016a].

To validate the analytical models for round wire skin resistance, see Figure 5.3. Several analytical models are given and well match measured resistance for 40 inches (not precisely measured) of 26-gauge magnet wire. It can be noted that Rayleigh's begins to fail its assumptions at approximately 1 MHz and thereafter blows up, but the other references for skin factor are accurate across frequency.

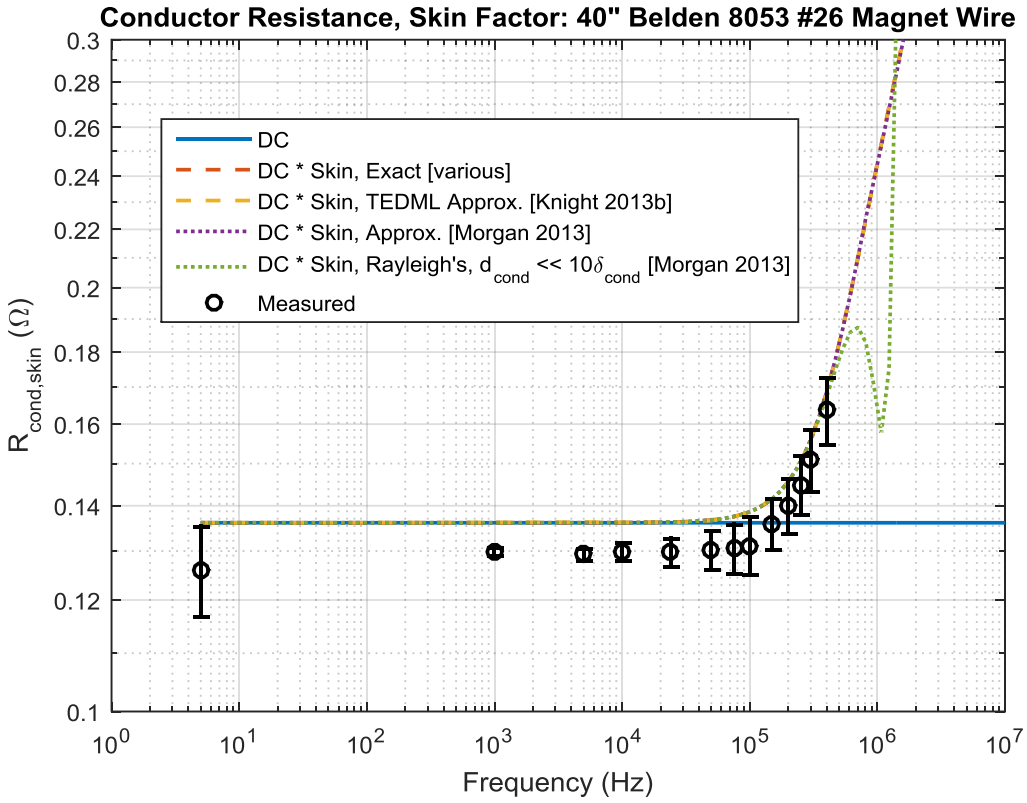

Figure 5.3 – Measured and Theoretical Round Wire Skin Resistance

Litz Wire

Litz wire DC resistance $R_{dc,Litz}$ is [Kazimierczuk 2014, eq. (5.372)]:

$$R_{dc,Litz} \approx \frac{4 n_{turn} d_{coil}}{n_{strand} \sigma_{cond} \pi d_{strand}^2} \approx \frac{R_{dc,strand}}{n_{strand}} \quad [\![minimal\ twisting]\!] \quad \Omega$$

$$R_{dc,strand} = \frac{l_{wire}}{\sigma_{cond} \pi r_{strand}^2} \quad \Omega$$

where n_{strand} is the total number of strands in the wire and r_{strand} & d_{strand} are the radius and diameter of a bare strand conductor, respectively.

Since Litz wire includes twisting to decrease eddy current effects, the length of conductor is longer than the wire's outer physical length implies. Two different approaches exist, the first found commonly by industry (e.g. [http://www.litz-wire.com/]) and the second analytical (e.g. [Xu Tang and Sullivan 2003, eq. (4)]). Note that bunching

and cabling operations occur as individual strands are bunched into a bundle, a group of which may be bundled again and/or cabled inside of the overall cable. The references' approaches are:

$$R_{dc,Litz} \approx \begin{cases} \frac{R_{dc,strand}}{n_{strand}} (1.015)^{n_{bunching}} (1.025)^{n_{cabling}} \\ \frac{R_{dc,strand}}{n_{strand}} \left(1 + \frac{\pi^2 n_{strand} d_{strand}^2}{4 K_a p_{twist}^2}\right) \end{cases} \quad \Omega$$

where the strand packing factor $K_a \approx 0.6$ [Hämäläinen et al. 2014, pg. 694]; $n_{bunching}$ & $n_{cabling}$ are the number of bunching and cabling operations, respectively; and p_{twist} is the pitch of the wire twisting.

A selection of analytical approaches are presented in Table B.3 and optimization approaches in Table 5.1 for Litz wire. It is difficult to separate which analytical equation is most accurate when, but appropriate assumptions and noted applicable ranges have been included where possible. Unfortunately, it is difficult to solder Litz wire without proper equipment (e.g. solder pot); measurements were not made here. It can be confidently stated that Dowell's method is hugely varying in its accuracy [Wojda and Kazimierczuk 2012] and that Bartoli et al.'s method is likely better than Dowell's when applicable ($\frac{r_{strand}}{p} < 0.04$) [Väisänen et al. 2013]. Otherwise, Dowell's, Tourkhani and Viarouge's, Bartoli et al.'s, and Sullivan's methods "lead to similar results" [Barrios et al. 2015]. The optimum Litz strand diameter is found when $F_R = 1.5 - 2$ [Kazimierczuk 2014; Sullivan 1999].

Table 5.1 – Litz Design Optimization Equations

<table>
<tr><th>Description</th><th>Optimization Equations</th><th>Reference</th></tr>
<tr><td>Dowell's method, multi-layer</td><td>$$d_{strand,opt} = \frac{3.10445\ \delta_{cond}}{\sqrt[4]{\eta^2(5n_l^2 n_{strand} - 1)}}\ m$$
$$[\![*, \mu_{int} \to \infty, \pm 60\%, 0.4 \le \eta \le 0.7, n_l \gg 1, A \le 2]\!]$$
$$A = \left(\frac{\pi}{4}\right)^{\frac{3}{4}} \frac{d_{strand}}{\delta_{cond}} \sqrt{\eta}$$
$$\eta = \frac{d_{strand}}{p_{strand}} = \frac{n_{strand}\pi d_{strand}^2}{\pi d_{wire}^2}$$
$$n_{strand,opt} = \frac{5n_l^2 + \sqrt{25n_l^4 - \frac{371.538}{\eta^2}\left(\frac{\delta_{cond}}{d_{strand}}\right)^4}}{\frac{185.769}{\eta^2}\left(\frac{\delta_{cond}}{d_{strand}}\right)^4}$$</td><td>[Kazimierczuk 2014, eq. (5.388) & (5.392)] or [Wojda and Kazimierczuk 2012, eq. (24) & (27)]</td></tr>
<tr><td>Tourkhani and Viarouge's method</td><td>$$d_{strand,opt} = \frac{3.0393\ \delta_{cond}}{\sqrt[4]{1 + \frac{\pi^2 n_{strand}\beta}{4}\left(16n_l^2 - 1 + \frac{24}{\pi^2}\right)}}\ m$$
$$\beta = \frac{n\pi r_{strand}^2 n_{strand}}{l_{coil} t_{coil}}$$</td><td>[Tourkhani and Viarouge 2001, eq. (22)-(23) & (31)] and [Barrios et al. 2015, eq. (17)]</td></tr>
<tr><td>Sullivan's method</td><td>See reference</td><td>[Sullivan 1999]</td></tr>
<tr><td>Sullivan's economical method</td><td>$n_{strand,opt} = k\frac{\delta_{cond}^2 l_{coil}}{n_{turn}}$ $[\![d_{strand} < \delta_{cond}, ungapped]\!]$
k – see reference, Table I
$n_1 = 4\frac{\delta_{cond}^2}{d_{strand}^2}$ $[\![d_{strand} < \delta_{cond}]\!]$ strands in 1st bunching
$n_b = 3, 4, or\ 5$ bundles per bunching operation (> 1st)</td><td>[Sullivan and Zhang 2014, eq. (2) & (4)]</td></tr>
<tr><td>Industry suggested strand size</td><td>
<table>
<tr><th>Frequency</th><th>Recommended Wire Gauge</th><th>Nominal Diameter over Copper</th><th>D.C. Resistance Ohms/M' (Max)</th><th>Single Strand R_{AC} / R_{DC} "S"</th></tr>
<tr><td>60 HZ - 1 KHZ</td><td>28 AWG</td><td>0.0126</td><td>66.37</td><td>1.0000</td></tr>
<tr><td>1 KHZ – 10 KHZ</td><td>30 AWG</td><td>0.0100</td><td>105.82</td><td>1.0000</td></tr>
<tr><td>10 KHZ – 20 KHZ</td><td>33 AWG</td><td>0.0071</td><td>211.70</td><td>1.0000</td></tr>
<tr><td>20 KHZ – 50 KHZ</td><td>36 AWG</td><td>0.0050</td><td>431.90</td><td>1.0000</td></tr>
<tr><td>50 KHZ – 100 KHZ</td><td>38 AWG</td><td>0.0040</td><td>681.90</td><td>1.0000</td></tr>
<tr><td>100 KHZ – 200 KHZ</td><td>40 AWG</td><td>0.0031</td><td>1152.3</td><td>1.0000</td></tr>
<tr><td>200 KHZ – 350 KHZ</td><td>42 AWG</td><td>0.0025</td><td>1801.0</td><td>1.0000</td></tr>
<tr><td>350 KHZ – 850 KHZ</td><td>44 AWG</td><td>0.0020</td><td>2873.0</td><td>1.0003</td></tr>
<tr><td>850 KHZ – 1.4 MHZ</td><td>46 AWG</td><td>0.0016</td><td>4544.0</td><td>1.0003</td></tr>
<tr><td>1.4 MHZ – 2.8 MHZ</td><td>48 AWG</td><td>0.0012</td><td>7285.0</td><td>1.0003</td></tr>
</table>
</td><td>[litz-wire.com; litzwire.com]</td></tr>
<tr><td colspan="3">∗ Full list of assumptions found in [Kazimierczuk 2014, pg. 266]</td></tr>
</table>

In the above table, Sullivan's economical method contains guidance beyond just the total number of strands; although technically for an un-gapped transformer core, it does not appear egregious to apply the method to loop antennas whether they be open- (e.g. rod) or closed-path. As pointed out, for optimal efficacy of the Litz wire

construction, the 1st bunching operation should not have more strands than calculated for n_1 [Sullivan and Zhang 2014]. This first bunching level can then be bunched at the 2nd level with 3-5 bundles (each with n_1 strands); then the next bunching level comprised of these sub-bundles, ad nausea, until the total number of strands have been reached [Sullivan and Zhang 2014]. The previous guidance is for minimizing bundle-level skin effect; for minimizing bundle-level proximity effect, the twisting pitch should be small relative to the overall length of wire [Sullivan and Zhang 2014]. The complexity and design care needed to maximize Litz wire's benefits again distinguishes Litz from common stranded wire.

The thickness of magnet wire insulation on individual Litz strands can be estimated according to [Sullivan 1999, eq. (3)-(4)] which includes an additional estimating equation to increase the applicability (AWG 30-60) beyond the standard equation given by the National Electrical Manufacturer's Association (which Sullivan states is only practical for AWG 14-30). A very good table of four different insulation sizes can be found in [Kazimierczuk 2014, Table 10.2]. Bare magnet wire diameters and DC resistances can be estimated according to [Kazimierczuk 2014, eq. (10.1)-(10.5) or Table 10.1] or by Internet search. Manufacturer data should also be available.

For Litz wire, some literature recommends calculating an equivalent round-wire diameter (see [Biela and Kolar 2008] and references therein):

$$r_{cond\,\{Litz \rightarrow round\}} = r_{wire\,\{Litz\}} - t_{ins,wire} - t_{ins,strand} \;\; m$$

where $t_{ins,wire}$ & $t_{ins,strand}$ are the thicknesses of the outer wire and strands, respectively.

The outer diameter of Litz wire can be estimated, per [Biela and Kolar 2008, eq. (16)-(17)], by the following:

$$r_{wire\,\{Litz\}} \approx \begin{cases} r_{strand,ins.}\sqrt{\dfrac{4n_{strand}}{\pi}} \\ 2.7\times10^{-4}\left(\dfrac{n_{strand}}{3}\right)^{0.45}\left(\dfrac{d_{strand}}{4\times10^{-5}}\right)^{0.85} - t_{ins,wire} \end{cases} \quad m$$

where $r_{strand,ins.}$ is the radius of the insulated strand and d_{strand} is the radius of the bare strand.

Conductor Internal Inductance Equations

While coil external inductance is typically the dominant inductance factor, a complete analysis should include the inductance internal to the conductor wire. Similarly as to resistance, conductor inductance includes skin and proximity effects because it is due to the internal magnetic field created by a flowing current. As the cross-sectional area of the current decreases due to these effects—proportionally increasing the resistance—so too does the inductance decrease. It will be noticed that quite un-intuitively, the internal DC inductance $L_{cond,dc}$ is independent of conductor cross-section—proven by triple integral of a round wire [Paul 2011]. The internal DC inductance $L_{cond,dc}$, solved by [Paul 2011, eq. (4.80)], is:

$$L_{cond,dc} = \frac{\mu_0\mu_{cond}l_{wire}}{8\pi} \quad [\![f \to 0]\!] \quad H$$

where μ_{cond} is the relative permeability of the conductor. The internal AC inductance is:

$$L_{cond,ac} = L_{dc}\left(F_{L,skin} + F_{L,prox}\right) \quad H$$

where $F_{L,skin}$ & $F_{L,prox}$ are the skin and proximity inductance factors, respectively.

The following sub-sections aren't strictly needed to calculate these factors, as conductor resistance and inductance are inversely related:

$$F_{L,skin} = 1/F_{R,skin}$$

$$F_{L,prox} = 1/\left(F_{R,prox} + 1\right) - 1$$

If the above approach isn't desired for internal inductance skin effect in round wires, equations in Table B.4 can be utilized. Again, for small stranded wires, it should be safe to assume a simple round conductor of equivalent diameter. Literature regarding skin and proximity effects in Litz wire is limited; for skin effects, see [Sinha et al. 2010, eq. (1)-(2)].

To correct for proximity effect in round wire, the following by [Kazimierczuk 2014, eq. (5.290) & (5.349)] can be used:

$$F_{L,prox} = \frac{\sinh(A)+\sin(A)}{\cosh(A)+\cos(A)} = \frac{e^{A}-e^{-A}+2\sin(A)}{e^{A}+e^{-A}+2\cos(A)} \quad [\![Dowell's\ assumptions, \mu_{int} \to \infty]\!]$$

$$A = \begin{cases} \frac{r_{cond}}{\delta_{cond}}\sqrt{\frac{\pi d_{cond}}{p}} \\ or \\ \left(\frac{\pi}{4}\right)^{\frac{3}{4}}\frac{d_{cond}}{\delta_{cond}}\sqrt{\frac{d_{cond}}{p}} \end{cases}$$

A straight wire also has external inductance, which may not be obviously differentiated from the internal inductance in some literature (e.g. [Grover 1946, pg. 35; Terman 1943, pg. 43]). Unlike DC internal inductance, external inductance is a function of wire cross-section. The full expression can be quite complicated and originates with Neumann [Rosa 1907-8]. The appropriate external inductance depends on the geometry—single, straight wire; pair of straight wires; coil; etc. Coil external inductance formulas are presented in Chapter 6.

The GMD of a wire can be derived from the net DC inductance $L_{dc,net}$ of a straight wire with some simplifications [Paul 2011, pg. 275]. The equation for a straight wire much longer than its GMD, derived in [Paul 2011, eq. (6.44c)], is:

$$L_{dc,net} = \frac{\mu_0\mu_{cond}}{2\pi}\left[\log\left(\frac{2l_{wire}}{GMD_{wire}}\right) - 1\right] \quad [\![straight\ wire, l_{wire} \gg GMD_{wire}]\!]\ H$$

Wire Leads

Practical coils will have wire leads that connect the coil to a transmission line or connector. These leads will have the same internal impedance as described in the previous sections; proximity effect can typically be neglected. In addition, the leads' external inductance $L_{ext,leads}$ and self-capacitance $C_{self,leads}$ should be considered. These can be done by modeling the leads as two parallel, round wires (two-wire transmission line) neglecting end effects as in [Kazimierczuk 2014, eq. (1.448), (9.69), & (9.90)]:

$$L_{ext,leads} = \begin{cases} \frac{\mu_0 \mu_r l_{leads}}{\pi} \cosh^{-1}\left(\frac{d_{sep}}{2r_{cond}}\right) & exact \\ \frac{\mu_0 \mu_r l_{leads}}{\pi} \ln\left(\frac{d_{sep}}{r_{cond}}\right) & [\![d_{sep} \gg \sqrt{2r_{cond}}]\!] \end{cases} H$$

$$[\![round\ wire, no\ end\ effects]\!]$$

$$C_{self,leads} = \frac{\pi \varepsilon_0 \varepsilon_r l_{leads}}{\cosh^{-1}\left(\frac{d_{sep}}{2r_{cond}}\right)} \quad [\![round\ wire, \varepsilon_{ins,wire} \approx 1]\!] \ F$$

where d_{sep} is the separation distance between the leads; l_{leads} is the length of each lead wire; and $\varepsilon_{ins,wire}$ is the relative permittivity of the wire insulation.

CHAPTER 6

COIL INDUCTANCE AND SELF-CAPACITANCE

When wire is bent, its external inductance is no longer that of a straight wire's and must instead account for geometry, mutual inductance to nearby conductors, and magnetic core permeability. A similar consideration must be made for self-capacitance. Furthermore, the effects of a conducting core and shield upon impedance are presented.

Coil External Inductance

The dominant inductance in an ESL is typically the coil external inductance L_{coil}; this section will focus on the external inductance due to the coil shape and not the internal inductance of the wire employed. The external inductance of both rings and solenoids will be discussed and analyzed in this section including the concept of a current-sheet and appropriate corrections for such. This includes analytical and empirical equations, which since there are so many conflicting equations, we will give recommendations. Some calculations are also plotted to aid in comparing formulas.

For a simple ring that has negligible length and thickness ($l_{coil} \to 0, t_{coil} \to 0$), the ESL's coil inductance is well understood and scales by n^2. Coils with finite length are more difficult to analyze—though even "simple" rings' exact equations are cumbersome without simplifications—so many analytical and empirical fits have been established over more than a century. Knight and Weaver give an excellent introduction and step-by-step through the history of calculating coil self-inductance for a solenoidal coil, then extends their applicability and accuracy [Knight 2013a; Weaver 2016]. Some of the simplest and most-quoted solenoidal coil equations are based on Wheeler's

empirical fits (see [Wheeler 1928]) but are superseded in accuracy by fuller, more complex equations.

An assortment of equations and references for various geometries are listed in Table C.1 for rings (zero length) and Table C.2 for solenoids and coils of length. This includes most common equations but does not include various approximate equations (e.g. Coffin's, Havelock's, Stefan's) when better exist (more accuracy and/or less constraints) as concluded by [Rosa and Grover 1916]. The following equations are recommended after validating by our measurements (see Chapter 8) for thin single- or multi-layer solenoids: Snow/Weaver for general solenoids including polygonal coils with $l_{coil} \gg 0.1A_{coil}$; Grover/Knight/Weaver (corrected) for an air-core toroidal solenoid; and the analytical toroidal current-sheet solenoid for an air-core toroid. Thick multi-layer solenoids and rings were not studied in detail here, but ring equations expressed in [Grover 1946] or [Terman 1943] would be expected to be highly accurate (assuming the ring, if multi-turn, meets assumptions of thin and short else a solenoid equation should be used). General solenoid equations (corrected) like Knight/Rosa/Weaver are also accurate for rings (which are just a special case of a solenoid); Snow/Weaver does not natively handle a single-turn ring.

For a comprehensive compilation of inductance (self and mutual) formulas and analysis for some more existing formulas in the early 1900s, [Rosa and Grover 1916] and [Grover 1946] would be recommended. For a simple but useful compilation, [Terman 1943] further narrows down equations per coil type, simplifies equations with more tables and figures, cuts out most discussion (including, alas, references to many equations' origin), and uses units of inches. Many of the equations and tables/figures of [Terman 1943, §2.7-11] can be shown to be the same as that presented in references by Rosa and/or Grover with few—but not necessarily trivial—resulting differences (and

oddly, commonly replacing ln() with the approximation $2.303\log_{10}()$, though this may have been preferred in 1943).

Analytical or numerical equations for self-inductance come about via one of two ways: volumetric flux integrals or the limit of mutual inductance for two identical, co-located coils [Conway 2013]. The most prevalent, closed-form analytical equations are based on the assumption of a thin, current-sheet (CS) solenoid, of which Lorenz's (1879) is exact and has no restrictions when its assumptions are valid [Rosa 1906]. More recent literature attempts to approximate or handle the complete elliptic integral functions required in Lorenz's shape correction factor k_L to handle computational errors such as round-off [Nagaoka 1909; Lundin 1985; Miller 1987; Fincan and Üstün 2015; Weaver 2016; Knight 2016].

The only full corrections for both CS assumptions (infinitely thin and continuous sheet) are limited to two methods: Rosa's and Snow's [Rosa and Grover 1916; Knight 2013a; De Queiroz 2014; Snow 1939]. Snow's method also incorporates helicity, although Knight extends Rosa's method for large pitch angles [Knight 2013a]. Another plausible approach is by considering the mutual flux between circular filaments (infinitely thin)—known as the summation method—such as Maxwell's approach (see [Rosa and Grover 1916; Weaver 2016; De Queiroz 2014]) which can handle any coil shape due to iterative calculation of the flux between turns, but doesn't natively include round wire corrections (though they can be added). Note that Rosa's current-sheet corrections for self- and mutual-inductance of round wire are commonly given the symbols G and H respectively (or A and B), but Knight's convention of k_s and k_m will be used herein. Further note that Knight recommends using an effective coil diameter for current-sheet inductance calculations, where refinements are due to skin and proximity effects' impact on the current distribution [Knight 2016b, eq. (6.6)-(6.7)], but such was not used herein.

The CS assumptions may be minor—likely of concern for coils with significant gaps between conductor turns and/or extremely thick wire (or thick layers)—because the accuracy is typically good (~1 %) without the correction after analyzing example results in [Ishida et al. 2011; Rosa and Grover 1916]. Grover states that the "inductance of the coil is to a first approximation the same as that of the equivalent current sheet" and "the correction [factor] is unimportant in many cases met in practice" (except, for example, when the winding pitch is greater than the wire thickness) [Grover 1946, pg. 15, 149, & 163]. Our measurements show that the CS assumptions can cause significant errors.

At first, it isn't exactly clear how to use mutual inductance approaches to calculate the self-inductance. The process is to calculate the mutual inductance M "for every combination of pairs of turns between the first and second coil and add up the results" for two over-lapping coils of the same dimensions and using the appropriate geometric mean distance (GMD) [Weaver 2016]. The GMD between coil turns is simply the distance between the turns' centers, but overlapping turns use the self-GMD of a wire, which is not zero [Weaver 2016; Knight]. A list of mutual inductance references are presented in the next sub-section. The following, taken from [Weaver 2016], demonstrates how to use mutual inductance to calculate inductance L_{coil} of a single-layer coil, with the first term calculating the overlapping first turns and the second term summing the rest of the coil turns (with $2(n-i)$ handling the repeating pairs) for a single-layer ($n_l = 1$) coil:

$$L_{coil} = n \times M_{ring}\{r_{coil\,\{1\}}, r_{coil\,\{2\}}, GMD_{wire}\} + \sum_{i=1}^{n-1}\left[2(n-i) \times M_{ring}\{r_{coil\,\{1\}}, r_{coil\,\{2\}}, ip\}\right] \quad H$$

$$[\![n_l = 1, no\ helicity, d_{cond} \ll r_{coil}]\!]$$

where M_{ring} is the mutual inductance between rings and the GMD of a thin tube is $GMD_{wire} = r_{cond}$ [Weaver 2016]. Note that the GMD for other types of wire can be found in literature (e.g. [Queiroz 2014, Paul 2011, §6; Grover 1946, pg. 21-3]).

Wire GMD includes both internal and external inductance, therefore it is a function of current distribution. With the exception of older literature (e.g. works by Rosa and/or Grover, or [Terman 1943]), most literature instead separate internal and external inductance, which reduces confusion—though they could be recombined for a more accurate GMD. In practice, it is better to separate internal and external inductance, therefore the GMD of a thin ring/tube should be used for round wire when calculating external coil inductance and accurate equations used for the wire's internal inductance (presented in Chapter 5).

In recent decades, a preponderance of numerical and analytical approaches have been presented in literature for various shapes of solenoidal coils or generalized cases, although they too share the assumption of uniform current, and some the thin coil assumption ($t_{coil} \to 0$) [Luo and Chen 2013; Babic and Akyel 2000; Župan et al. 2014; Conway 2010; Pankrac 2012; Ishida et al. 2011; Hurley et al. 2015]. Most equations are for single-layer coils, but some handle multi-layer coils such as in [Rosa 1907; Rosa and Grover 1916, §7; Yuanren Qui et al. 1993; Wheeler 1928; Kazimierczuk 2014; Terman 1943]; the correction factor for a thick coil can be non-trivial (e.g. 10%) [Rosa 1907].

There are numerous analytical equations for a circular ring. Interestingly, it is shown that the classic exact equation is less accurate than the extremely-simple Kirchhoff thin ring equation (with "- 2" instead of "- 1.75") when compared to another analytical derivation as well as method of moments numerical analysis [Carobbi and Bonci 2014]. It is possible that Carobbi and Bonci had round-off errors, a known concern for functions with elliptic integral functions [Knight 2016b, pg. 59], but we did not investigate their results. Instead, Maxwell's second algebraic arrangement of mutual inductance should be used in [Maxwell 1873, §701] and a computationally-accurate approach for subtraction of the elliptical integrals $K_{ei1}() - E_{ei2}()$ used [Knight 2016b, pg. 60].

The common expression for a thin-ring using the natural logarithm $\ln() - 2$ is actually an approximation of $K_{ei1}() - 2$ (which is rarely seen in literature) which itself is a thin-ring approximation of Maxwell's mutual inductance equation solved for coil inductance [Knight 2016b, pg. 58; Paul 2011, pg. 129-30]. Note that some literature use 1.75 instead of 2, but it can be shown that the difference is due to whether or not the internal inductance of the wire is included, not a rounding choice. Most expressions for ring and coil inductance are explicitly external inductance, so "2" should be used for such to foment comparison (and allow frequency effects to be factored into the internal inductance).

Most of the literature has focused on round objects, not rectangular, due to relative simplicity and popularity. However, it is useful to explore how similar the results are between a square coil (which is also practical) and a round coil of equivalent area, since such is typically a reasonable first-order approximation. Results for several references are plotted below in Figure 6.1 for both solenoidal coils and rings ($l_{coil} \to 0$) for a very thin filament; note that the circle solenoids of (Lorenz/Weaver), (Lundin), and (Ishida et al.) overlap. As can be seen, square solenoids have a higher inductance relative to area than circular for coil lengths significantly less than coil area (seen also in the ring curves), but the inductance/area converges regardless of geometry for increasing coil length. Therefore, for coils with $l_{coil} \gg 0.1A_{coil}$, using a round coil of equivalent area is accurate regardless of shape; this conclusion matches literature [Grover 1946, pg. 171]. The calculation of a circular coil (Lorenz, direct) may have computational errors, which is one reason why numerous authors present alternate formulas or calculation approaches such as that of Weaver and Lundin. The circular coil (Yao and Chen) errors may be due to underlying assumptions by the authors. As expected, solenoidal inductance is less than that of a ring due to being inversely proportional to coil length. For rings, the inductance order goes as square > circle > isosceles triangle > equilateral triangle. No

current-sheet corrections for round wire have been applied, as the conductor was made small to simulate a filament. Note that it can be shown that a single-turn solenoid corrected for actual dimensions is approximately equal to that of a single-turn ring, as a ring is merely a special case of a solenoid.

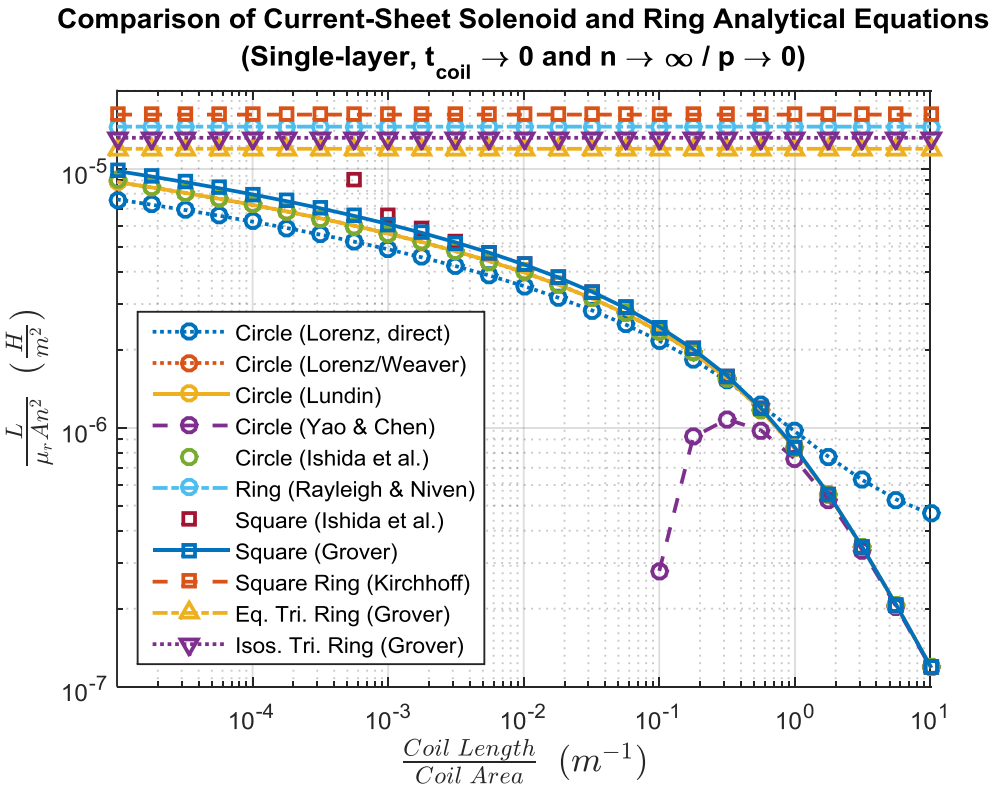

Figure 6.1 – Comparison of Inductance Equations for Rings and Solenoids

We will conclude this section by stating that the literature for coil inductance is large and multi-faceted. Choosing one approach over another can be difficult, but some equations handle a wide, general array of inputs like Knight/Rosa/Weaver and Snow/Weaver albeit with complex formulas requiring use of a computer script. It can also be important to apply corrections to formulas used for solenoids, unless their assumptions are met as a tightly-wound, thin coil (of any length)—but if using a computer, there is no excuse to not program in the corrections.

Mutual Inductance

In most ESL applications, there is only one coil. However, in some applications it makes sense to have multiple coils in parallel to increase the effective height and/or perpendicular/orthogonal coils to receive perpendicular/orthogonal signals. For example, a very simplistic omni-directional loop (sensitive to any direction) designed for a space mission consisted of three rods conjoined near their centers (to save space, presumably) with each oriented in one axis as seen in Figure 6.2 [Coillot and Leroy 2012]. There are interesting ways that multiple antennas' output signals can be combined beyond omni-directional coverage, such as beam steering. This section will describe the analytical treatment of mutual inductance as well as references for predicting it. A description of measurement approaches is also given along with plots of measured data for validation.

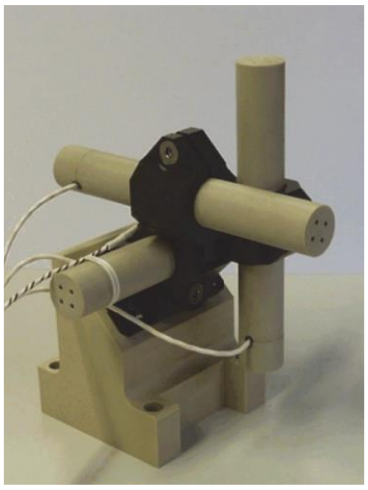

Figure 6.2 – Illustration of Tri-Axis, Omni-Directional ESL for a Space Mission [Coillot and Leroy 2012, Fig. 1]

When electrically-connected coils are in the near vicinity of each other, they can cause proximity inductive effects including mutual flux, though orthogonal coils have minimal mutual flux effects. The net external coil inductance L_{coil} includes each coils'

self-inductance L_{self} (that is, their external coil inductance when alone) and their mutual inductance L_{mut}. For two coils, this is [Kazimierczuk 2014, eq. (7.156) & (7.158)]:

$$L_{coil} = L_1 + L_2 \pm 2L_{mut} = L_1 + L_2 \pm 2k_{mut}\sqrt{L_1 L_2}\ \ H$$

where L_1 & L_2 are the self-inductances of the two coils and k_{mut} is the mutual coupling factor which ranges between zero and one. Assuming two equivalent inductor coils, the net external coil inductance L_{coil} and mutual coupling factor k_{mut} can be simplified:

$$L_{coil} = 2L_1(1 \pm k_{mut})\ \ [\![two\ equivalent\ inductors]\!]\ \ H$$

The mutual coupling factor can be found from the mutual inductance or from the leakage inductance as in [Kazimierczuk 2014, eq. (7.129)]:

$$k_{mut} = \frac{L_{mut}}{L_1} = 1 - \frac{L_{leak\{1\}}}{L_1}\ \ [\![two\ equivalent\ inductors]\!]$$

where $L_{leak\{1\}}$ is the leakage inductance from one of the coils. Note that when calculating magnetic core loss, the net external coupling inductance should be used (verified by measurements as presented later).

Mutual flux can be series-aiding or series-opposing, hence the ±; it is a function of the coil winding direction and the series connection wire between the two coils. This translates to the potential of having an ESL with twice the effective height and low inductance via two coils connected series-opposing; Spears patented such an antenna with two pairs of orthogonal, series-opposing coils on a closed-flux magnetic core (see Figure 6.3) [U.S. Patent 3,495,264; M. F. Spears, 1970]. Achieving a high mutual coupling coefficient k_{mut} may not be easy depending on the geometry, nor is it easy to calculate the leakage flux's mean magnetic path length.

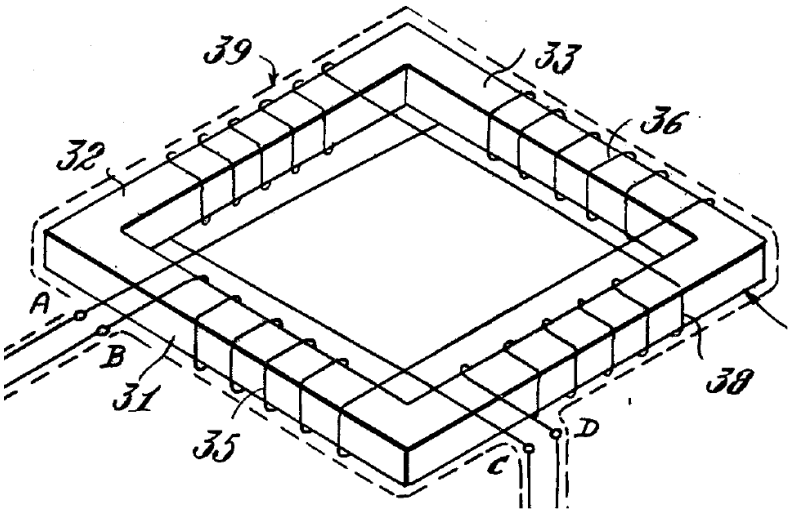

Figure 6.3 – Illustration of Two Orthogonal Coil pairs on Closed-Flux Magnetic Core [U.S. Patent 3,495,264; M. F. Spears, 1970, Fig. 5]

Equations for leakage and mutual inductance abound for various geometries and for single- or multi-turn coils; see Table 6.1 for references. For two circular filaments with arbitrary lateral and angular misalignment, [Babic et al. 2010] states to supersede various other works by Grover, Snow, etc. with generalized equations and proves it by comparing to Grover's examples and numerical modeling. Mutual inductance calculations for a square coil can also be approximated by using an equivalent diameter circular coil and then multiplying the final mutual inductance by a factor of 1-1.6 [Cheng and Shu 2014a]. Literature for solenoidal coils' mutual flux appears to be limited to solenoids with parallel axes (e.g. [Conway 2007]), but an approximation could be performed by breaking each solenoid into sets of circular filaments and evaluating the net mutual flux from each pair.

Table 6.1 – Mutual Flux Equation References

Description	References
General-shape air-core coil	[Pankrac 2012]
Air-core circular coil	[Babic et al. 2010, eq. (24)-(26); Conway 2007; Conway 2008; Conway 2010; Hurley et al. 2015; Yuanren Qui et al. 1993; Rosa and Grover 1916; Župan et al. 2014; Grover 1946; Terman 1943]
Air-core rectangular coil mutual inductance	[Cheng and Shu 2014a; Cheng and Shu 2014b; Rosa and Grover 1916; Grover 1946; Terman 1943]
Low-frequency (e.g. 50/60 Hz) transformer leakage inductance	[Hurley and Wilcox 1994; Janse van Rensburg and Ferreira 2004; De León et al. 2014]
High-frequency transformer leakage inductance	[Bahmani and Thiringer 2015, eq. (13)-(14); Ouyang et al. 2015; Wilson and Brown 2008]

Leakage inductance decreases with frequency due to conductor skin effect, which results in a higher mutual coupling coefficient. However, most equations neglect frequency effects—not surprising given that 50/60 Hz transformers are a primary interest for such calculations [Bahmani and Thiringer 2015]. According to the literature reviews summarized in [Bahmani and Thiringer 2015] and [De León et al. 2014], it is difficult to come up with precise, general-case, closed-form equations—therefore, the literature typically attempts to provide simplified, engineering-accuracy formulae for specific applications. Complex antennas requiring high accuracy mutual inductance prediction should be simulated.

The separate inductances of two coils can be measured in various ways—see Table 6.2—giving several different measurement methods to determine the mutual coupling coefficient (other inductances, such as internal wire inductance, are neglected) . For example, the self-inductance is the inductance of a singular coil, therefore the leakage inductance is the difference in the coil's inductances with and without the secondary coil (open-circuited) present. The net leakage inductance (referred to the primary) is the inductance measured when the secondary coil is short-circuited [Kazimierczuk 2014].

Finally, the mutual flux can be determined by measuring the two coils' inductance when connected in series-aiding ($L_{series-aid}$) and series-opposing ($L_{series-oppose}$) configurations; ideally, both should be measured to compute L_{mut} using the following equation as per [Kazimierczuk 2014, eq. (7.204)]:

$$L_{mut} = \frac{1}{4}\left(L_{series-aid} - L_{series-oppose}\right)\ H$$

Table 6.2 – Self, Leakage, and Mutual Inductance Measurements with Two Coils

	Coil(s) Measured			**Coil #2**		
L_{meas}	**Coil #1**	**Coils #1 & 2, Series-Aiding**	**Coils #1 & 2, Series-Opposing**	**Not Present**	**Open-Circuited**	**Short-Circuited**
$= L_1$	X			X		
$= L_1 + L_{leak,1}$	X				X	
$= L_{leak,1} + \left(\frac{n_1}{n_2}\right)^2 L_{leak,2}$ [Kazimierczuk 2014, eq. (7.201)]	X					X
$= L_1 + L_2 + 2L_{mut}$		X				
$= L_1 + L_2 - 2L_{mut}$			X			

In general, mutual inductance effects are more difficult to analyze than the external coil inductance of a single coil, the latter being a special case of mutual inductance (discussed earlier). We show in Chapter 8 that predictions reasonably match measured data for the case of mutual coils on a toroid, but references have also been given for analyzing other cases. However, small differences between predicted and measured mutual coupling have large repercussions in predicting the net external inductance and core resistance.

Coil Self-Capacitance

There are various capacitances that can be involved in a loop antenna. They can be divided into two types: self and external. Self-capacitance effects arise due to the coil, core, shield, medium, and wire leads; these are expanded upon here. External capacitances are typically a capacitor wired in parallel with the intention of resonating the loop antenna at a particular frequency; there is no need to expand upon such here. Self-capacitance is a contentious topic [Knight 2013c] and goes by other names such as stray, distributed, or parasitic capacitance. Care must be taken in how self-capacitance is measured (see Chapter 1).

There is a plethora of literature including various analytical and empirical approaches to deriving self-capacitance; see Table C.3 for a list. Note that Palermo's work (sometimes referenced in literature) is not included here due to Medhurst's work believed to supersede it [Medhurst 1947; Knight 2013c]. For Litz wire, some literature recommends calculating an equivalent round-wire diameter (see previous chapter). Our measurements did not clearly indicate which formulas were most appropriate, but Medhurst's, Kazimierczuk's non-conducting #2, and the parallel-ring electrode equations were relevant in many cases for both air-core and ferrite-core. Despite analytical treatment specific to ferrite-cores in literature, other empirical analysis has also found air- and ferrite-core to be the same despite ferrite's high permittivity [Mel'nikov and Mel'nikova 1974].

The majority of our measurements were not measured by the two-capacitor method, therefore the self-capacitance had to be calculated from the measured SRF and assumed inductance. However, the measured SRF for the ferrite-cores were typically at a frequency where MN60's relative permeability has to be extrapolated by the dispersion formula—which is necessary to calculate inductance and thence capacitance—and was assumed to be approximately equal to one at very high frequencies. Measured data for

the ferrite-cores where the two-capacitor method was also employed show a significant difference (several orders of magnitude) between these two methods, implying that MN60's relative permeability is higher than one at these frequencies. An underlying assumption is that the permittivities of the relevant materials are relatively independent of frequency (see Chapter 2).

One way to decrease C_{self} is to not wind the turns uniformly but rather divide the turns into several groups with gaps between the groups—this has the effect of adding capacitance in series, decreasing the net capacitance [Carr and Hippisley 2011, pg. 355]. We have not explored this experimentally, but it may be worth pursuing should self-capacitance be a limiting factor.

Conducting Core and Shield Effects upon Coil Impedance

As described previously, nearby conducting materials can impact the impedance of a coil. There has been significant rigorous literature on impacts both on coil inductance and self-capacitance, and will be discussed here along with references. The effects by a conducting core upon coil resistance have been previously mentioned.

There are a handful of analytical literature on a shielded air-core coil's inductance (with the assumptions previously mentioned), with the conclusion that a shielded coil's inductance will be equal or less than when un-shielded. It is likely that as a core's internal permeability approaches infinity, the closer the shield must be to impact the coil impedance as the flux is more concentrated in a permeable core. Bogle presented a simple inductance correction factor equation for a coil surrounded by a cylindrical shield (also referred to in [Rhea 2000]) that is expanded upon with more applicability by Phillips [Phillips 1949]. Simpson as well as Young and Butler also analyze a coil within a cylindrical shield including empirical data, which agree with Bogle and Phillips that the shielded coil's inductance can be significantly less than when un-shielded but is a

function of shield/loop diameter and coil length/diameter ratios [Simpson 1999; Young and Butler 2001]. Young and Butler also analyzes the cylindrical shield with a slit, showing how more slit area in a shield results in less reduction of inductance [Young and Butler 2002]. Padhi analytically explores the inner transmission line's admittance but neglects the proximity eddy-current effects [Padhi 1965]. Lindsay derives the transmission line voltage transfer function of a single-gap loop which compares well to measured data [Lindsay and Münter 1983].

Equations for self-capacitance effects for conducting cores and shields are included in Table C.3. In [Kazimierczuk 2014], conducting cores and shields are treated as conducting planes that create an image for a nearby wire, adding parallel capacitance to each wire turn. For single-layer coils, [Grandi et al. 1999] indicate that a conducting core or shield plays a major role, which is best seen in the difference in equations in Table C.3 for a single-layer coil with and without conducting core/shield. However, multi-layer coils are negligibly impacted by a conducting core or shield (even close-fitting, with axial cut), with a maximum increase in self-capacitance less than 20% for widely-spaced windings [Hole and Appel 2005]. Some shield capacitance formulas are given in [Rhea 2000] including cylindrical, square, and other geometries surrounding the loop. Literature typically include complicated circuit models and make assumptions, so high accuracy may require general electromagnetic modeling. Otherwise, the approximate equations in Table C.3 are reported to fairly match measured.

The effect of a conducting medium in the vicinity of an ESL should be considered in a similar manner as turn-to-core/-shield if the loop does not have a shield. If the medium has both relatively-low conductivity and permittivity, as well as a significant separation distance from the ESL, then it can likely be ignored. A numerical approach to the inductance of a coil as modified by surrounding media, including eddy effects in nearby metal, is presented in [Mayer 2009].

CHAPTER 7

OPTIMIZATION AND DESIGN EXAMPLE

Optimizing an ESL means maximizing its sensitivity (or resolution) for a particular application. Sensitivity and signal/noise ratio (SNR) are metrics for evaluating antenna performance, and will be discussed along with simpler figures of merit. This chapter also expands upon some optimizing strategies such as geometry and layout considerations, as well as numerical optimization routines to select the best design. An application example of optimization is given at the end including design methodology, laboratory measurements, and field measurements along with discussion of the results.

Sensitivity, SNR, and Figure of Merit

Calculating an ESL's sensitivity and SNR allows for quantitative analysis (and comparison) of antenna performance. This section will describe sensitivity and SNR calculations as well as discussing sources and prediction of noise. Some references are given for matching and pre-amplifying, which assist in maximizing sensitivity and SNR. Further, some figures of merit are given as a different way of comparing antenna performance.

The sensitivity S_{min} (as per [Macintyre 1999 (48.12)-(48.13)]) and SNR of an ESL are defined relative to an antenna output voltage V_{ant} as in the following equations:

$$S_{min} = \frac{V_{ant}}{H\omega} = \mu_0 \mu_{ext} nA \quad \frac{Vms}{A}$$

$$SNR = \frac{V_{ant}}{V_n}$$

where V_n is the effective noise voltage referred to the antenna output.

There are various noise sources to consider: ambient/atmospheric, vibration in Earth's magnetic field, and internal noise. Of course, whether these are noise sources depends on the application: for example, a system designed to measure atmospheric noise (e.g. lightning) would not consider such to be noise but rather the signal of interest. These noise sources are described in more detail in the following sub-section. They are generally un-correlated, therefore their aggregate sum is a geometric mean (all referred to a common point such as the input):

$$V_n = \sqrt{\sum V_{n,i}^2} \quad [\![uncorrelated\ noise\ voltages]\!]\ V$$

Ambient and atmospheric noises include natural and man-made. For statistical noise values, see International Telecommunications Union report ITU-R P.372. Note that man-made signals include spurious (e.g. automobile engine sparks) and intentional (e.g. radio stations); ITU-R P.372 focuses on the former while the latter can be explored in relevant national/international codes and licenses.

Moving and vibration can cause two notable noises: magnetorestrictive and geomagnetic. The first is primarily a concern in magnetic materials, so ideally a material with low magnetorestriction is chosen if this may be a concern; for further analysis of this noise source, see literature (e.g. [Burrows 1976]). The second noise is caused by rotating through Earth's DC magnetic field, which can cause significant noise especially at extremely low frequencies [Dinger and Davis 1976]. The intensity of Earth's magnetic field vector varies as a function of location and time, but the flux magnitude is approximately $2.5 - 6.5 \times 10^{-5}$ T [http://www.ngdc.noaa.gov/geomag/faqgeom.shtml, accessed 2015-09-17]; a common magnitude given is 5×10^{-5} (e.g. [Dinger and Davis 1976]). For more analysis, see the literature.

Internal noise can be divided into three primary sources: thermal noise due to the antenna's equivalent series resistance R_{ant}, amplifier input noise voltage e_n, and amplifier input noise current i_n. There are additional noise contributions that may

possibly be significant: transformer coupled negative feedback (if any), feedback resistor, and amplifier resistors [Yan et al. 2013]. Assuming un-correlated noise, the noise voltage is as per [Yan et al. 2013, eq. (15)]:

$$V_n = \sqrt{k_B T R_{ant} + e_n^2 + (i_n | R_{ant} + j2\pi L_{ant}|)^2} \ \frac{V}{\sqrt{Hz}}$$

where k_B is Boltzmann's constant and T is temperature (in Kelvin).

Noise voltage may also be represented as equivalent input magnetic noise B_n using the following, taken from [Grosz and Paperno 2012, eq. (9)]:

$$B_n = \frac{V_n}{2\pi \mu_{ext} n A} \ \frac{T}{\sqrt{Hz}}$$

System design must factor in matching and amplifying of an antenna to maximize its sensitivity. The matching circuit and preamplifier are ideally electrically close to the antenna—this minimizes losses. The common approach for an ESL is to follow the antenna with a transformer and then the preamplifier circuit [Harriman et al. 2010]. Full treatment of this subject is left to the literature for ESLs (air- or magnetic-core) such as [Liu et al. 2015; Ozaki et al. 2014; Rhouni et al. 2013; Trask 2008; Warnick and Jensen 2007; Harriman et al. 2010; Paschal 1988]. The latter by Paschal is very comprehensive. A practical consideration can be to settle on a common impedance to allow for interchangeability of antennas with a standard matching and amplifying circuit such as in [Cohen et al. 2010].

As can be seen from the legion equations presented heretofore, simplifying everything into one comprehensive equation is daunting. The closest to this—though not fully simplified—is for a long, cylindrical, high-permeability rod in [Nourmohammadi et al. 2014]. Sometimes, it is simpler to compare antennas' performance by a figure of merit F_{merit}. The following by [Hansen and Collin 2011, eq. (3.70)-(3.71)] is not simple per se, but it is at least a closed-form equation as compared to full analytical treatment:

$$F_{merit} = \frac{nk_\lambda^2 \mu_{ext} r_{coil}^2 X_{coil}}{2(R_{rad} + R_{core})} = \frac{3nk_\lambda^2 \mu_{ext} r_{coil}^2}{k_\lambda^2 l_{core} \mu_{ext} r_{coil}^2 + 6\tan(\delta_m)} \quad [\![long\ coil, n \gg 1, ESL]\!]$$

An even simpler figure of merit is the following, as recommended by [Alvandian 2012]:

$$F_{merit} = \frac{h_e^2}{|Z_{ant}|}$$

where Z_{ant} is the antenna impedance.

Optimization Strategies

Some ESL optimization strategies and notes that have been found in various literature are given here for optimum coil/core ratio (or core permeability), optimum core length/diameter ratio, and multi-layer coil layout on a magnetic core. It turns out that the former is quite contested, and will be discussed here in detail. Numerical strategies for down-selecting between various designs are also given.

Some literature calculates the optimum coil/core length ratio for a single-layer winding being generally approximated as 0.9 (that is, a coil occupies 90% of the magnetic core length) or close to unity [Grosz and Paperno 2012; Yan et al. 2013; Pettengill et al. 1977, who cite Snelling]. Indeed, [Maksimenko 1991] calculated it as 0.89 for a simple, general case using a high-permeability core; he also calculated that a ratio between 0.55 and 1 does not change the SNR by more than 10% from optimum. Simpson's article on designing a ferrite-core ESL doesn't specify coil length but shows simulation results for a full-length coil, implying such to be optimal [Simpson 2007].

However, measurements by Belrose indicate that the maximum sensitivity is obtained with a short-/medium-length coil (he states "short") with data indicating the coil length should be approximately 1/3 – 1/2 the rod length for maximum sensitivity [Belrose 1955, Fig. 5]. Observing Figure 4.7 and Figure 4.8, it seems that Belrose's conclusion has more merit for optimizing SNR. Indeed, the fact that a lot of demagnetization

analysis and fluxmeter designs use short coils suggest a short coil is optimal. The following section's design example also concludes short coils can be optimal, but it may be application dependent due to balancing other design parameters like impedance.

Optimum magnetic core length/diameter ratio or permeability can be hard to quantify at high accuracy without interpolating tables. However, Pettengill et al.'s equation (presented in Chapter 4)—which is reasonably accurate within its applicability range, although it is for $\mu_{a,f}$ (short coil) though the authors argue for a long coil—foments a simple analytical approach which prioritizes compactness. The authors use it to suggest the following optimal length/diameter ratio:

$$(l/d)_{core,opt,compact} \approx 0.92(\mu_i - 1)^{0.69} \ \ [\![2 \leq (l/d)_{core} < 20]\!]$$

Re-arranged for optimum initial permeability, this is:

$$\mu_{i,opt,compact} \approx [1.09(l/d)_{core}]^{1.45} + 1 \ \ [\![2 \leq (l/d)_{core} < 20]\!]$$

Some calculations using [Chen et al. 2006] show that the above can be significantly misleading. For example, the above equation computes for $(l/d)_{core} = 15$ that $\mu_{i,opt,compact} \approx 58 \rightarrow \mu_{a,m} = 33$, but a very reasonable, higher-permeability material of $\mu_i = 250 \rightarrow \mu_{a,m} = 63$—practically doubling the antenna's effective height. Therefore, it is not recommended to use Pettengill et al.'s approach.

It has been suggested that the ideal magnetic core shape for axial demagnetization is a hyperboloid [Mel'nikov and Mel'nikova 1974]. An easier manifestation of such is a dumb-bell shape—a cylindrical rod with end-caps [Mel'nikov and Mel'nikova 1974; Coillot et al. 2007; Tashiro et al. 2015]. Mel'nikov and Mel'nikova cite a reference that states empirical measurements that achieved an effective permeability to weight ratio improvement over a cylindrical core of "roughly 1.8 times" for a hyperboloid and 1.2 times for a dumb-bell. Coillot et al. state a "higher than 50%" increase in apparent permeability for a dumb-bell over a cylinder [Coillot et al. 2012]. Further numerical

simulation or empirical evaluation is recommended. It should be noted that ferrite is difficult to machine and fabricate for complex shapes.

When using multi-layer coils, there is also some literature on optimized coil layout. [Spang and Albach 2008] show that for a multi-layer coil with a magnetic core, the optimum coil layout for minimum resistance is trapezoidal (shorter length closest to the core) in order to minimize the proximity effect. From a simple SNR-optimization approach (which neglects proximity effects), [Maksimenko 1991] found that a trapezoidal (longest length closest to the core) multi-layer coil out-performed the optimal single-layer coil by approximately 2%.

Sometimes, the optimization approach is to minimize mass/weight while maximizing SNR or sensitivity; space applications are a good example [Coillot et al. 2007]. In this case, aluminum wiring can be more effective than copper [Burrows 1976]. Paschal shows an air-core loop's sensitivity to be proportional to $\sqrt{Area \times Mass}$, though this includes numerous simplifications and assumptions [Paschal 1988].

Otherwise, optimization relationships or routines are utilized, as in [Duan and Luo 2014], [Coillot et al. 2007], [Grosz and Paperno 2012], and [Yan et al. 2013]. In [Duan and Luo 2014], various evolutionary algorithms are compared—differential evolution (DE), particle swarm optimization (PSO), artificial bee colony (ABC), backtracking search algorithm (BSA), and adaptive BSA (ABSA)—which all arrive to a similar optimal result but differ primarily in the computation time, with ABSA dominant. Of course, brute-force iterative, numerical evaluation can also be employed if processing time/efficiency is not a concern. Regardless of the optimization evaluation routine, constraints and weights (or conversely, penalties) must be decided upon to narrow down to the optimal design.

We can conclude by stating that various ideas of optimum strategies abound but analytical or numerical simulation is recommended to validate the strategy. However,

these notes still have merit and can aid in determining which approaches to calculate or simulate for. The concept of an optimal core shape such as hyperboloid or dumb-bell is interesting and is also worth pursuing for applications where (literally) "squeezing out every ounce of performance" is worthwhile.

Optimization Design Example

As an illustrative example for applying the lessons learned herein, it was decided to explore optimal designs for use with the "AWESOME" receiver used to measure low frequency signals in the ambient (see [Cohen et al. 2010] for more details on the receiver). Unfortunately, attempting a design example wherein the ESL is immersed in a dissipative medium was ruled out for logistical reasons. For time constraint reasons, it was decided to program a brute-force, iterative routine to analytical analyze various input antenna designs and find the optimum thereby. Analytical, numerical, and (pseudo-) empirical approaches as deemed best (as outlined in the previous chapters) were used to numerically evaluate each iteration. An illustration of the calculation procedure for axial magnetic-core loops is presented in Figure 7.1; toroidal ESLs are similar but should calculate $\mu_{ext} = \mu_{a,toroidal}$, add θ_{coil} correction, and any mutual inductance effects.

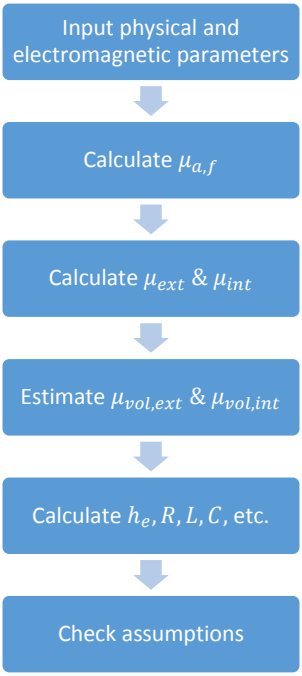

Figure 7.1 – Flow-Chart for Axial Magnetic-Core ESL Calculations

For the AWESOME receiver, the optimum antenna impedance is $R_{ant} = 1\ \Omega, L_{ant} = 0.5 - 1\ mH$ over the frequency span 0 – 100 kHz. The input variables are: magnetic core, turns n (4:4:120), coil layers n_l (1/2/4), coil length l_{coil} (up to l_{core}), and type of wire. The magnetic cores used were MN60 or air/wood/PE and were of the shapes listed in Table 8.1, up to 12 inches in length; the MN60 toroids included single-coil and series-opposing coils (on opposing sides). The wire types consisted of #24 stranded, #26 magnet wire, 60/36 Litz (60 strands of #36 magnet wire), and 120/36 Litz. The frequency span was simplified to 1/10/100/10^3/10^4/10^5 Hertz. Wire leads of 12 inches were assumed. Coil diameters were calculated at the minimum possible. Although not displayed, nine ESL assumptions were also programmed (e.g. $f \leq 0.25\ SRF, l_{wire} \leq 0.1\lambda_{free-pace}$) and were met for the most part; the primary exception was seen in some MN60 cores being thicker than the skin depth in the core for some higher frequencies, but this will be ignored for a first-order approximation.

To narrow down the choices, a weighting function is applied. In a high-value application, a very complicated weighting function should be found that takes into consideration impedance, effective height, volume, mass, etc. A very simplistic weighting function was chosen instead for brevity reasons as the purpose is to illustrate the lessons learned herein. The weighting function is a binary check that the median resistance and inductance are within reasonable bounds for the AWESOME receiver specification:

$$w = \begin{cases} [0.8 < median(R_{ant}) < 1.2\ \Omega\,] \,\&\, [0.5 < median(L_{ant}) < 1.1\ \text{mH}] & 1 \\ else & 0 \end{cases}$$

The resulting effective heights after weighting were then calculated. Since it is difficult to plot concisely, the results will be described. The vast majority of designs were excluded by the binary weighting operation, indicating that the resistance and inductance combination is difficult to meet with these inputs. The two antenna cores with the highest effective height will be considered the top two optimal antenna designs; their design parameters are listed in Table 7.1. These designs had at least double the effective height of the next closest designs for other core geometries, except for a close MN60 toroid design (which was surprising but not investigated further). Not surprisingly, the top two performing antennas were cores with large cross-sectional area and solidly ferrite, both important to having as high of an effective height as possible. Also, the optimum designs had short coils, which is intuitive for maximizing effective height as the external flux is peaked with a short coil, while internal flux (affecting coil inductance and ferrite loss) is minimal which then allows for more coil turns.

Table 7.1 – Design Example: Optimal ESL Design Parameters by Effective Height

Material	l_{core} (in)	d_{core} (in)	d_{hollow} (in)	Wire Type	l_{coil} (in)	n turns	n_l layers
MN60	12	1.75	0	#24 Stranded	2	60	1
MN60	12	1.5	0	#24 Stranded	2	60	1

It also worth presenting the weighted designs' effective height divided by mass, illustrating the concept of physical attributes having design importance. Again, it is difficult to present a concise plot, so the results will be described. The optimal effective height to mass ratio was exemplified by the smallest MN60 ferrite core which was also hollow: $l_{core} = 2.5\ in, d_{core} = 1\ in, d_{hollow} = 0.75\ in, \#24\ stranded\ wire, l_{coil} = 2.25\ in, n = 120, \& \ n_l = 1$. This illustrates that physical attributes such as mass or volume can add complexity to designing an optimal weighting function. It is also interesting to note that the optimal coil length was most of the length of the core, not a short coil; this underscores the difficulty in definitively stating a general optimal coil/core length ratio for magnetic cores.

The top two effective height designs of Table 7.1 were built and measured. Physically, the two antennas were practically the same except for diameter (1.5 vs. 1.75 inches); see Figure 7.2 for a photograph of one antenna with transmission line added to the antenna's wire leads (added after laboratory measurements). The ESLs' turns were close but less than 60 (56 and 58) and the coil lengths longer than 2 inches (2.5 and 2.44 inches) which implies that the wire diameter was larger than mistakenly input. Measured effective heights versus predicted are shown in Figure 7.3, resistance in Figure 7.4, and inductance in Figure 7.5; note that the predictions were re-run based on the actual prototype dimensions (only n & l_{coil} changed) but were close to that originally calculated.

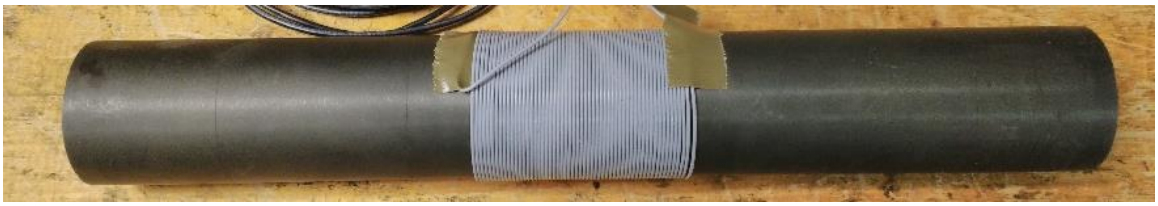

Figure 7.2 – Photo of 1.75-inch Diameter MN60 ESL for Design Example

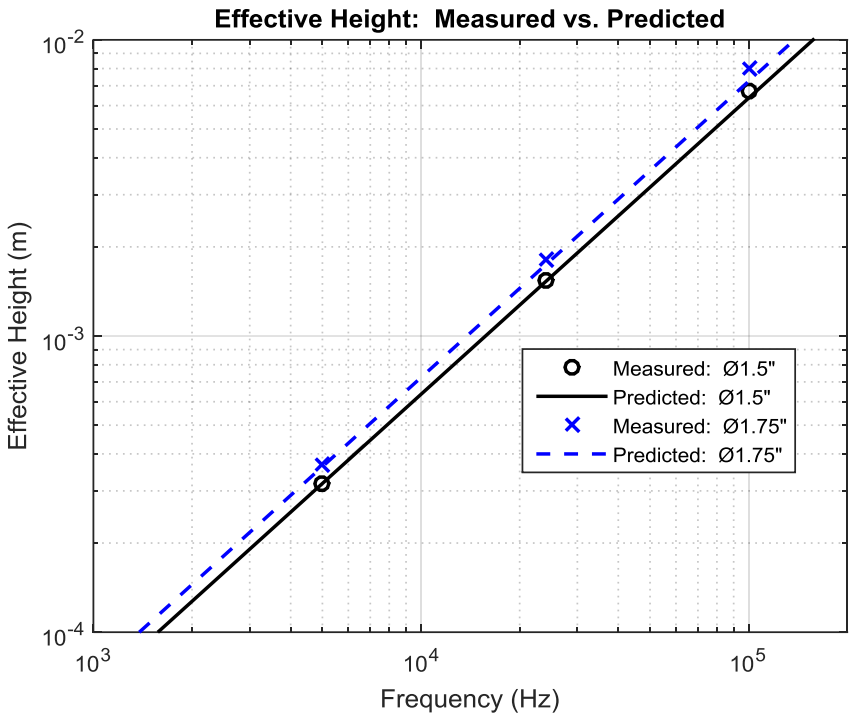

Figure 7.3 – Design Example: Measured vs. Predicted Effective Height

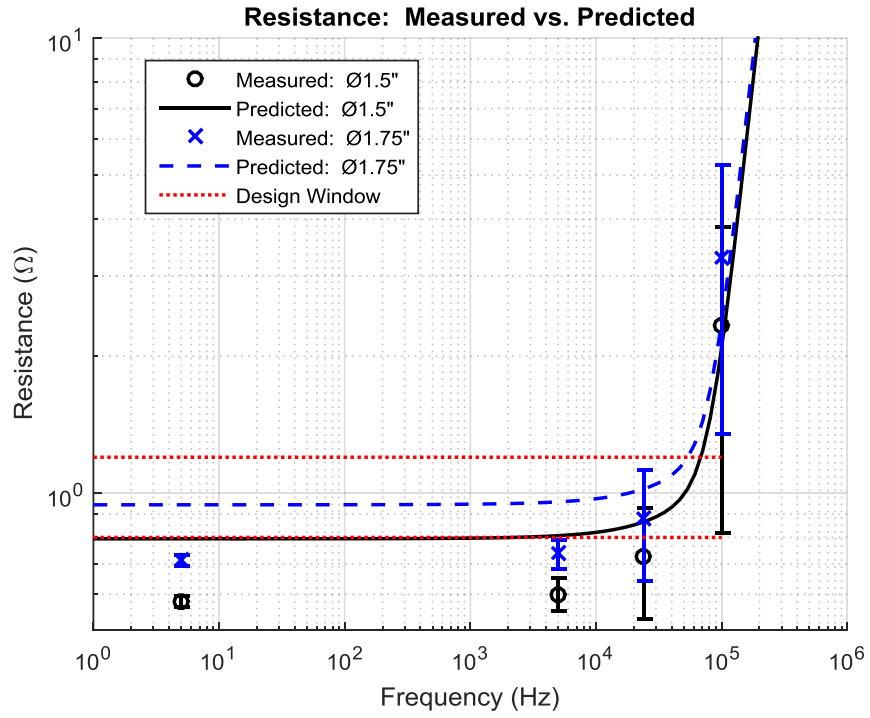

Figure 7.4 – Design Example: Measured Resistance vs. Predicted, Take 1

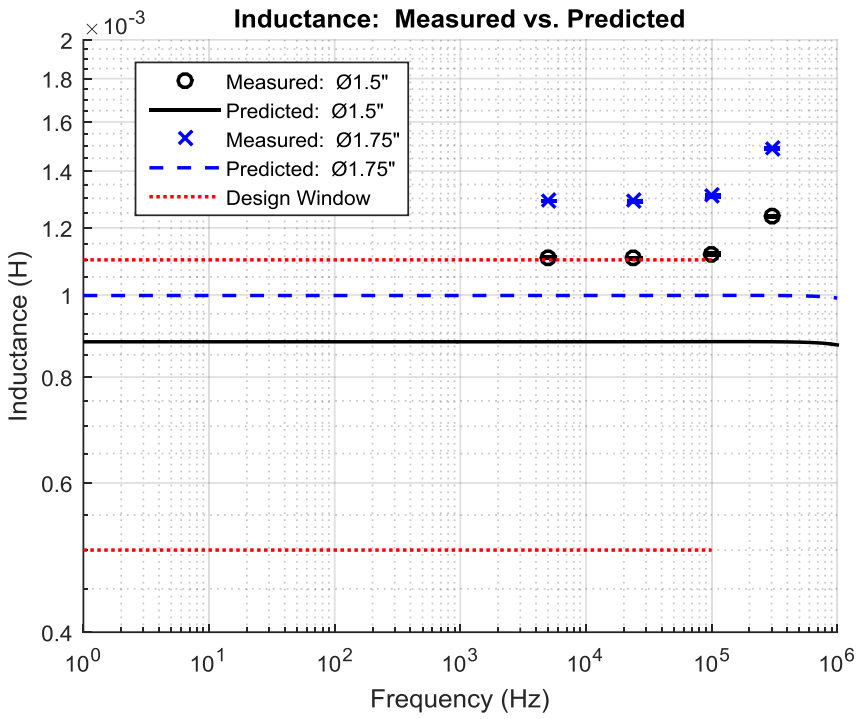

Figure 7.5– Design Example: Measured Inductance vs. Predicted, Take 1

As can be seen, the effective height predictions well matched measured, implying that the apparent and external permeabilities were calculated accurately. The resistance and inductance, however, have noticeable discrepancies between measured and predicted. At lower frequencies, DC wire resistance dominates, which after analysis showed that the input wire conductor's (bare) diameter was mistakenly input, which did not show up as clearly until such a long amount of wire was used. The measured inductance was higher than predicted, which can be traced to the calculated $\mu_{int,vol} \approx 0.95\mu_{int}$ being less than measured, partially due to using the first-order approximation of k_L for μ_{int}. Note that the increase in measured inductance at 300 kHz is due to parallel self-capacitance starting to become significant, as the measured SRFs were 820-917 kHz.

After fixing the wire physical parameters and choosing to instead use Smith's correction $\mu_{int}/\mu_{a,f}$ (for inductance), the resistance and inductance calculations were re-run—see Figure 7.6 and Figure 7.7. As can be seen, the predicted resistance now

reasonably matches measured. Predicted inductance is now closer to measured, but is still noticeably different. The latter is due to the same reason as the measured factor in Figure 4.7 varies vs. Smith's (discussed prior). Indeed, in that figure the measured factor at the same l_{coil}/l_{core} (0.2) is ~1.2 times Smith's, a similar proportion as for the measured vs. predicted inductance in Figure 7.6.

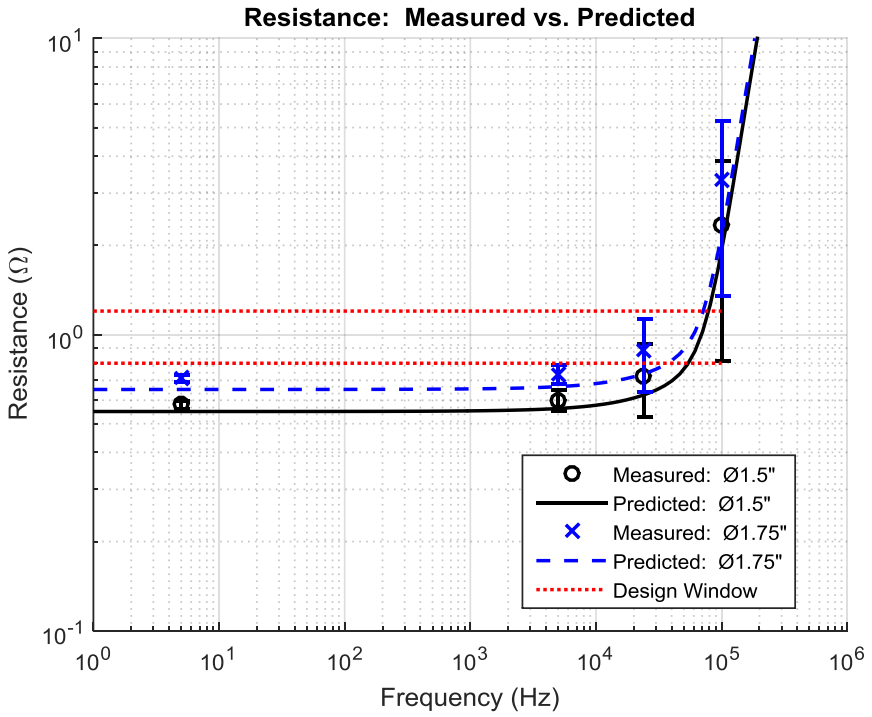

Figure 7.6 – Design Example: Measured Resistance vs. Predicted, Take 2

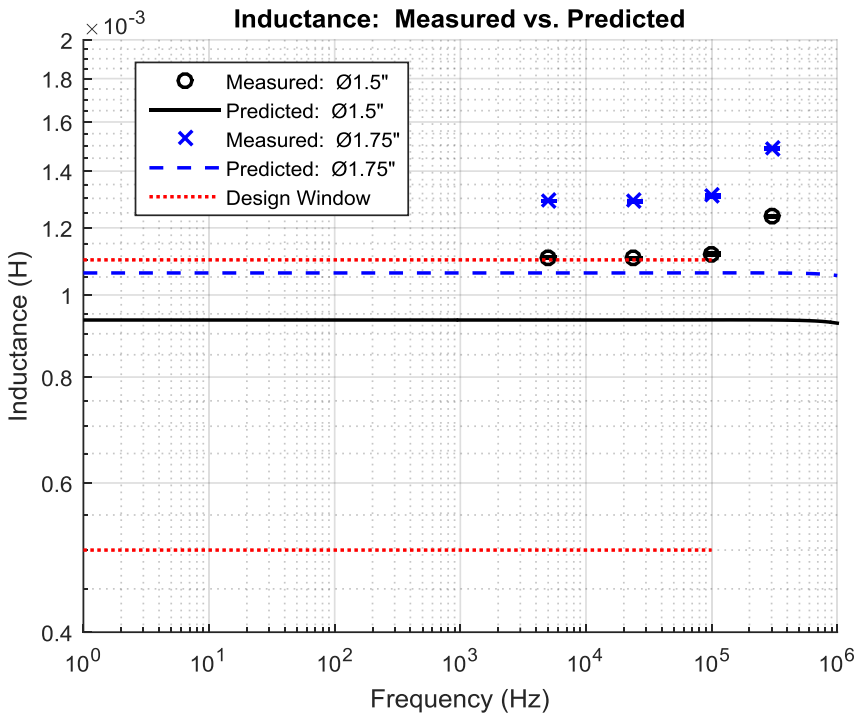

Figure 7.7 – Design Example: Measured Inductance vs. Predicted, Take 2

Next, the prototypes were tested in the field with the AWESOME receiver. For comparison, they were tested against a 2.6 meter (base) by 1.3 meter (height) isosceles triangle air-core loop. A plot of typical single-sided spectrums, taken over 10-second periods, is shown in Figure 7.8 for the three antennas. For more fidelity in analysis, a narrower spectrum is shown in Figure 7.9 with a sub-plot for each antenna; for convenience, the magnitudes are normalized to the air-core loop's peak at 24 kHz, which is the United States transmitting station "NAA" at Cutler, Maine. Although there is a two hour difference between measurements between measuring the ferrite-core antennas and the air-core (due to technical issues), data from a nearby site indicated negligible amplitude differences in the NAA signal (24 kHz) over the elapsed time period. The noise at such frequencies is typically dominated by atmospheric noise such as lightning, which can cause saturation for particular strong, nearby events. Because of that fact and the disparate times of measurement, quantitative SNR analysis is limited.

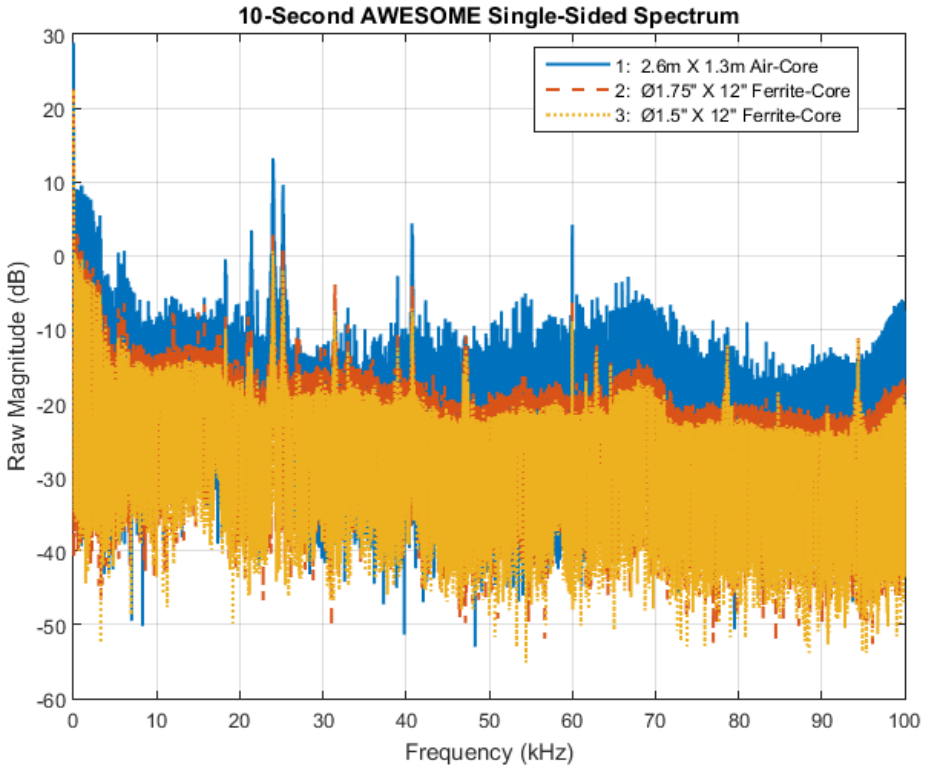

Figure 7.8 – Design Example: Measured Spectrum with AWESOME Receiver

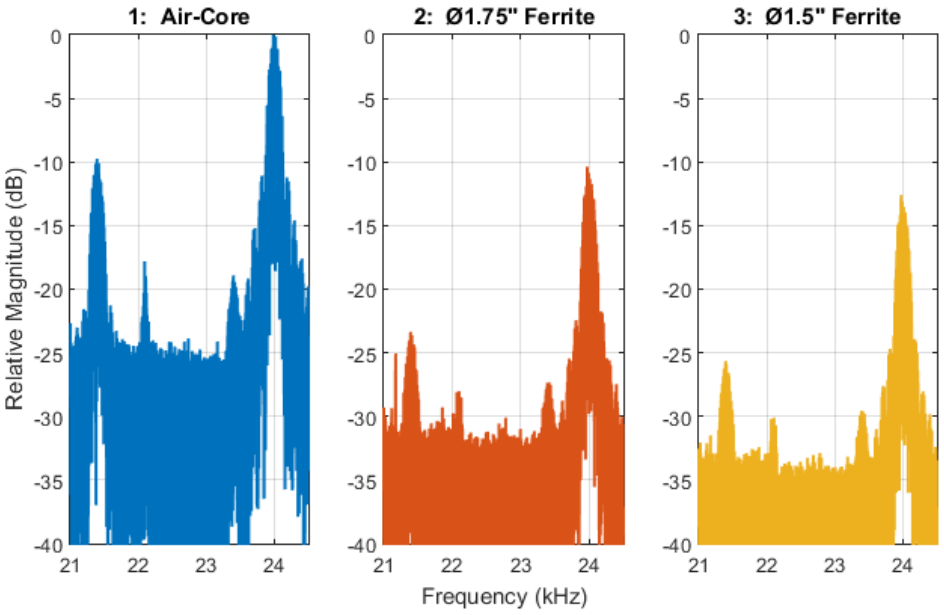

Figure 7.9 – Design Example: Measured Spectrum, Narrowed for Each Antenna

As expected, the spectrum plots show that the air-core loop greatly out-performed the ferrite-core designs as seen by the higher spectrum magnitudes—the air-core was more sensitive by 11 and 13 decibels, respectively, over the 1.75- and 1.5-inch diameter ferrite loops as seen by the relative peaks at 24 kHz. This can be primarily attributed to the significantly larger coil area of the air-core loop, against which the ferrite-cores still could not compete even including their effective permeability enhancement. The larger coil area of the 1.75-inch diameter prototype likewise allowed it to out-perform the smaller 1.5-inch, by approximately 2 decibels. Higher precision comparisons could be made using statistical signal processing, but without side-by-side testing (which was planned), the simple analysis here will suffice. An additional effect, though likely minor, would be differences due to the AWESOME receiver's impedance matching—which would favor the air-core loop as it has an impedance ($R = 0.99\ \Omega, L = 0.86\ mH$) closest to the AWESOME specification [Cohen 2016].

It is worth comparing the field measurement results to predicted. The sensitivity (see earlier in this chapter) of the air-core loop is predicted to be 15 decibels better than the 1.75-inch diameter ferrite-core, which is optimistic by 4 decibels over the field data but not necessarily unreasonable given the overall measurement uncertainty. The 1.75-inch diameter ferrite loop's sensitivity measured higher than the 1.5-inch diameter loop's by 1.4 decibels in the lab, which was similar to the approximate 2 decibels in field testing. Overall, this validates the AWESOME receiver results as reasonable.

For the example given here, the relatively-compact 1.75-inch diameter by 12-inch length ferrite-core loop can be used as a portable antenna as compared to an air-core loop with equivalent sensitivity. Example dimensions of such an air-core loop would be $d_{coil} = 0.5\ m\ (19.7\ inches), n = 19$ which corresponds to the conservative, predicted sensitivity difference of 15 decibels between the triangular air-core and 1.75-inch ferrite-core loop [Cohen 2016]. The example loop is one of many suggested for use with the

AWESOME receiver [Cohen 2016]. The ferrite-core loop would weigh approximately sixteen times more (2.3 kg vs. 0.14 kg) than the equivalent air-core loop as a trade-off.

From this design example, it has been shown that calculations can reasonably predict performance with some inaccuracy for magnetic-core inductance, validated by laboratory and measurements in the field. This design example has also illustrated general concepts for optimal design, such as large coil area being always preferred for better sensitivity and that magnetic cores can aid compact designs. Further, it was illustrated that when considering other parameters such as mass, a more efficient antenna might consider a hollow and shorter core. In general, the optimal coil/core length ratio can depend on the optimization weighting.

CHAPTER 8

MEASURED DATA AND CALCULATIONS

Measured and calculated data for various air- and Ceramics Magnetics, Inc. MN60 ferrite-core ESLs are presented and discussed in this chapter. The first section describes background measurement details for posterity. The following sections present measured and calculated results for rod ESLs and for toroid ESLs, along with discussion. See Figure 8.1 for a photo of some of the MN60 ferrite cores measured.

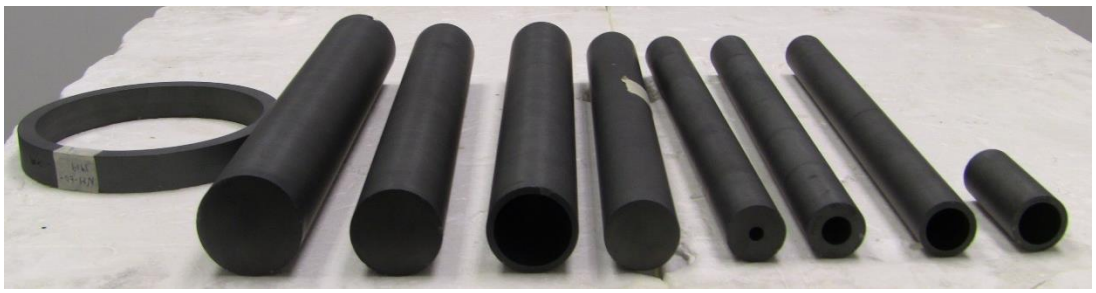

Figure 8.1 – Photo of Some MN60 Ferrite Cylindrical Cores Measured

Measurement Details

Air-cores used wood or polyethylene (PE). Rod cores were comprised of circular or square prisms, the latter represented in the following tables by their equivalent physical diameter. Wire used included #24 stranded and #26 magnet wire. Effective height measurements were made in a screen(ed) room to minimize interference using an Agilent 35670A Dynamic Signal Analyzer and a Stoddart 90114-3 (equivalent to AT-205/URM-6 except connector) 36-turn, 5.25-inch diameter air-core loop with electrostatic shield (see Figure 1.1 (right)). Notable settings chosen for the Agilent 35670A include: floating input low, DC input coupling, flat-top FFT analysis window, and 10 averages. Impedance measurements were made with an HP 4192A LF Impedance

Analyzer with a 16047C Test Fixture (0-13 MHz) and short/open compensation. Instruments were energized for at least 30 minutes prior to taking data to meet stated specification and were within U.S. Navy "METCAL" calibration.

Impedance and effective height measurements included lead wires, which were attempted to be factored out of any results presented herein and were sometimes negligible, but were added as a series resistance and inductance for predictions. Self-capacitance was measured using the self-resonant frequency and the two-capacitor methods as described in Chapter 1. Core and coil dimensions were not measured to high precision nor accuracy. Coil diameters were estimated as the minimum possible or estimated from measured wire length (minus leads), the latter being necessary for prisms wound with #24 stranded wire due to the coil not fitting tightly; for all other cases, the coil was wound reasonably tight upon the core.

Effective height measurements involve measuring the signal received $V_{in(meas)}$ on the connected antenna relative to that received on a reference (standard) antenna. Nominally, the analyzer's input impedance Z_{in} is infinite (or at least, infinitely greater than the connected antenna's impedance), but it is specified as 1 mega-ohm (not independently measured) for this instrument; note that there is no specified reactance due to using DC input coupling. There were some measured cases where the infinite impedance assumption might break down somewhat, so to be safe, a voltage divider effect is factored out using the known impedances to calculate the actual voltage on the antenna V_{ant}:

$$V_{ant} = V_{in(meas)} \left(\frac{Z_{in} + Z_{antenna}}{Z_{in}} \right) \ V$$

Measured Air- and Ferrite-Core Rod ESLs

This section presents measured and predicted data for air- and ferrite-core rod ESLs using an axial winding. Data includes physical dimensions, permeability, resistance, inductance, and capacitance. Some discussion of the data will be given and compared to theoretical predictions.

The following tables present the physical description of the various air- and ferrite-core ESL variations (Table 8.1); measured effective height, resistance, and inductance vs. frequency (Table 8.2); and measured and calculated permeability (at 5 kHz), SRF, coil self-capacitance (by SRF method and/or two-capacitor method), and estimated leads' capacitance (Table 8.3). In these tables, physical values are bolded to assist in demarcating changes between items. Note that effective volumetric external permeability $\mu_{vol,ext}$ was measured by comparing its effective height h_e to a calculated equivalent air-core; eff. vol. internal permeability $\mu_{vol,int}$ was measured by comparing its inductance L to that measured on the same-size air-core or a calculated air-core (which uses [Snow/Weaver] for predicted inductance). Thirty-seven axial builds were measured and one radial; while the radial is not examined further, the measured data is given here for posterity. Unfortunately, effective height measurements on the air-core (wood and PE) ESLs were not significantly above the background picked up by the cabling, invalidating their results and therefore are not presented. See Figure 1.1 (top) for a photo of an axial and Figure 8.2 for a radial ferrite-core ESL.

Figure 8.2 – Photo of Radial Ferrite-Core ESL

Table 8.1 – Physical Descriptions of Measured Rod ESLs

					Core Geometry (Effective Circular)					Coil Geometry			
#	Shape	Wind. Type	Wire Type	Core Mat'l	ID (in)	OD (in)	L (in)	$\frac{ID}{OD}$	$\frac{L}{OD}$	# Turns	# Layers	$\frac{d_{coil}}{d_{core}}$	$\frac{l_{coil}}{l_{core}}$
1	●	Axial	#24 str.	MN60	0	1.75	12	0	6.9	20	1	1.03	1.00
2	●	Axial	#24 str.	MN60	0	1.75	12	0	6.9	**58**	1	1.03	**0.21**
3	●	Axial	#24 str.	MN60	0	**1.5**	12	0	**8.0**	**20**	1	1.03	**1.00**
4	●	Axial	#24 str.	MN60	0	1.5	12	0	8.0	**56**	1	1.03	**0.20**
5	●	Axial	**#26**	MN60	0	1.5	12	0	8.0	**20**	1	1.01	**1.00**
6	○	Axial	**#24 str.**	MN60	**1.25**	1.5	12	**0.83**	8.0	20	1	1.03	1.00
7	●	Axial	#24 str.	MN60	**0**	**1.25**	12	**0**	**9.6**	20	1	1.04	1.00
8	●	Axial	**#26**	MN60	0	1.25	12	0	9.6	20	1	1.01	1.00
9	●	Axial	**#24 str.**	MN60	0	1.25	12	0	9.6	20	**2, rev**	1.05	1.00
10	●	Axial	#24 str.	MN60	0	1.25	12	0	9.6	20	**2, fly**	1.05	1.00
11	●	Axial	#24 str.	MN60	0	1.25	12	0	9.6	**10**	1	1.04	1.00
12	●	Axial	#24 str.	MN60	0	1.25	12	0	9.6	**20**	1	1.04	**0.92**
13	●	Axial	#24 str.	MN60	0	1.25	12	0	9.6	20	1	1.04	**0.83**
14	●	Axial	#24 str.	MN60	0	1.25	12	0	9.6	20	1	1.04	**0.67**
15	●	Axial	#24 str.	MN60	0	1.25	12	0	9.6	20	1	1.04	**0.50**
16	●	Axial	#24 str.	MN60	0	1.25	12	0	9.6	20	1	1.04	**0.33**
17	●	Axial	#24 str.	MN60	0	1.25	12	0	9.6	20	1	1.04	**0.17**
18	●	Axial	#24 str.	MN60	0	1.25	12	0	9.6	20	1	1.04	**0.08**
19	●	Axial	#24 str.	MN60	0	1.25	12	0	9.6	20	**2, rev**	1.05	0.08
20	●	Axial	#24 str.	MN60	0	1.25	12	0	9.6	20	**3, rev**	1.05	0.08
21	●	Axial	**#26**	**Wood**	0	1.25	12	0	9.6	20	**1**	1.01	**1.00**
22	□	Axial	**#24 str.**	**MN60**	**0.28**	**1.13**	**3**	**0.25**	**2.7**	20	1	1.22	1.00
23	□	Axial	#24 str.	MN60	0.28	1.13	**6**	0.25	**5.3**	20	1	1.22	1.00
24	□	Axial	#24 str.	MN60	0.28	1.13	**18**	0.25	**16.0**	20	1	1.22	1.00
25	□	Axial	**#26**	MN60	0.28	1.13	**18**	0.25	16.0	20	1	1.02	1.00
26	▫	Axial	**#24 str.**	**Wood**	0	1.13	**3**	**0**	**2.7**	20	1	1.22	1.00
27	▫	Axial	#24 str.	Wood	0	1.13	**6**	0	**5.3**	20	1	1.22	1.00
28	▫	Axial	#24 str.	Wood	0	1.13	**18**	0	**16.0**	20	1	1.22	1.00
29	▫	Axial	**#26**	Wood	0	1.13	**18**	0	16.0	20	1	1.02	1.00
30	●	Axial	#26	Wood	0	**1**	**12**	0	**12.0**	20	1	1.02	1.00
31	○	Axial	**#24 str.**	**MN60**	**0.25**	1	12	**0.25**	12.0	20	1	1.05	1.00
32	○	Axial	**#26**	MN60	0.25	1	12	0.25	12.0	20	1	1.02	1.00
33	○	Axial	**#24 str.**	MN60	**0.5**	1	12	**0.5**	12.0	20	1	1.05	1.00
34	○	Axial	#24 str.	MN60	**0.75**	1	12	**0.75**	12.0	20	1	1.05	1.00
35	○	Axial	#24 str.	MN60	0.75	1	**2.5**	0.75	**2.5**	20	1	1.05	1.00
36	○	Axial	#24 str.	MN60	**4.75**	**5.5**	**2.25**	**0.86**	**0.4**	20	1	1.01	1.00
37	●	Axial	**#26**	**PE**	**0**	**1.25**	**0.16**	**0**	**0.1**	**7**	1	1.01	1.00
38	○	**Radial**	**#24 str**.	**MN60**	**4.75**	**5.5**	**0.75**	**0.86**	**2.4**	**20**	1	1.01	**0.18**

Table 8.2 – Measured Rod ESLs' Eff. Height, Resistance, and Inductance

	Eff. Height (dB//m)			Series Resistance (Ω)					Series Inductance (μH)			
#	5 kHz	24 kHz	100 kHz	5 Hz	5 kHz	24 kHz	100 kHz	300 kHz	5 kHz	24 kHz	100 kHz	300 kHz
1	-80.0	-66.4	-54.6	0.268	0.274	0.281	0.419	2.431	76.5	76.3	76.5	77.0
2	-68.7	-54.8	-41.9	0.712	0.736	0.883	3.305	47.992	1290.9	1290.5	1310.2	1488.4
3	-81.2	-67.5	-55.7	0.238	0.243	0.245	0.332	1.979	65.8	65.7	65.8	66.1
4	-70.0	-56.2	-43.5	0.579	0.601	0.727	2.331	35.017	1106.6	1105.5	1118.9	1237.6
5	-81.0	-67.5	-55.9	0.388	0.391	0.400	0.485	2.164	65.9	65.8	65.9	66.4
6	-81.7	-67.9	-56.2	0.239	0.244	0.246	0.326	1.295	63.2	63.1	63.2	63.5
7	-81.8	-68.1	-56.6	0.204	0.209	0.211	0.298	2.131	63.2	63.1	63.2	63.5
8	-81.5	-67.9	-56.4	0.320	0.325	0.335	0.424	2.196	61.4	61.2	61.4	61.8
9	-81.6	-68.0	-56.5	0.204	0.208	0.209	0.296	2.143	64.2	64.1	64.2	64.5
10	-81.7	-68.1	-56.8	0.226	0.232	0.237	0.330	2.176	64.0	63.9	64.0	64.2
11	-88.0	-74.3	-62.6	0.112	0.115	0.117	0.140	0.588	16.4	16.4	16.4	16.4
12	-81.3	-67.8	-56.4	0.199	0.204	0.206	0.301	2.239	67.0	66.9	67.1	67.4
13	-81.1	-67.4	-56.0	0.199	0.205	0.207	0.308	2.511	75.9	75.8	75.9	76.3
14	-80.5	-66.8	-55.4	0.200	0.207	0.212	0.334	2.930	89.4	89.3	89.5	90.0
15	-80.0	-66.3	-54.8	0.187	0.196	0.201	0.336	3.242	102.4	101.9	102.0	102.6
16	-79.7	-66.1	-54.5	0.187	0.194	0.199	0.357	3.589	120.4	120.2	120.4	121.2
17	-79.6	-65.9	-54.3	0.186	0.194	0.201	0.373	3.848	141.5	141.4	141.6	142.6
18	-79.5	-65.8	-54.3	0.187	0.196	0.207	0.432	4.223	157.4	157.2	157.5	158.4
19	-79.5	-65.8	-54.1	0.187	0.195	0.205	0.428	4.197	156.1	155.8	156.1	157.5
20	-79.4	-65.8	-54.1	0.187	0.196	0.207	0.431	4.227	157.2	157.0	157.3	158.6
21				0.325	0.328	0.329	0.333	0.379	2.96	2.95	2.94	2.93
22	-97.1	-83.3	-71.8		0.185	0.189	0.217	0.421	39.0	38.9	38.8	38.8
23	-90.1	-76.5	-64.9	0.187	0.191	0.191	0.214	0.412	46.5	46.4	46.4	46.4
24	-77.4	-63.6	-52.0	0.208	0.214	0.219	0.274	1.076	69.4	69.3	69.3	69.6
25	-77.1	-63.5	-51.9	0.361	0.365	0.375	0.430	1.322	71.4	71.3	71.3	71.8
26				0.206	0.197	0.196	0.209	0.662	6.03	6.01	6.00	5.97
27				0.196	0.199	0.198	0.209	0.266	3.80	3.77	3.76	3.74
28				0.214	0.217	0.218	0.228	0.289	2.84	2.83	2.82	2.80
29				0.364	0.367	0.368	0.373	0.424	2.96	2.96	2.95	2.94
30				0.273	0.276	0.277	0.281	0.321	2.34	2.33	2.33	2.32
31	-83.5	-69.7	-58.0	0.163	0.167	0.170	0.238	1.354	51.7	51.6	51.7	52.1
32	-82.8	-69.5	-57.9	0.285	0.288	0.295	0.369	1.524	53.4	53.3	53.3	53.9
33	-83.5	-69.8	-58.0	0.162	0.167	0.169	0.249	1.335	51.6	51.5	51.6	52.0
34	-83.9	-70.2	-58.4	0.163	0.167	0.169	0.248	1.216	49.2	49.1	49.1	49.3
35	-100.0	-86.5	-74.8	0.147	0.150	0.153	0.210	0.539	34.4	34.3	34.2	34.1
36	-83.0	-69.4	-58.0	0.738	0.738	0.745	0.879	2.112	160.1	159.9	160.3	164.6
37				0.128	0.132	0.131	0.141	0.187	3.37	3.36	3.36	3.34
38	-84.9	-71.3	-59.7	0.530	0.533	0.536	0.695	2.140	151.1	151.0	151.0	151.3

Table 8.3 – Measured Rod ESLs' Permeability, SRF, and Capacitance

		Coil/Core Geometry				Rel. Permeability (5 kHz), Real								
#	Shape	$\frac{ID}{OD}$	$\frac{L}{OD}$	$\frac{l_{coil}}{l_{core}}$	n	Spec. μ_i	$\mu_{vol,ext}$ (h_e) Calc. // Air	$\mu_{vol,int}$ (L_{coil}) Meas. // Air	$\mu_{vol,int}$ (L_{coil}) Calc. // Air	Mean $\frac{\mu_{vol,ext}}{\mu_{ext}}$	SRF (MHz)	C_{self} from SRF (pF)	C_{self} from 2 Cap.'s (pF)	Est. C_{leads} (pF)
1	●	0	6.9	1.00	20	6500	29.1		18.6	0.95	3.65	425.0		0.50
2	●	0	6.9	**0.21**	**58**	6500	37.2		15.7	0.95	0.82	0.12		0.88
3	●	0	8.0	1.00	**20**	6500	34.4		20.1	0.94	4.40	358.6		0.52
4	●	0	8.0	**0.20**	**56**	6500	44.6		18.5	0.94	0.92	0.16		0.85
5	●	0	8.0	**1.00**	**20**	6500	36.5		19.7	0.98	3.53	550.7	0.50	0.45
6	○	**0.83**	8.0	1.00	20	6500	32.6		19.3	0.31	4.63	323.2		0.53
7	●	**0**	**9.6**	1.00	20	6500	45.7		24.9	0.93	4.39	451.9		0.52
8	●	0	9.6	1.00	20	6500	49.3	23.9	23.8	0.97	3.46	734.3	0.26	0.37
9	●	0	9.6	1.00	20	6500	45.8		24.9	0.91	4.86	374.0		0.40
10	●	0	9.6	1.00	20	6500	45.2		24.9	0.91	4.88	371.0		0.40
11	●	0	9.6	1.00	**10**	6500	44.7		13.8	0.93	11.10	141.2		0.40
12	●	0	9.6	**0.92**	**20**	6500	48.3		25.8	0.93	4.36	457.7		0.45
13	●	0	9.6	**0.83**	20	6500	49.8		28.4	0.93	4.20	477.8		0.48
14	●	0	9.6	**0.67**	20	6500	53.2		30.6	0.93	4.03	480.1		0.51
15	●	0	9.6	**0.50**	20	6500	56.2		30.4	0.93	3.98	448.1		0.34
16	●	0	9.6	**0.33**	20	6500	58.1		28.1	0.93	3.76	400.0		0.36
17	●	0	9.6	**0.17**	20	6500	59.2		20.7	0.93	3.49	297.8		0.41
18	●	0	9.6	**0.08**	20	6500	59.6		14.8	0.93	3.62	180.1		0.47
19	●	0	9.6	0.08	20	6500	58.4		14.4	0.91	3.04	250.8		0.45
20	●	0	9.6	0.08	20	6500	57.9		14.4	0.90	3.07	243.8		0.43
21	●	0	9.6	**1.00**	20	**1**			0.98	1			4.09	0.42
22	□	**0.25**	**2.7**	1.00	20	**6500**	6.95	6.72	6.70	0.67	12.10	29.1		0.35
23	□	0.25	**5.3**	1.00	20	6500	15.4	13.3	12.4	0.65	10.10	62.9		0.36
24	□	0.25	**16.0**	1.00	20	6500	67.2	28.8	26.9	0.63	7.42	154.8		0.49
25	□	0.25	16.0	1.00	20	6500	100.1	30.3	32.6	0.91	5.10	360.3	1.81	0.58
26	◘	**0**	**2.7**	1.00	20	**1**			0.99	1				0.38
27	◘	0	**5.3**	1.00	20	1			0.94	1				0.34
28	◘	0	**16.0**	1.00	20	1			0.90	1				0.50
29	◘	0	16.0	1.00	20	1			1.12	1			3.69	0.48
30	●	0	**12.0**	1.00	20	1			1.01	1			0.49	0.41
31	○	**0.25**	12.0	1.00	20	**6500**	57.9		27.4	0.86	5.78	348.1		0.40
32	○	0.25	12.0	1.00	20	6500	65.8	28.7	27.7	0.91	4.76	480.3	2.22	0.51
33	○	**0.5**	12.0	1.00	20	6500	57.9		27.3	0.69	5.58	372.0		0.42
34	○	**0.75**	12.0	1.00	20	6500	55.4		26.0	0.41	6.17	305.6		0.40
35	○	0.75	**2.5**	1.00	20	6500	8.65		8.52	0.48	7.71	102.6		0.31
36	○	**0.86**	**0.4**	1.00	20	6500	2.16		2.40	0.69	1.74	0.66		0.41
37	●	**0**	**0.1**	1.00	**7**	**1**			1.09	1				0.40

Some analysis can be made on the preceding data. Trends can be seen that validated concepts presented in earlier sections. For example, items 7 & 12-18 show that $\mu_{vol,ext}$ increases as $l_{coil}/l_{core} \to 0$. Another example is items 22-24, which differ in ferrite-core length and coil length (l_{coil}/l_{core} stayed constant) but clearly show the increasing effective permeabilities due to a higher core length/diameter ratio; self-capacitance also increased with coil length. A third example is seen in items 5-6 and 31/33/34, where the major difference varied in each set is the hollow diameter, showcasing that effective permeability slightly decreases as the core is increasingly hollow ($ID/OD \to 1$); the impact is much less than a linear proportionality. It can also be seen that the multi-layer winding style (reverse vs. fly-back) has no noticeable effect except that fly-back will have more wire length (and thusly more conductor resistance).

Continuing the analysis: items 7-11 have the same build except wire type, number of turns, and number of layers, with results that show that external effective permeability is practically equivalent, but the self-capacitance is not (higher for more turns, less for more coil layers, and less for thicker wire). Items 18-20 varied number of layers and, contrary to items 7-11, showed self-capacitance increased for having more than one layer—but this may be due to the relative differences in pitch, as items 7-11 had a coil length of 12 inches as compared to items 18-20's length of 1 inch. In general, the self-capacitance values determined from measuring the SRF (and extrapolating the ferrite-cores' relative permeability) varied distinctly from that measured by the two-capacitors method, likely due to the difference in actual permeability compared to extrapolated (assuming constant permittivity influence). The estimated leads' capacitance was often on the order of that measured from the two-capacitor method, which indicates that the leads' capacitance can be significant and should not be ignored.

Items 24-25 are interesting as they are the same build except for wire type and coil diameter; item 25's thinner wire allowed for a tight coil, which correspondingly

results in higher effective permeabilities. However, the resulting effective height is practically unchanged, as expected—it is taken care of by the volumetric averaging of the effective external permeability and free-space permeability as well as higher coil area (not shown). However, the inductance is affected, being higher for the tighter coil due to less leakage flux. The mean of predicted $\mu_{vol,ext}/\mu_{ext}$ is shown in Table 8.3 to demonstrate the effect of incorporated air volume for the built coil.

At first, the $\mu_{vol,int}$ values did not show as good of agreement between that measured relative to an air-core and to a calculated air-core. Investigation into the calculation revealed a difference in calculation methodology: that measured relative to an air-core simply divided the respective inductances, while that relative to a calculated air-core isolated coil external inductance from wire internal inductance and leads' external inductance (both modeled as in series with the coil external inductance). Upon further consideration, the coil external inductance should always be isolated—even though the wire internal inductance and leads' external inductance to be subtracted will typically have to be predicted. This approach is validated for the air-cores by noticing that their effective internal permeabilities (calculated air-core) are reasonably close to one; note that the predicted leads' external inductance can be similar in magnitude to the air-core's external coil inductance, so it is important to consider. It is further validated by the very good agreement between direct measurement and calculation for ferrite cores.

Calculated fluxmetric demagnetization factors (converted into apparent permeability and averaged volumetrically) from some of the references are compared versus measured fluxmetric apparent permeability (at 5 kHz) in Table 8.4. The measured apparent permeability was back-calculated from the core's measured effective vol. external permeability $\mu_{vol,ext}$ (see previous table) by assuming a coil/core length ratio effect as described and recommended in Chapter 4; such is neglected for the hollow spheroid per [Wait 1953; Simpson & Zhu 2006] for hollow cores measured (as the

hollow is already factored in the calculation). Values are presented as error/difference in units of decibels ($10\log_{10}()$). For convenience, any cell that does not match its reference's requisite assumptions is put into red text. The same approach is presented in Table 8.5 for magnetometric demagnetization factors as well as spheroidal (which also used a magnetometric basis for measured when calculating error, as $N_{ell} \approx N_{m\{rod\}}$ for the length/diameter ratios measured—see Chapter 4). Note that only ferrite cores are presented as the relative apparent permeability of an air-core is one. Further, the lowest error per row per table is bolded and italicized to foment comparison. Finally, the local toroidal factor of [Sandomirskii 2008] was converted to fluxmetric by means of [Primdahl et al. 2002], which is analyzed further in the following section for toroidal measurements; it is presented here merely for comparison.

Table 8.4 – Measured Rod ESLs' Flux. Apparent Permeability vs. Theoretical

	Core Geom.			Error: Theoretical // Measured Fluxmetric Apparent Permeability $\mu_{a,f}$ (dB)								
#	Shape	$\frac{ID}{OD}$	$\frac{L}{OD}$	Solid Cyl. [Poole 2004]	Solid Cyl., 2 < L/OD < 20 [Pettengill et al. 1977]	Solid Cyl. [Cross 2007]	Solid Cyl. [Chen et al. 2006]	Solid Rect. Prism [Chen et al. 2005]	N_{tor} -> N_i, Hollow Cyl, $\mu_i \to \infty$ [Sandomirskii 2008]	Hollow Cyl, 0.1 ≤ L/OD ≤ 8, 0.2 ≤ ID/OD ≤ 0.8 [Kobayashi & Iijima	Hollow Cyl,, L/OD ≥ 7 [Rosenblat's]	General, $\mu_i \to \infty$ [Rosenblat's]
1	●	0	6.9	-1.81	0.25	-0.31	-0.10	***0.00***	-15.97	-0.11	0.27	-0.18
2	●	0	6.9	-1.79	0.26	-0.30	-0.08	***0.02***	-15.96	-0.10	0.28	-0.16
3	●	0	**8.0**	-1.56	0.42	-0.15	***0.02***	0.10	-16.87	-0.04	0.23	-0.16
4	●	0	8.0	-1.55	0.42	-0.14	***0.02***	0.11	-16.86	-0.04	0.24	-0.16
5	●	0	8.0	-1.66	0.32	-0.25	-0.08	***0.00***	-16.80	-0.14	0.13	-0.26
6	○	**0.83**	8.0	-6.17	-4.31	-4.85	-4.69	-4.61	-15.74	-1.23	***0.44***	-4.86
7	●	**0**	**9.6**	-1.63	0.23	-0.32	-0.22	-0.14	-18.30	-1.37	***-0.11***	-0.46
8	●	0	9.6	-1.77	***0.09***	-0.46	-0.37	-0.28	-18.24	-1.51	-0.25	-0.60
9	●	0	9.6	-1.73	***0.13***	-0.43	-0.33	-0.24	-18.52	-1.48	-0.22	-0.56
10	●	0	9.6	-1.68	0.18	-0.38	-0.28	-0.19	-18.47	-1.43	***-0.17***	-0.51
11	●	0	9.6	-1.53	0.33	-0.22	-0.12	-0.04	-18.20	-1.27	***-0.01***	-0.36
12	●	0	9.6	-1.65	0.22	-0.34	-0.24	-0.16	-18.32	-1.39	***-0.13***	-0.47
13	●	0	9.6	-1.59	0.27	-0.28	-0.18	-0.10	-18.26	-1.33	***-0.07***	-0.42
14	●	0	9.6	-1.57	0.30	-0.26	-0.16	-0.08	-18.24	-1.31	***-0.05***	-0.39
15	●	0	9.6	-1.59	0.28	-0.28	-0.18	-0.10	-18.26	-1.33	***-0.07***	-0.41
16	●	0	9.6	-1.57	0.29	-0.26	-0.17	-0.08	-18.25	-1.31	***-0.05***	-0.40
17	●	0	9.6	-1.56	0.30	-0.25	-0.16	-0.07	-18.24	-1.30	***-0.04***	-0.39
18	●	0	9.6	-1.57	0.29	-0.26	-0.16	-0.08	-18.24	-1.31	***-0.05***	-0.40
19	●	0	9.6	-1.58	0.29	-0.27	-0.17	-0.09	-18.37	-1.32	***-0.06***	-0.41
20	●	0	9.6	-1.59	0.27	-0.28	-0.19	-0.10	-18.44	-1.33	***-0.07***	-0.42
22	□	**0.25**	**2.7**	-2.73	-1.04	-1.22	-0.43	-0.20	-7.86	***-0.08***	5.45	-0.94
23	□	0.25	**5.3**	-2.36	-0.28	-0.79	-0.52	-0.38	-12.76	***-0.22***	0.57	-1.74
24	□	0.25	**16**	-1.55	***-0.09***	-0.48	-0.43	-0.38	-20.00	-1.21	-0.26	-1.55
25	□	0.25	16	-1.69	***-0.22***	-0.62	-0.56	-0.51	-18.85	-1.35	-0.40	-1.69
31	○	**0.25**	**12**	-1.50	0.20	-0.31	-0.22	-0.14	-16.76	0.83	***0.03***	-0.54
32	○	0.25	12	-1.82	***-0.12***	-0.63	-0.54	-0.46	-16.94	0.51	-0.29	-0.86
33	○	**0.5**	12	-2.45	-0.76	-1.26	-1.18	-1.09	-1.04	-0.12	***0.03***	-1.50
34	○	**0.75**	12	-4.53	-2.86	-3.36	-3.27	-3.19	-17.26	-2.23	***0.19***	-3.59
35	○	0.75	**2.5**	-5.38	-3.93	-4.05	-3.27	-3.06	-8.98	***0.15***	7.38	0.57
36	○	**0.86**	**0.4**	-2.96	-5.32	-3.56	-2.40		-3.53	***-0.34***		-5.09

Table 8.5 – Measured Rod ESLs' Magnet. Apparent Permeability vs. Theoretical

	Core Geom.			Error: Theoretical // Measured Magnetometric Apparent Permeability $\mu_{a,m}$ (dB)									
#	Shape	$\frac{ID}{OD}$	$\frac{L}{OD}$	Solid Cyl., $\mu_i \to \infty$, L >> D [Chen et al. 2002]	Solid Cyl., $\mu_i > 1000$, L >> D [Macintyre 1999]	Solid Cyl. [Chen et al. 2006]	Solid Cyl. [Poole 2004]	Hollow Cyl., L $\to \infty$ [Prat-Camps et al. 2012]	Rect. Prism [Chen et al. 2005]	Prolate Spheroid [Wait 1953; Simpson & Zhu 2006]	Hollow Prolate Spheroid [Wait 1953; Simpson 2008]	Spheroid [Bozorth & Chapin 1942; Chen et al. 2002]	General, $\mu_i \to \infty$, mod. Rosenblat's [Musmann & Afanassiev 2010]
1	●	0	6.9	0.18	0.98	-0.10	-1.74	23.27	***0.00***	-0.39	-0.39	-0.39	-1.42
2	●	0	6.9	0.20	0.99	-0.08	-1.73	23.29	***0.02***	-0.38	-0.38	-0.38	-1.40
3	●	0	**8.0**	0.12	1.09	***0.02***	-1.45	22.51	0.10	-0.18	-0.18	-0.18	-1.40
4	●	0	8.0	0.13	1.10	***0.02***	-1.44	22.51	0.10	-0.17	-0.17	-0.17	-1.40
5	●	0	8.0	0.02	1.00	-0.08	-1.54	22.42	***0.00***	-0.27	-0.27	-0.27	-1.50
6	○	**0.83**	8.0	-4.53	-3.61	-4.62	-5.98	-14.62	-4.55	-4.81	***0.00***	-4.81	-6.03
7	●	**0**	**9.6**	-0.24	0.90	-0.22	-1.46	21.22	***-0.11***	-0.27	-0.27	-0.27	-1.70
8	●	0	9.6	-0.38	0.76	-0.37	-1.60	21.09	***-0.25***	-0.42	-0.42	-0.42	-1.84
9	●	0	9.6	-0.34	0.80	-0.33	-1.56	21.12	***-0.21***	-0.38	-0.38	-0.38	-1.80
10	●	0	9.6	-0.29	0.85	-0.28	-1.51	21.17	***-0.16***	-0.33	-0.33	-0.33	-1.75
11	●	0	9.6	-0.14	1.00	-0.12	-1.36	21.32	***-0.01***	-0.17	-0.17	-0.17	-1.60
12	●	0	9.6	-0.25	0.88	-0.24	-1.48	21.21	***-0.13***	-0.29	-0.29	-0.29	-1.71
13	●	0	9.6	-0.20	0.94	-0.18	-1.42	21.26	***-0.07***	-0.23	-0.23	-0.23	-1.66
14	●	0	9.6	-0.17	0.96	-0.16	-1.40	21.29	***-0.05***	-0.21	-0.21	-0.21	-1.63
15	●	0	9.6	-0.19	0.94	-0.18	-1.42	21.27	***-0.07***	-0.23	-0.23	-0.23	-1.65
16	●	0	9.6	-0.18	0.96	-0.16	-1.40	21.28	***-0.05***	-0.22	-0.22	-0.22	-1.64
17	●	0	9.6	-0.17	0.97	-0.15	-1.39	21.29	***-0.04***	-0.21	-0.21	-0.21	-1.63
18	●	0	9.6	-0.17	0.96	-0.16	-1.40	21.29	***-0.05***	-0.21	-0.21	-0.21	-1.64
19	●	0	9.6	-0.18	0.95	-0.17	-1.41	21.28	***-0.06***	-0.22	-0.22	-0.22	-1.64
20	●	0	9.6	-0.20	0.94	-0.18	-1.42	21.26	***-0.07***	-0.23	-0.23	-0.23	-1.66
22	□	**0.25**	**2.7**	11.32	2.23	-0.39	-2.97	1.75	***-0.16***	-1.13	-0.90	-1.13	-2.11
23	□	0.25	**5.3**	***0.33***	0.68	-0.49	-2.35	-1.72	-0.35	-0.89	-0.63	-0.89	-2.94
24	□	0.25	**16.0**	-0.64	0.78	-0.42	-1.26	-8.11	-0.35	-0.22	***0.05***	-0.22	-2.77
25	□	0.25	16.0	-0.78	0.64	-0.56	-1.40	-8.36	-0.49	-0.36	***-0.09***	-0.36	-2.92
31	○	0.25	**12.0**	-0.37	0.92	-0.22	-1.27	-6.21	-0.11	-0.17	***0.10***	-0.17	-1.78
32	○	0.25	12.0	-0.69	0.60	-0.54	-1.60	-6.55	-0.43	-0.49	***-0.22***	-0.49	-2.10
33	○	**0.5**	12.0	-1.32	***-0.04***	-1.17	-2.22	-12.77	-1.06	-1.12	0.09	-1.12	-2.72
34	○	**0.75**	12.0	-3.39	-2.13	-3.24	-4.28	-16.26	-3.14	-3.20	***0.25***	-3.20	-4.80
35	○	0.75	**2.5**	8.02	***-0.37***	-3.15	-5.49	-8.19	-2.96	-3.85	-1.01	-3.85	-0.60
36	○	**0.86**	**0.4**	-4.69	-4.80	***-2.21***	-3.19	-2.99		-3.53	-4.13	-2.63	-5.05

Some conclusions can be drawn from Table 8.4 and Table 8.5. For cylinders and rectangular prisms which were mostly solid ($ID/OD \leq 0.25$), the best overall reference was the numerical tables for a solid rectangular prism in [Chen et al. 2005]—though solid cylinders per [Chen et al. 2006] were reasonably close. For hollow cores, [Kobayashi and Iijima 1996] is excellent when their assumptions are met and even for $ID/OD < 0.2$. Otherwise, Rosenblat's for a hollow cylinder is excellent for either solid or hollow (when its assumptions are met)—which is remarkable for a relatively-simple equation (but only for infinite permeability)—as is the hollow prolate spheroid for $L/OD \geq 6.9$ (which is understandable as generally, an ellipsoid is only a good approximation of a cylinder for $l_{core} \gg d_{core}$). The solid prolate spheroid factors are further remarkable (note that Wait's calculates equivalently as Simpson's) in that they are equivalent to that of a simple spheroid (by Bozorth/Chapin or Chen et al.) for very high initial permeability, validating the former's complex math. Some of the other approaches are also very good, with the equation of [Cross 2007] reasonably tracking the numerical tables of [Chen et al. 2006] for solid cylinders. The conversion of local toroidal of [Sandomirskii 2008] to fluxmetric by means of [Primdahl et al. 2002] is terrible, and as seen later in the section on toroidal data, shows that the simple conversion approach is not accurate.

Also validated is the conversion of square prisms to equivalent-diameter cylinders, seen by the close agreement between theoretical for cylinder or prism. Conversion between fluxmetric and magnetometric using the recommended parabolic fit approach in Chapter 4 is validated by the close agreement between theoretical for converting the measured apparent permeability to fluxmetric or magnetometric. Note that the modified Rosenblat's for general shapes per [Musmann & Afanassiev 2010] modifies Rosenblat's per their parabolic fit approach to coil distribution, which is not intended for full-length (magnetometric) coils—hence their notable errors in Table 8.5. Finally, using the magnetometric basis for prolate spheroids was validated.

Calculated inductance values are compared to measured in the following two tables in order to compare sixteen theoretical approaches for rings and solenoids from references. The measured volumetric effective internal permeability $\mu_{vol,int}$ (see Table 8.3) was used for the ferrite cores and a relative permeability of one used for air-cores; items which had their effective internal permeability derived relative to a calculated air-core would be biased towards the reference used to calculate it and so will not presented below. Values are presented as error/difference in units of decibels ($10\log_{10}()$) relative to the measured inductance at 5 kHz. For convenience, the lowest error per row is bolded and italicized. Also for convenience, any cell that does not match its reference's requisite assumptions is put into red text. Note that some of the solenoids are presented both un-corrected as a current-sheet (CS) solenoid and some corrected (Corr.) for round wire.

Table 8.6 – Measured Rod ESLs' Inductance vs. Theoretical, Part 1

	Coil Geometry				Error: Theoretical // Measured Inductance (dB)							
#	Shape	l_{coil} (in)	n	n_l	Thin Ring, $r_{coil} \gg r_{cond}$, l_{coil} & $t_{coil} \to 0$, Elliptical	Thin Ring, $r_{coil} \gg r_{cond}$, l_{coil} & $t_{coil} \to 0$, Log.	Wheeler, Corr. Solenoid, $l_{coil} > 0.4d_{coil}$ [Kazimierczuk 2014]	Corr. Sol. [Knight]/[Rosa]	CS Sol., $l_{coil} \gg d_{coil}$, $\pi d_{coil} \gg p$, $r_{cond} \to 0$ [Kazimierczuk 2014]	CS Sol., $l_{coil} \gg d_{coil}$, $d_{cond} \gg \delta_{cond}$, $r_{cond} \to 0$ [Kazimierczuk 2014]	CS Sol. [Knight]/ Rosa/Weaver]	Corr. Sol. [Knight/Rosa/Weaver]
8	●	12	20	1	11.05	11.40	-0.49	-0.57	-2.89	-2.89	-3.08	-0.48
21	●	12	20	1	11.12	11.47	-0.42	-0.50	-2.82	-2.82	-3.01	-0.41
22	□	**3**	20	1	7.76	8.13	-0.08	-0.10	0.44	0.44	-0.36	-0.07
23	□	**6**	20	1	9.94	10.31	0.12	0.10	-0.39	-0.39	-0.80	0.13
24	□	**18**	20	1	11.56	11.93	-0.33	-0.47	-3.54	-3.53	-3.67	-0.33
25	□	18	20	1	10.79	11.15	-1.31	-1.48	-5.24	-5.24	-5.35	-1.31
26	▫	**3**	20	1	7.76	8.13	-0.08	-0.10	0.44	0.44	-0.36	-0.07
27	▫	**6**	20	1	9.92	10.29	0.10	0.08	-0.41	-0.41	-0.82	0.11
28	▫	**18**	20	1	11.57	11.94	-0.32	-0.46	-3.53	-3.53	-3.67	-0.32
29	▫	18	20	1	10.63	10.99	-1.47	-1.65	-5.40	-5.40	-5.52	-1.47
30	●	**12**	20	1	11.08	11.45	-0.69	-0.81	-3.57	-3.57	-3.73	-0.69
32	○	12	20	1	11.26	11.63	-0.51	-0.63	-3.39	-3.39	-3.55	-0.51
37	●	**0.16**	**7**	1	1.14	1.49	-0.81	-0.40	6.02	6.02	-0.26	-0.43

Table 8.7 – Measured Rod ESLs' Inductance vs. Theoretical, Part 2

	Coil Geometry				Error: Theoretical // Measured Inductance (dB)							
#	Shape	l_{coil} (in)	n	n_l	Solenoid [Snow/Weaver]	Square CS Sol. [Niwa/Grover/Wheeler]	Corr. Square Sol., [Niwa/Grover/Wheeler]	Corr. Rect. Sol., [Ishida et al. 2010]	$6r_{coil} \approx 9l_{coil} \approx 10t_{coil}$, $n_l > 1$ [Wheeler 1928]	CS Sol., $n_l > 1$ [Kazimierczuk 2014]	Corr. Sol., $n_l > 1$, non-helical [Rosa 1907]	Corr. Sol., $n_l > 1$, non-helical, $l_{coil} \leq 2d_{coil}$ [Weinstein's]
8	●	12	20	1	***-0.07***	-3.19	-1.53	-1.53	-3.57	-0.51	2.84	13.96
21	●	12	20	1	***-0.01***	-3.13	-1.46	-1.46	-3.50	-0.44	2.91	14.03
22	□	**3**	20	1	***0.03***	-1.95	-1.75	-1.76	-0.73	-0.13	3.27	0.40
23	□	**6**	20	1	0.30	-2.46	-1.81	-1.81	-1.25	***0.08***	3.65	-8.49
24	□	**18**	20	1	***0.31***	-5.39	-2.85	-2.85	-4.17	-0.35	1.94	18.96
25	□	18	20	1	***-0.51***	-5.48	-2.73	-2.73	-5.86	-1.33	1.37	20.35
26	▫	**3**	20	1	***0.03***	-1.95	-1.75	-1.76	-0.73	-0.13	3.27	0.40
27	▫	**6**	20	1	0.28	-2.48	-1.83	-1.84	-1.27	***0.06***	3.63	-8.52
28	▫	**18**	20	1	***0.31***	-5.38	-2.84	-2.84	-4.16	-0.35	1.95	18.96
29	▫	18	20	1	***-0.68***	-5.65	-2.90	-2.90	-6.02	-1.49	1.21	20.18
30	●	**12**	20	1	***-0.13***	-3.87	-1.88	-1.88	-4.22	-0.72	3.11	17.19
32	○	12	20	1	***0.05***	-3.69	-1.70	-1.71	-4.04	-0.54	3.29	17.37
37	●	**0.16**	**7**	1	-0.34	***-0.18***	-0.27	-0.27	-0.30	-0.90	7.81	-0.30

Some conclusions can be drawn from the results of Table 8.6 and Table 8.7. Most noticeably, the thin-ring approximations are not good for any of these geometries, underscoring why a solenoidal approach should be used. The best overall theoretical approaches is clearly [Snow/Weaver] followed by [Knight/Rosa/Weaver] (Corr. Sol.), valid for all cases but sometimes with significant error (e.g. $-0.68\ dB = -14\%$). It can be seen that the round-wire correction for solenoids can sometimes be significant (up to several decibels) and should not be neglected. For square air-core solenoids, [Niwa/Grover/Wheeler] (Corr.) (or equivalently, Ishida et al.) was worse than using the equivalent circular solenoid by [Snow/Weaver], the error primarily being attributable to the round wire correction. Some other references were reasonable (within their

assumptions), but we conclude that [Snow/Weaver] should be used as it has no known limitations except for the caveat of some complexity (requiring a computer).

It is likely that some of the general error is a result of the physical build of a coil: looking at Figure 1.1 (top), it can be seen that the coil pitch is not uniform, despite positing such as an assumption. This is because the coils were built by hand without significant attention given to constant pitch, and the coils sometimes moved slightly as they were not fully constrained. Supporting this, it can be seen that the calculated errors tend toward zero as $l_{coil} \to 0$, where the pitch would be closer to uniform as $p \to 0$; item 37 is an exception. Again, no precise physical measurements (e.g. d_{coil}) were made.

Although calculated errors are not shown for ferrite cores whose internal permeability was derived from a calculated air-core (using [Snow/Weaver]), some relative analysis was made and can be described. For multi-layer solenoids, Weinstein's is very close to [Snow/Weaver]—within 0.04 dB—when the very-limiting assumptions were met (only items 19-20); small errors are seen in items 26 & 37 in Table 8.7 as they approach the required assumptions. Otherwise, single- and multi-layer approaches were interchangeable as coil thickness was kept thin. Note that winding pitch p was herein calculated only using the coil length l_{coil} and number of turns n, without regard for number of layers n_l; this caused no noticeable errors.

Calculated self-capacitance values are presented in the following tables, single-layer in Table 8.8 and multi-layer in Table 8.9. For convenience, the closest calculation to measured is bolded and italicized per row and per single-/multi-layer section; the closest amongst both sections is underlined per row. The measured capacitance used for comparison is the minimum of the self-capacitance as calculated from measured SRF and that measured from the two-capacitor method, where data for both exist. Also for convenience, any cell that does not match its reference's requisite assumptions is put into red text. Empty cells were due to non-number values.

Table 8.8 – Measured Rod ESLs' Theoretical Self-Capacitance, Single-Layer

	Core & Coil Geometry					Meas. and Est. C (pF)			Theoretical C_{self} (pF)						
#	Shape	d_{core} (in)	n	n_l	l_{coil} (in)	C_{self} from SRF	C_{self} from 2 Cap.'s	Est. C_{leads}	Air-core, no shield [Medhurst 1947b]	#1, Non-Cond. Core [Kazimierczuk 2014]	#2, Non-Cond. Core [Kazimierczuk 2014]	Semi-empirical, L >> D [Knight 2013c]	Electrode [Knight 2013c]	Solid Prolate Spheroid [Simpson and Zhu 2007]	Hollow Prolate Spheroid [Simpson 2008]
1	●	1.75	20	1	12	425.0			***4.27***	0.05	2.86	28,400	0.64	1.24	
2	●	1.75	**58**	1	**2.5**	0.12		0.88	2.12	***0.08***	116	40,700	0.85	1.24	
3	●	**1.5**	**20**	1	**12**	358.6		0.50	***4.13***	0.04	2.47	23,900	0.55	1.14	
4	●	1.5	**56**	1	**2.44**	0.16		0.85	1.85	***0.06***	95.1	33,800	0.73	1.14	
5	●	1.5	**20**	1	**12**	550.7	0.50	0.45	4.11	0.04	1.79	23,500	***0.47***	1.14	
6	○	1.5	20	1	12	323.2		0.52	***4.13***	0.04	2.47	23,900	0.55	1.14	1.14
7	●	**1.25**	20	1	12	451.9		0.50	***3.99***	0.04	2.07	19,600	0.46	1.04	
8	●	1.25	20	1	12	734.3	0.26	0.37	3.97	0.03	1.5	19,200	***0.39***	1.04	
9	●	1.25	20	**2, rev**	12	374.0		0.39	***4***	0.04	2.09	19,900	0.46	1.04	
10	●	1.25	20	**2, fly**	12	371.0		0.39	***4***	0.04	2.09	19,900	0.46	1.04	
11	●	1.25	**10**	1	12	141.2		0.39	***3.99***	0.07	0.52	20,900	0.46	1.04	
12	●	1.25	**20**	1	**11**	457.7		0.43	***3.71***	0.04	2.25	19,800	0.46	1.04	
13	●	1.25	20	1	**10**	477.8		0.47	***3.44***	0.04	2.48	20,100	0.47	1.04	
14	●	1.25	20	1	**8**	480.1		0.49	2.91	0.04	***3.1***	20,800	0.49	1.04	
15	●	1.25	20	1	**6**	448.1		0.33	2.39	0.05	***4.13***	21,900	0.52	1.04	
16	●	1.25	20	1	**4**	400.0		0.35	1.91	0.05	***6.2***	23,800	0.56	1.04	
17	●	1.25	20	1	**2**	297.8		0.39	1.55	0.07	***12.4***	28,500	0.64	1.04	
18	●	1.25	20	1	**1**	180.1		0.45	1.56	0.12	***24.8***	35,500	0.76	1.04	
19	●	1.25	20	**2, rev**	1	250.8		0.43	1.58	0.12	***25.1***	36,100	0.77	1.04	
20	●	1.25	20	**3, rev**	1	243.8		0.41	1.59	0.12	***25.2***	36,400	0.77	1.04	
21	●	1.25	20	**1**	**12**		4.09	0.42	***3.97***	0.03	1.5	4.47	0.39	1.04	
22	□	**1.13**	20	1	**3**	29.1		0.33	1.78	0.06	***8.8***	27,700	0.63	0.59	0.6
23	□	1.13	20	1	**6**	62.9		0.35	2.45	0.05	***4.4***	23,600	0.55	0.72	0.72
24	□	1.13	20	1	**18**	154.8		0.48	***5.69***	0.04	1.47	20,300	0.46	1.25	1.25
25	□	1.13	20	1	18	360.3	1.81	0.58	5.58	0.03	0.9	16,700	0.33	1.25	***1.25***
26	◘	1.13	20	1	**3**			0.36	1.78	0.06	8.8	2.24	0.63	0.59	
27	◘	1.13	20	1	**6**			0.33	2.45	0.05	***4.4***	2.91	0.55	0.72	
28	◘	1.13	20	1	**18**			0.49	5.69	0.04	1.47	***6.39***	0.46	1.25	
29	◘	1.13	20	1	18		3.69	0.48	***5.58***	0.03	0.9	6.31	0.33	1.25	
30	●	**1**	20	1	**12**		0.49	0.41	3.84	0.03	1.2	4.31	***0.31***	0.94	
31	○	1	20	1	12	348.1		0.39	***3.86***	0.03	1.67	15,500	0.37	0.94	0.94
32	○	1	20	1	12	480.3	2.22	0.51	3.84	0.03	***1.2***	15,100	0.31	0.94	0.94
33	○	1	20	1	12	372.0		0.40	***3.86***	0.03	1.67	15,500	0.37	0.94	0.94
34	○	1	20	1	12	305.6		0.39	***3.86***	0.03	1.67	15,500	0.37	0.94	0.94
35	○	1	20	1	**2.5**	102.6		0.30	1.39	0.05	***8***	20,500	0.49	0.52	0.52
36	○	**5.5**	20	1	**2.3**	0.66		0.40	7.74	***0.28***	47.2	194,000	2.67	1.91	-0.4
37	●	**1.25**	**7**	1	**0.2**			0.40	2.77	0.56	14	2.53	0.97	1.04	

Table 8.9 – Measured Rod ESLs' Theoretical Self-Capacitance, Multi-Layer

	Core & Coil Geometry					Meas. and Est. C (pF)			Theoretical C_{self} (pF)						
#	Shape	d_{core} (in)	n	n_l	l_{coil} (in)	C_{self} from SRF	C_{self} from 2 Cap. 's	Est. C_{leads}	#1, $n_l = 2$, $n \geq 10$, Non-Cond. Core Kazimierczuk 2014]	#2, $n_l = 2$, $n \geq 10$, Non-Cond. Core [Kazimierczuk 2014]	#1, $n_l = 2/3$, $n \geq 10$, Cond. Core/Shield [Kazimierczuk 2014]	#2, $n_l = 2/3$, $n \geq 10$, Cond. Core/Shield [Kazimierczuk 2014]	Multi-Layer [Macintyre 1999]	Multi-Layer [Biela and Kolar 2008]	Multi-Layer [Coillot and Leroy 2011]
1	●	1.75	20	1	12	425.0		0.49	1.54	-6.06				***52.8***	
2	●	1.75	**58**	1	**2.5**	0.12		0.88	***1.54***	-1.26				152	
3	●	**1.5**	**20**	1	**12**	358.6		0.50	1.32	-6.06				***45.6***	
4	●	1.5	**56**	1	**2.4**	0.16		0.85	***1.32***	-1.23				127	
5	●	1.5	**20**	1	**12**	550.7	0.50	0.45	***7.87***	83.7				117	
6	○	1.5	20	1	12	323.2		0.52	1.32	-6.06				***45.6***	
7	●	**1.25**	20	1	12	451.9		0.50	1.11	-6.06				***38.3***	
8	●	1.25	20	1	12	734.3	0.26	0.37	***6.57***	83.7				97.9	
9	●	1.25	20	**2, rev**	12	374.0		0.39	1.12	-6.06	1.27	-6.86	***463***	32.2	1,220
10	●	1.25	20	**2, fly**	12	371.0		0.39	1.12	-6.06	1.27	-6.86	***463***	32.2	1,220
11	●	1.25	**10**	1	12	141.2		0.39	1.11	-6.06				***19.8***	
12	●	1.25	**20**	1	**11**	457.7		0.43	1.11	-5.56				***38.3***	
13	●	1.25	20	1	**10**	477.8		0.47	1.11	-5.05				***38.2***	
14	●	1.25	20	1	**8**	480.1		0.49	1.11	-4.04				***38.1***	
15	●	1.25	20	1	**6**	448.1		0.33	1.11	-3.03				***38***	
16	●	1.25	20	1	**4**	400.0		0.35	1.11	-2.02				***38***	
17	●	1.25	20	1	**2**	297.8		0.39	1.11	-1.01				***37.9***	
18	●	1.25	20	1	**1**	180.1		0.45	1.11	-0.51				***37.9***	
19	●	1.25	20	**2, rev**	1	250.8		0.43	1.12	-0.51	1.27	-0.57	38.6	31.9	***101***
20	●	1.25	20	**3, rev**	1	243.8		0.41	1.13	-0.51	0.4	-0.18	34.5	29.9	***53.2***
21	●	1.25	20	**1**	**12**		4.09	0.42	***6.57***	83.7				97.9	
22	□	**1.13**	20	1	**3**	29.1		0.33	1.18	-1.52				***40.4***	
23	□	1.13	20	1	**6**	62.9		0.35	1.18	-3.03				***40.5***	
24	□	1.13	20	1	**18**	154.8		0.48	1.18	-9.09				***41.2***	
25	□	1.13	20	1	18	360.3	1.81	0.58	***5.94***	126				90.2	
26	◘	1.13	20	1	**3**			0.36	1.18	-1.52				40.4	
27	◘	1.13	20	1	**6**			0.33	***1.18***	-3.03				40.5	
28	◘	1.13	20	1	**18**			0.49	***1.18***	-9.09				41.2	
29	◘	1.13	20	1	18		3.69	0.48	***5.94***	126				90.2	
30	●	**1**	20	1	**12**		0.49	0.41	5.27	83.7				79.1	
31	○	1	20	1	12	348.1		0.39	0.9	-6.06				***31.1***	
32	○	1	20	1	12	480.3	2.22	0.51	5.27	83.7				79.1	
33	○	1	20	1	12	372.0		0.40	0.9	-6.06				***31.1***	
34	○	1	20	1	12	305.6		0.39	0.9	-6.06				***31.1***	
35	○	1	20	1	**2.5**	102.6		0.30	0.9	-1.26				***30.6***	
36	○	**5.5**	20	1	**2.3**	0.66		0.40	4.75	-1.14				162	
37	●	**1.25**	**7**	1	**0.2**			0.40	6.57	1.1				33.9	

The preceding self-capacitance calculations compared to measured highlight some trends. First, it is noticed that there are significant differences between the formulas and that there isn't typically one analytical approach that consistently compared well to measured (noting, as discussed earlier, the differences in measured data between the SRF method and the two-capacitor method). Second, the data supports the conclusion that the air- and ferrite-cores had similar self-capacitances, so air-core formulas like Medhurst's can be used; this may not be true for magnetic cores of high conductivity. Third, most of the formulas predict self-capacitances on the order of pico-farads or less for these coil builds (except for Knight's semi-empirical when using the ferrite-core with high permittivity) which generally matched that measured by the two-capacitor method. Fourth, there was no noticeable difference between multi-layer coils of the same overall geometry in the measured data, despite the analytical treatments that vary against the number of coil layers. Oddly, items 7/9/10 and 18-20 show that single- and multi-layer coils have different self-capacitances, but whether it increased or decreased going from single- to multi-layer depended on the build, while analytical theories predict that it should go down as number of layers n_l increases.

Measured Ferrite-Core Toroidal ESLs

This section presents measured and predicted data for toroidal MN60 ferrite cores with a toroidal winding. Data includes physical dimensions, permeability, resistance, inductance, and capacitance. Some discussion of the data will be given and compared to theoretical predictions, similarly as to the preceding section for axial rod ESLs. At the end, plots of measured and theoretical data are given to foment comparison.

The following tables present the physical description of the three toroidal ESL variations tested (Table 8.10); measured resistance (Table 8.11), inductance (Table 8.12), and effective height (Table 8.13) vs. frequency as well as for a single coil ("Coil 1") and

two equivalent coils series-opposing ("Coil 1 CW Coil 2"); and measured and calculated permeability (at 5 kHz), SRF, coil self-capacitance (by SRF method and/or two-capacitor method), and estimated leads' capacitance for one coil (Table 8.14). Data for more combinations of Coil 1 and Coil 2 were taken but are not listed for brevity. In these tables, physical values are bolded to assist in demarcating changes between items. Note that effective external permeability μ_{ext} was measured by comparing its effective height h_e to a calculated equivalent air-core; effective internal permeability μ_{int} was measured by comparing its inductance L to a calculated equivalent air-core (which uses [Kazimierczuk 2014] (empirical toroid) for predicted inductance). See Figure 8.3 for a photo of a toroidal ferrite-core ESL with two equivalent coils on opposite sides.

Figure 8.3 – Photo of Toroidal Ferrite-Core ESL with Two Equal Coils

Table 8.10 – Physical Descriptions of Measured Toroidal ESLs

#	Core Material	Wire Type	d_{hollow} (in)	d_{core} (in)	l_{core} (in)	$\frac{ID}{OD}$	$\frac{L}{OD}$	n	n_l	l_{coil} (in)	d_{coil} (in)	θ_{coil} (º)
1	MN60	#24 str.	4.75	5.5	0.75	0.86	0.1	20	1	1	0.64	21
2	MN60	#24 str.	4.75	5.5	0.75	0.86	0.1	20	1	**4.32**	0.64	**90**
3	MN60	#24 str.	4.75	5.5	**2.25**	0.86	**0.4**	20	1	4.32	**1.08**	90

Table 8.11 – Measured Toroidal ESLs' Series Resistance

			Measured Series Resistance (Ω)									
			Coil 1					Coil 1 CW Coil 2				
#	l_{core} (in)	l_{coil} (in)	5 Hz	5 kHz	24 kHz	100 kHz	300 kHz	5 Hz	5 kHz	24 kHz	100 kHz	300 kHz
1	0.75	1	0.112	1.061	6.52	172.3	2864	0.231	0.239	0.247	0.439	2.027
2	0.75	**4.32**	0.112	1.053	6.59	175.9	3008	0.231	0.235	0.237	0.333	1.368
3	**2.25**	4.32	0.236	2.753	16.47	548.5	10338	0.468	0.475	0.510	2.010	32.09

Table 8.12 – Measured Toroidal ESLs' Series Inductance

			Measured Series Inductance (mH)							
			Coil 1				Coil 1 CW Coil 2			
#	l_{core} (in)	l_{coil} (in)	5 kHz	24 kHz	100 kHz	300 kHz	5 kHz	24 kHz	100 kHz	300 kHz
1	0.75	1	1.897	1.864	2.004	1.536	0.154	0.154	0.154	0.154
2	0.75	**4.32**	1.834	1.804	1.947	1.470	0.101	0.101	0.101	0.101
3	**2.25**	4.32	5.267	5.185	5.726	3.748	0.154	0.154	0.155	0.149

Table 8.13 – Measured Toroidal ESLs' Effective Height

	Core and Coil Geometry			θ_{coil} Factor upon h_e (dB)		Measured Effective Height					
						Coil 1 (dB // m)			(Coil 1 CW Coil 2) // Coil 1 (dB)		
#	l_{core} (in)	l_{coil} (in)	θ_{coil} (°)	Sum	Est.	5 kHz	24 kHz	100 kHz	5 kHz	24 kHz	100 kHz
1	0.75	1	21	-0.05	-0.06	-91.6	-77.9	-65.1	6.6	6.5	5.1
2	0.75	**4.32**	**90**	-0.92	-1.13	-92.1	-78.5	-65.8	6.0	6.0	4.7
3	**2.25**	4.32	90	-0.92	-1.13	-88.5	-74.5	-54.7	6.0	5.6	-2.3

Table 8.14 – Measured Toroidal ESLs' Permeability, SRF, and Cap. (One Coil)

			Relative Permeability (5 kHz), Real						
#	l_{core} (in)	θ_{coil} (°)	μ_i	$\mu_{vol,ext}$ (h_e)	$\mu_{vol,int}$ (L_{coil})	Mean $\frac{\mu_{vol,ext}}{\mu_{ext}}$	SRF (MHz)	C_{self} from SRF (pF)	Est. C_{leads} (pF)
1	0.75	21	6500	60.2	8500	0.87	0.57	74.6	0.34
2	0.75	**90**	6500	62.7	8438	0.87	0.52	85.6	0.34
3	**2.25**	90	6500	33.8	7976	0.92	0.43	36.1	0.33

From the preceding tables, several conclusions can be made. First, having a coil spread out over a large angle causes a noticeable drop in effective height, as predicted by the θ_{coil} factor—comparing items 1-2, there is a measured difference in effective height of 0.5-0.7 decibels while the summation prediction was 0.9 decibels. The latter difference between measured and predicted is possibly due to the coil build which may have had an uneven spread favoring the center, or may be within measurement error. Second, adding a second coil series-opposing ("CW") doubled the effective height (+6 dB) for low frequencies, as expected. Third, the measured volumetric effective internal permeability $\mu_{vol,int}$ at 5 kHz is significantly higher than the initial permeability μ_i specified—above the maximum including 25% tolerance (8125) for items 1-2. The measured permeability is somewhat affected by the winding of the coils, which were not very tight on the core (as seen in Figure 8.3) and not necessarily of even pitch, and there may be error in the formula used to calculate the inductance of an equivalent air-core. Fourth, adding the series-opposing second coil significantly drops the net inductance while doubling the resistance; primarily because of the lower inductance, the SRF increased by a factor of ten (measured data not shown for brevity). Fifth, there are high frequency effects seen at 100 kHz in the effective height data—going from 24 to 100 kHz should result in a 12.4 dB increase in effective height, which is approximately true for items 1-2 while item 3 instead increases approximately 20 dB; note also the effective height differences of Coil 1 CW Coil 2 // Coil 1. It is not clear why there is a disparity vs. frequency—the resonant frequency assumption is satisfied for one coil and especially for two series-opposing—but the estimated skin depth of the core relative to its cross-section (in either dimension) is approximately one or less (using either the volumetric external permeability or estimated initial permeability) at 100 kHz, which violates one of our assumptions and may have a significant effect.

The mutual coupling between two coils on opposing sides can be further investigated by the measurement approaches tabulated in Table 6.2. Data from these measurements are presented in Table 8.15 and compared to theoretical predictions. As seen, the various measurement techniques net approximately the same measured mutual coupling factor k_{mut}; note that item 3's "Coil 1 CW/CCW 2" would have a mean factor of 1.01 (instead of 0.79) if the 300 kHz data was not included; 1.01 is not theoretically possible but is the result of calculations including individual inductances. The theoretical predictions reasonably matched measured—even for an EE core—with [Hurley and Wilcox 1994] being the best (shown bolded and italicized). However, accuracy in the mutual coupling factor is very important, e.g. a factor of 0.99 yields vastly different results than a factor of 0.9 (discussed further later).

Table 8.15 – Measured Toroidal ESLs' Mutual Coupling Factor

			Measured k_{mut}				**Error: Theoretical // Measured k_{mut} (dB)**		
#	**l_{core} (in)**	**θ_{coil} (°)**	**Coil 1**	**Coil 1 (2 S.C.)**	**Coil 2 (1 S.C.)**	**Coil 1 CW /CCW 2**	**Toroid [Hurley & Wilcox 1994]**	**Toroid (Meas. L) [de Leon et al. 2014]**	**EE Core [Bahmani and Thiringer 2015]**
1	0.75	21	0.96	0.96	0.96	0.98	***0.09***	-0.23	-0.39
2	0.75	**90**		0.97	0.97	1.00	***0.02***	-0.05	-0.29
3	**2.25**	90		0.98	0.98	0.79	***-0.03***	-0.04	-0.16

The measured external permeability is compared to theoretical at 5 kHz in Table 8.16 as an error expressed in decibels. Unlike rods, there is not much literature for toroids, so some of the analytical formulas used are actually radial, fluxmetric apparent permeabilities transformed into toroidal ("$N_f \rightarrow N_{tor}$") according to [Primdahl et al. 2002]. For convenience, the smallest errors are bolded and italicized per row. From the results, it is clear that the coil distribution (i.e. θ_{coil}) did not have a significant impact but core length did, with the latter obfuscating which literature approach was best for general prediction. We do, however, conclude that our simple correction to a pseudo-empirical

model best fit our data for items 1-2 while none fit item 3 very well; in general, [Sandomirskii 2008] was good for all cases, making it a general recommendation. It seems accidental that the transformed Rosenblat's works so well with no information given about the core's inner diameter; the (inputs) used for Rosenblat's were $(k) = 3.6, (l_{core}) = d_{core}, (A_{core}) = d_{core} l_{core}, (a) = l_{core}, (b) = d_{core}$. Further, the radial permeability of [Kobayashi and Iijima 1996] (which is shown earlier to be accurate) when transformed by [Primdahl et al. 2002] is decidedly not accurate (it is also shown un-transformed as "$N_{f,rad}$"); similar occurs transforming radial (or even axial) for other literature approaches (e.g. solid cylinder per [Chen et al. 2006]), with the conclusion that transforming fluxmetric to local toroidal according to [Primdahl et al. 2002] is not recommended.

Table 8.16 – Measured Toroidal ESLs' External Permeability vs. Theoretical

	Core & Coil Geometry				**Error: Theoretical // Measured μ_{ext} (dB)**							
#	**l_{core} (in)**	**$\frac{ID}{OD}$**	**$\frac{L}{OD}$**	**θ_{coil} (°)**	**Pseudo-Empirical, $\mu_i \to \infty$ [Primdahl et al. 2002]**	**Pseudo-Empirical, $\mu_i \to \infty$ [De Graef and Beleggia 2006]**	**Pseudo-Empirical Fit to Our Data, $\mu_i \to \infty$, Based On [De Graef and Beleggia 2006]**	**$\mu_i \to \infty$, $ID/OD \to 1$ De Graef and Beleggia 2006]**	**$N_{f,rad} \to N_{tor}$, General, $\mu_i \to \infty$ [Rosenblat]**	**$\mu_i \to \infty$ [Sandomirskii 2008]**	**$N_{f,rad}$, $0.1 \leq L/D \leq 8$, $0.2 \leq ID/OD \leq 0.8$ [Kobayashi & Iijima 1996]**	**$N_{f,rad} \to N_{tor}$, $0.1 \leq L/D \leq 8$, $0.2 \leq ID/OD \leq 0.8$ [Kobayashi & Iijima 1996]**
1	0.75	0.86	0.1	21	-1.37	-0.75	0.48	-0.77	0.32	***-0.11***	-10.4	-10.9
2	0.75	0.86	0.1	**90**	-1.55	-0.93	0.30	-0.95	***0.14***	-0.29	-10.6	-11.0
3	**2.25**	0.86	**0.4**	90	-3.34	-2.72	-1.48	***-0.66***	2.28	-0.77	-8.71	-5.10

Comparing the pseudo-empirical calculations, our fit was best for items 1-2, followed by [De Graef and Beleggia 2006]. Our fit multiplies 0.75 times the constant of [De Graef and Beleggia 2006], the latter being a slight modification of [Primdahl et al. 2002], both of which using a constant derived from linear trend fitting to cited empirical

data (with a large standard deviation). The cited empirical data all used core length/diameter ratios approximately the size of items 1-2 or smaller, therefore the fact that item 3 was poorly predicted by the pseudo-empirical approaches isn't surprising. This implies that the pseudo-empirical model may not adequately handle core length/diameter ratio.

Measured and theoretical inductance are compared in Table 8.17, as an error expressed in decibels and using the initial permeability at 5 kHz. For convenience, the smallest errors are bolded and italicized per row. Again, there is limited literature for toroids, so some general solenoid approaches are given alongside those explicitly for toroids. The calculated errors clearly show, however, that general solenoid approaches (the first four in the table) greatly over-estimate the inductance, which was a very surprising result; however, they divide by the actual coil length, not assuming fully-wound as in the toroid equations. The analytical approaches explicitly given for toroids can also significantly over-estimate the inductance (as seen in the last two columns) and are generally for a coil fully-wound around the perimeter of the toroid. The accuracy of these errors is subject to the large manufacturer tolerances in initial permeability (e.g. ±25% or -1.25/+1 dB) and the coil geometry, which was not wound tightly onto the core nor necessarily of even pitch and was not fully-wound around the toroid (the latter's error is supposedly minimal for MN60's high permeability [Clarke 2014]). Further measurements are recommended using a fully-wound and tight coil, but we suspect that for these high-permeability cores, either the toroid "CS Sol." or empirical by [Kazimierczuk 2014] are accurate as the closed-path through the core will dominate.

For air-cores, the corrected solenoid equations should be used. Therefore, unlike the axial rod section where the correction for round wires is important even with a high-permeability core because the fringing flux outside the core is still relatively significant, it may not be correct to simply divide the inductance between a toroidal coil measured on

an air-core and a magnetic-core to derive initial permeability. As supporting evidence, note the large difference (several decibels) between "CS Sol." and corrected.

Table 8.17 – Measured Toroidal ESLs' Inductance vs. Theoretical

			Error: Theoretical // Measured Inductance (dB)								
#	l_{core} (in)	l_{coil} (in)	Corr. CS Sol. [Knight/Rosa/Weaver]	Solenoid [Snow/Weaver]	Square Solenoid (Corr. CS) [Niwa/Grover/Wheeler]	Square Sol., Corr. CS [Ishida et al. 2010]	Toroid, CS Sol. ($p \to 0$), Fully-Wound	Toroid, CS Sol. ($p \to 0$), Empirical, Fully-Wound [Kazimierczuk 2014]	Toroid, Sol. (Corr. CS), Fully-Wound [Rosa and Grover 1916]	Toroid, Sol. (Corr. CS), Fully-Wound [Grover/Knight]	Toroid, Sol. (Corr. CS), Fully-Wound [Grover/Knight/Weaver]
1	0.75	1	10.36	10.45	25.01	25.09	***-1.16***	-1.16	-1.38	4.66	4.36
2	0.75	**4.32**	6.15	6.46	22.68	22.07	***-1.01***	-1.01	2.88	4.81	4.51
3	**2.25**	4.32	5.50	5.67	18.09	17.48	***-0.82***	-0.83	2.46	4.21	3.93

Theoretical self-capacitances were calculated from literature to compare to the measured data; see Table 8.18 for single-layer calculations and Table 8.19 for multi-layer (even though all three builds were single-coil). For convenience, the closest calculation to measured is bolded and italicized per row and per single-/multi-layer section; the closest amongst both sections is underlined per row. The measured capacitance used for comparison is the minimum of the self-capacitance as calculated from measured SRF. Also for convenience, any cell that does not match its reference's requisite assumptions is put into red text. Empty cells were due to non-number values.

Table 8.18 – Measured Toroidal ESLs' Theoretical Self-Capacitance, Single-Layer

			Meas. and Est. C (pF)		Theoretical C_{self} (pF)						
#	l_{core} (in)	l_{coil} (in)	C_{self} from SRF	Est. C_{leads}	Air-core, no shield [Medhurst 1947b]	#1, Non-Cond. Core [Kazimierczuk 2014]	#2, Non-Cond. Core [Kazimierczuk 2014]	Semi-empirical, L >> D [Knight 2013c]	Electrode [Knight 2013c]	Solid Prolate Spheroid [Simpson and Zhu 2007]	Hollow Prolate Spheroid [Simpson 2008]
1	0.75	1	72.4	0.33	0.77	0.06	***12.3***	14,100	0.38	6.78	-0.14
2	0.75	**4.32**	83.1	0.33	1.54	0.03	2.85	10,200	0.27	***6.78***	-0.14
3	**2.25**	4.32	35.5	0.32	1.83	0.04	***4.79***	18,800	0.46	1.91	-0.41

Table 8.19 – Measured Toroidal ESLs' Theoretical Self-Capacitance, Multi-Layer

			Meas. and Est. C (pF)		Theoretical C_{self} (pF)						
#	l_{core} (in)	l_{coil} (in)	C_{self} from SRF	Est. C_{leads}	#1, $n_l = 2$, $n \geq 10$, Non-Cond. Core Kazimierczuk 2014]	#2, $n_l = 2$, $n \geq 10$, Non-Cond. Core [Kazimierczuk 2014]	#1, $n_l = 2/3$, $n \geq 10$, Cond. Core/Shield [Kazimierczuk 2014]	#2, $n_l = 2/3$, $n \geq 10$, Cond. Core/Shield [Kazimierczuk 2014]	Multi-Layer [Macintyre 1999]	Multi-Layer [Biela and Kolar 2008]	Multi-Layer [Coillot and Leroy 2011]
1	0.75	1	72.4	0.33	0.55	-0.51				***18.8***	
2	0.75	**4.32**	83.1	0.33	0.55	-2.18				***18.9***	
3	**2.25**	4.32	35.5	0.32	0.93	-2.18				***31.7***	

Similarly as for the rods, the self-capacitance calculated from measured SRF had to extrapolate permeability. However, the SRF for the three items was on the order of 400-600 kHz, where it would be expected that the extrapolated permeability would be more accurate than at several megahertz. If the measured self-capacitance is accurate, then the multi-layer formula (though it can handle multi-layer) by [Biela and Kolar 2008] was best followed by Kazimierczuk's #2 for a non-conducting core. It appears that at best, a good prediction is within an order of magnitude of the measured.

The preceding data can be more readily compared via graph—consider item 1 as an example. The measured mutual coupling factor k_{mut} is compared with several

analytical literature approaches in Figure 8.4. Abbreviations are used for the various measured coil scenarios, e.g. “Coil 1 (Coil 2 O.C.)” means coil 1’s inductance was measured while coil 2 was open-circuited (O.C.); S.C. is short-circuited; CW/CCW are series-opposing and series-aiding respectively. It can be seen that [Hurley and Wilcox 1994] matched the series-aiding/-opposing measurement very well and was the best analytical approach. Similar is seen for the other two items.

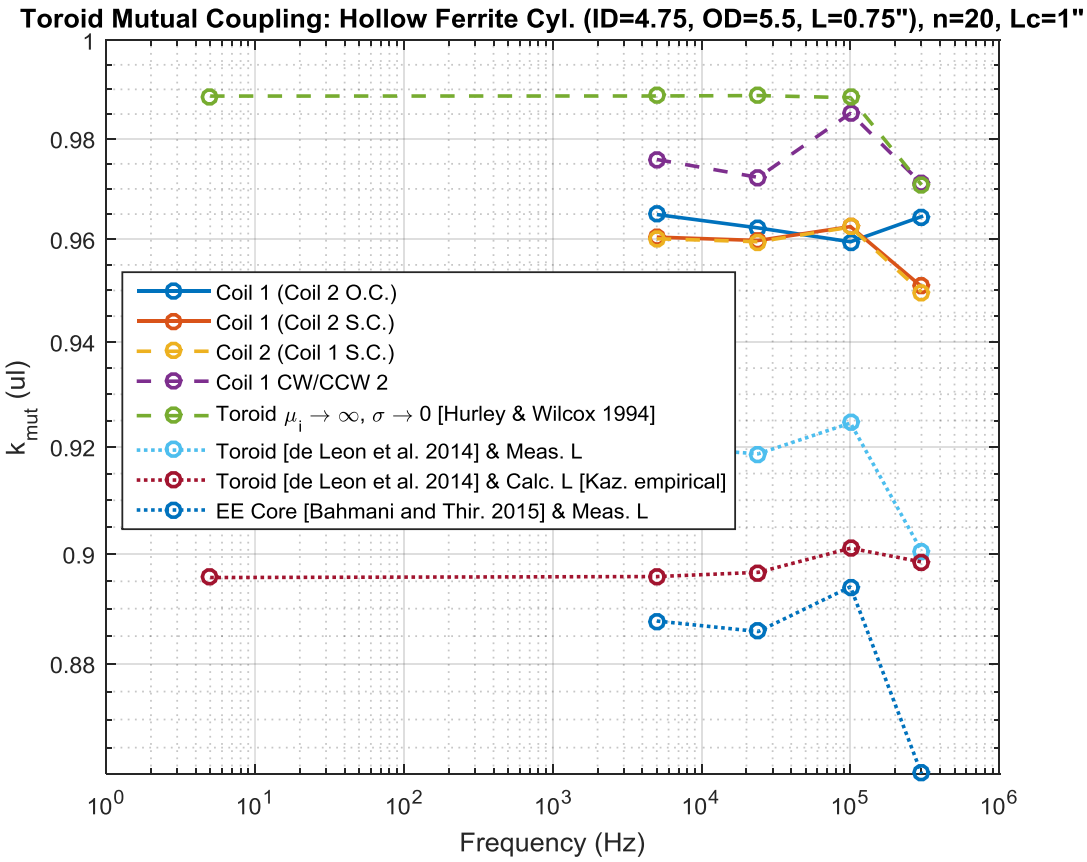

Figure 8.4 – Measured and Analytical Toroid Mutual Coupling

The mutual coupling effect upon net coil inductance and ferrite loss were also explored by measurement of the two coils when connected series-opposing for item 1. See comparisons of measured vs. theoretical for inductance (Figure 8.5) and resistance

(Figure 8.6). Calculations included the wire conductor skin effect. Inductance measurements are given for measured series-opposing ("Coil 1 CW 2") but also double that of coil 1's inductance measured alone multiplied by theoretical $(1 - k_{mut})$. From both figures, it can be seen how difficult it is to accurately predict the mutual coupling effect as the multiplication factor $(1 - k_{mut})$ is very sensitive to small values of k_{mut}. For resistance, Kazimierczuk's approach for core resistance ($\omega L \tan \delta_m$) was more accurate than Hurley and Wilcox's calculation for all three toroid and coil geometries measured herein.

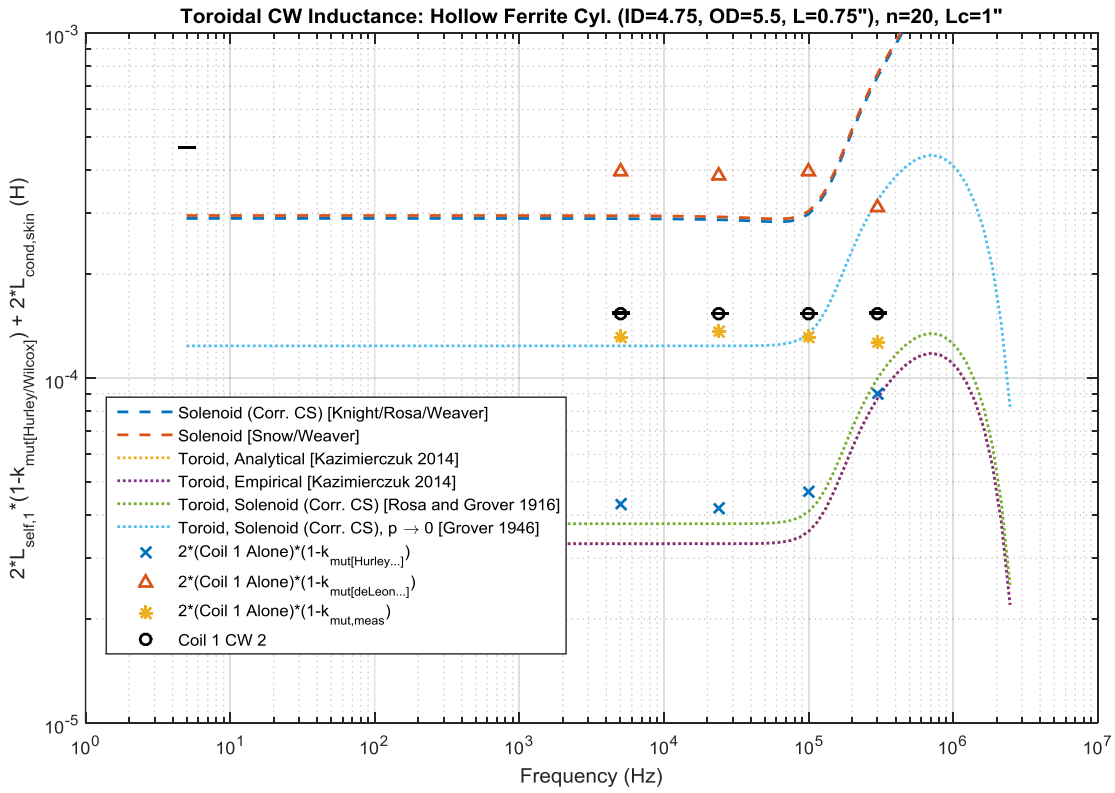

Figure 8.5 – Series-Opposing Toroid Inductance, Measured and Analytical

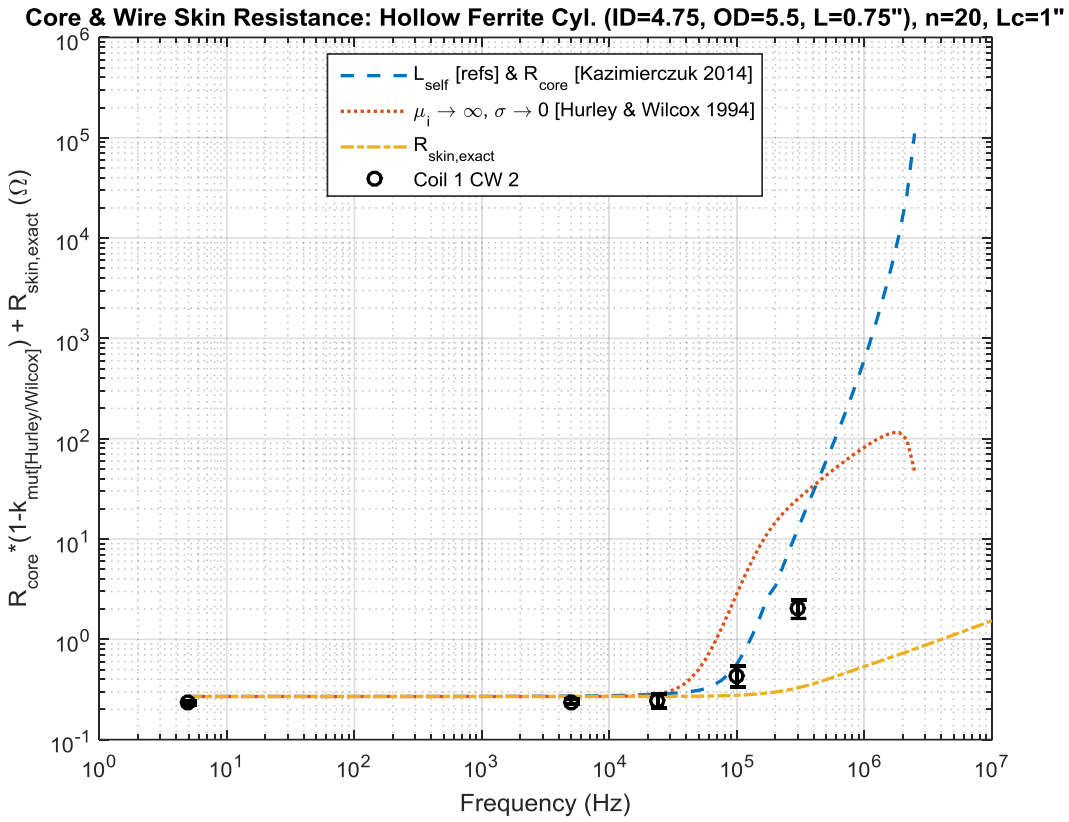

Figure 8.6 – Series-Opposing Toroid Resistance, Measured and Analytical

Measurements also investigated the net effective height for one or two coupled toroidal coils. Measured effective height h_e is shown in Figure 8.7 for the above toroidal case for different coil combinations. Nominally, the effective height of one coil is independent of a second coil unless they are connected, which is generally seen in the measurements. If connected series-aiding (CCW), the effective height should approach zero as the coils' effective heights have opposing phases while the mutual coil flux is aiding. When connected series-opposing (CW), the effective height should double (+6 dB) that of one coil as their phases are in-phase while the mutual coil flux is opposing; this apparently also occurs even if the second coil is connected by mutual flux though un-connected by conductor. It is not clear why the effective height varies strongly at 10^5 hertz when the mutual coupling factor was relatively constant across the measured

frequencies; coil SRF was added to show that it should not be a self-resonance issue. Analysis earlier in this section show that it may be due to the skin depth in the core no longer being greater than the core's cross-section (in either dimension).

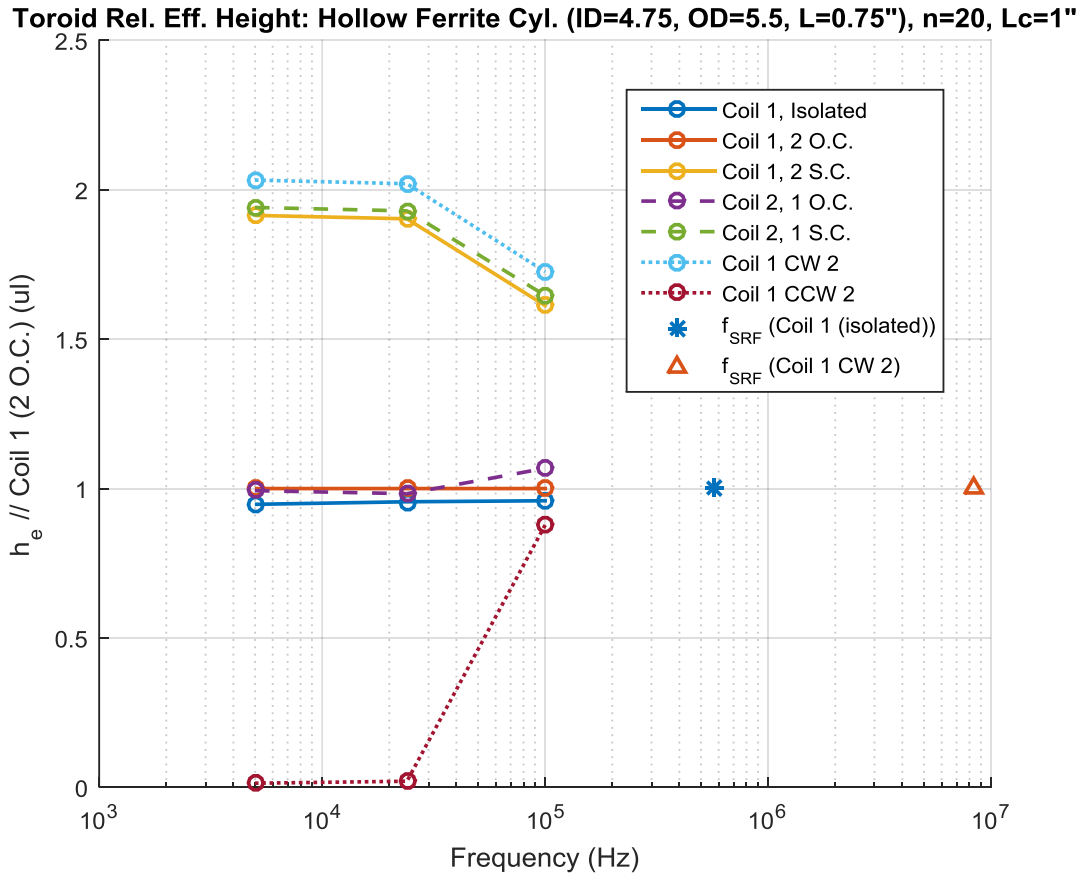

Figure 8.7 – Toroidal Coils' Measured Effective Height

CHAPTER 9

CONCLUSION

From the extensive analysis and exhaustive literature review given here for electrically-small loop antennas, we hope to have furthered scientific understanding of the subject matter in totality—not just the important consideration of when immersed in a conducting medium. We have given formulas, references, data, and analysis for the following: material properties (with a focus on ferrites), impedance effects due to a surrounding medium, antenna effective height and absolute gain, shielding, demagnetization factor, effective permeability, wire impedance, coil external inductance, coil mutual inductance, coil self-capacitance, impedance effects due to a conducting core and shield, sensitivity and signal/noise ratio, and optimization strategies.

An example of optimization was given with two optimal designs built, tested in the lab with good comparison to predicted, and then tested in the field using ambient external signals with the "AWESOME" receiver. Measured lab data were given for 41 unique loops of varying parameters (core material, core shape, axial rod or toroid, coil length, etc.) including resistance, inductance, and effective height versus frequency as well as resonant frequency and toroidal mutual coupling. Finally, recommendations were given in each section for use in predictions after comparing many theoretical and empirical references against measured data.

Measurements and analysis have shown that resistance, inductance, and magnetic core apparent/effective permeability can be accurately predicted, although the latter's accuracy is less for internal permeability (used for coil inductance and core losses) and more research is recommended. It can also be difficult to accurately predict coil external inductance and mutual coupling except for coils of even pitch that are tightly-wound to the core, and possibly for toroids that are also not wound fully around their perimeter.

APPENDIX A : DEMAGNETIZATION FACTOR TABLES

The following tables list exact and approximated (or tabulated) demagnetization factor equations, values, and references for ellipsoid, fluxmetric, magnetometric, and local toroidal, respectively. See Chapter 4 for a description of demagnetization.

Table A.1 – Ellipsoidal Demagnetization Factors

Geometry	$\widetilde{N}$	N_f (ul)	
		Exact	**Approximate or Tabulated**
Sphere	N_x, N_y, N_z	$= {}^{1}/_{3}$	
Ellipsoid	N_x, N_y, N_z (Principal axes)	$= \begin{cases} \frac{\cos(\varphi)\cos(\vartheta)}{\sin^3(\vartheta)\sin^2(\alpha)}\left[K_{ei1}(\sin(\alpha),\vartheta) - E_{ei2}\left((\sin(\alpha),\vartheta)\right)\right] & \hat{x} \\ \frac{\cos(\varphi)\cos(\vartheta)}{\sin^3(\vartheta)\sin^2(\alpha)\cos^2(\alpha)}\left[E_{ei2}\left((\sin(\alpha),\vartheta)\right) - \cos^2(\alpha)K_{ei1}(\sin(\alpha),\vartheta) - \frac{\sin^2(\alpha)\sin(\vartheta)\cos(\vartheta)}{\cos(\varphi)}\right] & \hat{y} \\ \frac{\cos(\varphi)\cos(\vartheta)}{\sin^3(\vartheta)\cos^2(\alpha)}\left[\frac{\sin(\vartheta)\cos(\varphi)}{\cos(\vartheta)} - E_{ei2}\left((\sin(\alpha),\vartheta)\right)\right] & \hat{z} \end{cases}$ $[\![x \geq y \geq z \geq 0]\!]$ $\vartheta = \cos^{-1}({}^{z}/_{x})$ $\varphi = \cos^{-1}\left({}^{y}/_{x}\right)$ $\alpha = \frac{\sin(\varphi)}{\sin(\vartheta)}$ [Osborn 1945, eq. (2.1)-(2.6)] or [Chen et al. 2002, eq. (3)-(5)]	See [Osborn 1945, eq. (2.14)-(2.18) or (2.23)-(2.25)]

Table A.1 – Ellipsoidal Demagnetization Factors (Continued)

Spheroid (Symmetric Ellipsoid)	N_{axial}	$= \begin{cases} \frac{1}{1-l/{d_{core}}^2}\left[1-\frac{l/d_{core}\cos^{-1}(l/d_{core})}{\sqrt{1-l/{d_{core}}^2}}\right] & [\![l/d_{core}<1]\!] \ (Oblate) \\ \frac{1}{3} & [\![l/d_{core}=1]\!] \ (Sphere) \\ \frac{1}{l/{d_{core}}^2-1}\left[\frac{l/d_{core}\cosh^{-1}(l/d_{core})}{\sqrt{l/{d_{core}}^2-1}}-1\right] & [\![l/d_{core}>1]\!] \ (Prolate) \\ \approx \frac{\ln(2\,l/d_{core})-1}{l/{d_{core}}^2} & [\![l/d_{core}>12]\!] \ (Prolate) \end{cases}$ [Chen et al. 2006, eq. (16)-(17)] or $= \begin{cases} \frac{l/{d_{core}}^{-2}}{l/{d_{core}}^{-2}-1}-\left(\frac{l/{d_{core}}^{-2}}{(l/{d_{core}}^{-2}-1)^{3/2}}\right)\sin^{-1}\left(\frac{\sqrt{l/{d_{core}}^{-2}-1}}{l/d_{core}}\right) & [\![l/d_{core}<1]\!] \ (Oblate) \\ \frac{1}{3} & [\![l/d_{core}=1]\!] \ (Sphere) \\ \frac{1}{l/{d_{core}}^2-1}\left[\left(\frac{l/d_{core}}{2\sqrt{l/{d_{core}}^2-1}}\right)\ln\left(\frac{l/d_{core}+\sqrt{l/{d_{core}}^2-1}}{l/d_{core}-\sqrt{l/{d_{core}}^2-1}}\right)-1\right] & [\![l/d_{core}>1]\!] \ (Prolate) \end{cases}$ [Bozorth and Chapin 1942, eq. (1b) & (2a)] or see [Beleggia et al. 2009b, eq. (2.26)] or see [Osborn 1945, eq. (2.10) or (2.20)]	$= \begin{cases} 1-\frac{\pi\,l/d_{core}}{2} & [\![l/d_{core}\ll 1]\!] \ (Oblate) \\ \frac{\ln(2\,l/d_{core})-1}{l/{d_{core}}^2} & [\![l/d_{core}\gg 1]\!] \ (Prolate) \end{cases}$ [Bozorth and Chapin 1942, eq. (1b) & (2a) or see [Beleggia et al. 2009b, eq. (3.26, right), Table 2 (lemon), $\omega = \bar{R}/r$, & Figure 1c] or see [Osborn 1945, eq. (2.12) or (2.22)]

Table A.1 – Ellipsoidal Demagnetization Factors (Continued)

Spheroid (Symmetric Ellipsoid)	N_{axial}	or $= \frac{\mu_i/\mu_{a\,\{prolate\}} - 1}{\mu_i - 1} \quad \left[\!\left[\begin{matrix} l/d_{core} > 1 \\ (Prolate) \end{matrix} \right]\!\right]$ $\mu_{a\,\{prolate\}} = 1 + F(\mu_i - 1) = 1 + BQ_1'(a)$ $F = \frac{aQ_1'(a)}{aQ_1'(a) - \mu_i Q_1(a)}$ $B = \frac{(\mu_i - 1)P_1(a)}{Q_1'(a)P_1(a) - \mu_i Q_1(a)}$ $a = \frac{l_{core}}{\sqrt{l_{core}^2 - d_{core}^2}}$ where P_v is the associated Legendre polynomial (order zero, degree v) [Simpson and Zhu 2006, eq. (12), (23), & (32)] and [Wait 1953b, eq. (3), (10), & (13)] or see [Simpson and Cahill 2007] or [Wait 1953a] for oblate spheroid	
	N_{radial}	$= \begin{cases} \frac{1}{2}\left[\left(\frac{l/d_{core}{}^{-2}}{\left(l/d_{core}{}^{-2}-1\right)^{3/2}}\right)\sin^{-1}\left(\frac{\sqrt{l/d_{core}{}^{-2}-1}}{l/d_{core}}\right) - \frac{1}{l/d_{core}{}^{-2}-1}\right] & \left[\!\left[l/d_{core} < 1 \right]\!\right] \; (Oblate) \\ \frac{1}{3} & \left[\!\left[l/d_{core} = 1 \right]\!\right] \; (Sphere) \\ \frac{1}{2}\left[\frac{l/d_{core}{}^{2}}{l/d_{core}{}^{2}-1} - \left(\frac{l/d_{core}}{\left(l/d_{core}{}^{2}-1\right)^{3/2}}\right)\ln\left(\frac{l/d_{core}+\sqrt{l/d_{core}{}^{2}-1}}{l/d_{core}-\sqrt{l/d_{core}{}^{2}-1}}\right)\right] & \left[\!\left[l/d_{core} > 1 \right]\!\right] \; (Prolate) \end{cases}$ [Bozorth and Chapin 1942, eq. (1a) & (2b) or see [Osborn 1945, eq. (2.11) or (2.19)]	$= \begin{cases} \frac{\pi\, l/d_{core} - 2}{4\, l/d_{core}{}^{-2}} & \left[\!\left[l/d_{core} \ll 1 \right]\!\right] \; (Oblate) \\ \frac{1}{2}\left(1 - \frac{\ln(2\, l/d_{core})}{l/d_{core}{}^{2}}\right) & \left[\!\left[l/d_{core} \gg 1 \right]\!\right] \; (Prolate) \end{cases}$ [Bozorth and Chapin 1942, eq. (1a) & (2b) or see [Osborn 1945, eq. (2.13) or (2.21)]

Table A.1 – Ellipsoidal Demagnetization Factors (Continued)

Hollow Spheroid	N_{axial}	$= \frac{\mu_i/\mu_{a\,\{hollow\ prolate\}} - 1}{\mu_i - 1} \quad \left[\!\left[\begin{matrix} l/d_{core} > 1 \\ (Prolate) \end{matrix} \right]\!\right]$ $\mu_{a\,\{hollow\ prolate\}} = F\left[\frac{(l_{core}^2 - d_{core}^2)}{d_{core}^2}\right] = 1 + BQ_1'(a)$ $F = \frac{\mu_i[1+GQ_1'(a)]}{\mu_i Q_1(a) + GQ_1'(a)Q_1(a)[\mu_i - 1] - aQ_1'(a)}$ $G = \frac{b[(\mu_i/\mu_{r\{hollow\}}) - 1]}{Q_1(b) - (\mu_i/\mu_{r\{hollow\}})bQ_1'(b)}$ $B = -\frac{a(\mu_i - 1) + B_1[\mu_i aQ_1'(a) - Q_1(a)]}{[\mu_i Q_1(a) - aQ_1'(a)] + B_1[(\mu_i - 1)Q_1(a)Q_1'(a)]}$ $B_1 = -\frac{b(\mu_i - 1)}{b\mu_i Q_1'(b) - Q_1(b)}$ $a = \frac{l_{core}}{\sqrt{l_{core}^2 - d_{core}^2}}$ $b = \sqrt{1 + \frac{d_{hollow}^2(a^2 - 1)}{d_{core}^2}}$ [Simpson 2008, eq. (2), (5), & (13)] and [Wait 1953b, eq. (3)-(4), (10), & (15)-(16)]	

Table A.2 – Fluxmetric Demagnetization Factors for Various Geometries

Geometry	$\widetilde{N}$	N_f (ul)	
		Exact	**Approximate or Tabulated**
Cube	N_x, N_y, N_z	$= {}^{1}/_{3}$	
Sphere	N_x, N_y, N_z	$= {}^{1}/_{3}$	
Hollow Sphere	N	$= \frac{1}{3} - \frac{2p^2[3+(\mu_i-1)(1+p+p^2)]}{9(1+p)+6(\mu_i-1)(1+p+p^2)}$ $p = \frac{r_{hollow}}{r_{core}}$ [Prat-Camps et al. 2016, eq. (9)]	
Circular Cylinder, Solid	N_{axial}	$= 1 - \frac{8\pi \frac{l}{d_{core}}}{4+\frac{l}{d_{core}}^2}\left[K_{ei1}\left(\frac{4}{4+\frac{l}{d_{core}}^2}\right) - E_{ei2}\left(\frac{4}{4+\frac{l}{d_{core}}^2}\right)\right]$ $[\![\mu_i \to 1]\!]$ [Chen et al. 2002, eq. (22)]	$= N_{f,axial}\{spheroid\}\frac{1+2.35\ln\left(1+0.137\frac{l}{d_{core}}\right)}{1+2.28\ln\left(1+0.284\frac{l}{d_{core}}\right)}$ $[\![\mu_i \to \infty]\!]$ [Sandomirskii 2008, eq. (4)-(5)] or $= \frac{4.02\log_{10}(l/d_{core})-0.92}{2\,(l/d_{core})^2}$ $[\![l/d_{core} \geq 10, \mu_i \to \infty]\!]$ [Bozorth and Chapin 1942, pg. 323] or $= \begin{cases} \frac{1}{2\,l/d_{core}^2} & [\![l/d_{core} \geq 20, \mu_i \to 1]\!] \\ \frac{1}{l/d_{core}^2}\left[\ln(2\,l/d_{core}) - \frac{3}{2}\right] & [\![l/d_{core} \gg 1, \mu_i \to \infty]\!] \end{cases}$ [Chen et al. 2002, eq. (24) & (26)] or see [Chen et al. 2006, Table 1] including correction for μ_i or $= N_{f,axial}\{spheroid\}$ $[\![\mu_i \to \infty]\!]$ [Chen et al. 2006]

Table A.2 – Fluxmetric Demagnetization Factors for Various Geometries (Continued)

	N_{radial}		$= \frac{1}{2}$ $[\![l_{core} \to \infty]\!]$ [Prat-Camps et al. 2012] or see [Kobayashi et al. 1996, Table I] including correction for μ_i Note: some inaccuracy when converted to axial and compared with [Chen et al. 2006, Table 1] or $= \left(1 + \frac{b_{\{elliptical\}}}{c_{\{elliptical\}}}\right)^{-1}$ $[\![l_{core} \to \infty]\!]$ [Musmann and Afanassiev 2010, eq. (1.51)]
Circular Cylinder, Hollow	N_{axial}		See [Kobayashi and Iijima 1996, Table I-III] including correction for μ_i or see [Matyuk et al. 2007, eq. (19)] or $= \frac{d_{core}^2 - d_{hollow}^2}{l_{core}^2}\left[\ln\left(\frac{0.6 l_{core}}{r_{core}}\right) - 1\right]$ $[\![\mu_i \to \infty]\!]$ Rosenblat's [Matyuk et al. 2007, eq. (1)]
	N_{radial}		$= \frac{1}{2}\left(1 - \frac{d_{hollow}}{d_{core}}\right)$ $[\![l_{core} \to \infty, any\ \mu_i]\!]$ [Prat-Camps et al. 2012, eq. ((27)]
Rect. Prism	N_x, N_y, N_z $(a \times b \times c)$	See [Chen et al. 2002, eq. (1)] for $\mu_r = 1$	$= \begin{cases} N_f\{cylinder\} & [\![a = b]\!] \\ N_x, N_z = \frac{2}{\pi}\tan^{-1}\left(\frac{2a}{c}\right) - \frac{c}{2\pi a}\ln\left(1 + \frac{4a^2}{c^2}\right) & [\![b \gg \sqrt{ac},\ b \to \infty,\ \mu_i \to 1]\!] \\ N_c = \frac{2ab}{\pi c^2} & \left[\!\left[\frac{\sqrt{ac}}{b} \to \infty, c > 10a\right]\!\right] \end{cases}$ [Chen et al. 2002, eq. (6) & (17)] and [Brown 1962] or see [Matyuk and Osipov 1999]

Table A.2 – Fluxmetric Demagnetization Factors for Various Geometries (Continued)

			or see [Chen et al. 2005, Table II] (which otherwise supersedes [Chen et al. 2002]) including correction for μ_i or see [Pardo et al. 2004, Table I] for square bars with correction for μ_i
Eq. Triangular Prism	N_x, N_y, N_z		
Dumbbell	N_{axial}		See [Tashiro et al. 2015, eq. (21)]
General, Pseudo-Empirical			$= \begin{cases} \frac{4A_{core,cs}\left[\ln\left(\frac{kl_{core}}{a+b}\right)-1\right]}{\pi\left(l_{core}^2-0.25\,l_{coil}^2\right)} & Open-Core, \pm 4\% \\ \frac{4A_{core,cs}\left[\ln\left(\frac{kl_{core}}{a+b}\right)-1\right]}{v\pi\left(l_{core}^2-0.25\,l_{coil}^2\right)} & Closed-Core, \pm 10\% \end{cases}$ $[\![\mu_i \to \infty, l_{coil} \leq 0.5\, l_{core}]\!]$ ul, modified Rosenblat's [Musmann and Afanassiev 2010, eq. (1.52)-(1.54)] $k = \begin{cases} 2.4 & Circular/Elliptical\ Cross-Section \\ 3.6 & Rectangular\ Cross-Section \end{cases}$ [Musmann and Afanassiev 2010, Table 1.1] $v = \begin{cases} 1.3 & Ellipsoid \\ 1 & Rod \\ 1.4 & Square\ Frame \end{cases}$ [Musmann and Afanassiev 2010, Table 1.1] where l_{core} is in the desired demagnetization direction; a, b are orthogonal dimensions of the core; and $A_{core,cs}$ is the core cross-sectional area perpendicular to l_{core} or see [Matyuk and Osipov 2000, eq. (12)] for a higher-accuracy but significantly more complicated modification of Rosenblat's

Table A.3 – Magnetometric Demagnetization Factors for Various Geometries

Geometry	$\widetilde{N}$	N_m (ul)	
		Exact	**Approximate or Tabulated**
Cube	N_x, N_y, N_z	$= {}^{1}/_{3}$	
Sphere	N_x, N_y, N_z	$= {}^{1}/_{3}$	
Hollow Sphere	N	$= \frac{1}{3} - \frac{2p^3(\mu_i - 1)}{6(\mu_i - 1) + 9}$ $p = \frac{r_{hollow}}{r_{core}}$ [Prat-Camps et al. 2016, eq. (8)]	
Circular Cylinder, Solid	N_{axial}	See [Beleggia et al. 2006, eq. (7) for circular or (18)-(19) for elliptical] or $= 1 - \frac{4}{3\pi}\left\{\sqrt{1 + l/d_{core}{}^{-2}}\left[l/d_{core}{}^{2} K_{ei1}\left(\frac{1}{1 + l/d_{core}{}^{2}}\right) + \left(1 - l/d_{core}{}^{2}\right) E_{ei2}\left(\frac{1}{1 + l/d_{core}{}^{2}}\right)\right] - \frac{1}{l/d_{core}}\right\}$ $[\![\mu_i \to 1]\!]$ [Chen et al. 2002, eq. (23)] and see [Chen et al. 2006, Table 2] for correction for μ_i	$N_{axial}\{spheroid\}$ $[\![\mu_i \to \infty]\!]$ [Chen et al. 2006] or $= \begin{cases} \frac{4}{3\pi\, l/d_{core}} - \frac{1}{8\, l/d_{core}{}^{2}} & [\![l/d_{core} \geq 1.4, \mu_i \to 1]\!] \\ \frac{3}{2\, l/d_{core}{}^{2}}\left[\ln(4\, l/d_{core}) - \frac{7}{3}\right] & [\![l/d_{core} \gg 1, \mu_i \to \infty]\!] \end{cases}$ [Chen et al. 2002, eq. (25) & (27)] or see [Chen et al. 2006, Table 2] (which supersedes [Chen et al. 1991]) including correction for μ_i or $= \frac{2.01 \log_{10}(l/d_{core}) - 0.46}{(l/d_{core})^2}$ $[\![l/d_{core} > 10, \mu_i > 1000]\!]$ [Macintyre 1999, eq. (48.22)]

Table A.3 – Magnetometric Demagnetization Factors for Various Geometries (Continued)

Circular Cylinder, Solid	N_{radial}	See [Chen et al. 2001, Table I] for correction for μ_i	$= \frac{1}{2}\ [\![l_{core} \to \infty]\!]$ [Prat-Camps et al. 2012] or see [Chen et al. 2006, Table 3] (which supersedes [Chen et al. 2001, Table I]) including correction for μ_i or see [Chen et al. 2006, eq. (26)-(27)]
Circular Cylinder, Hollow	N_{axial}	See [Beleggia et al. 2009a, eq. (11) & Table 1 or (14)-(15)] or $= 1 - 4N_{local,toroidal} - \frac{2}{\mu_i - 1}$ [Primdahl et al. 2002, eq. (12)]	
	N_{radial}	$= 2N_{local,toroidal} + \frac{1}{\mu_i - 1}$ [Primdahl et al. 2002, eq. (12)]	$= \frac{1}{2}\left(1 - \left(\frac{d_{hollow}}{d_{core}}\right)^2 \frac{\mu_i - 1}{\mu_i + 1}\right)\ [\![l_{core} \to \infty]\!]$ [Prat-Camps et al. 2012, eq. (25)]
Torus	N_{axial}	See [Beleggia et al. 2009a, eq. (2.26)]	$= {}^{1}/_{2}$ [Beleggia et al. 2009a]
Oval Ring	$N_{rad,long}$		$= 6.58 \frac{l_{core\ //\ axis}(d_{core} - d_{hollow})}{\left(min(l_{core\ \perp axis}) + 1.8 max(l_{core\ \perp axis})\right)^2} + \frac{0.2}{\mu_i} + 15 \times 10^{-6}$ [Kubik and Ripka 2008, eq. (15)-(16)]
Eq. Triangular Prism	N_x, N_y, N_z	See [Tang et al. 2005]	
Cyl. Rod with Disk Ends	N_{axial}		$= N_{axial,cyl.}\{l_{core}, d_{disk}\}\left(\frac{d_{core}}{d_{disk}}\right)^2$ $\left[\!\left[l_{disk} \approx 0.1\, l_{core}, \pm 10\%\ for\ 1 \le \frac{d_{disk}}{d_{core}} \le 15 \right]\!\right]$ [Coillot et al. 2007, eq. (4); Grosz et al. 2010, eq. (3)]

Table A.3 – Magnetometric Demagnetization Factors for Various Geometries (Continued)

Rectangular Prism	N_x, N_y, N_z $(a \times b \times c)$	See [Aharoni 1998, eq. (1)] or see [Beleggia et al. 2006, eq. (21)-(22) or (22)-(25)] or see [Chen et al. 2002, eq. (2)] or see [Chen et al. 2005, Table I] for correction for μ_i	$N_m\{cylinder\}$ $= \begin{cases} N_x, N_z = \frac{1}{2\pi}\left[4\tan^{-1}\left(\frac{a}{c}\right) + \frac{2c}{a}\ln\left(\frac{c}{a}\right) + \left(\frac{a}{c} - \frac{c}{a}\right)\ln\right. \end{cases}$ [Chen et al. 2002, eq. (7)] or see [Chen et al. 2005, Table I] (which otherwise supersedes [Chen et al. 2002])including correction for μ_i or see [Pardo et al. 2004, Table II] for square bars with correction for μ_i or $N_z = (2c/a + 1)^{-1}$ $[\![a = b, \pm 5.5\%]\!]$ [Chen et al. 2002, pg. 1746] from [Sato and Ishii 1989]

Table A.4 – Local Toroidal Demagnetization Factors

Geometry	$N_{local,toroidal}$ (ul)	
	Exact	**Approximate or Tabulated**
Relation to $N_{f,rad}$	$= 0.5\left(N_{f,radial,hollow\ cyl.} - \frac{1}{\mu_i - 1}\right)$ [Primdahl et al. 2002, eq. (12)] Note: not found to be accurate	
Analytical	See [De Graef and Beleggia 2006, eq. (11)] or see [Vuillermet 2010] (numerical)	$= \left[\ln\left(\frac{16 d_{core}^2}{l_{core}^2}\right) - 1\right] \frac{l_{core}(d_{core} - d_{hollow})}{2\pi d_{core}^2}$ $\left[\left[\frac{d_{hollow}}{d_{core}} \to 1, \mu_i \to \infty\right]\right]$ [De Graef and Beleggia 2006, eq. (20)] or $= \frac{1}{2}\left(1 - \frac{d_{hollow}}{d_{core}}\right)\left[1 - N_{f,axial}\{spheroid\} \frac{1 + 2.35 \ln(1 + 0.137\ l/d_{core})}{1 + 2.28 \ln(1 + 0.284\ l/d_{core})}\right]$ $[\![\mu_i \to \infty]\!]$ [Sandomirskii 2008, eq. (13)]
Pseudo-Empirical		$= \frac{1.83(r_{core} - r_{hollow}) l_{core}}{(0.5 d_{core} + 0.5 d_{hollow})^2}$ $[\![\mu_i \to \infty, \pm 0.0003]\!]$ [Primdahl et al. 2002, eq. (37)] or $= \frac{1.826(r_{core} - r_{hollow}) l_{core}}{d_{core}^2}$ $[\![\mu_i \to \infty]\!]$ [De Graef and Beleggia 2006, eq. (2) and pg. 406] or $= \frac{1.37(r_{core} - r_{hollow}) l_{core}}{d_{core}^2}$ $[\![\mu_i \to \infty]\!]$ Better fit to our data using the model of [De Graef and Beleggia 2006, eq. (2) and pg. 406]

APPENDIX B : WIRE SKIN AND PROXIMITY FACTOR TABLES

The following tables present equations for skin and proximity factor for round and Litz conductors, used for impedance calculations. See Chapter 5 for more description and discussion.

The following sections commonly use the following variables:

$$q = \frac{r_{cond}\sqrt{2}}{\delta_{cond}}$$

$$\delta_{cond} \approx \sqrt{\frac{1}{\pi f \mu_0 \mu_{cond} \sigma_{cond}}} \quad [\![good\ conductor]\!]\ m$$

Zero-order Kelvin functions $ber() + bei()$ and their derivatives $ber'() + bei'()$ are also used, which per [Olver and Maximon 2010, eq. (10.61.1) & (10.63.4, re-arranged)] are:

$$ber(x) + jbei(x) = J_0\left(xe^{j3\pi/4}\right)$$

$$ber'(x) + jbei'(x) = -J_1\left(xe^{j3\pi/4}\right)e^{j3\pi/4}$$

where $J_n()$ is the Bessel function of order n.

Table B.1 – Round Conductor Resistance Skin Factor Equations

Description	$F_{R,skin}$ (ul)	Reference
Exact	$= \frac{q}{2}\left[\frac{ber(q)bei'(q)-bei(q)ber'(q)}{(ber'(q))^2+(bei'(q))^2}\right]$	[Knight 2013b, eq. (5.1); Morgan 2013, eq. (7); Dimitrakakis and Tatakis 2009, eq. (5)-(7)]
Thick conductor approx.	$= \frac{r_{cond}^2}{2r_{cond}\delta_{cond}-\delta_{cond}^2} \quad [\![r_{cond} \gg \delta_{cond}]\!]$	[Knight 2013b, eq. (6.2)]
Butterworth's	See reference	[Terman 1943, pg. 77-82]
"TEDML" (±0.09%)	$= \frac{r_{cond}^2}{(2r_{cond}a-a^2)(1+b)}$ $a = \delta_{cond}\left[1-e^{-r_{cond}/\delta_{cond}}\right]$ $b = \frac{0.189774}{(1+0.272481[c^{1.82938}-c^{-0.99457}]^2)^{1.0941}}$ $c = 0.62006\, r_{cond}/\delta_{cond}$	[Knight 2013b, pg. 31]
Approximate	$= 1+\frac{q^4}{192}-\frac{q^8}{46{,}080}+\frac{q^{12}}{41{,}287{,}680} \quad Rayleigh\ (1886)$ $[\![d_{cond} \ll 10\ \delta_{cond}]\!]$ or $=\begin{cases} 1+\frac{q^4}{192+0.8q^4} & q \le 2.8 \\ 0.864-0.0177q+0.0563q^2 & 2.8 < q \le 3.8 \quad (\pm 0.6\%) \\ \frac{q}{2\sqrt{2}}+\frac{4}{15} & q > 3.8 \end{cases}$	[Morgan 2013, eq. (8)-(11)]
Dowell's method	$= A\left[\frac{\sinh(2A)+\sin(2A)}{\cosh(2A)-\cos(2A)}\right] = A\left[\frac{e^{2A}-e^{-2A}+2\sin(2A)}{e^{2A}+e^{-2A}-2\cos(2A)}\right]$ $[\![*, \mu_{int} \to \infty]\!]$ $A = \begin{cases} \frac{r_{cond}}{\delta_{cond}}\sqrt{\frac{\pi d_{cond}}{p}} \\ or \\ \left(\frac{\pi}{4}\right)^{\frac{3}{4}}\frac{d_{cond}}{\delta_{cond}}\sqrt{\frac{d_{cond}}{p}} \end{cases}$	[Dimitrakakis and Tatakis 2009, eq. (3)-(4)] or [Kazimierczuk 2014, eq. (5.110), (5.290), & (5.293)]
Semi-empirical, single-layer	$= \Psi\left[\frac{\sinh(2\Psi)+\sin(2\Psi)}{\cosh(2\Psi)-\cos(2\Psi)}\right] \quad [\![*, \mu_{int} \to \infty, \pm\sim 10\%]\!]$ $F = \frac{n\pi r_{cond}^2}{l_{coil}t_{coil}}$ $\Psi = \frac{r_{cond}\sqrt{\pi}}{\delta_{cond}}\sqrt[4]{F}$ $t_{coil} = n_l\left(d_{cond}+t_{ins,l}\right)-t_{ins,l}$	[Dimitrakakis et al. 2008, eq. (5)-(7)]
∗ Full list of assumptions found in [Kazimierczuk 2014, pg. 266]		

Table B.2 – Round Conductor Resistance Proximity Factor Equations

Description	$F_{R,prox}$ (ul)	Reference
Butterworth's, air-core	$= F_{R,skin}(\Psi - 1)k_{end}$ $[\![d_{cond}/p < 0.5\ (single\ layer), d_{cond} \gg \delta_{cond}]\!]$ ** Ψ - see reference $k_{end} \approx \frac{(n-1)}{n}$ ul [Knight 2016a, eq. (4.1)] Note: [Medhurst 1947a] discusses validity/accuracy	[Terman 1943, pg. 77-82]
Medhurst's empirical, single-layer. air-core	$= F_{R,skin}(\Psi - 1)k_{end}$ $[\![d_{cond} \gg \delta_{cond}]\!]$ ** Ψ - see reference, Table VIII $k_{end} \approx \frac{(n-1)}{n}$ ul [Knight 2016a, eq. (4.1)]	[Medhurst 1947b]
Knight's Frequency-Extension of Medhurst	$= 1 - F_{R,skin} + \Psi\left(F_{R,skin} - 1\right)(n - 1 + 1/\Psi)/n$ ** Ψ - see [Medhurst 1947b, Table VIII]	[Medhurst 1947b] and [Knight 2016a, pg. 10]
Analytical, single-layer	$= F_{R,skin}\left(R_p - 1\right)$ $[\![d_{cond} \gg \delta_{cond}]\!]$ ** R_p - see references	[Smith 1971] or [Smith 1972]
Semi-empirical, single-layer	$= \frac{2}{3} g \Psi \left[\frac{t_{coil}^2 F}{\pi r_{cond}^2} - 1\right]\left[\frac{\sinh(\Psi)-\sin(\Psi)}{\cosh(\Psi)+\cos(\Psi)}\right]$ $[\![*, \mu_{int} \to \infty, \pm\sim 10\%]\!]$ $g = \left(1 - \frac{0.03782}{F}\right)\left(\frac{r_{cond}}{\delta_{cond}}\right)^{[0.15456-(0.06279/F)]}$ $F = \frac{n\pi r_{cond}^2}{l_{coil} t_{coil}}$ $\Psi = \frac{\mathrm{r_{cond}}\sqrt{\pi}}{\delta_{cond}} \sqrt[4]{F}$ $t_{coil} = n_l\left(d_{cond} + t_{ins,l}\right) - t_{ins,l}$	[Dimitrakakis et al. 2008, eq. (5)-(7)]
Modified Ferreira's method, multi-layer	$-\pi q \left(\frac{d_{cond}}{p}\right)^2 \left(\frac{4(n_l^2-1)}{3} + 1\right) \frac{ber_2(q)ber'(q)+bei_2(q)bei'(q)}{(ber(q))^2+(bei(q))^2}$ $[\![*, \mu_{int} \to \infty]\!]$	[Dimitrakakis and Tatakis 2009, eq. (5)-(8)]
Dowell's method, multi-layer	$= A \frac{2(n_l^2-1)}{3}\left[\frac{\sinh(A)-\sin(A)}{\cosh(A)+\cos(A)}\right] =$ $A \frac{2(n_l^2-1)}{3}\left[\frac{e^A - e^{-A} - 2\sin(A)}{e^A + e^{-A} + 2\cos(A)}\right]$ $[\![*, \mu_{int} \to \infty, \pm 60\%]\!]$ $A = \begin{cases} \frac{r_{cond}}{\delta_{cond}}\sqrt{\frac{\pi d_{cond}}{p}} \\ or \\ \left(\frac{\pi}{4}\right)^{\frac{3}{4}} \frac{d_{cond}}{\delta_{cond}}\sqrt{\frac{d_{cond}}{p}} \end{cases}$	[Dimitrakakis and Tatakis 2009, eq. (3)-(4)] or [Kazimierczuk 2014, eq. (5.110), (5.290), & (5.293)]

Table B.2 – Round Conductor Resistance Proximity Factor Equations (Continued)

Modified Dowell's method	$= (1-w)G_1 + wG_2 \ [\![*, \mu_{int} \to \infty, \pm 4\%]\!]$ $G_1 = \frac{3\pi}{16} k^{-3} X \frac{\sinh(kX) - \sin(kX)}{\cosh(kX) + \cos(kX)}$ $G_2 = \frac{\pi X}{32(X^{-3} + b^3)}$ $X = \frac{d_{cond}}{\delta_{cond}}$ $w = \frac{t_{ins,layer}}{d_{cond}} w_1 + w_2$ $w_1 = 0.0596 - \left(0.1558 - 0.3477 e^{\left\{\frac{p - d_{cond}}{1.0673 d_{cond}}\right\}}\right)^2$ $w_2 = 0.0018 + \left(0.1912 - 0.2045 e^{\left\{\frac{p - d_{cond}}{1.3839 d_{cond}}\right\}}\right)^2$ $b = \frac{b_1 - b_2}{\frac{d_{cond}}{p - d_{cond}} + \frac{1}{b_3}} + b_2$ $b_1 = \frac{-0.0037 - 0.0432}{\frac{d_{cond}}{t_{ins,layer}} + \frac{1}{-0.0661}} + 0.0432$ $b_2 = \frac{1.8167 - 0.0074}{\frac{d_{cond}}{t_{ins,layer}} + \frac{1}{0.2195}} + 0.0074$ $b_3 = \frac{0.7053 - 0.8378}{\frac{d_{cond}}{t_{ins,layer}} + \frac{1}{23.8755}} + 0.8378$ $k = \frac{k_1 - k_2}{\frac{d_{cond}}{t_{ins,layer}} + \frac{1}{k_3}} + k_2$ $k_1 = \frac{1.0261 - 0.8149}{\frac{d_{cond}}{p - d_{cond}} + \frac{1}{9.3918}} + 0.8149$ $k_2 = \frac{0.4732 - 0.8023}{\frac{d_{cond}}{p - d_{cond}} + \frac{1}{1.2225}} + 0.8023$ $k_3 = \frac{0.0930 - 0.2588}{\frac{d_{cond}}{p - d_{cond}} + \frac{1}{-0.0334}} + 0.2588$	[Xi Nan and Sullivan 2004, eq. (4)-(12) and Table 1]
Pseudo-empirical transformer	See reference	[Bahmani et al. 2014]
Toroid	See reference	[Cheng and Evans 1994]
$*$ Full list of assumptions found in [Kazimierczuk 2014, pg. 266]		
** Formulas have been re-arranged as they are derived originally for $R_{ac} = R_{dc} F_{R,skin} F_{R,prox,2}$		

Table B.3 – Litz Wire Resistance Skin and Proximity Factors

Description	$F_R = F_{R,skin} + F_{R,prox}$ (ul)	Reference
Numerical, rod core	See reference	[Spang and Albach 2008]
Dowell's method, multi-layer	$= A\left[\frac{\sinh(2A)+\sin(2A)}{\cosh(2A)-\cos(2A)} + \frac{2(n_l^2 n_{strand}-1)}{3}\left(\frac{\sinh(A)-\sin(A)}{\cosh(A)+\cos(A)}\right)\right]$ $[\![*, \mu_{int} \to \infty, \pm 60\%, 0.4 \le \eta \le 0.7, n_l \gg 1]\!]$ $A = \left(\frac{\pi}{4}\right)^{\frac{3}{4}} \frac{d_{strand}}{\delta_{cond}}\sqrt{\eta}$ $\eta = \frac{d_{strand}}{p_{strand}} \approx \frac{n_{strand} d_{strand}^2}{d_{wire}^2} \approx 0.7$ (typ. [Kaz. 2014])	[Kazimierczuk 2014, eq. (5.378)-(5.379)] or [Wojda and Kazimierczuk 2012, eq. (1), (16), & (19)]
Tourkhani and Viarouge's method	$= \frac{q}{2}\left[\frac{ber(q)bei'(q)-bei(q)ber'(q)}{(ber'(q))^2+(bei'(q))^2} - \frac{\pi^2 n_{strand}\beta}{24}\left(16n_l^2 - 1 + \frac{24}{\pi^2}\right)\left(\frac{ber_2(q)ber'(q)+bei_2(q)bei'(q)}{(ber(q))^2+(bei(q))^2}\right)\right]$ Note likely typo in reference (yellow highlight) $q = \frac{r_{strand}\sqrt{2}}{\delta_{cond}}$ ul $\delta_{cond} = \sqrt{\frac{1}{\pi f \mu_0 \mu_{cond} \sigma_{cond}}}$ m $\beta = \frac{n_{turn} n_{strand} \pi r_{strand}^2}{l_{coil} t_{coil}}$ ul	[Tourkhani and Viarouge 2001, eq. (22)-(23) & (31)] and [Barrios et al. 2015, eq. (17)]
Bartoli et al.'s method	$= \frac{q}{2}\left\{\frac{ber(q)bei'(q)-bei(q)ber'(q)}{(ber'(q))^2+(bei'(q))^2} - 2\pi\left[\left(\frac{4(n_l^2-1)}{3} + 1\right) n_{strand}^2 \left(\eta_{ext}^2 + \frac{\eta_{int}^2 x}{2\pi n_{strand}}\right)\right]\left(\frac{ber_2(q)ber'(q)+bei_2(q)bei'(q)}{(ber(q))^2+(bei(q))^2}\right)\right\}$ $\left[\!\left[\frac{r_{strand}}{p} < 0.04\right]\!\right]$ $\eta_{ext} = d_{strand}\frac{\sqrt{\pi}}{2p}$, $\eta_{int} = d_{strand}\frac{\sqrt{\pi}}{2p_{strand}} = \frac{n_{strand} d_{strand}^2}{d_{wire}^2}$ $x = \frac{n d_{strand}^2}{(d_{wire}-2t_{ins,wire})^2}$	[Bartoli et al. 1996, eq. (12), (14), (17), & (19) – has erroneous $\left(\frac{1}{n_{strand}}\right)$ term] or [Väisänen et al. 2013, eq. (1)]
Sullivan's method	$\approx 1 + \frac{(\pi\omega\mu_{cond}\sigma_{cond} n_{turn} n_{strand})^2 d_{strand}^6}{768\, l_{coil}^2} k$ $= 1 + \frac{(\pi\, n_{turn}\, n_{strand})^2 d_{strand}^6}{192\, \delta_{cond}^4\, l_{coil}^2} k$ $[\![d_{strand} < \delta_{cond}]\!]$ k is a factor for the field distribution (typ. ≈ 1 for an un-gapped transformer core, unknown for a rod core)	[Sullivan 1999, eq. (2)] or [Sullivan and Zhang 2014, eq. (10)]
Complex permeability model	See references	[Etemadrezaei and Lukic 2012] or [Xi Nan and Sullivan 2009]
Litz industry	$= S + K\left(\frac{n_{strand} d_{strand,inches}}{d_{wire,inches}}\right)^2 \left(\frac{d_{strand,inches}\sqrt{f}}{10.44}\right)^4$ $S \approx 1, K \approx 2$ (see references)	[litz-wire.com; litzwire.com]
∗ Full list of assumptions found in [Kazimierczuk 2014, pg. 266]		

Table B.4 – Solid Round Wire Inductance Skin Factor Equations

Description	$F_{L,skin}$ (ul)	Reference
Exact	$= \frac{4}{q}\left[\frac{ber(q)ber'(q)-bei(q)bei'(q)}{(ber'(q))^2+(bei'(q))^2}\right]$	[Knight 2013b, eq. (16.2)] or [Morgan 2013, eq. (16)]
Polynomial asymptotically-correct approximation, with modified-Lorentzian correction (±0.016%)	$= a(1-b)\left[1-e^{\{-(1/a)^{1.5819}\}}\right]^{(1/1.5819)}$ $a = \frac{4}{q\sqrt{2}}\left(1+\frac{0.01209}{q+1}-\frac{0.63523}{q^2+1}+\frac{0.16476}{q^3+1}\right)$ ul $b = \frac{-0.198584}{(1+[(0.38691q)^{1.2652}-(0.38691q)^{-0.39709}]^2)^{2.62343}}$ ul	[Knight 2013b, pg. 44 & 46]
Thick conductor approximation	$= \frac{2\delta_{cond}}{r_{cond}}$ $[\![r_{cond} \gg \delta_{cond}]\!]$	[Knight 2013b, pg. 40] or [Morgan 2013 ,eq. (13)]
Rayleigh's approximation	$= 1-\frac{q^4}{384}+\frac{13q^8}{1{,}105{,}920}$ $[\![r_{cond} \ll 10\,\delta_{cond}]\!]$	[Morgan 2013, eq. (15)]
Dowell's method	$= \frac{\sinh(2A)-\sin(2A)}{\cosh(2A)-\cos(2A)} = \frac{e^{2A}-e^{-2A}-2\sin(2A)}{e^{2A}+e^{-2A}-2\cos(2A)}$ $[\![*$ $,\mu_{int} \to \infty]\!]$ $A = \begin{cases} \frac{r_{cond}}{\delta_{cond}}\sqrt{\frac{\pi d_{cond}}{p}} \\ or \\ \left(\frac{\pi}{4}\right)^{\frac{3}{4}}\frac{d_{cond}}{\delta_{cond}}\sqrt{\frac{d_{cond}}{p}} \end{cases}$	[Dimitrakakis and Tatakis 2009, eq. (4)] or [Kazimierczuk 2014, eq. (5.290) & (5.349)]
$*$ Full list of assumptions found in [Kazimierczuk 2014, pg. 266]		

APPENDIX C: COIL INDUCTANCE AND SELF-CAPACITANCE TABLES

The following tables present equations and references for calculating ring coil inductance, solenoidal single- and multi-layer coil inductance, and coil self-capacitance, respectively. See Chapter 6 for more description and discussion.

Table C.1 – Ring (Zero Coil Length) Inductance Equations

Description	L_{coil} (H)	Reference
Exact for a ring, Legendre Polynomials	$= n^2 \frac{\mu_0 \mu_{int} \pi^2 r_{coil} \sqrt{1-\frac{1}{\rho^2}}}{\frac{Q^1_{-1/2}(\rho)}{P^1_{-1/2}(\rho)} - 2\sum_{n=1}^{\infty}\left[\frac{Q^1_{n-1/2}(\rho)}{(4n^2-1)P^1_{n-1/2}(\rho)}\right]}$ $\rho = r_{coil}/r_{cond}$ ul where P^1_{ν} & Q^1_{ν} are Associated Legendre functions (order one, degree ν)	[Carobbi and Bonci 2014, eq. (4)]
Exact for a ring, Maxwell's	$= n^2 M_{ring,1}\{r_{coil}, r_{coil} - r_{wire}, 0\} = \mu_0 \mu_{int} n^2 (2r_{coil} - r_{cond}) \left[\left(1 - \frac{k^2}{2}\right) K_{ei1}(k) - E_{ei2}(k)\right]$ $k = \frac{2\sqrt{r_{coil}(r_{coil}-r_{cond})}}{2r_{coil}-r_{cond}}$ Note: this formula appears with various algebraic arrangements	[Paul 2011, eq. (4.27); Knight 2016b, eq. (10.2); Carobbi and Bonci 2014, eq. (6); Maxwell 1873, §701]
Exact for a ring, Maxwell's alternate	$= n^2 M_{ring,2}\{r_{coil}, r_{coil}, GMD_{wire}\}$ $M_{ring,2}\{r_1, r_2, s\} = 2\mu_0 \mu_{int} \sqrt{\frac{r_1 r_2}{k}} [K_{ei1}(k) - E_{ei2}(k)]$ $k = \frac{s_1 - s_2}{s_1 + s_2}, s_1 = \sqrt{(r_1 + r_2)^2 + s^2}, s_2 = \sqrt{(r_1 - r_2)^2 + s^2}$	[Knight 2016b, eq. (M701.2); Maxwell 1873, §701]

Table C.1 – Ring (Zero Coil Length) Inductance Equations (Continued)

Thin-wire approximation of Maxwell's	$= \mu_0 \mu_{int} r_{coil} n^2 \left[K_{ei1} \left(\frac{\sqrt{r_{coil}^2 - r_{cond}^2}}{r_{coil}} \right) - 2 \right] \quad [\![r_{coil} \gg r_{cond}]\!]$	[Kraichman 1962, eq. (14); Knight 2016b, pg. 58; Paul 2011, pg. 129]
Thin-wire approximation for a ring, Kirchhoff's	$= \mu_0 \mu_{int} r_{coil} n^2 \left[\ln\left(\frac{8 r_{coil}}{r_{cond}}\right) - 2 \right] \quad [\![r_{coil} \gg r_{cond}]\!]$ Note: in [Rosa and Grover 1916; Grover 1946, eq. (119b)], the highlighted value is presented as 1.75 but should be 2 when used for external inductance only	Kirchhoff (1864) as in [Rosa and Grover 1916, eq. (59) ; Grover 1946, eq. (119b)] or [Carobbi and Bonci 2014, eq. (5); Paul 2011, eq. (4.28); Kazimierczuk 2014, eq. (3.13); Maxwell 1873, §706]
Thin-wire approximation, Rayleigh & Niven	$= \mu_0 \mu_{int} r_{coil} n^2 \left[\left(1 + \frac{r_{cond}^2}{8 r_{coil}^2}\right) \ln\left(\frac{8 r_{coil}}{r_{cond}}\right) + \frac{r_{cond}^2}{24 r_{coil}^2} - 2 \right] \quad [\![r_{coil} \gg r_{cond}]\!]$ Note: the highlighted value is presented as 1.75 but should be 2 when used for external inductance only	Rayleigh and Niven as in [Rosa and Grover 1916, eq. (63)]
Ring	See reference **	[Snow 1954, eq. (2.15)-(2.16) & (5.43)]
Ring, numerical	See reference (note: could not replicate results)	[Babic and Akyel 2000, eq. (2) & (9)]
Square Ring	See references*	[Rosa and Grover 1916, eq. (105), Kirchhoff's] or [Grover 1946, eq. (60)]
Polygonal ring	See reference*	[Grover 1946, pg. 59-65]
Short Loop, any shape	$= 276 \log\left(\frac{2 A_{coil}}{P}\right) n^2 \tan\left(k_{wave} \frac{P}{2}\right) \quad [\![P \leq 0.8\lambda]\!]$ $P = Perimeter$ (m)	[Awadalla and Sharshar 1984, eq. (1)-(2)]
Flat/planar spiral	See reference which includes a comprehensive list and comparison of analytical and empirical equations for various shapes, incl. by Rosa, Grover, and Terman	[Kazimierczuk 2014, pg. 488-506]
* Rosa and/or Grover references' formulas generally assume lengths in cm and inductance L in μH or cm		
** [Snow 1954] formulas generally assume lengths in cm and inductance L in nH		
Note: many of the above references of [Rosa and Grover 1916; Grover 1946] can be found in [Terman 1943] albeit simplified (sometimes diminishing their applicability and/or accuracy) and using units of inches		

Table C.2 – Solenoidal Coil Inductance Equations

Description	L_{coil} (H)	Reference
Wheeler's intermediate current-sheet solenoid	$= \frac{0.4\pi^2\mu_0\mu_{int}r_{coil}^2n^2}{l_{coil}+0.9r_{coil}}$ $[\![l_{coil} > 0.4d_{coil}, \pm 1\%]\!]$	[Kazimierczuk 2014, eq. (1.310)]
Long current-sheet solenoid	$= \frac{\mu_0\mu_{int}n^2\pi r^2}{l_{coil}}$ $[\![l_{coil} \gg d_{coil}, r_{cond} \to 0, QS]\!]$ $r = \begin{cases} = r_0 = r_{coil}[1-(r_{cond}/r_{coil})^2] & f \to 0 \ [\![r_{coil} \gg r_{cond}, 2\pi r_{coil} \gg p]\!] \\ \frac{2r_0+\frac{2r_{coil}+d_{cond}(2/n-1)}{(p/d_{cond})-1}}{2+\frac{4}{(p/d_{cond})-1}} & f \to \infty \ [\![d_{cond} \gg \delta_{cond}]\!] \end{cases}$	[Knight 2013a, eq. (1.1), (3.1), & (4.1)-(4.2)] and/or [Kazimierczuk 2014, eq. (1.308)]
Lorenz's Solenoid, Current-Sheet	See references	(Lorenz 1879) see [Nagaoka 1909; Rosa and Grover 1916, eq. (73)] For computing see [Wheeler 1982, eq. (1)-(2); Lundin 1985; Miller 1987, eq. (1)-(2); Weaver 2016]
Solenoid, Current-Sheet, Analytical	See reference (note: could not replicate results)	[Babic and Akyel 2000, eq. (2) & (8)]
Solenoid, Current-Sheet, Numerical	See references	[Luo and Chen 2013, eq. (20)-(21)] or [Ishida et al. 2011]
Rosa's Corrected Solenoid	See references *	[Rosa 1906; Rosa and Grover 1916; Grover 1946]

Table C.2 – Solenoidal Coil Inductance Equations (Continued)

Knight/Rosa Corrected Solenoid	$= \frac{\mu_0 \mu_{int} \pi r_{coil}^2 n^2 k_L}{l_{coil}} - \mu_0 \mu_{int} r_{coil} n (k_s + k_m) = \mu_0 \mu_{int} r_{coil} n \left[\frac{\pi r_{coil} n k_L}{l_{coil}} - k_s - k_m \right]$ $k_L = \begin{cases} \frac{4}{3\pi\sqrt{1-\kappa^2}} \left\{ \frac{1-\kappa^2}{\kappa^2} [K_{ei1}(\kappa) - E_{ei2}(\kappa)] + E_{ei2}(\kappa) - \kappa \right\} & Exact\ (Nagaoka) \\ \frac{2l_{coil}}{\pi d_{coil}} \left[\frac{2.666}{1+1.877 l_{coil}/d_{coil}} + \ln\left(1 + \frac{0.161 d_{coil}}{l_{coil}}\right) \right] & Simple, Optimized, \pm 0.7\% \\ \frac{2l_{coil}}{\pi d_{coil}} \left[\frac{\left[\ln\left(\frac{4d_{coil}}{l_{coil}}\right) - \frac{1}{2}\right]\left[1 + 0.383901\left(\frac{l_{coil}}{d_{coil}}\right)^2 + 0.017108\left(\frac{l_{coil}}{d_{coil}}\right)^4\right]}{1 + 0.258952\left(\frac{l_{coil}}{d_{coil}}\right)^2} + a \right] & l_{coil} \le d_{coil}, \pm 0.0002\%\ (Lundin) \\ \frac{1 + 0.383901 (d_{coil}/l_{coil})^2 + 0.017108 (d_{coil}/l_{coil})^4}{1 + 0.258952 (d_{coil}/l_{coil})^2} - \frac{4 d_{coil}}{3\pi l_{coil}} & l_{coil} > d_{coil}, \pm 0.0003\%\ (Lundin) \end{cases}$ $\kappa = d_{coil} / \sqrt{d_{coil}^2 + l_{coil}^2}$ $a = 0.093842 \left(\frac{l_{coil}}{d_{coil}}\right)^2 + 0.002029 \left(\frac{l_{coil}}{d_{coil}}\right)^4 - 0.000801 \left(\frac{l_{coil}}{d_{coil}}\right)^6$ $k_s = \begin{cases} \frac{\pi d_{coil} k_L \{l_{coil} \to p\}}{2p} - \frac{2}{\sqrt{\kappa_1}} [K_{ei1}(\kappa_1) - E_{ei2}(\kappa_1)] & exact\ (Rosa) \\ \ln\left(1 + \frac{\pi d_{coil}}{2p}\right) + \frac{1}{a} - \ln\left(\frac{8 d_{coil}}{d_{cond}}\right) + 2 - \frac{d_{cond}^2 \left[\ln(8 d_{coil}/d_{cond}) + \frac{1}{3}\right]}{8 d_{coil}^2} & approximate \end{cases}$ $\kappa_1 = \frac{\sqrt{(2r_{coil}/r_{cond})^2 + 1} - 1}{\sqrt{(2r_{coil}/r_{cond})^2 + 1} + 1}$ $a = \frac{1}{\ln(8/\pi) - 0.5} + 3.437 \left(\frac{p}{d_{coil}}\right) + 1.76356 \left(\frac{p}{d_{coil}}\right)^2 + \frac{-0.47}{\left(0.755 + {}^{d_{coil}}/_{p}\right)^{1.44}}$ $k_m(\pm 0.00008) = \begin{cases} \ln(2\pi) - 1.5 & p d_{coil} \le 0 \\ [\ln(2\pi) - 1.5] e^{-2.3736 p d_{coil}} + a & p d_{coil} > 0 \end{cases}$ $a = \ln(1 + p d_{coil}) [-0.0905 b^3 + 1.7565 b^4 - 2.1277 b^5 + 1.0967 b^6 - 0.664 b^7 - 0.4186 b^8 - 0.363 b^9 + 0.499 b^{10}]$ $b = 1/(1 + p d_{coil})$	[Knight 2013a, pg. 29, 38, 62-63, 78, 83]

Table C.2 – Solenoidal Coil Inductance Equations (Continued)

Knight/Rosa/Weaver Corrected Solenoid	Use "Knight/Rosa Corrected Solenoid" (above) using Knight's k_m but use Weaver's k_L & k_s	[Knight 2013a, pg. 29, 38, 62-63, 78, 83] and [Weaver 2016]
Snow's Corrected Solenoid	See reference **	[Snow 1954, eq. (2.26)-(2.27)]
Snow/Weaver Corrected Solenoid	See reference	[Weaver 2016]
Rosa's Corrected Multilayer Solenoid	$= m^4 L_{CS}\{n \to x\} - \Delta_1 + \Delta_2 = \mu_0 \mu_{int} r_{coil} \left[x m^4 \left(\frac{\pi r_{coil} x k_L}{l_{coil}} - A_s - B_s \right) + \frac{n}{n_l l_{coil}} \left\{ \ln\left(\frac{d_{wire}}{d_{cond}}\right) + F + E \right\} \right] \quad [\![p \to 0]\!]$ Note: highlighted terms are only made clear in [Rosa 1907 Multi-Layer] and results can be significantly erroneous if using that presented in [Rosa and Grover 1916]. Note: $d_{wire} \to p$ (noted unceremoniously in [Terman 1943]) as most of Rosa's work were tight coils, so the two would effectively be synonymous k_L – Lorenz/Nagaoka correction factor (see previous) $\Delta_1 = \mu_0 \mu_{int} r_{coil} x m^4 (A_s + B_s)$ $\Delta_2 = \frac{\mu_0 \mu_{int} r_{coil} n}{n_l l_{coil}} \left[\ln\left(\frac{d_{wire}}{d_{cond}}\right) + F + E \right]$ $m = \frac{n t_{coil}}{n_l l_{coil}}$ $x = l_{coil}/t_{coil}$ $A_s = 0.6949 - \frac{t_{coil}^2}{96 r_{coil}^2} \left[\ln\left(\frac{8 r_{coil}}{t_{coil}}\right) + 2.76 \right]$ $B_s = \begin{cases} 0 & x \le 1 \\ -0.3751 x^{-0.5967} + 0.3727 & x > 1 \end{cases}$ (Curve fitting to [Rosa and Grover 1916, Table X]) $F = 0.13806$ (round wire)	[Rosa 1907a; Rosa 1907b, pg. 375; Rosa and Grover 1916, pg. 91, eq. (91) & (93)] or [Terman 1943, eq. (49)-(50); note that simplifications can cause notable errors]

Table C.2 – Solenoidal Coil Inductance Equations (Continued)

	$E \approx \begin{cases} n \approx 10 & 0.015 \\ n \to \infty & 0.01806 \end{cases}$ (see [Rosa and Grover 1916, pg. 141 or explicit definition in [Rosa and Grover 1907]) Note: although the reference calculations were reproduced and should work for any coil length accd. to Rosa, it is very cumbersome and did not do well for the coils measured herein	
Multilayer Solenoid	$= \frac{\mu_0 \mu_{int} \pi r_{coil}^2 n^2}{l_{coil}\left[1+0.9\left(\frac{r_{coil}}{l_{coil}}\right)+0.32\left(\frac{b}{r_{coil}}\right)+0.84\left(\frac{b}{l_{coil}}\right)\right]}$ $[\![\pm 2\%]\!]$ $b = t_{coil} = layers\ thickness\ ("coil\ build")$	[Kazimierczuk 2014, eq. (1.312)]
Multilayer Solenoid	See reference	[Wheeler 1928, eq. (1)]
Multilayer Solenoid, iterative, semi-independent layers	See reference $[\![no\ helicity, d_{wire} \ll r_{coil}]\!]$	[Weaver 2016]
Torus, Corrected	See reference*	[Grover 1946, pg. 169-170]
Torus, Analytical	See reference	[Kazimierczuk 2014, eq. (1.335) or (1.336)]
Torus, Analytical (Images)	See reference	[Hurley and Wilcox 1994, eq. (1-4)]
Rect. Toroid, Corrected	See reference Note: use [Knight 2013/2016] for k_m ("H" in Grover). Can also use [Weaver 2016] for k_s ("G" in Grover).	[Grover 1946, pg. 170] which supersedes [Rosa and Grover 1916]
Rect. Toroid, Current-Sheet	$= \begin{cases} \frac{\mu_0 \mu_{int} l_{core} n^2}{2\pi} \ln\left(\frac{d_{core}}{d_{hollow}}\right) & Analytical \\ 4.6\mu_0 \mu_{int} l_{core} n^2 \log_{10}\left(\frac{d_{core}}{d_{hollow}}\right) \times 10^{-7} & Empirical \end{cases}$	[Kazimierczuk 2014, eq. (1.323), (1.331), & (1.334)]; "analytical" is common-place (e.g. [Rosa and Grover 1916; Grover 1946]).

Table C.2 – Solenoidal Coil Inductance Equations (Continued)

Rect. Coil, Single-layer, Corrected	See references*	[Grover 1946, pg. 70-74] and correction in [Wheeler 1982 eq. (8)-(9)]
Rect. Coil, Multi-Layer, Corrected	See reference (note: units of inches)	[Terman 1943, §2 eq. (55) & (59)]
Polygonal Coil, Multi-Layer	To a first-order assumption, transform the polygon into an effective circular radius [Grover 1946, eq. (150)] and use the desired circular, multi-layer coil equation	
Square Coil, Current-Sheet, Approx.	See reference	[Wheeler 1982, eq. (14)]
Short Polygonal Coil, Corrected	See reference*	[Grover 1946, pg. 170-176]
Polygonal Coil, Current-Sheet, Numerical	See reference	[Ishida et al. 2011]
General	$= \frac{\mu_0 \mu_{int} n^2 S_{coil}}{\text{MPL}} = \frac{\mu_0 \mu_{int} n^2 S_{coil}}{l_{coil}} K_{shape}$ $0 \leq K_{shape} \leq 1 -$ shape factor (e.g. k_L for round solenoid, not including round wire corrections)	
* Rosa and/or Grover references' formulas generally assume lengths in cm and inductance L in μH or cm		
** [Snow 1954] formulas generally assume lengths in cm and inductance L in nH		
Note: any "current-sheet" calculation can be corrected as $L_{self} = L_{self,C.S.} - \mu_0 \mu_{int} r_{coil} n(k_s + k_m)$ though the correction for non-circular coils should use the effective radius (see [Grover 1946, eq. (150)]). [Weaver 2016] and [Knight 2013/2016] can be used for k_s & k_m.		
Further note: many of the above references of [Rosa and Grover 1916; Grover 1946] can be found in [Terman 1943] albeit simplified (sometimes diminishing their applicability and/or accuracy) and using units of inches		

Table C.3 – Coil Self-Capacitance Equations

Description	C_{self} (F)	Reference
Parallel-Ring Electrodes	$= \frac{\varepsilon_0 \varepsilon_r \pi^2 d_{coil}}{\cosh^{-1}(l_{coil}/d_{wire})} \quad [\![ESL]\!]$	[Knight 2013c, eq. (8.1)]
Single-layer	$= d_{coil}\left(\frac{0.1126\, l_{coil}}{d_{coil}} + 0.08 + \frac{0.27}{\sqrt{l_{coil}/d_{coil}}}\right) \times 10^{-10}$	[Medhurst 1947b]
Single-layer, doubly-asymptotic, empirically-corrected (±2.1%)	$= \frac{4\varepsilon_0 \varepsilon_{ins} l_{coil}}{\pi(\cos(\psi))^2}\left[1 + 0.5k_c\left(1 + \frac{\varepsilon_{core}}{\varepsilon_{ins}}\right)\right] \quad [\![ESL, l_{coil} \gg d_{coil}]\!]$ $k_c = 0.717439\left(\frac{d_{coil}}{l_{coil}}\right) + 0.933048\left(\frac{d_{coil}}{l_{coil}}\right)^{3/2} + 0.106\left(\frac{d_{coil}}{l_{coil}}\right)^2$ ul	[Knight 2013c, eq. (5.3)]
Single-layer	$= \begin{cases} \begin{cases} \frac{4\varepsilon_0 \varepsilon_r \pi^2 r_{coil} r_{cond} n^2}{l_{coil}} & Approximate \\ \frac{C_{tt}}{n-1} & Analytical \end{cases} & [\![Non-conducting\ core, no\ shield]\!] \\ \begin{cases} 2C_{tt} & n = 1,2 \\ 1.5C_{tt} & n = 3 \\ \rightarrow 1.366C_{tt} & n \geq 4 \end{cases} & [\![Conducting\ core/shield]\!] \end{cases}$ $C_{tt} = \frac{\varepsilon_0 \varepsilon_r \pi^2 d_{coil}}{\ln\left\{\left[\frac{p}{2r_{cond}\left(1+\frac{t_{ins,wire}}{r_{cond}}\right)^{1-1/\varepsilon_r}}\right] + \sqrt{\left[\frac{p}{2r_{cond}\left(1+\frac{t_{ins,wire}}{r_{cond}}\right)^{1-1/\varepsilon_r}}\right]^2 - \left(1+\frac{t_{ins,wire}}{r_{cond}}\right)^{2/\varepsilon_r}}\right\}}$	[Kazimierczuk 2014, eq. (9.104), (9.105), (9.114), & (9.205)-(9.216)]
Multi-layer	$= \left[\frac{\varepsilon_{ins,wire}\varepsilon_{ins,layer}}{\varepsilon_{ins,wire}t_{ins,layer} + \varepsilon_{ins,layer}t_{ins,wire}}\right]\frac{0.018544 d_{coil} l_{coil}(n_l - 1)}{n_l^2} \times 10^{-9}(?)$	[Macintyre 1999, eq. (48.18)]
Multi-layer	$= \frac{8\pi\varepsilon_0\varepsilon_r l_{coil}(n_l - 1)[d_{coil,inner} + d_{wire,outer} - n_l(\pm t_{ll})]}{6n_l^2(1.26d_{wire,outer} - 1.15d_{wire,inner} + p - 2t_{ins,wire})} \quad [\![ESL, tightly\ packed]\!]$	[Martínez et al. 2014, eq. (46)]

Table C.3 – Coil Self-Capacitance Equations (Continued)

Multi-layer, hexagonal winding	$= \begin{cases} 1.618C_{tt} & [\![Two\ layers, non-conducting\ core, no\ shield]\!] \\ 1.83C_{tt} & [\![Two\ layers, conducting\ core/shield]\!] \quad [\![n \geq 10]\!] \\ 0.5733C_{tt} & [\![Three\ layers, conducting\ core/shield]\!] \end{cases}$ $C_{tt} = \begin{cases} \varepsilon_0 l_{coil}\left[\frac{\varepsilon_r \theta_1}{\ln(r_{wire}/r_{cond})} + \cot\left(\frac{\theta_1}{2}\right) - 3.732\right] & Approximate \\ \frac{2\varepsilon_0\varepsilon_r \pi d_{coil}}{\sqrt{\left[2\varepsilon_r + \ln\left(\frac{r_{wire}}{r_{cond}}\right)\right]\ln\left(\frac{r_{wire}}{r_{cond}}\right)}} \tan^{-1}\left(\frac{\sqrt{3}-1}{\sqrt{3}+1}\sqrt{\frac{2\varepsilon_r + \ln\left(\frac{r_{wire}}{r_{cond}}\right)}{\ln\left(\frac{r_{wire}}{r_{cond}}\right)}}\right) & Analytical \end{cases}$ $\theta_1 = \cos^{-1}(1 - \ln(r_{wire}/r_{cond})/\varepsilon_r)$ $r_{wire} = r_{cond} + t_{ins,wire}$	[Kazimierczuk 2014, eq. (9.127)-(9.130) & (9.147)]
Multi-layer, tightly-packed	$= \frac{1}{n^2}\left\{n_l C_{tt}\left(n_{\frac{t}{l}} - 1\right) + C_{ll}\sum_{i=1}^{n_{\frac{t}{l}}}[(n_l - 1)(2i-1)^2]\right\}$ $[\![ESL, tightly\ packed]\!]$ $C_{tt} = \frac{4\pi a_0 \varepsilon_0 r_{coil}}{\sqrt{1-a_0^2}} \tan^{-1}\left[\sqrt{\frac{1+a_0}{1-a_0}}\tan\left(\frac{\pi}{8}\right)\right]$ $a_0 = \frac{1}{\left(1 + \frac{\pm t_{ll}}{2\left(r_{wire,outer}\right)}\right) - \varepsilon_r^{-1}\ln\left(1 - \frac{t_{ins,wire}}{r_{wire,outer}}\right)}$ $\frac{4\pi b_0 \varepsilon_0 r_{coil}}{\sqrt{1-b_0^2}} \tan^{-1}\left[\sqrt{\frac{1+b_0}{1-b_0}}\tan\left(\frac{\pi}{8}\right)\right]$ $b_0 = \frac{1}{\left(1 + \frac{p - 2t_{ins,wire}}{2\left(r_{wire,outer}\right)}\right) - \varepsilon_r^{-1}\ln\left(1 - \frac{t_{ins,wire}}{r_{wire,outer}}\right)}$ $C_{ll} = \frac{4\pi b_0 \varepsilon_0 r_{coil}}{\sqrt{1-b_0^2}} \tan^{-1}\left[\sqrt{\frac{1+b_0}{1-b_0}}\tan\left(\frac{\pi}{8}\right)\right]$ $b_0 = \frac{1}{\left(1 + \frac{p - 2t_{ins,wire}}{2\left(r_{wire,outer}\right)}\right) - \varepsilon_r^{-1}\ln\left(1 - \frac{t_{ins,wire}}{r_{wire,outer}}\right)}$	[Martínez et al. 2014, eq. (20) & (25)-(28), ref. 23]

Table C.3 – Coil Self-Capacitance Equations (Continued)

Multi-layer	$= 4C_{ll}\left(\frac{n_l-1}{n_l^2}\right)\ [\![QS]\!]$ $C_{ll\,\{ortho\}} = \frac{\varepsilon_0 l_{wire}}{n_l\left(1-\frac{t_{ins,wire}}{\varepsilon_{ins,wire} r_{wire}}\right)}\left[a_1 + \frac{a_2 t_{ins,wire}^2}{2\varepsilon_{ins,wire} r_{wire}^2\left(1-\frac{t_{ins,wire}}{\varepsilon_{ins,wire} r_{wire}}\right)}\right]$ $a_1 = \frac{b}{\sqrt{b^2-1}}\tan^{-1}\left(\sqrt{\frac{b+1}{b-1}}\right) - \frac{\pi}{4}$ $a_2 = \frac{b(b^2-2)}{(b^2-1)^{3/2}}\tan^{-1}\left(\sqrt{\frac{b+1}{b-1}}\right) - \frac{b}{2(b^2-1)} - \frac{\pi}{4}$ $b = \frac{1}{1-\frac{t_{ins,wire}}{\varepsilon_{ins,wire} r_{wire}}}\left(1 + \frac{t_{ins,ll}}{2\varepsilon_{ins,layer} r_{wire}}\right)$ $C_{ll\,\{cyclic\}} = \frac{4\varepsilon_0\varepsilon_r l_{wire}}{n_l\sqrt{2\varepsilon_r \ln(r_{wire}/r_{cond}) + [\ln(r_{wire}/r_{cond})]^2}}$ $\tan^{-1}\left\{\frac{(\sqrt{3}-1)(2\varepsilon_r + \ln(r_{wire}/r_{cond}))}{(\sqrt{3}+1)\sqrt{(2\varepsilon_r + \ln(r_{wire}/r_{cond}))\ln(r_{wire}/r_{cond})}}\right\}$ $C_{ll} \approx 0.5\left(C_{ll\,\{ortho\}} + C_{ll\,\{cyclic\}}\right)$ $r_{wire} = r_{cond} + t_{ins,wire}$	[Biela and Kolar 2008, eq. (9)-(10), (14), & (23)]
Multi-layer	$= \frac{\pi\varepsilon_0\varepsilon_r l_{coil}}{t_{ins,wire}(n_l-1)}\left[d_{coil} + 2n_l\left(d_{cond} + t_{ins,wire}\right)\right]$	[Coillot and Leroy 2012, eq. (11)]
Oblate spheroidal, solid	See reference	[Simpson and Cahill 2007]
Toroid, single-layer	See references	[Pasko et al. 2015; Middelstädt et al. 2014; Wang et al. 2010]

Table C.3 – Coil Self-Capacitance Equations (Continued)

Prolate spheroidal, solid	$= \frac{\pi\varepsilon_0}{50}\left[12K_1 + \frac{K_3}{7}\right]\begin{cases}\frac{d_{core}^2}{\sqrt{l_{core}^2 - d_{core}^2}} & l_{core} > d_{core} \\ l_{core} & l_{core} = d_{core}\ (sphere)\end{cases} [\![QS]\!]$ $K_1 = \begin{cases}\frac{\varepsilon_r P_1'(a)}{P_1(a)} - \frac{Q_1'(a)}{Q_1(a)} & l_{core} > d_{core} \\ \varepsilon_r + 2 & l_{core} = d_{core}\ (sphere)\end{cases}$ $K_3 = \begin{cases}\frac{\varepsilon_r P_3'(a)}{P_3(a)} - \frac{Q_3'(a)}{Q_3(a)} & l_{core} > d_{core} \\ 3\varepsilon_r + 4 & l_{core} = d_{core}\ (sphere)\end{cases}$ $a = \frac{l_{core}}{\sqrt{l_{core}^2 - d_{core}^2}}$ where P_v' is the derivative of the associated Legendre function P_v (order zero, degree v)	[Simpson and Zhu 2007, eq. (51)-(53)] and [Wait 1953b, eq. (3)]
Prolate spheroidal, hollow	$= \frac{\pi\varepsilon_0}{50}\left[12G_1 + \frac{G_3}{7}\right]\frac{d_{core}^2}{\sqrt{l_{core}^2 + d_{core}^2}}\ [\![QS]\!]$ $G_1 = \varepsilon_r\left[\frac{P_1'(a) + U_1 Q_1'(a)}{P_1(a) + U_1 Q_1(a)}\right] - \frac{Q_1'(a)}{Q_1(a)}$ $G_3 = \varepsilon_r\left[\frac{P_3'(a) + U_3 Q_3'(a)}{P_3(a) + U_3 Q_3(a)}\right] - \frac{Q_3'(a)}{Q_3(a)}$ $U_1 = \frac{\varepsilon_r - 1}{\frac{Q_1(b)}{P_1(b)} - \varepsilon_r\frac{Q_1'(b)}{P_1'(b)}}$ $U_3 = \frac{\varepsilon_r - 1}{\frac{Q_3(b)}{P_3(b)} - \varepsilon_r\frac{Q_3'(b)}{P_3'(b)}}$ $a = \frac{l_{core}}{\sqrt{l_{core}^2 - d_{core}^2}}$ $b = \sqrt{1 + \frac{d_{hollow}^2(a^2-1)}{d_{core}^2}}$	[Simpson 2008, eq. (21)-(22)] and [Wait 1953b, eq. (3)-(4)]

REFERENCES

[Abdeen 1999] A.M. Abdeen, “Dielectric behaviour in Ni-Zn ferrites,” in *Journal of Magnetism and Magnetic Materials*, vol. 192, pp. 121-129, 1999.

[Aharoni 1998] A. Aharoni, “Demagnetizing factors for rectangular ferromagnetic prisms,” in *Journal of Applied Physics*, vol. 83, pp. 3432-3434, 1998.

[Albach et al. 2007] M. Albach, A. Stadler and M. Spang, "The Influence of Ferrite Characteristics on the Inductance of Coils With Rod Cores," in *IEEE Transactions on Magnetics*, vol. 43, no. 6, pp. 2618-2620, June 2007.

[Alvandian 2012] Correspondence with G. Alvandian, 2012.

[An and Smith 1980] L. N. An and G.S. Smith, “The eccentrically insulated circular loop antenna,” in *Radio Science*, vol. 15, no. 6, pp. 1067-1081, Nov.-Dec. 1980.

[An and Smith 1982] L. N. An and G.S. Smith, “The horizontal circular loop antenna near a planar interface,” in *Radio Science*, vol. 17, no. 3, pp. 483-502, May-June 1982.

[Ancona 1978] C. Ancona, "On small antenna impedance in weakly dissipative media," in *IEEE Transactions on Antennas and Propagation*, vol. 26, no. 2, pp. 341-343, Mar 1978.

[Awadalla and Sharshar 1984] K. Awadalla and A. E. M. Sharshar, "A simple method to determine the impedance of a loop antenna," in *IEEE Transactions on Antennas and Propagation*, vol. 32, no. 11, pp. 1248-1251, Nov 1984.

[Babic and Akyel 2000] S. Babic and C. Akyel, "Improvement in calculation of the self- and mutual inductance of thin-wall solenoids and disk coils," in *IEEE Transactions on Magnetics*, vol. 36, no. 4, pp. 1970-1975, July 2000.

[Babic et al. 2010] S. Babic, F. Sirois, C. Akyel and C. Girardi, "Mutual Inductance Calculation Between Circular Filaments Arbitrarily Positioned in Space: Alternative to Grover's Formula," in *IEEE Transactions on Magnetics*, vol. 46, no. 9, pp. 3591-3600, Sept. 2010.

[Bahmani et al. 2014] M. A. Bahmani, T. Thiringer and H. Ortega, "An Accurate Pseudoempirical Model of Winding Loss Calculation in HF Foil and Round Conductors in Switchmode Magnetics," in *IEEE Transactions on Power Electronics*, vol. 29, no. 8, pp. 4231-4246, Aug. 2014.

[Bahmani and Thiringer 2015] M. A. Bahmani and T. Thiringer, "Accurate Evaluation of Leakage Inductance in High-Frequency Transformers Using an Improved Frequency-Dependent Expression," in *IEEE Transactions on Power Electronics*, vol. 30, no. 10, pp. 5738-5745, Oct. 2015.

[Balanis 2012] C.A. Balanis, *Advanced Engineering Electromagnetics*, Wiley Press, Second Edition, 1040 pages, 2012.

[Barrios et al. 2015] E. L. Barrios, A. Ursúa, L. Marroyo and P. Sanchis, "Analytical Design Methodology for Litz-Wired High-Frequency Power Transformers," in *IEEE Transactions on Industrial Electronics*, vol. 62, no. 4, pp. 2103-2113, April 2015.

[Bartoli et al. 1996] M. Bartoli, N. Noferi, A. Reatti and M. K. Kazimierczuk, "Modeling Litz-wire winding losses in high-frequency power inductors," *Power Electronics Specialists Conference, 1996. PESC '96 Record., 27th Annual IEEE,* Baveno, 1996, pp. 1690-1696 vol.2.

[Beleggia et al. 2006] M. Beleggia, M. De Graef, and Y.T. Miller, "The equivalent ellipsoid of a magnetized body," in *Journal of Physics D: Applied Physics*, vol. 39, pp. 891-899, 2006.

[Beleggia et al. 2009a] M. Beleggia, D. Vokoun, and M. De Graef, "Demagnetization factors for cylindrical shells and related shapes," in *Journal of Magnetism and Magnetic Materials*, vol. 321, pp. 1306-1315, 2009.

[Beleggia et al. 2009b] M. Beleggia, M. De Graef, and Y.T. Millev, "Magnetostatics of the uniformly polarized torus," in *Proceedings of the Royal Society A*, vol. 465, pp. 3581-3604, Sep. 2009.

[Belrose 1955] J.S. Belrose, "Ferromagnetic Loop Aerials," in *Wireless Engineer*, vol. 32, pp. 41-46, Feb. 1955.

[Best 2007] S.R. Best, "Small Antennas," Chapter 6 in J. L. Volakis, *Antenna Engineering Handbook*, Fourth Edition, pp. 6-1 – 6-33, McGraw-Hill, 2007.

[Biela and Kolar 2008] J. Biela and J. W. Kolar, "Using Transformer Parasitics for Resonant Converters—A Review of the Calculation of the Stray Capacitance of Transformers," in *IEEE Transactions on Industry Applications*, vol. 44, no. 1, pp. 223-233, Jan.-Feb. 2008.

[Bjork and Bahl 2013] R. Bjork and C.R.H. Bahl, "Demagnetization factor for a powder of randomly packed spherical particles," in *Applied Physics Letters*, vol. 103, no. 10, 2013.

[Bozorth and Chapin 1942] R.M. Bozorth and D.M. Chapin, "Demagnetizing Factors of Rods," in *Journal of Applied Physics*, vol. 13, pp. 320-326, May 1942.

[Brockman et al. 1950] F.G. Brockman, P.H. Dowling, and W.G. Steneck, "Dimensional Effects Resulting from a High Dielectric Constant Found in a Ferromagnetic Ferrite," in *Physical Review*, vol. 77, no. 1, Jan. 1950.

[Burrows 1976] M.L. Burrows, "The submarine-towed ELF loop antenna," in *Radio Science*, vol. 11, no. 4, pp. 357-366, Apr. 1976.

[Butler and Van Bladel 1964] C. Butler and J. Van Bladel, "Electromagnetic fields in a spherical cavity embedded in a dissipative medium," in *IEEE Transactions on Antennas and Propagation*, vol. 12, no. 1, pp. 110-118, Jan 1964.

[Carobbi et al. 2000] C. F. M. Carobbi, L. M. Millanta and L. Chiosi, "The high-frequency behavior of the shield in the magnetic-field probes," *Electromagnetic Compatibility, 2000. IEEE International Symposium on*, Washington, DC, vol.1, pp. 35-40, 2000.

[Carobbi and Bonci 2014] C. F. M. Carobbi and A. Bonci, "Electromotive Force Induced in and Inductance of an Electrically Small Circular Loop Antenna," in *IEEE Transactions on Electromagnetic Compatibility*, vol. 56, no. 4, pp. 780-783, Aug. 2014.

[Carr and Hippisley 2011] J. Carr and G. Hippisley, *Practical Antenna Handbook*, McGraw-Hill Education TAB, Fifth Edition, 784 pages, 2011.

[Chen and King 1963] C. L. Chen and R. King, "The small bare loop antenna immersed in a dissipative medium," in *IEEE Transactions on Antennas and Propagation*, vol. 11, no. 3, pp. 266-269, May 1963.

[Chen et al. 1991] D. X. Chen, J. A. Brug and R. B. Goldfarb, "Demagnetizing factors for cylinders," in *IEEE Transactions on Magnetics*, vol. 27, no. 4, pp. 3601-3619, July 1991.

[Chen et al. 2001] Du-Xing Chen, E. Pardo and A. Sanchez, "Radial magnetometric demagnetizing factor of thin disks," in *IEEE Transactions on Magnetics*, vol. 37, no. 6, pp. 3877-3880, Nov 2001.

[Chen et al. 2002] Du-Xing Chen, E. Pardo and A. Sanchez, "Demagnetizing factors of rectangular prisms and ellipsoids," in *IEEE Transactions on Magnetics*, vol. 38, no. 4, pp. 1742-1752, Jul 2002.

[Chen et al. 2005] D. X. Chen, E. Pardo and A. Sanchez, "Demagnetizing factors for rectangular prisms," in *IEEE Transactions on Magnetics*, vol. 41, no. 6, pp. 2077-2088, June 2005.

[Chen et al. 2006] D.X. Chen, E. Pardo, and A. Sanchez, "Fluxmetric and magnetometric demagnetizing factors for cylinders," in *Journal of Magnetism and Magnetic Materials*, vol. 306, pp. 135-146, 2006.

[Cheng and Evans 1994] K. W. E. Cheng and P. D. Evans, "Calculation of winding losses in high-frequency toroidal inductors using single strand conductors," in *IEE Proceedings - Electric Power Applications*, vol. 141, no. 2, pp. 52-62, Mar 1994.

[Cheng and Shu 2014a] Yuhua Cheng and Yaming Shu, "Mutual inductance calculation between arbitrarily positioned rectangular filaments," in *International Journal of Applied Electromagnetics and Mechanics*, vol. 46, pp. 287-298, 2014.

[Cheng and Shu 2014b] Y. Cheng and Y. Shu, "A New Analytical Calculation of the Mutual Inductance of the Coaxial Spiral Rectangular Coils," in *IEEE Transactions on Magnetics*, vol. 50, no. 4, pp. 1-6, April 2014.

[Clarke 2014] R. Clarke, "Magnetism: quantities, units and relationships," July 2014, <http://info.ee.surrey.ac.uk/Workshop/advice/coils/terms.html>.

[CMI MN60] Ceramic Magnetics, Inc., MN60 material specification, <http://www.cmi-ferrite.com/Materials/Datasheets/MnZn/MN60.pdf>.

[Cohen et al. 2010] M. B. Cohen, U. S. Inan and E. W. Paschal, "Sensitive Broadband ELF/VLF Radio Reception With the AWESOME Instrument," in *IEEE Transactions on Geoscience and Remote Sensing*, vol. 48, no. 1, pp. 3-17, Jan. 2010.

[Cohen 2016] Correspondence with M.B. Cohen (thesis advisor), 2016.

[Coillot and Leroy 2012] C. Coillot and P. Leroy, "Induction Magnetometers Principle, Modeling and Ways of Improvement," Chapter 3 in K. Kuang, *Magnetic Sensors – Principles and Applications*, InTech, 2012.

[Coillot et al. 2007] C. Coillot, J. Moutoussamy, P. Leroy, G. Chanteur, and A. Roux, "Improvements on the Design of Search Coil Magnetometers for Space Experiments," in *Sensor Letters*, vol. 5, no. 1, pp. 1-4, 2007.

[Coillot et al. 2014] C. Coillot, J. Moutoussamy, M. Boda, and P. Leroy, "New ferromagnetic core shapes for inducting sensors," in *J. Sens. Sens. Syst.*, vol. 3, pp. 1-8, 2014.

[Coillot et al. 2015] C. Coillot, M. El Moussalim, E. Brun, A. Rhouni, R. Lebourgeois, G. Sou, and M. Mansour, "Magnetic noise contribution of the ferromagnetic core of induction magnetometers," in *J. Sens. Sens. Syst.*, vol. 4, pp. 229-237, 2015.

[Conway 2001] J. T. Conway, "Exact solutions for the magnetic fields of axisymmetric solenoids and current distributions," in *IEEE Transactions on Magnetics*, vol. 37, no. 4, pp. 2977-2988, Jul 2001.

[Conway 2006] J. T. Conway, "Trigonometric Integrals for the magnetic field of the coil of rectangular cross section," in *IEEE Transactions on Magnetics*, vol. 42, no. 5, pp. 1538-1548, May 2006.

[Conway 2007] J. T. Conway, "Inductance Calculations for Noncoaxial Coils Using Bessel Functions," in *IEEE Transactions on Magnetics*, vol. 43, no. 3, pp. 1023-1034, March 2007.

[Conway 2008] J. T. Conway, "Noncoaxial Inductance Calculations Without the Vector Potential for Axisymmetric Coils and Planar Coils," in *IEEE Transactions on Magnetics*, vol. 44, no. 4, pp. 453-462, April 2008.

[Conway 2010] J. T. Conway, "Inductance Calculations for Circular Coils of Rectangular Cross Section and Parallel Axes Using Bessel and Struve Functions," in *IEEE Transactions on Magnetics*, vol. 46, no. 1, pp. 75-81, Jan. 2010.

[Conway 2013] J. T. Conway, "Analytical Solutions for the Self- and Mutual Inductances of Concentric Coplanar Disk Coils," in *IEEE Transactions on Magnetics*, vol. 49, no. 3, pp. 1135-1142, March 2013.

[Corum and Corum 1987] J. Corum and K. Corum, "Toroidal helix antenna," *Antennas and Propagation Society International Symposium, 1987*, Blacksburg, VA, USA, 1987, pp. 832-835.

[Corum et al. 2006] K.L. Corum, P.V. Pesavento, and J.F. Corum, "Multiple Resonances in RF Coils and the Failure of Lumped Inductance Models," in *Sixth International Symposium Nikola Tesla,* Oct. 2006.

[Cross 2007] R. Cross, "Ferrite Rod Receiving Loop Antenna Analysis and Modeling," spreadsheet and documentation, Sept. 2007. <http://raylcross.net/murod_mm/index.html>

[Cruzan 1959] O. Cruzan, "Radiation properties of a thin wire loop antenna embedded in a spherical medium," in *IRE Transactions on Antennas and Propagation*, vol. 7, no. 4, pp. 345-352, October 1959.

[Davis et al. 1977] J. Davis, R. Dinger and J. Goldstein, "Development of a superconducting ELF receiving antenna," in *IEEE Transactions on Antennas and Propagation*, vol. 25, no. 2, pp. 223-231, Mar 1977.

[DeBonte and Butherus 1977] W. DeBonte and A. Butherus, "Magnetically permeable adhesives and adhesive-joined shield structures," in *IEEE Transactions on Magnetics*, vol. 13, no. 5, pp. 1376-1378, Sep 1977.

[De Graef and Beleggia 2006] M. De Graef and M. Beleggia, "The fluxgate ring-core demagnetization field," in *Journal of Magnetism and Magnetic Materials*, vol. 305, pp. 403-409, 2006.

[De León et al. 2014] F. de León, S. Purushothaman and L. Qaseer, "Leakage Inductance Design of Toroidal Transformers by Sector Winding," in *IEEE Transactions on Power Electronics*, vol. 29, no. 1, pp. 473-480, Jan. 2014.

[De Queiroz 2014] A.C.M. de Queiroz, "Mutual Inductance and Inductance Calculations by Maxwell's Method," Oct. 2014, <http://www.coe.ufrj.br/~acmq/tesla/maxwell.pdf>.

[Deschamps 1962] G. Deschamps, "Impedance of an antenna in a conducting medium," in *IRE Transactions on Antennas and Propagation*, vol. 10, no. 5, pp. 648-650, September 1962.

[DeVore and Bohley 1977] R. DeVore and P. Bohley, "The electrically small magnetically loaded multiturn loop antenna," in *IEEE Transactions on Antennas and Propagation*, vol. 25, no. 4, pp. 496-505, Jul 1977.

[Dimitrakakis et al. 2008] G. S. Dimitrakakis, E. C. Tatakis and E. J. Rikos, "A Semiempirical Model to Determine HF Copper Losses in Magnetic Components With Nonlayered Coils," in *IEEE Transactions on Power Electronics*, vol. 23, no. 6, pp. 2719-2728, Nov. 2008.

[Dimitrakakis and Tatakis 2009] G. S. Dimitrakakis and E. C. Tatakis, "High-Frequency Copper Losses in Magnetic Components With Layered Windings," in *IEEE Transactions on Magnetics*, vol. 45, no. 8, pp. 3187-3199, Aug. 2009.

[Dinger and Davis 1976] R. J. Dinger and J. R. Davis, "Adaptive methods for motion-noise compensation in extremely low frequency submarine receiving antennas," in *Proceedings of the IEEE*, vol. 64, no. 10, pp. 1504-1511, Oct. 1976.

[Duan and Luo 2014] H. Duan and Q. Luo, "Adaptive Backtracking Search Algorithm for Induction Magnetometer Optimization," in *IEEE Transactions on Magnetics*, vol. 50, no. 12, pp. 1-6, Dec. 2014.

[Etemadrezaei and Lukic 2012] M. Etemadrezaei and S. M. Lukic, "Equivalent complex permeability and conductivity of Litz wire in wireless power transfer systems," *2012 IEEE Energy Conversion Congress and Exposition (ECCE)*, Raleigh, NC, 2012, pp. 3833-3840.

[Ferroxcube] Ferroxcube, “Soft Ferrites and Accessories Data Handbook,” 2013. <http://www.ferroxcube.com/FerroxcubeCorporateReception/datasheet/FXC_HB 2013.pdf>.

[Fincan and Üstün 2015] B. Fincan and Ö Üstün, "A study on comparing analytical methods for coil design in high frequency wireless energy transfer," *Emerging Technologies: Wireless Power (WoW), 2015 IEEE PELS Workshop on*, Daejeon, 2015, pp. 1-5.

[Fiorillo et al. 2009] F. Fiorillo, C. Beatrice, M. Coisson and L. Zhemchuzhna, "Loss and Permeability Dependence on Temperature in Soft Ferrites," in *IEEE Transactions on Magnetics*, vol. 45, no. 10, pp. 4242-4245, Oct. 2009.

[Fiorillo et al. 2010] F. Fiorillo, E. Ferrara, M. Coisson, C. Beatrice, and N. Banu, “Magnetic properties of soft ferrites and amorphous ribbons up to radiofrequencies,” in *Journal of Magnetism and Magnetic Materials*, vol. 322, pp. 1497-1504, 2010.

[Fiorillo and Beatrice 2011] F. Fiorillo and C. Beatrice, “Energy Losses in Soft Magnets from DC to Radiofrequencies: Theory and Experiment,” in *Journal of Superconductivity and Novel Magnetism*, vol. 24, pp. 559-566, 2011.

[Fiorillo et al. 2014] F. Fiorillo, C. Beatrice, O. Bottauscio and E. Carmi, "Eddy-Current Losses in Mn-Zn Ferrites," in *IEEE Transactions on Magnetics*, vol. 50, no. 1, pp. 1-9, Jan. 2014.

[Fiorillo and Beatrice 2015] F. Fiorillo and C. Beatrice, “A comprehensive approach to broadband characterization of soft ferrites,” in *International Journal of Applied Electromagnetics and Mechanics*, vol. 48, pp. 283-294, 2015.

[Fraga et al. 1998] E. Fraga, C. Prados and D. X. Chen, "Practical model and calculation of AC resistance of long solenoids," in *IEEE Transactions on Magnetics*, vol. 34, no. 1, pp. 205-212, Jan 1998.

[Galejs 1963] J. Galejs, “Small Electric and Magnetic Antennas with Cores of a Lossy Dielectric,” in *Journal of Research of the National Bureau of Standards*, vol. 67D, no. 4, pp. 445-451, Aug. 1963.

[Galejs 1965] J. Galejs, "Admittance of insulated loop antennas in a dissipative medium," in *IEEE Transactions on Antennas and Propagation*, vol. 13, no. 2, pp. 229-235, Mar 1965.

[Giri and King 1978] D.V. Giri and R.W.P. King, "Electrically Small Loop Antenna Loaded by a Homogenous and Isotropic Ferrite Cylinder-Part II," technical report 668 for *Office of Naval Research*, July 1978.

[Grandi et al. 1999] G. Grandi, M. K. Kazimierczuk, A. Massarini and U. Reggiani, "Stray capacitances of single-layer solenoid air-core inductors," in *IEEE Transactions on Industry Applications*, vol. 35, no. 5, pp. 1162-1168, Sep/Oct 1999.

[Green 2001] L. Green, "RF-inductor modeling for the 21st century," in *EDN Magazine*, p.p. 67-74, Sept. 2001.

[Grosz et al. 2010] A. Grosz, E. Paperno, S. Amrusi, and E. Livertis, "Integration of the electronics and batteries inside the hollow core of a search coil," in *Journal of Applied Physics*, vol. 107, 09E703, 2010.

[Grosz and Paperno 2012] A. Grosz and E. Paperno, "Analytical Optimization of Low-Frequency Search Coil Magnetometers," in *IEEE Sensors Journal*, vol. 12, no. 8, pp. 2719-2723, Aug. 2012.

[Grover 1946] F.W. Grover, *Inductance Calculations*, Dover Publications, 304 pages, 2013, reprint of 1946 original.

[Hämäläinen et al. 2014] H. Hämäläinen, J. Pyrhönen, J. Nerg and J. Talvitie, "AC Resistance Factor of Litz-Wire Windings Used in Low-Voltage High-Power Generators," in *IEEE Transactions on Industrial Electronics*, vol. 61, no. 2, pp. 693-700, Feb. 2014.

[Hamilton 2015] N.C. Hamilton, "The complex initial reluctivity, permeability and susceptibility spectra of magnetic materials," in *Journal of Magnetism and Magnetic Materials*, vol. 377, pp. 496-501, 2015.

[Hansen 1963] R. Hansen, "Radiation and reception with buried and submerged antennas," in *IEEE Transactions on Antennas and Propagation*, vol. 11, no. 3, pp. 207-216, May 1963.

[Hansen and Collin 2011] R.C. Hansen and R.E. Collin, *Small Antenna Handbook*, Wiley Press, 360 pages, 2011.

[Harriman et al. 2010] S. K. Harriman, E. W. Paschal and U. S. Inan, "Magnetic Sensor Design for Femtotesla Low-Frequency Signals," in *IEEE Transactions on Geoscience and Remote Sensing*, vol. 48, no. 1, pp. 396-402, Jan. 2010.

[Hole and Appel 2005] M. J. Hole and L. C. Appel, "Stray capacitance of a two-layer air-cored inductor," in *IEE Proceedings - Circuits, Devices and Systems*, vol. 152, no. 6, pp. 565-572, 9 Dec. 2005.

[Huang and Zhang] R. Huang and D. Zhang, "Theoretical and Experimental Comparison of Different Lumped Circuit Methods for Determination of Mn–Zn Ferrites' Intrinsic Complex Permeability and Permittivity," in *IEEE Transactions on Magnetics*, vol. 44, no. 6, pp. 846-849, June 2008.

[Hurley and Wilcox 1994] W. G. Hurley and D. J. Wilcox, "Calculation of leakage inductance in transformer windings," in *IEEE Transactions on Power Electronics*, vol. 9, no. 1, pp. 121-126, Jan 1994.

[Hurley et al. 2015] W. G. Hurley, M. C. Duffy, J. Zhang, I. Lope, B. Kunz and W. H. Wölfle, "A Unified Approach to the Calculation of Self- and Mutual-Inductance for Coaxial Coils in Air," in *IEEE Transactions on Power Electronics*, vol. 30, no. 11, pp. 6155-6162, Nov. 2015.

[Ishida et al. 2011] K. Ishida, T. Itaya, A. Tanaka, N. Takehira and T. Miki, "Arbitrary-shaped single-layer coil self-inductance using shape functions," in *IET Science, Measurement & Technology*, vol. 5, no. 1, pp. 21-27, January 2011.

[Islam 1963] M.A. Islam, "Mathematical Analysis on the Effect of a Prolate Spheroidal Core in a Magnetic Dipole Field," in *Journal of Mathematical Physics*, vol. 4, no. 9, pp. 1206-1212, Sept. 1963.

[Janse van Rensburg and Ferreira 2004] P.A. Janse van Rensburg and H.C. Ferreira, "The Role of Magnetizing and Leakage Inductance in Transformer Coupling Circuitry," presentation in *2004 8th IEEE International Symposium on Power Line Communications and Its Applications (ISPLC)*, 2004.

[Jenkins et al. 2014] A. Jenkins, V. Bana and G. Anderson, "Impedance of a coil in seawater," *Antennas and Propagation Society International Symposium (APSURSI), 2014 IEEE*, Memphis, TN, 2014, pp. 625-626.

[Jordan et al. 2009] J.W. Jordan, B.K. Sternberg, and S.L. Dvorak, "Development and validation of a low-frequency modeling code for high-moment transmitter rod antennas," in *Radio Science*, vol. 44, RS6008, 2009.

[Kazimierczuk 2014] M.K. Kazimierczuk, *High-Frequency Magnetic Components*, Wiley Press, Second Edition, 756 pages, 2014.

[King et al. 1964] R. King, C. Harrison and D. Tingley, "The admittance of bare circular loop antennas in a dissipative medium," in *IEEE Transactions on Antennas and Propagation*, vol. 12, no. 4, pp. 434-438, Jul 1964.

[King and Smith 1981] R.W.P. King and G.S. Smith, *Antennas in Matter: Fundamentals, Theory and Applications*, MIT Press, 868 pages, 1981.

[King et al. 1992] R.W.P. King, M. Owens, and T.T. Wu, *Lateral Electromagnetic Waves*, Springer Press, 746 pages, 1992.

[Knight 2013a and 2016b] D.W. Knight, "An introduction to the art of Solenoid Inductance Calculation with emphasis on radio-frequency applications," un-published, version 0.20, Feb. 2016, <http://g3ynh.info/zdocs/magnetics/>.

[Knight 2013b] D.W. Knight, "Practical continuous functions for the internal impedance of solid cylindrical conductors," un-published, version 2.06, Apr. 2013, <http://www.g3ynh.info/>.

[Knight 2013c] D.W. Knight, "The self-resonance and self-capacitance of solenoid coils," un-published, version 0.08, July 2013, <http://www.g3ynh.info/>.

[Knight 2016a] D.W. Knight, "An introduction to the art of Solenoid Inductance Calculation Part II Solenoid Impedance and Q," un-published, version 0.01, Jan. 2016, <http://g3ynh.info/zdocs/magnetics/>.

[Kobayashi and Iijima 1996] M. Kobayashi and H. Iijima, "Surface magnetic charge distributions of cylindrical tubes," in *IEEE Transactions on Magnetics*, vol. 32, no. 1, pp. 270-273, Jan 1996.

[Kobayashi et al. 1996] M. Kobayashi, Y. Ishikawa and S. Kato, "Magnetizing characteristics of circular cylinders in perpendicularly applied magnetic field," in *IEEE Transactions on Magnetics*, vol. 32, no. 1, pp. 254-258, Jan 1996.

[Kraichman 1962] M.B. Kraichman, "Impedance of a Circular Loop in an Infinite Conducting Medium," in *Journal of Research of the National Bureau of Standards*, vol. 66D, no. 4, July-Aug. 1962.

[Kraichman 1970] M.B. Kraichman, *Handbook of Electromagnetic Propagation in Conducting Media*, University of Michigan Library Press, 140 pages, 1970.

[Kubik and Ripka 2008] J. Kubik and P. Ripka, "Racetrack fluxgate sensor core demagnetization factor," in *Sensors and Actuators A*, vol. 143, pp. 237-244, 2008.

[Liao et al. 2012] Y. Liao, T. H. Hubing and D. Su, "Equivalent Circuit for Dipole Antennas in a Lossy Medium," in *IEEE Transactions on Antennas and Propagation*, vol. 60, no. 8, pp. 3950-3953, Aug. 2012.

[Libby 1946] L. L. Libby, "Special Aspects of Balanced Shielded Loops," in *Proceedings of the IRE*, vol. 34, no. 9, pp. 641-646, Sept. 1946.

[Lindsay and Münter 1983] J. E. Lindsay and K. Münter, "Distributed Parameter Analysis of Shielded Loops Used for Wide-Band H-Field Measurements," in *IEEE Transactions on Instrumentation and Measurement*, vol. 32, no. 1, pp. 241-244, March 1983.

[Liu et al. 2015] K. Liu, W. Zhu, B. Yan, L. Liu and G. Fang, "Ultralow Noise Preamplifier and Optimization Method for Induction Magnetometers," in *IEEE Sensors Journal*, vol. 15, no. 6, pp. 3293-3300, June 2015.

[Lundin 1985] R. Lundin, "A handbook formula for the inductance of a single-layer circular coil," in *Proceedings of the IEEE*, vol. 73, no. 9, pp. 1428-1429, Sept. 1985.

[Luo and Chen 2013] Y. Luo and B. Chen, "Improvement of Self-Inductance Calculations for Circular Coils of Rectangular Cross Section," in *IEEE Transactions on Magnetics*, vol. 49, no. 3, pp. 1249-1255, March 2013.

[Macintyre 1999] S.A. Macintyre, "Magnetic Field Measurement," Chapter 48 in J.G. Webster, *The Measurement, Instrumentation and Sensors Handbook*, First Edition, pp. 48-1 – 48-33, CRC Press, 1999.

[Magni et al. 2012] A. Magni, F. Fiorillo, E. Ferrara, A. Caprile, O. Bottauscio and C. Beatrice, "Domain Wall Processes, Rotations, and High-Frequency Losses in Thin Laminations," in *IEEE Transactions on Magnetics*, vol. 48, no. 11, pp. 3796-3799, Nov. 2012.

[Maksimenko 1991] V.G. Maksimenko, "The Optimization of a VLF-Band Magnetic Antenna," in *Telecommunications and Radio Engineering*, vol. 45, no. 5, pp. 119-121, 1991.

[Manteghi and Ibraheem 2014] M. Manteghi and A. A. Y. Ibraheem, "On the Study of the Near-Fields of Electric and Magnetic Small Antennas in Lossy Media," in *IEEE Transactions on Antennas and Propagation*, vol. 62, no. 12, pp. 6491-6495, Dec. 2014.

[Martínez et al. 2014] J. Martínez, S. Babic and C. Akyel, "On Evaluation of Inductance, DC Resistance, and Capacitance of Coaxial Inductors at Low Frequencies," in *IEEE Transactions on Magnetics*, vol. 50, no. 7, pp. 1-12, July 2014.

[Martinez-Huerta et al. 2013] J.M. Martinez-Huerta, J. De La Torre Medina, L. Piraux, and A. Encinas, "Configuration dependent demagnetizing field in assemblies of interacting magnetic particles," in *Journal of Physics: Condensed Matter*, vol. 25, 2013.

[Massarini et al. 1996] A. Massarini, M. K. Kazimierczuk and G. Grandi, "Lumped parameter models for single- and multiple-layer inductors," *Power Electronics Specialists Conference, 1996. PESC '96 Record., 27th Annual IEEE*, Baveno, vol. 1, pp. 295-301, 1996.

[Matyuk and Osipov 2000] V.F. Matyuk and A.A. Osipov, "Central Demagnetization Factor for Bodies with Difference Shapes. II. Rectangular Rods," in *Russian Journal of Nondestructive Testing*, vol. 36, no. 1, pp. 27-32, 2000.

[Matyuk et al. 2007] V.F. Matyuk, A.A. Osipov, and A.V. Strelyukhin, “Central Demagnetization Coefficient for Hollow Cylindrical Bars Made of Soft Magnetic Materials,” in *Russian Journal of Nondestructive Testing*, vol. 43, no. 3, pp. 154-162, 2007.

[Maxwell 1873] J.C. Maxwell, *A Treatise on Electricity and Magnetism*, vol. 2, 1873.

[Mayer 2009] D. Mayer, "Inductance of Coil in Nonhomogeneous Surrounding," in *IEEE Transactions on Magnetics*, vol. 45, no. 3, pp. 1032-1035, March 2009.

[Medhurst 1947] R.G. Medhurst, “H.F. Resistance and Self-Capacitance of Single-Layer Solenoids,” in *Wireless Engineer*, pp. 35-43 (Feb. 1947) and 80-92 (Mar. 1947).

[Mel’nikov and Mel’nikova 1974] E.A. Mel’nikov and L.N. Mel’nikova, “Receiving Induction Ferrite Antennas,” in *Izvestiya Vysshikh Uchebnykh Zavendeniy: Radioelektronika*, vol. 17, no. 10, 1974.

[Middelstädt et al. 2014] L. Middelstädt, S. Skibin, R. Döbbelin and A. Lindemann, "Analytical determination of the first resonant frequency of differential mode chokes by detailed analysis of parasitic capacitances," *Power Electronics and Applications (EPE'14-ECCE Europe), 2014 16th European Conference on*, Lappeenranta, 2014, pp. 1-10.

[Miller 1987] H. C. Miller, "Inductance formula for a single-layer circular coil," in *Proceedings of the IEEE*, vol. 75, no. 2, pp. 256-257, Feb. 1987.

[Miron 2006] D. B. Miron, *Small Antenna Design*, Newnes, 304 pages, 2006.

[Moore 1963] R. Moore, "Effects of a surrounding conducting medium on antenna analysis," in *IEEE Transactions on Antennas and Propagation*, vol. 11, no. 3, pp. 216-225, May 1963.

[Moore 1967] R. K. Moore, "Radio communication in the sea," in *IEEE Spectrum*, vol. 4, no. 11, pp. 42-51, Nov. 1967.

[Morgan 2013] V. T. Morgan, "The Current Distribution, Resistance and Internal Inductance of Linear Power System Conductors—A Review of Explicit

Equations," in *IEEE Transactions on Power Delivery*, vol. 28, no. 3, pp. 1252-1262, July 2013.

[Musmann and Afanassiev 2010] G. Musmann and Y. Afanassiev, *Fluxgate Magnetometers for Space Research*, Books on Demand, 292 pages, 2010.

[Nagaoka 1909] H. Nagaoka, "The Inductance Coefficients of Solenoids," in *Journal of the College of Science (Imperial University, Tokyo, Japans)*, vol. 27, no. 6, 1909.

[Ng 2004] K.Y. Ng, "Coherent parasitic energy loss of the recycler beam," report TM-2249 for *Fermi National Accelerator Laboratory*, May 2004. <http://lss.fnal.gov/archive/test-tm/2000/fermilab-tm-2249.pdf>

[NMG MN60] National Magnetics Group, Inc., MN60 material specification. <http://www.magneticsgroup.com/pdf/MN60%20.pdf>

[Nikolova 2014] N.K. Nikolova, "Loop Antennas," lecture notes, McMaster University, 2014, <http://www.ece.mcmaster.ca/faculty/nikolova/antenna_dload/current_lectures/L12_Loop.pdf>.

[Nourmohammadi et al. 2014] A. Nourmohammadi, S.M.H. Feiz, and M.H. Asteraki, "Investigation of Noise Reduction and SNR Enhancement in Search Coil Magnetometers at Low Frequencies," submitted Sep. 2014, <http://arxiv.org/abs/1409.7267>.

[Olver and Maximon 2010] F.W.J. Olver and L.C. Maximon, "Bessel Functions," Chapter 10 in Olver et al., *NIST Handbook of Mathematical Functions*, pp. 215-286, Cambridge University Press and National Institute of Standards and Technology, 2010.

[Osborn 1945] J.A. Osborn, "Demagnetizing Factors of the General Ellipsoid," in *Physical Review*, vol. 67, no. 11-12, pp. 351-357, June 1945.

[Ouyang et al. 2015] Z. Ouyang, J. Zhang and W. G. Hurley, "Calculation of Leakage Inductance for High-Frequency Transformers," in *IEEE Transactions on Power Electronics*, vol. 30, no. 10, pp. 5769-5775, Oct. 2015.

[Ozaki et al. 2014] M. Ozaki, S. Yagitani, H. Kojima, K. Takahashi and A. Kitagawa, "Current-Sensitive CMOS Preamplifier for Investigating Space Plasma Waves by Magnetic Search Coils," in *IEEE Sensors Journal*, vol. 14, no. 2, pp. 421-429, Feb. 2014.

[Padhi 1965] T. Padhi, "Theory of Coil Antennas," in *Radio Science Journal of Research NBS/USNC-URSI*, vol. 69D, no. 7, July 1965.

[Pankrac 2012] V. Pankrac, "The Algorithm for Calculation of the Self and Mutual Inductance of Thin-Walled Air Coils of General Shape With Parallel Axes," in *IEEE Transactions on Magnetics*, vol. 48, no. 5, pp. 1875-1889, May 2012.

[Pardo et al. 2004] E. Pardo, Du-Xing Chen and A. Sanchez, "Demagnetizing factors for square bars," in *IEEE Transactions on Magnetics*, vol. 40, no. 3, pp. 1491-1498, May 2004.

[Paschal 1988] E.W. Paschal, *The Design of Broad-Band VLF Receivers with Air-Core Loop Antennas*, Second Edition, May 1988.

[Pasko et al. 2015] S. W. Pasko, M. K. Kazimierczuk and B. Grzesik, "Self-Capacitance of Coupled Toroidal Inductors for EMI Filters," in *IEEE Transactions on Electromagnetic Compatibility*, vol. 57, no. 2, pp. 216-223, April 2015.

[Paul 2011] C.R. Paul, *Inductance: Loop and Partial*, Wiley-IEEE Press, 220 pages, 2011.

[Pavlov 1963] P.P. Pavlov, "Insulated loop antenna with a spherical ferrite core in a conducting medium," in *Radio Eng. Electron. Phys. (USSR)*, vol. 8, pp. 1461-1466, 1963.

[Pettengill et al. 1977] R. Pettengill, H. Garland and J. Meindl, "Receiving antenna design for miniature receivers," in *IEEE Transactions on Antennas and Propagation*, vol. 25, no. 4, pp. 528-530, Jul 1977.

[Phatak et al. 2011] C. Phatak, R. Pokharel, M. Beleggia, and M. De Graef, "On the magnetostatics of chains of magnetic nanoparticles," in *Journal of Magnetism and Magnetic Materials*, vol. 323, pp. 2912-2922, 2011.

[Phillips 1949] F. M. Phillips, "A Note on the Inductance of Screened Single-Layer Solenoids," in *Proceedings of the IEE - Part III: Radio and Communication Engineering*, vol. 96, no. 40, pp. 138-140, March 1949.

[Poole 2004] R.H.M. Poole, "Ferrite Rod Antennas for HF?," R&D White Paper WHP 091 for *British Broadcasting Corporation (BBC)*, July 2004.
(and)
Accompanying spreadsheet < http://downloads.bbc.co.uk/rd/pubs/whp/whp-pdf-files/whp091excel.xls>.

[Pozar 2011] D.M. Pozar, *Microwave Engineering*, Wiley Press, Fourth Edition, 752 pages, 2011.

[Prat-Camps et al. 2012] J. Prat-Camps, C. Navau, D. X. Chen and A. Sanchez, "Exact Analytical Demagnetizing Factors for Long Hollow Cylinders in Transverse Field," in *IEEE Magnetics Letters*, vol. 3, 2012.

[Prat-Camps et al. 2016] J. Prat-Camps, C. Navau, A. Sanchez and D. X. Chen, "Demagnetizing Factors for a Hollow Sphere," in *IEEE Magnetics Letters*, vol. 7, no. , pp. 1-4, Dec. 2016.

[Primdahl et al. 2002] F. Primdahl, P. Brauer, J.M.G. Merayo, and O.V. Nielsen, "The fluxgate ring-core internal field," in *Meas. Sci. Technol.*, vol. 13, pp. 1248-1258, 2002.

[Rhea 2000] R. Rhea, "Filters and an Oscillator Using a New Solenoid Model," in *Applied Microwave & Wireless*, pp. 30-42, Nov. 2000.

[Rhouni et al. 2013] A. Rhouni, G. Sou, P. Leroy and C. Coillot, "Very Low 1/f Noise and Radiation-Hardened CMOS Preamplifier for High-Sensitivity Search Coil Magnetometers," in *IEEE Sensors Journal*, vol. 13, no. 1, pp. 159-166, Jan. 2013.

[Roc'h et al. 2009] A. Roc'h, R. Iannarelli and F. Leferink, "New materials for inductors," *Electromagnetic Compatibility - EMC Europe, 2009 International Symposium on*, Athens, 2009, pp. 1-4.

[Roc'h and Leferink 2012] A. Roc'h and F. Leferink, "Nanocrystalline Core Material for High-Performance Common Mode Inductors," in *IEEE Transactions on Electromagnetic Compatibility*, vol. 54, no. 4, pp. 785-791, Aug. 2012.

[Rosa 1906] E.B. Rosa, “Calculation of the Self-Inductance of Single-Layer Coils,” in *Bulletin of the Bureau of Standards,* vol. 2, no. 2, pp. 161-187.

[Rosa 1907a] E.B. Rosa, “On the Geometrical Mean Distances of Rectangular Areas and the Calculation of Self-Inductance,” in the *Bulletin of the Bureau of Standards,* vol. 3, no. 1, pp. 1-41, 1907.

[Rosa 1907b] E.B. Rosa, “The Self-Inductance of a Coil of any Length Wound with any Number of Layers of Wire,” in *Bulletin of the Bureau of Standards*, vol. 4, no. 3, pp. 369-381, 1907.

[Rosa 1907-8] E.B. Rosa, “The Self and Mutual Inductances of Linear Conductors,” in *Bulletin of the Bureau of Standards*, vol. 4, Science Paper 80, 1907-1908.

[Rosa and Grover 1916] E.B. Rosa and F.W. Grover, “Formulas and Tables for the Calculation of Mutual and Self-Inductance,” in *Bulletin of the Bureau of Standards*, vol. 8, no. 1, 1916.

[Row 1965] R. Row, "Insulated loop antenna in a conducting spherical shell," in *IEEE Transactions on Antennas and Propagation*, vol. 13, no. 2, pp. 216-218, Mar 1965.

[Row 1969] R. Row, "On the receiving properties of a small horizontal bare circular loop antenna buried in the ground," in *IEEE Transactions on Antennas and Propagation*, vol. 17, no. 5, pp. 563-567, Sep 1969.

[Sandomirskii 2008] S.G. Sandomirskii, “Analysis of Formulas for Computation of Central Demagnetization Coefficient for Hollow Cylinders Made of a Material with a High Magnetic Permeability under Magnetization Across the Generatrix,” in *Russian Electrical Engineering,* vol. 79, no. 3, pp. 155-160, 2008.

[Sato and Ishii 1989] M. Sato and Y. Ishii, “Simple and approximate expressions of demagnetizing factors of uniformly magnetized rectangular rod and cylinder,” in *Journal of Applied Physics*, vol. 66, pp. 983-985, 1989.

[Shinagawa et al. 2009] H. Shinagawa, T. Suzuki, M. Noda, Y. Shimura, S. Enoki and T. Mizuno, "Theoretical Analysis of AC Resistance in Coil Using Magnetoplated Wire," in *IEEE Transactions on Magnetics*, vol. 45, no. 9, pp. 3251-3259, Sept. 2009.

[Simpson 1999] T. L. Simpson, "Effect of a conducting shield on the inductance of an air-core solenoid," in *IEEE Transactions on Magnetics*, vol. 35, no. 1, pp. 508-515, Jan 1999.

[Simpson and Zhu 2006] T. Simpson and Y. Zhu, "The Electrically Small Multi-Turn Loop Antenna with a Spheroidal Core," in *IEEE Antennas and Propagation Magazine*, vol. 48, no. 5, pp. 54-66, Oct. 2006.

[Simpson 2007] T. L. Simpson, "Designing an electrically small ferrite-loaded loop antenna for Optimum Performance," *Antennas and Propagation Society International Symposium, 2007 IEEE*, Honolulu, HI, 2007, pp. 5427-5430.

[Simpson and Cahill 2007] T. Simpson and J. Cahill, "The Electrically Small Elliptical Loop with an Oblate Spheroidal Core," in *IEEE Antennas and Propagation Magazine*, vol. 49, no. 5, pp. 83-92, Oct. 2007.

[Simpson and Zhu 2007] T. Simpson and Y. Zhu, "Correction to "The electrically small multi-turn loop antenna with a spheroidal core" [Oct 06 54-66]," in *IEEE Antennas and Propagation Magazine*, vol. 49, no. 2, pp. 80-81, April 2007.

[Simpson 2008] T. Simpson, "Electrically Small Spheroidal Loops Wound on Hollow Ferrite Cores," in *IEEE Antennas and Propagation Magazine*, vol. 50, no. 3, pp. 88-94, June 2008.

[Sinha et al. 2010] D. Sinha, P. K. Sadhu, N. Pal and A. Bandyopadhyay, "Computation of inductance and AC resistance of a twisted litz-wire for high frequency induction cooker," *Industrial Electronics, Control & Robotics (IECR), 2010 International Conference on*, Orissa, 2010, pp. 85-90.

[Smith 1976] G. Smith, "On the electrically small bare loop antenna in a dissipative medium," in *IEEE Transactions on Antennas and Propagation*, vol. 24, no. 4, pp. 533-537, Jul 1976.

[Smith 2007] G.S. Smith, "Loop Antennas," Chapter 5 in J. L. Volakis, *Antenna Engineering Handbook*, Fourth Edition, pp. 5-1 – 5-25, McGraw-Hill, 2007.

[Smith 2016] Correspondence with G.S. Smith (thesis committee member), 2016.

[Snelling 1969] E.C. Snelling, *Soft Ferrites: Properties and Applications*, Iliffe, 390 pages, 1969.

[Snow 1939] C. Snow, "Mutual Inductance and Force Between Two Coaxial Helical Wires," in *Journal of Research of the National Bureau of Standards*, Research Paper RP1178, vol. 22, Feb. 1939.

[Snow 1954] C. Snow, "Formulas for Computing Capacitance and Inductance," Circular 544 in *National Bureau of Standards*, Sep. 1954.

[Spang and Albach 2008] M. Spang and M. Albach, "Optimized Winding Layout for Minimized Proximity Losses in Coils With Rod Cores," in *IEEE Transactions on Magnetics*, vol. 44, no. 7, pp. 1815-1821, July 2008.

[Stadler et al. 2010] A. Stadler, M. Albach and A. Lindner, "A Practical Method to Measure Electrical AC Conductivity of MnZn Ferrites Using Conventional Toroids," in *IEEE Transactions on Magnetics*, vol. 46, no. 2, pp. 678-681, Feb. 2010.

[Stadler 2011] A. Stadler, "Radiated magnetic field of a low-frequency ferrite rod antenna," *Compatibility and Power Electronics (CPE), 2011 7th International Conference-Workshop*, Tallinn, 2011, pp. 283-288.

[Stuart 1966] I.D. Stuart, "Practical Considerations in the Design of Ferrite Cored Aerials for Broadcast Receivers," in *Proceedings I.R.E.E. Australia*, vol. 27, pp. 329-338, Dec. 1966.

[Sullivan 1999] C. R. Sullivan, "Optimal choice for number of strands in a litz-wire transformer winding," in *IEEE Transactions on Power Electronics*, vol. 14, no. 2, pp. 283-291, Mar 1999.

[Sullivan and Harris 2011] C.R. Sullivan and J.H. Harris, "Testing Core Loss for Rectangular Waveforms, Phase II Final Report," Sept. 2011. <http://www.psma.com/coreloss/phase2.pdf>

[Sullivan 2013] C.R. Sullivan, "High-Frequency Core and Winding Loss Modeling," copy of IEMDC talk, 2013. <http://sites.dartmouth.edu/power-magnetics/files/2013/05/sullivan-iemdc_for-web1.pdf>

[Sullivan and Zhang 2014] C. R. Sullivan and R. Y. Zhang, "Simplified design method for litz wire," *2014 IEEE Applied Power Electronics Conference and Exposition - APEC 2014*, Fort Worth, TX, 2014, pp. 2667-2674.

[Tang et al. 2005] K. Tang, H.W. Zhang, Q.Y. Wen, and Z.Y. Zhong, "Demagnetization field of ferromagnetic equilateral triangular prisms," in *Physica B*, vol. 363, pp. 96-101, 2005.

[Tashiro et al. 2015] K. Tashiro, H. Wakiwaka and G. Y. Hattori, "Estimation of Effective Permeability for Dumbbell-Shaped Magnetic Cores," in *IEEE Transactions on Magnetics*, vol. 51, no. 1, pp. 1-4, Jan. 2015.

[Terman 1943] F.E. Terman, *Radio Engineers' Handbook*, McGraw-Hill Book Company, Inc., 1019 pages, 1943.

[Tourkhani and Viarouge 2001] F. Tourkhani and P. Viarouge, "Accurate analytical model of winding losses in round Litz wire windings," in *IEEE Transactions on Magnetics*, vol. 37, no. 1, pp. 538-543, Jan 2001.

[Trask 2008] C. Trask, "An Active Ferrite Rod Antenna with Remote Tuning," unpublished, Feb. 2008, <http://www.home.earthlink.net/~christrask/Active%20Ferrite%20Rod%20Antenna.pdf>.

[Tsutaoka 2003] T. Tsutaoka, "Frequency Dispersion of Complex Permeability in MnZn and NiZn Spinel Ferrites and Their Composite Materials," in *Journal of Applied Physics*, vol. 93, no. 5, pp. 2789-2796, 2003.

[Tumanski 2011] S. Tumanski, *Handbook of Magnetic Measurements*, CRC Press, 404 pages, 2011.

[Väisänen et al. 2013] V. Väisänen, J. Hiltunen, J. Nerg and P. Silventoinen, "AC resistance calculation methods and practical design considerations when using litz wire," *Industrial Electronics Society, IECON 2013 - 39th Annual Conference of the IEEE*, Vienna, pp. 368-375, 2013.

[Van Uitert 1956] L. G. Van Uitert, "Dielectric Properties of and Conductivity in Ferrites," in *Proceedings of the IRE*, vol. 44, no. 10, pp. 1294-1303, Oct. 1956.

[Vuilletermet 2010] Y. Vuillermet, “About the use of numerical integral methods to simulate a fluxgate magnetometer: The ring-core example,” in *Sensors and Actuators A: Physical*, vol. 163, pp. 48-53, 2010.

[Wait 1952] J. R. Wait, "The Magnetic Dipole Antenna Immersed in a Conducting Medium," in *Proceedings of the IRE*, vol. 40, no. 10, pp. 1244-1245, Oct. 1952.

[Wait 1953a] J.R. Wait, “The receiving properties of a wire loop with a spheroidal core,” in *Canadian Journal of Technology*, vol. 31, pp. 9-14, Jan. 1953.

[Wait 1953b] J.R. Wait, “The receiving loop with a hollow prolate spheroidal core,” in *Canadian Journal of Technology*, vol. 31, pp. 132-137, June 1953.

[Wait 1957] J.R. Wait, “Insulated Loop Antenna Immersed in a Conducting Medium,” in *Journal of Research of the National Bureau of Standards*, vol. 59, no. 2, pp. 133-137, Aug. 1957.

[Wait and Spies 1964] J.R. Wait and K.P. Spies, “A Note on the Insulated Loop Antenna Immersed in a Conducting Medium,” in *Radio Science Journal of Research NBS/USNC-URSI*, vol. 68D, no. 11, Nov. 1964.

[Wait 1966] J.R. Wait, “Theories of Prolate Spheroidal Antennas,” in *Radio Science*, vol. 1, no. 4, pp. 475-512, April 1966.

[Wait 1995] J. R. Wait, "Excitation of a conducting half-space by a toroidal coil," in *IEEE Antennas and Propagation Magazine*, vol. 37, no. 4, pp. 72-74, Aug 1995.

[Wait 1998] J. R. Wait, "The ancient and modern history of EM ground-wave propagation," in *IEEE Antennas and Propagation Magazine*, vol. 40, no. 5, pp. 7-24, Oct 1998.

[Wang et al. 2010] S. Wang, Liu Zeyuan and Y. Xing, "Extraction of parasitic capacitance for toroidal ferrite core inductor," *2010 5th IEEE Conference on Industrial Electronics and Applications*, Taichung, 2010, pp. 451-456.

[Warnick and Jensen 2007] K. F. Warnick and M. A. Jensen, "Signal and Noise Analysis of Small Antennas Terminated with High-Impedance Amplifiers," *Antennas and*

Propagation, 2007. EuCAP 2007. The Second European Conference on, Edinburgh, 2007, pp. 1-6.

[Weaver 2016] R. Weaver, "Numerical Methods for Inductance Calculation," accessed March 2016, parts 1-2 starting on <http://electronbunker.ca/eb/CalcMethods.html>.

[Werner 1996] D. H. Werner, "An exact integration procedure for vector potentials of thin circular loop antennas," in *IEEE Transactions on Antennas and Propagation*, vol. 44, no. 2, pp. 157-165, Feb 1996.
(and)
D. H. Werner, "Correction to "An Exact Integration Procedure for Vector Potentials of Thin Circular Loop Antennas"," in *IEEE Transactions on Antennas and Propagation*, vol. 44, no. 8, pp. 1199-, Aug. 1996.

[Wheeler 1928] H. A. Wheeler, "Simple Inductance Formulas for Radio Coils," in *Proceedings of the Institute of Radio Engineers*, vol. 16, no. 10, pp. 1398-1400, Oct. 1928.

[Wheeler 1982] H. A. Wheeler, "Inductance formulas for circular and square coils," in *Proceedings of the IEEE*, vol. 70, no. 12, pp. 1449-1450, Dec. 1982.

[Williams 1965] R.H. Williams, "Insulated and Loaded Loop Antenna Immersed in a Conducting Medium," in *Radio Science Journal of Research NBS/USNC-URSI*, vol. 69D, no. 2, Feb. 1965.

[Wilson and Brown 2008] P. R. Wilson and A. D. Brown, "Effective modeling of leakage inductance for use in circuit simulation," *Applied Power Electronics Conference and Exposition, 2008. APEC 2008. Twenty-Third Annual IEEE*, Austin, TX, 2008, pp. 391-395.

[Wojda and Kazimierczuk 2012] R. P. Wojda and M. K. Kazimierczuk, "Winding resistance of litz-wire and multi-strand inductors," in *IET Power Electronics*, vol. 5, no. 2, pp. 257-268, Feb. 2012.

[Xi Nan and Sullivan 2003] Xi Nan and C. R. Sullivan, "An improved calculation of proximity-effect loss in high-frequency windings of round conductors," *Power Electronics Specialist Conference, 2003. PESC '03. 2003 IEEE 34th Annual*, 2003, pp. 853-860 vol.2.

[Xi Nan and Sullivan 2004] Xi Nan and C. R. Sullivan, "Simplified high-accuracy calculation of eddy-current loss in round-wire windings," *Power Electronics Specialists Conference, 2004. PESC 04. 2004 IEEE 35th Annual*, 2004, pp. 873-879 Vol.2.

[Xi Nan and Sullivan 2009] X. Nan and C. R. Sullivan, "An Equivalent Complex Permeability Model for Litz-Wire Windings," in *IEEE Transactions on Industry Applications*, vol. 45, no. 2, pp. 854-860, March-April 2009.

[Xu Tang and Sullivan 2003] Xu Tang and C. R. Sullivan, "Stranded wire with uninsulated strands as a low-cost alternative to litz wire," *Power Electronics Specialist Conference, 2003. PESC '03. 2003 IEEE 34th Annual*, vol. 1, pp. 289-295, 2003.

[Yan et al. 2013] B. Yan, W. Zhu, L. Liu, K. Liu and G. Fang, "An Optimization Method for Induction Magnetometer of 0.1 mHz to 1 kHz," in *IEEE Transactions on Magnetics*, vol. 49, no. 10, pp. 5294-5300, Oct. 2013.

[Young and Butler 2001] J. C. Young and C. M. Butler, "Inductance of a shielded coil," in *IEEE Transactions on Antennas and Propagation*, vol. 49, no. 6, pp. 944-953, Jun 2001.

[Young and Butler 2002] J. C. Young and C. M. Butler, "Inductance of a coil in a slotted shield," in *IEEE Transactions on Antennas and Propagation*, vol. 50, no. 4, pp. 475-484, Apr 2002.

[Yuanren Qui et al. 1993] Yuanron Qui and Qinke Zhang, "Numerical Calculation on Multi-Layer Solenoidal Coil," *Electromagnetic Field Computation, 1992. Digest of the Fifth Biennial IEEE Conference on*, Claremont, CA, USA, 1992, pp. TP30-TP30.

[Zaman et al. 1981] A. J. M. Zaman, S. A. Long and C. G. Gardner, "Impedance of a loop surrounding a conducting cylinder," in *IEEE Transactions on Instrumentation and Measurement*, vol. IM-30, no. 1, pp. 41-45, March 1981.

[Zhang 2007] D. Zhang, “Permeability enhancement by induced displacement current in magnetic material with high permittivity,” in *Journal of Magnetism and Magnetic Materials*, vol. 313, pp. 47-51, 2007.

[Zhu et al. 2000] J. Zhu, K. J. Tseng, C. F. Foo and J. X. Wang, "Experimental investigations into the effects of multi-segment structure on core losses in MnZn ferrites at high frequencies," *Magnetics Conference, 2000. INTERMAG 2000 Digest of Technical Papers. 2000 IEEE International*, Toronto, ON, Canada, 2000, pp. 450-450.

[Župan et al. 2014] T. Župan, Ž Štih and B. Trkulja, "Fast and Precise Method for Inductance Calculation of Coaxial Circular Coils With Rectangular Cross Section Using the One-Dimensional Integration of Elementary Functions Applicable to Superconducting Magnets," in *IEEE Transactions on Applied Superconductivity*, vol. 24, no. 2, pp. 81-89, April 2014.

[Zverev et al. 2011] V.I. Zherev, R.R. Gimaev, A.M. Tishin, Ya. Mudryk, K.A. Gschneidner Jr., and V.K. Pecharsky, "The role of demagnetization factor in determining the 'true' value of the Curie temperature," in *Journal of Magnetism and Magnetic Materials*, vol. 323, pp. 2453-2457, 2011.